eISSN: 2789-858X

Scientific Journal for the Faculty of Science - Sirte University (SJFSSU)

Bi-annual, Peer- Reviewed, and Open Accessed e-Journal

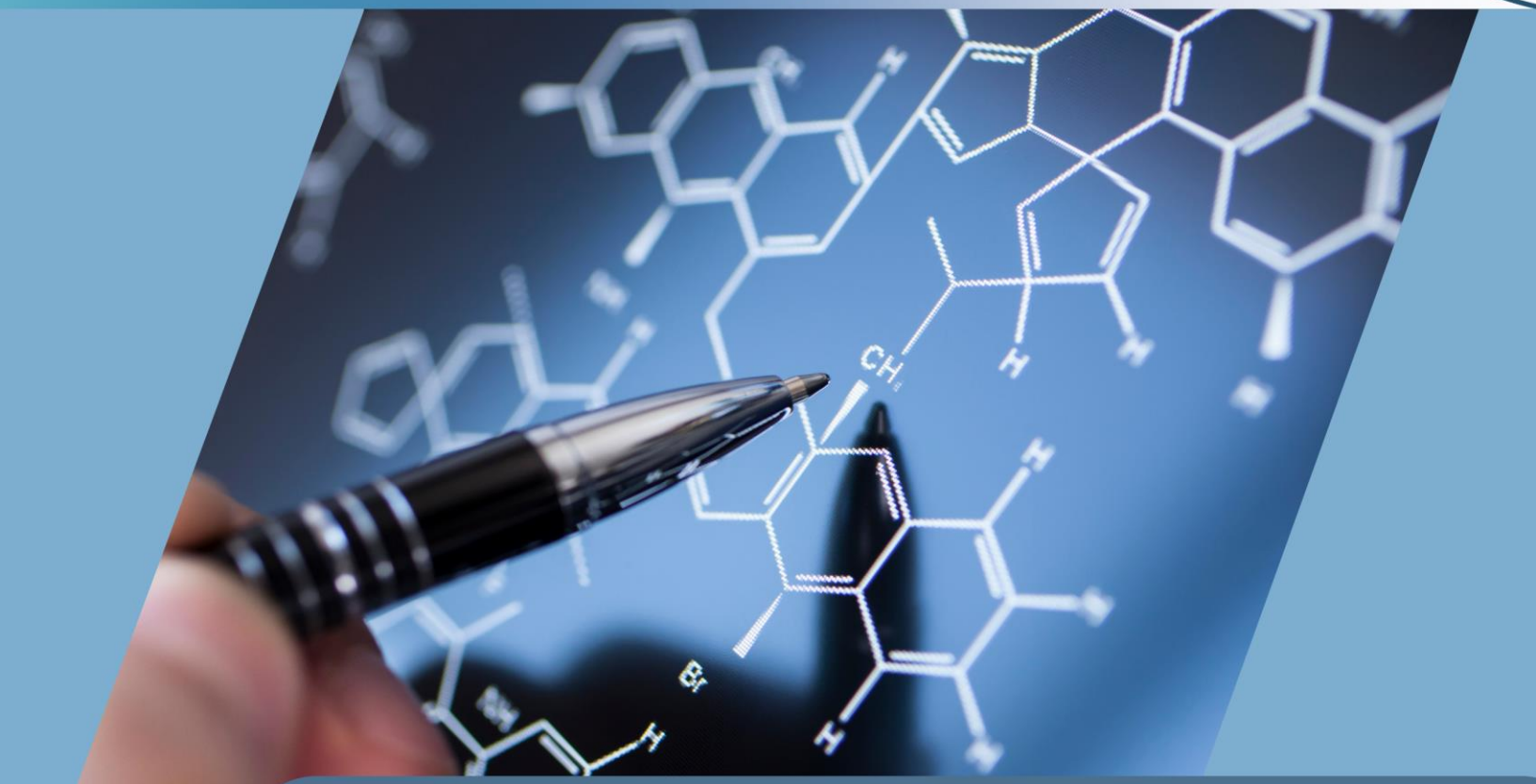

VOLUME 4 ISSUE 1 APRIL 2024

10.37375/issn.2789-858X

Legal Deposit Number@National Library (Benghazi): 990/2021

jsfsu@su.edu.ly

Scientific Journal for Faculty of Science-Sirte University (SJFSSU)

Bi-annual, Peer-Reviewed, Indexed, and Open Accessed e-Journal

DOI: 10.37375/issn.2789-858X (Indexed by Crossref, USA)

Volume 4, Issue 1, April 2024

Advisory Scientific Committee of the SJFSSU

No	Name	Specialization	Organization	Country
1	**Prof. Dr. Ahmad F. Mahgoub**	Zoology	Science Faculty, **Sirte** University	Libya
2	**Prof. Dr. Salem A. Abuhassia**	Statistics	Science Faculty, **Omar Al-Mukhtar** University	Libya
3	**Prof. Dr. Marei M. El-Ajaily**	Chemistry	Science Faculty, **Benghazi** University	Libya
4	**Prof. Dr.Huda Shaaban Elgubbi**	Botany	Science Faculty, **Misurata** University	Libya
5	**Prof. Dr. Nasser H. Sweilam**	Applied Maths	Science Faculty, **Cairo** University	Egypt
6	**Prof. Dr. Osama Ahmed Hlal**	Geology	Science Faculty, **Tripoli** University	Libya
7	**Prof. Dr. Mohamed A. Elssaidi**	Environment Sciences	Engineering and Technical Sciences Faculty, **Sebha** University	Libya
8	**Prof. Dr. Ebrahim M. Daghman**	Microbiology	Science Faculty, **Misurata** University	Libya
9	**Prof. Dr. Ali Mohamed Awin**	Mathematics	Science Faculty, **Tripoli** University	Libya
10	**Prof. Dr. Ebrahim A. Elmerhaq**	Information Technology	Information Technology Faculty, **Tripoli** University	Libya
11	**Prof. Dr. Rafa A. Azzarroug**	Physics	Science Faculty, **Benghazi** University	Libya
12	**Prof. Dr. Osams M. Shalabiea**	Astronomy	Science Faculty, **Cairo** University	Egypt
13	**Prof. Dr. Abdualhamid S. Alhaddad**	**Environment Sciences & Natural Resources**	Science Faculty, **Misurata** University	Libya

Editor in-Chief's Word

Welcome, dear readers, to the first issue of the fourth volume of the Scientific Journal for the Faculty of Science-Sirte University (SJFSSU). We are thrilled to embark on this journey with you, and we hope that this collection of articles will spark curiosity, ignite discussion, and inspire further exploration.

We believe that the articles in this volume offer a diverse and thought-provoking perspective on this topic, and we encourage you to engage with them critically and openly.

As the Editor-in-Chief, I am particularly proud of the work that our team has put into curating this volume. We have carefully selected articles that represent a wide range of viewpoints and methodologies, ensuring that there is something for everyone within these pages. We are also grateful to the authors who have entrusted us with their work, and we hope that you will find their contributions to be both informative and engaging.

All articles published in SJFSSU will be assigned a DOI (Digital Object Identifier) to ensure their long-term accessibility and citability. Additionally, all submissions are carefully scanned using the Turnitin plagiarism checker to ensure originality and academic integrity.

In addition to the information already mentioned, we would like to highlight a few additional aspects of the SJFSSU that make it a valuable resource:

Rigorous Peer Review: All articles submitted to SJFSSU undergo a rigorous peer-review process to ensure that they meet the highest standards of academic excellence.

Open Access Policy: We believe that open access makes research more accessible and impactful, allowing anyone the full text of all articles freely available online, without any restrictions, and building upon our published work.

Citations in Scopus-Indexed Journals: Our journal is committed to publishing high-quality research that is relevant to the field. As such, we are proud to share that some of our articles have been cited in journals that are indexed in Scopus, a leading abstract and citation database. This demonstrates the impact and reach of our work.

If you are a researcher, scholar, or writer who is passionate about SJFSSU, we encourage you to submit your work to SJFSSU. We are particularly interested in articles that are original, insightful, and well-written. Thus you can help to ensure that SJFSSU continues to be a valuable resource for researchers, and scholars.

We at SJFSSU value your feedback and suggestions as they help us improve the quality and relevance of our content. There are several ways you can share your thoughts with us. You can submit a formal letter to the editor-in-chief outlining your feedback or suggestions. This is a good option if you have detailed comments or want to address a specific article or issue. Also, we are active on the social media platform Facebook, so you can send us a direct message or leave a comment on our posts to share your feedback.

Prof. Haniyah Saed Ben Hamdin
Editor-in-Chief, Scientific Journal for the Faculty of Science-Sirte University.

About the Scientific Journal of the Faculty of Science at the University of Sirte

DOI: http://www.doi.org/10.37375/issn.2789-858X

History of the journal

The Journal of the Faculty of Science at the University of Sirte is a biannual and electronic peer-reviewed scientific journal that is available free of charge on its website. The journal was established by the decision of the dean of Sirte University No. 11 which was issued on 29-4-2021 and decision No. 194 which was issued on 25-5-2021 on the formation of the editorial board of the journal.

The message

We hope that this journal will be a scientific platform that provides researchers, from inside and outside Sirte University, the chance to publish their scientific research according to the scientific development in the field of pure and applied Sciences. The editorial board of the journal will follow the approach of adhering to the scientific methodology, and ethics of scientific research, examining the accuracy, and scientific honesty during the procedures of evaluating the received manuscripts to ensure that the quality standards recognized in scientific publications are met.

Vision

Inclusion of international databases to contribute to raising the University's ranking and progress at the local and national ranks.

Objectives of the journal

1. This scientific journal was established by the faculty to meet the community's need for scientific research, including the scientific research it presents by specialists in various sciences. The publication of scientific research is essential in the career of any researcher. Moreover, the process of publishing research has developed and become an effective way to spread knowledge and communication between researchers.
2. The journal aims to encourage researchers to accelerate progress in scientific research and publish their works.
3. Providing an honorable image to the Faculty of Science in particular and Sirte University in general.

Scientific Disciplines

The Scientific Journal for the Faculty of Science-Sirte University (SJFSSU is concerned with publishing original research in all fields of applied and pure (theoretical) science, namely mathematics, statistics, physics, chemistry, zoology, botany, microbiology, astronomy, computer science, information technology, geology, environment science, and oceanography.

Policy and Publication Ethics of the Scientific Journal for the Faculty of Science-Sirte University (SJFSSU)

Publishing Cycle

The Scientific Journal of the Faculty of Science at Sirte University is published electronically on a semi-annual basis during April and October.

Open Access Policy

The Scientific Journal of the Faculty of Science at Sirte University is an open-access journal that allows readers, authors, and their institutions to obtain the full text of the articles published in it for free.

Copyright License Terms

All articles published in the Scientific Journal of the Faculty of Science at Sirte University are subject to the International Creative Commons License (CC BY 4.0 Creative Common Licence) and the author(s) retain copyright for the articles published by the journal with the guarantee of the following:

1- Making the article available on the journal's website.

2- Granting any third party the right to use the article without any restrictions provided that its contents and original authors are preserved and the source of publication is cited.

Intellectual Property Rights Copyrights

The Scientific Journal of the Faculty of Science at Sirte University possesses the copyright of the published articles without any restrictions.

Archiving Policy

The PKP Preservation Network (PN) provides free preservation services for a journal managed by Open Journal Systems (OJS) via the PKP PN plugin. Therefore, for SJFSSU to fulfill this essential criterion, this plugin has been activated.

Plagiarism Policy

1. To fulfill the academic integrity requirements, manuscripts submitted to the SJFSSU must adhere to ethical standards and refrain from plagiarism in any way. Thus all manuscripts submitted to the SJFSSU must be initially screened by plagiarism checker software.

2. If any plagiarism or scientific theft is detected before publication, then the SJFSSU will contact the author/s concerning this matter. If the editorial board of the SJFSSU is not satisfied with the justifications presented by the author, then the following strict actions will be taken against the author:

    i. Such manuscript(s) will be immediately rejected.

    ii. The editorial board forever will not consider any request for publication submitted by such author/s in the future.

    iii. An announcement will be placed in this regard on the journal website and in the author's institution.

3. If any plagiarism or scientific theft is detected after publication, then:
    a. Immediately this article will be withdrawn from publication and republished on the journal's website and in the next issue of the journal with a watermark (RETRACTED).
    b. An appropriate announcement will be placed in this regard through the journal website and in the author's institution.
    c. An official letter to the author's institution regarding taking legal measures in this regard.
    d. We can also consider more strict actions against authors based on the seriousness of the incident.

Complaints and Appeals

Anyone can submit his/her complaints/appeal to the Editor-in-Chief of the journal by email.

Publication fees

Publication in the journal is completely free and there are no fees either for submission, article processing APC or for publication, fees for the number of papers, or fees for coloured figures.

Publication Ethics:

1. Any manuscript submitted to the SJFSSU must contain an original work that has been neither previously published, nor is under consideration by another journal, conference, workshop, or symposium.
2. The submitted manuscript must fulfill the common requirements of scientific research, including presenting the problem, reviewing the relevant literature, analyzing data, discussing results, and drawing conclusions and recommendations.
3. The SJFSSU accepts all types of articles such as research articles, review articles, topical reviews, case study/case reports, monographs, short communication, letters, conference/symposium special issues, editorials, research articles, and methodology articles.
4. An author is required to write his or her manuscript carefully according to the basic and technical rules of the SJFSSU.
5. The SJFSSU only accepts manuscripts written in the English language.
6. The subject of the submitted manuscript must be in the specified categories of the SJFSSU.
7. All individuals involved in the publishing process: from authors, editorial board, and reviewers, must comply with standards of ethical behaviour.
8. All submitted manuscripts are subject to a double-blind and peer-review process that is the author will be unaware of the reviewer’s identity, and also the reviewer is unaware of the author’s identity.
9. The SJFSSU follows the Code of Conduct of the Committee on Publication Ethics (COPE) and follows COPE Flowcharts for resolving cases of suspected misconduct. The Journal is particularly committed to the COPE Code of Conduct for Journal Publishers. Journal editors follow COPE's Code of Conduct and best practice guidelines for journal editors.

Author/s Responsibility:

1. The author is alone responsible for the proofreading and spelling check of his or her submitted manuscript.
2. The SJFSSU editorial committee has the right to make any editorial changes to the manuscript which is accepted for publication.
3. The author/ authors is/are prohibited from publishing in the journal for three consecutive years if it appears that they have sent the manuscript to another journal at the same time that it was sent to the journal.
4. The author is not entitled to withdraw the manuscript during the evaluation process unless the peer-review process exceeds six months. Thus the author could withdraw the manuscript provided that he informs the journal of his desire.
5. Any author is kindly requested to disclose any affiliations, including financial, consultant, or institutional associations that might lead to bias or a conflict of interest.
6. Any author is required to understand, complete, and sign the 'Authorship, Copyright Transfer, Conflicts of Interest and Acknowledgments statement' which can be downloaded from the link:
   https://drive.google.com/file/d/1jvan4NOS_CFeqJzOw8LR6RwH0vXoiA29/view?usp=sharing

The signed form should be scanned and attached electronically along with the submitted manuscript.

7. An author has to submit his or her manuscript electronically as an MS Word file through the journal website via the link:
   https://journal.su.edu.ly/index.php/SJFSSU/information/authors
8. Without the need to contact the editorial committee about a submitted manuscript, an author can easily track his or her submitted manuscript electronically through the journal website via the link:
   https://journal.su.edu.ly/index.php/SJFSSU/information/authors

Author's Rights:

1. The Author retains the following rights:
   i. All proprietary rights, such as patent rights.
   ii. Using all or part of the material published in his or her article in further research of his or her filling, provided that permission is granted from the SJFSSU and an adequate acknowledgment should be appropriately credited and referenced for the SJFSSU.

Disclaimer

The author(s) of each article appearing in this Journal is/are solely responsible for the views, ideas expressed, and the accuracy of the data in his or her manuscript. Thus the published papers do not reflect the opinions or views of the SJFSSU or its members. Furthermore, the designation and the presentation of materials do not reflect any opinion whatsoever of the SJFSSU in terms of the legal status of any country, territory…etc.

Editors Responsibilities:

1. The editorial committee must ensure a fair double-blind peer-review of the submitted manuscript.
2. The editorial committee will strive to make sure there are no potential conflicts of interest between the author and the editorial and review personnel.
3. The editorial committee will ensure that all the information related to submitted manuscripts is sustained as confidential.

Reviewers Responsibilities:

1. The reviewers must ensure that all the information related to submitted manuscripts is kept confidential.
2. A reviewer who is unable to review the submitted manuscript for any reason should notify the editorial director to excuse himself or herself from the review process.
3. Reviewers must review the submitted manuscripts objectively according to the journal's evaluation forms and adhere to the specified evaluation period of three months at max.

Review Process

1. If the submitted manuscript initially meets the specified requirements of the SJFSSU and successfully passes the plagiarism check, then directly it should go through the double-blind and peer-review process.
2. The submitted manuscript is subject to double-blind review by specialized referees suggested by the editorial committee in an undisclosed manner to evaluate the submitted manuscript.

3. The editorial board of the journal informs the author of the opinions of the referees and forwards its assessment report if the manuscript needs any corrections.
4. Any Degree holder with a scientific degree (assistant professor or higher) who would like to be a referee in the SJFSSU should register and send his or her CV through the SJFSSU website.
5. An author is required to make any minor or major corrections that are suggested by the referees within a stipulated date.

Publishing Process

1. Once the decision is made to accept the manuscript for publication at the SJFSSU, the author will be notified and facilitated with an acceptance letter to confirm that his or her manuscript has been accepted for publication in the upcoming issue of the SJFSSU.
2. Once the issue of the journal has been realized, a soft copy of each published paper will be sent to the author via his or her email address.

Author Guidelines

All submissions should strictly be prepared according to the following typing guidelines for preparing the manuscript:

1. The submitted manuscript should be approximately up to a maximum of 20 pages and a minimum of 5 pages (including tables, figures, references list, appendixes, and supplements).
2. The submitted manuscript of types (review articles, topical review) should be approximately 45 pages maximum (including tables, figures, references list, appendixes, and supplements).

Rules for the Paper Structure

3. The first page should contain the full title of the manuscript (the title should be concise and informative), then the name(s) of the author(s).
4. Affiliation with contact information including the (Affiliation (s) of the author(s), i.e. institution, (department), city, (state), and country). A clear indication and an active, official university email address of the corresponding author.
5. This is followed by the abstract except for review article types which start with the introduction.

6. The abstract length should be (250) words at the maximum and (150) words at the minimum.
7. In the abstract of the submitted manuscript, the following main points must be available: -

    i. An introductory sentence related to the research topic to attract readers.
    ii. Presentation of the research's main point (purpose).
    iii. Description of the method used in the research.
    iv. Presentation of the achieved results.
    v. A concluding sentence that includes a recommendation.
8. The keywords should be 4 to 6, which can be used for indexing purposes.
9. In the introduction of the submitted manuscript, the following main points must be available: -
    i. Introductory sentences related to the research topic to attract readers.
    ii. An adequate background, then the relevant literature review.
    iii. Clearly state the object of the research.
    iv. The limitation of the research.
    v. The structure of the manuscript.
10. In the Material and Methods section of the submitted manuscript, the author should provide sufficient details to allow the work to be reproduced by an independent researcher. Methods that are already published should be summarized and indicated by a reference. If quoting directly from a previously published method, use quotation marks and also cite the source. Any modifications to existing methods should also be described.
11. Results should be clear and concise and presented separately from the discussion.
12. The discussion should explore the significance of the results of the work, not repeat them.
13. The main conclusions of the study may be presented in a short Conclusions section, which may stand alone or form a subsection of the Discussion section.
14. Collate acknowledgments in a separate section at the end of the article before the reference list and do not, therefore, include them on the title page, as a footnote to the title or otherwise. List contributions that need acknowledging (e.g., acknowledgments of technical help; acknowledgments of financial and material support, writing assistance or proofreading the article, financial arrangement, specifying the nature of the support).

15. Within the acknowledgments section, a conflict of interest statement must be included for all manuscripts even if there are no conflicts of interest.
16. If there is more than one appendix, they should be identified as A, B, etc. Formulae and equations in appendices should be given separate numbering: Eq. (A.1), Eq. (A.2), etc.; in a subsequent appendix, Eq. (B.1), and so on. Similarly for tables and figures: Table A.1; Fig. A.1, etc.
17. The author is asked to switch off the 'Track Changes' option in Microsoft Office files as these will appear in the published version.

Text Formatting Rules:

18. Use a normal, plain font (e.g., 10-point Times New Roman) for text.
19. Use italics for emphasis.
20. Use the equation editor or Math Type for equations.
21. Save your file in docx format (Word 2007 or higher).

Headings: Please use no more than three levels of displayed headings.

22. The manuscript (in two columns) should be single line space and the font type (Times New Roman) and the size should be as specified in this table:

Paper title	14 Bold
Authors names	10
Abstract	9
Address	10 Italic
Main headings	12 Bold
Subheadings	10 Bold
Text	10
Figure and table captions	9

23. The metric system should be used, and the Arabic numbers should be used for page numbers and throughout the running text.
24. Abbreviations, if used should be defined at their first mention in the text and used consistently thereafter, and the non-standard ones should be avoided.
25. Mathematical equations should appear in a sequential order and should be numbered between the brackets ( ).

Tables

26. All tables are to be numbered using Arabic numerals.
27. Tables should always be cited in text in consecutive numerical order. For each table, please supply a table caption (title) explaining the components of the table and an explanatory legend.
28. Identify any previously published material by giving the original source in the form of a reference at the end of the table caption.
29. Footnotes to tables should be indicated by superscript lower-case letters (or asterisks for significance values and other statistical data) and included beneath the table body.

Figures

30. High resolution is required in preparing the figures in the manuscript, the file formats JPEG, PNG are preferred for the figures, images, etc.
31. If the figure, photo… etc. has been published elsewhere, then the original source must be acknowledged and a written permission from the copyright holder must be obtained and submitted with the manuscript.
32. If photographs of people are used, then the photos must be obscured by clouds or a written permission by the concerned person must be obtained.
33. All figures are to be numbered using Arabic numerals.
34. Figure parts should be denoted by lowercase letters (a, b, c, etc)
35. References to figures and tables should be made in a sequential order as they appear in the running text, and should be numbered between the parentheses ( ), e.g. (Fig. 1) and (Tab. 1).
36. Ensure all figure and table citations in the text match the files provided.
37. When preparing your figures, pay attention to the size figures to fit in the column width.
38. Figures should have a short label.

References Style:

39. Enclose the references list at the end of the manuscript accordingly to the APA (American Psychological Association) style (5^{th} to 7^{th}) edition. A guide containing examples of common citation formats in APA can be found at the below link:

https://guides.libraries.psu.edu/apaquickguide/

40. How to create an APA cited paper in Microsoft Word:

https://support.microsoft.com/en-us/office/apa-mla-chicago-%E2%80%93-automatically-format-bibliographies-405c207c-7070-42fa-91e7-eaf064b14dbb

Page margins: The Page margins should be adjusted as,

Top	Bottom	left	Right
2	2	2.5	2

41. To prepare the manuscript, it is highly recommended to use the ready –template that is prepared by the editorial committee which is available electronically on the journal website at the ink:

https://docs.google.com/document/d/1Q7JFml7kjZAwr0qXLzv6L9nOoOdeRLtK/mobilebasic

Scientific Journal for Faculty of Science-Sirte University (SJFSSU)

DOI: 10.37375/issn.2789-858X (Indexed by Crossref, USA)

Volume 4, Issue 1, April 2024

DOI: https://doi.org/10.37375/sjfssu.v4i1

Scientific Journal for the Faculty of Science-Sirte University Vol. 4, No. 1 (2024) 1-8

Scientific Journal for the Faculty of Science-Sirte University

Journal home page: http://journal.su.edu.ly/index.php/JSFSU/index

DOI: 10.37375/issn.2789-858X

Efficient Removal of Methylene Blue Dyes from Aqueous Solutions Using Various Charcoal Adsorbents: A Comparative Thermodynamic and Isotherm Study of Olive, Pine, and Commercial Activated Carbon

Ezadeen Aboshaloa, Nura Ageel, khadeja Samoe and Ahlam Albashini

Chemistry Department, Education Faculty, Tripoli University, Libya.

DOI: https://doi.org/10.37375/sjfssu.v4i1.2605

ARTICLE INFO:

Received: 23 January 2023

Accepted: 31 April 2024

Published: 17 April 2024

***Keywords*:** *adsorption, activated carbon, methylene blue, pollution, dye.*

A B S T R A C T

In this study, the effectiveness of various types of charcoal, including pine, olive, and commercial activated carbon, as adsorbents for removing methylene blue dye from water is evaluated. The study was conducted by preparing aqueous solutions containing methylene blue dye and using the three types of charcoal as adsorbents. The main factors affecting the adsorption process were determined through laboratory experiments, which included varying temperature, contact time, pH, and the quantity of charcoal to optimize the dye removal process. Additionally, isotherm studies and thermodynamic analysis of the reaction were conducted. The results demonstrate the successful removal of methylene blue dye by all three types of charcoal, with maximum adsorption capacities of 346.02 mg/g, 283.28 mg/g, and 406.50 mg/g for commercial activated carbon, olive charcoal, and pine charcoal, respectively. The ΔH results indicate that the adsorption process for pine charcoal and activated carbon was physical, while it was chemical for olive charcoal. This research highlights the efficiency, cost-effectiveness, and sustainability of the adsorption process using charcoal as a promising solution for reducing dye pollution in water sources, contributing to the development of sustainable water purification strategies.

1 Introduction

The extensive use of synthetic dyes in the textile industry has led to the generation of colored wastewater, contributing to the pollution of water bodies and posing a significant environmental concern. Colored wastewater contains various organic and hazardous substances, which not only endanger aquatic life but also pose risks to public health (Ramakrishna & Viraraghavan, 1997). Synthetic dyes, known for their non-biodegradability and resistance to heat, light, and chemicals, exacerbate water contamination, potentially causing mutagenic, carcinogenic, or toxic effects (Almeida & Chemosphere, 2014). This pollution threatens the sustainability of ecosystems and compromises the availability of clean water resources for communities.

In addition to environmental pollution resulting from the dye industry, communities around the world face various environmental challenges arising from the use of chemicals, biological, and physical factors (Goudarzi & Mahvi, 2021). Pollution encompasses not only colored wastewater from industries but also air pollution caused by industrial emissions and volatile organic compounds, as well as soil pollution from the disposal of solid and hazardous wastes (Sarwar et al., 2020; Hahladakis & Iacovidou., 2020; Kim et al., 2017; Gyawali & Techato 2020).

Pollution is considered one of the most significant environmental challenges facing humanity in the modern age, adversely affecting the environment, human health, and animal life. Among the effects of environmental

***Corresponding author*: E-mail: e.pashloa@uot.edu.ly**

pollution are increased rates of chronic diseases such as asthma and respiratory diseases, deterioration of water quality affecting access to clean and potable water, and negative impacts on biodiversity and ecosystem stability (Landrigan et al., 2018; Prüss-Ustün et al., 2016; Patz et al., 2014)

Conventional wastewater treatment methods such as precipitation, coagulation, and filtration, while effective, are often time-consuming and expensive, limiting their widespread application (Crini, 2005). Therefore, addressing the issue of synthetic dye removal from wastewater requires exploring alternative, cost-effective solutions. Adsorption, a process involving the attachment of pollutant molecules to the surface of a material, particularly activated carbon, has emerged as a promising approach for the treatment of organic contaminants (Khettaf et al, 2016).

Moreover, the utilization of plant waste, such as seeds and roots, as eco-friendly and cost-effective adsorbents for dyes, has gained significant attention (Seow & Lim., 2016; Verma & EnviManag., (2016); Hassaan & El Nemr, 2017). Furthermore, the recent emphasis on producing activated carbon from agricultural and food waste offers a sustainable solution to address this environmental challenge (Aboushaloa et al., 2022; Alardhi et al., 2020; Maghni et al., 2017; Aboushloa & Etorki, 2015). Therefore, this study aims to assess the adsorption effectiveness of methylene blue onto olive, pine, and commercially produced activated carbon surfaces.

In this study, the adsorption capacity and efficiency of the three types of activated carbon, namely olive charcoal, pine charcoal, and commercially produced activated carbon, will be evaluated for the removal of methylene blue from wastewater. The findings of this research will contribute to the development of efficient and sustainable methods for dye removal, potentially leading to reduced environmental pollution and improved water quality.

2 Materials and Methods

2.1 Coal Preparation: Three coal samples (olive coal, pine coal, and commercial activated carbon) underwent drying at 105°C for 8 hours, followed by grinding and sieving for particle size standardization.

2.2 Effect of Initial Concentration on Adsorption Capacity: To establish the optimum initial concentration for dye (MB) adsorption, concentrations ranging from 5 to 25 ppm were prepared for olive coal, pine coal, and commercial activated carbon. After adding the coal, adsorption was measured following a 30-minute incubation.

2.3 Effect of Weight on Adsorption Capacity: The study explored the impact of coal weight (0.1-1.5 grams) on dye (MB) adsorption by assessing seven different weights for each type of coal at concentrations of 10, 10, and 25 ppm. Adsorption measurements were conducted after a 30-minute incubation.

2.4 Effect of Contact Time on Adsorption Capacity: Investigating the influence of contact time, olive coal and pine coal (0.4 grams each) and commercial activated carbon (0.1 grams) were added to dye solutions (10, 10, and 25 ppm). After a 30-minute incubation, adsorption was measured.

2.5 Effect of Temperature on Adsorption Capacity: The impact of temperature on adsorption capacity was evaluated by exposing olive coal and pine coal (0.4 grams each) and commercial activated carbon (0.1 grams) to dye solutions (10, 10, and 25 ppm) at different temperatures (25, 30, 40, and 70°C) for 30 minutes. Adsorption measurements were conducted after filtration.

Equations for Adsorption: The amount adsorbed (Qe) onto the silicon surface was determined using the following equation:

$$Q = \frac{Ci - Ce}{w} \times v \quad (1)$$

The removal efficiency (% Removal) was calculated as:

$$\%\text{Removal} = \frac{Ci - Ce}{Ce} \times 100 \quad (2)$$

Adsorption Isotherm Models: The Langmuir isotherm model, applicable to monolayer adsorption, is represented by:

$$Ce/\ Qe = 1\ /qmax\ Ce + 1/\ q\ maxb \quad (3)$$

where qmax is the maximum adsorption capacity (mg/g), and b is the adsorption energy (L/mg).

The Temkin model, considering the adsorption as a chemical process, is expressed as:

$$Qe = \frac{RT}{b}\ln(A) + \frac{RT}{b}\ln(Ce) \quad (4)$$

Where $B = \frac{RT}{B}$ (5)

Freundlich adsorption isotherm is calculated by:

$$\ln(Qe) = \ln(Kf) + \frac{1}{n}(Ce) \quad (6)$$

where Kf and n are proportional constants reflecting adsorption capacity and intensity.

These equations provide a foundation for evaluating the adsorption performance of the studied materials under various conditions. (Aboshaloa et al.,2022)

3 Results and Discussion

3.1 Effect of Initial Concentration: The influence of the initial concentration of methylene blue (MB) dye on the adsorption ratio was investigated using three types of charcoal (olive, pine, commercial) at different dye concentrations (5, 10, 15, 20, 25 ppm), as illustrated in Figure 1.

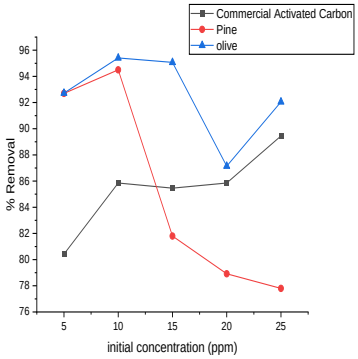

Figure (1) Effect of initial concentration (ppm) on Adsorption Process

The results demonstrate that the adsorption ratio for olive charcoal peaks at 10 ppm (95.41%), pine charcoal at 10 ppm (94.5%), and commercial activated charcoal at 25 ppm (89.45%). These findings align with previous studies (Rahman, et al., 2012; Li et al., 2016). suggesting an overall trend of increased adsorption rates with higher dye concentrations. The variation in optimal concentrations for each charcoal type emphasizes the need for tailored adsorption conditions based on specific adsorbent characteristics. Increased competition between dye molecules for scarce active sites on the charcoal surface or saturation of adsorption sites could be the cause of the plateau or minor decline in adsorption effectiveness at higher doses.

3.2 Effect of Weight on Adsorption Capacity: The impact of weight on the adsorption process of MB dye was explored using different weights of the three types of charcoal (0.1, 0.2, 0.4, 0.6, 0.8, 1.0, and 1.5 g), as depicted in Figure 2.

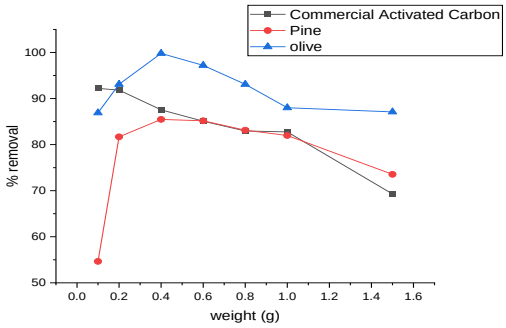

Figure (2) Effect of Weight (g) on Adsorption

Process results indicate that the adsorption rate for olive charcoal and pine charcoal is optimal at 0.4 g, with removal ratios of 99.8% and 85.4%, respectively. Commercial activated charcoal demonstrates the highest adsorption rate at 0.1 g, with a removal ratio of 92.2%. These outcomes align with a prior study (Aboushloa & Etorki, 2015). that identified the best dye adsorption rate at 0.3 g.

3.3 Effect of Contact Time on Adsorption Capacity: The influence of contact time on the adsorption process of MB dye was studied using three types of charcoal at different shaking times (10, 20, 30, 40, 50, 60, 90, 120 min), as presented in Figure 3.

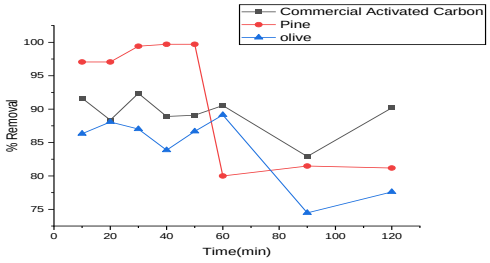

Figure (3) Effect of time(min) Values on Adsorption Process

Results indicate that the best adsorption rate for olive charcoal was observed at a contact time of 60 minutes (89.1%), while pine charcoal demonstrated optimal

adsorption at 40 minutes (99.42%). Commercial activated charcoal displayed the highest adsorption rate at 30 minutes (92.63%). These findings align with previous studies (Pathania et al., 2017; Rahman, et al, 2012; Li et al., 2016) reporting optimal shaking times for dye removal ranging from 30 to 60 minutes.

3.4 Effect of pH on Adsorption Capacity: The adsorption process of MB dye was influenced by the pH of the solution, adjusted using dilute solutions of sodium hydroxide and oxalic acid, over a pH range of 1 to 12, as illustrated in Figure 4.

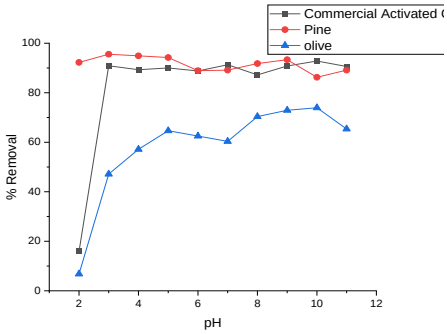

Figure (4) Effect of pH Values on Adsorption Process

Results showed that the highest adsorption rates for olive charcoal and commercial charcoal were observed at pH 10, with removal ratios of 73.93% and 92.8%, respectively. Pine coal exhibited the maximum adsorption rate at pH 3, with a removal ratio of 95.57%. These findings are consistent with previous studies (Pathania et al., 2017; Rahman, et al, 2012; Kumar et al., 2011). which reported higher adsorption rates in basic media. However, another study (Li et al, 2016) reported higher adsorption rates at pH 3, consistent with the results for pine coal.

3.5 Effect of Temperature on Adsorption Capacity: The effect of temperature on the adsorption process of methylene blue dye was investigated over a temperature range of 25-70°C, as shown in Figure 5.

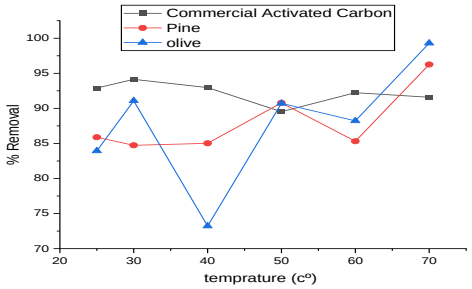

Figure (5) Effect of Temperature (c°) on Adsorption Process

The highest adsorption ratios for olive charcoal and pine charcoal were observed at 70°C, with removal ratios of 99.29% and 96.26%, respectively. For commercial activated charcoal, the highest adsorption rate was observed at 30°C, with a removal ratio of 94.14%. These results are consistent with previous studies (Rahman, et al, 2012; Kumar et al, 2011; Li et al, 2016; Aarfane et al., 2014). reporting an increase in adsorption rates with increasing temperature.

3.6 Isotherm Adsorption: Adsorption models, including Langmuir, Freundlich, and Temkin, were applied to the methylene blue dye, and the results are presented in Table 1. The isotherm of olive coal is also shown in the table1. Figures 6, 7 and 8 shows Langmuir, Freundlich and Temkin models.

Table (1) shows the isotherm of olive coal

Olive coal isothermates						
Isotherm models	Correlation Parameter					
Langmuir	Intercept 0.00353	Slope 0.00301	qmax(mg/g) 283.2861	AT 1.17257	RL 0.07857	R2 083665
Freundlich	Intercept 2.18097	Slope 0.87486	1/n 0.87486	Kf 151.6945	R2 0.79086	
Temkin	Intercept 168.814	Slope 108.26033	Pt (j mol-1) 108.26033	CT (j mg-1) 1.55933	R2 0.97174	

3.7 Isotherm Langmuir, Freundlich, Temkin for olivecoal

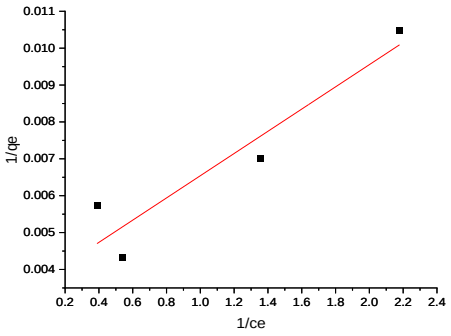

Figure (6) shows the Langmuir model

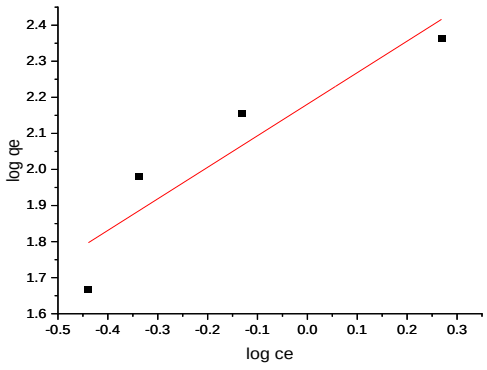

Figure (7) shows Freundlich model

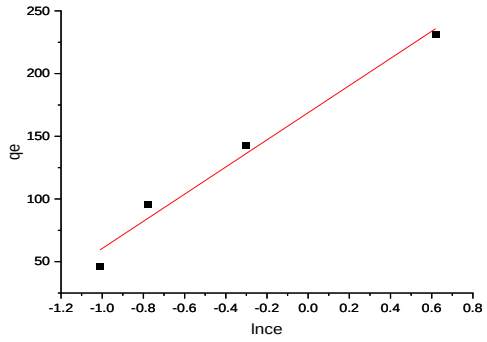

Figure (8) shows Temkin model of olive charcoal

Table (2) shows pine coal isotherm

Coal pine isothermate						
Isotherm models	Correlation Parameter					
Langmuir	Intercept 0.00246	Slope 0.00268	qmax(mg/g) 406.50406	AT 0.917910	RL 0.09824	R^2 0.70906
Freundlich	Intercept 2.24475	Slope 0.4006	1/n 0.4006	Kf 175.69119	R^2 0.68938	
Temkin	Intercept 194.27847	Slope 74.83377	Pt (j mol-1) 74.83377	CT (j mg-1) 2.596133	R^2 0.81187	

3.8 Isotherm Langmuir, Freundlich, Temkin for pine coal

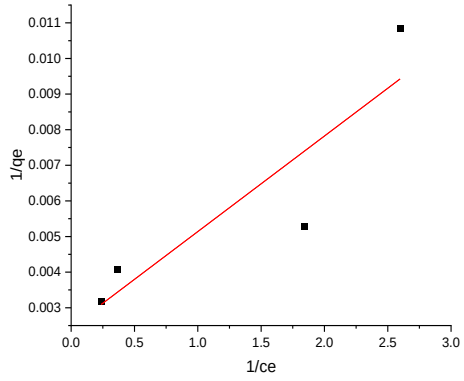

Figure (9) shows the Langmuir model

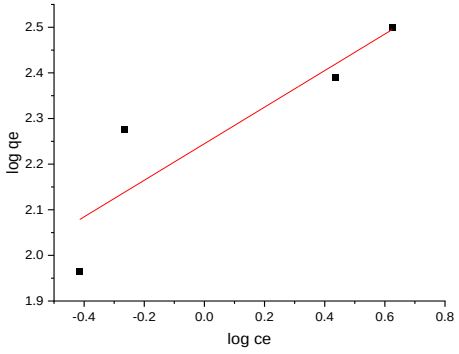

Figure (10) shows the Freundlich model

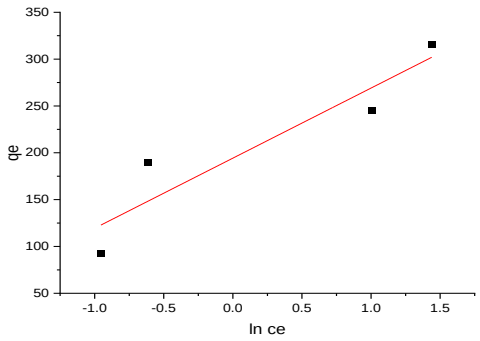

Figure (11) shows the Temkin model of pine charcoal

Table (3) shows the isotherm ate of commercial activated coal

Isothermate of commercial activated charcoal						
Isotherm models	Correlation Parameter					
Langmuir	Intercept 0.00289	Slope 0.01431	qmax(mg/g) 346.0207	AT 0.20195	RL 0.24698	R^2 0.93817
Freundlich	Intercept 1.95537	Slope 1.44764	1/n 1.44764	Kf 90.23395	R^2 0.92448	
Temkin	Intercept 84.51345	Slope 239.44749	Pt (j mol-1) 239.44749	CT (j mg-1) 0.35295	R^2 0.98687	

3.9 Isotherm Langmeier, Freundlich, Temkin Commercial Activated Coal

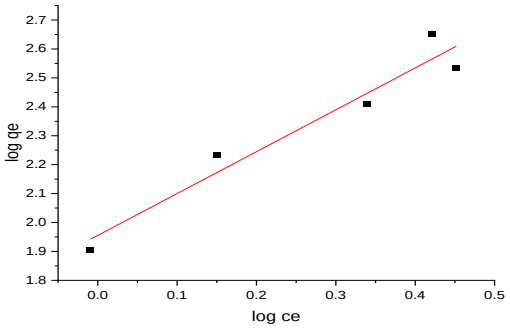

Figure (12) shows the Langmuir model

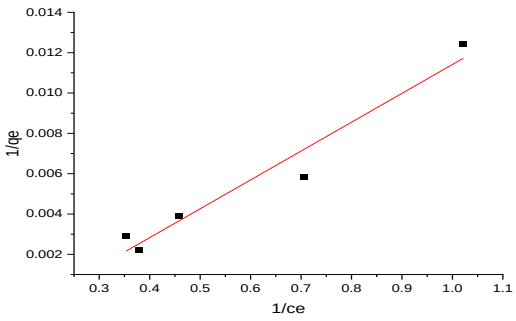

Figure (13) shows the Freundlich model

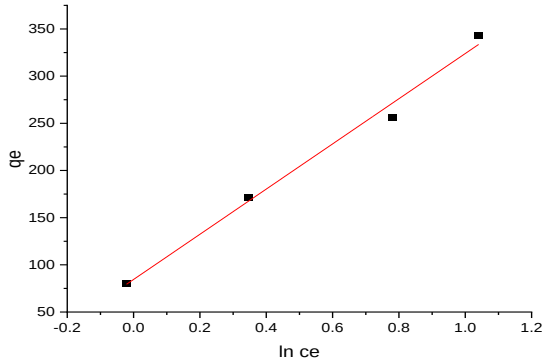

Figure (14) shows a model of Temkin isotherm

3.10 Thermodynamic functions of olive coal,

R^2 values of 0.97, 0.81, and 0.98 were found, respectively, when the Langmuir model was used to the adsorption of MB dye on the three forms of carbon (commercial activated charcoal, olive charcoal, and pine charcoal). The Temkin model was found to be most applicable to commercial activated charcoal and olive charcoal, but not to pine charcoal. The adsorption of MB dye on the three different forms of carbon (commercial activated charcoal, olive charcoal, and rosin charcoal) was found to have a correlation coefficient R^2 of 0.79, 0.68, and 0.92 for the Freundlich model. The results show that the Freundlich model is most applicable to commercial activated charcoal, while it is not suitable for olive charcoal or pine charcoal. The adsorption of methylene blue dye on the three different forms of carbon was also studied using the Temkin model; R^2 values of 0.97, 0.81, and 0.98 were found for commercial activated charcoal, olive charcoal, and pine charcoal, respectively. The results show that the Temkin model is most applicable to commercial activated charcoal and olive charcoal, but not to pine charcoal. The RL values obtained for the three types of carbon ranged from 0.07 to 0.24, indicating that the adsorption process is favorable. The RL values also suggest that the adsorption isotherm is not irreversible or linear but rather falls in the category of favorable or unfavorable, depending on the specific value of RL. (Junag et al., 1997; Aboushloa & Etorki., 2015). Overall, the Langmuir model was found to be applicable to all three types of carbon, while the Temkin and Freundlich models were most applicable to commercial activated charcoal and olive charcoal. The results suggest that the choice of adsorption model can depend on the specific type of carbon used and the properties of the dye being adsorbed.

3.11 Thermodynamic function of olive coal, commercial activated coal, pine coal.

Table (4) shows the thermodynamic functions of olive charcoal

Temperature	ΔG	ΔS	ΔH
298 K	- 12.6375KJ/mol	142.8124 J/molK	30.657649 KJ/mol
303 K	-12.6254KJ/mol		
313K	-13.0983KJ/mol		
323 K	-14.9518KJ/mol		
333 K	-17.6227KJ/mol		
343K	-18.5731KJ/mol		

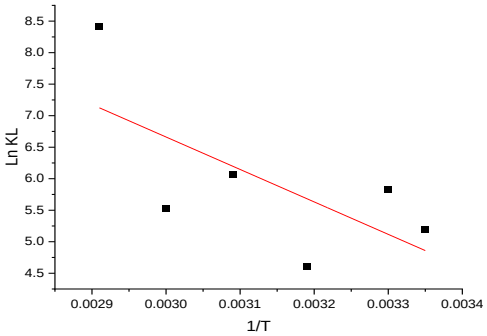

Figure (15) shows the thermodynamic functions of olive charcoal

Table (5) shows the thermodynamic functions of commercial activated coal

Temperature	ΔG	ΔS	ΔH
298 K	-11.3804KJ/mol	17.8261 J/mol.K	63.10450 KJ/mol
303 K	-12.3193KJ/mol		
313K	-11.9837KJ/mol		
323K	-11.0182KJ/mo1		
333 K	-12.4056KJ/mol		
343K	-12.8092KJ/mol		

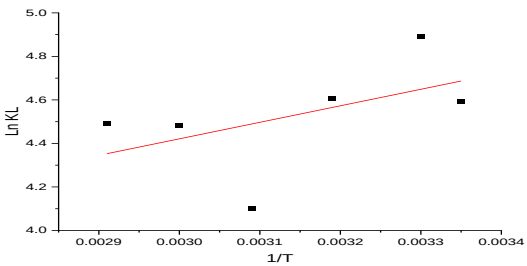

Figure (16) shows the thermodynamic functions of commercial activated coal.

Table (6) shows the thermodynamic functions of pine coal

Temperature	ΔG	ΔS	ΔH
298 K	-12.8719kJ/mol	183.8153 J/mol.K	42.810039 KJ/mol
303 K	-14.6896kJ/mol		
313K	-11.9907kJ/mol		
323K	-16.2900kJ/mol		
333K	-15.3231Jk/mol		
343K	-23.9816kJ/mol		

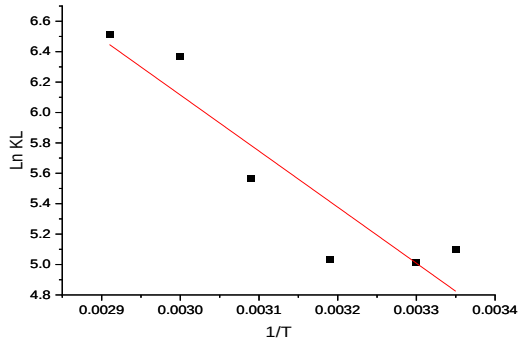

Figure (17) shows the thermodynamic functions of pine coal

The experimental results presented in Tables 4, 5, and 6 for the three types of carbon samples indicate that the adsorption of methylene blue decreases at lower temperatures and increases at higher temperatures. The negative values of ΔG suggest that the adsorption process is spontaneous (Aarfane et al., 2014). while the negative value of ΔS indicates a decrease in randomness at the solid-liquid interface. The positive value of ΔH indicates that the adsorption process is endothermic. The adsorption energy values for pine charcoal and commercial charcoal (> 40 KJ/mol) suggest that the adsorption is chemical in nature, while the adsorption energy value for olive charcoal (< 40 KJ/mol) suggests that the adsorption is physical in nature (Chawki, 2014).

4 Conclusion

Using various types of charcoal, including olive and pine activated charcoal, as well as commercially produced activated charcoal, the adsorption efficiency for removing Methylene Blue from industrial wastewater was evaluated. The results showed that all types of activated charcoal possessed high adsorption capacity for removing Methylene Blue from aqueous solution. This study provides support for the effectiveness of using activated charcoal in treating colored industrial wastewater contaminated with harmful organic substances. The results indicate that sustainable use of plant-based materials as adsorbents may be an effective alternative to relying on traditional activated charcoal. Based on these findings, further research in this field is recommended to enhance our understanding of adsorption processes and develop new, efficient methods for treating dye-contaminated water.

Additionally, industries generating colored industrial wastewater should adopt environmentally friendly practices and implement effective water treatment systems to mitigate pollution effects on the environment and human health. By investing in advanced environmental technology and embracing sustainability principles, a balance between industrial growth and environmental protection can be achieved.

Conflict of Interest: The authors declare that there are no conflicts of interest.

References

Aboshaloa, E., Asweisi, A., Almusrati, A., Almusrti, M., & Aljhane, H. (2022). *Asian Journal of Nanoscience and Materials*.

Aboushloa, E. M., & Etorki, A. M. (2015). Removal of synthetic dye acid red 186 from water by activated carbon. *British Journal of Environmental Sciences*, *3*(6), 54-64.

Alardhi, S. M., Alrubaye, J. M., & Albayati, T. M. (2020). Adsorption of Methyl Green dye onto MCM-41: equilibrium, kinetics and thermodynamic studies. *Desalin Water Treat*, *179*, 323-331.

Almeida, E. J. R., & Corso, C. R. (2014). Comparative study of toxicity of azo dye Procion Red MX-5B following biosorption and biodegradation treatments with the fungi Aspergillus niger and Aspergillus terreus. *Chemosphere*, *112*, 317-322.

Archna, L. K., & Siva, K. R. R. (2012). Biological methods of dye removal from textile effluents-A review. *J Biochem Tech*, *3*(5), 177.

Djelloul, C. (2014). *Expérimentation, modélisation et optimisation de l'adsorption des effluents textiles* (Doctoral dissertation, Faculté des sciences et de la technologie UMKBiskra).

Goudarzi, G., & Mahvi, A. H. (2021). Environmental Pollution Caused by Industrial Emissions: AGlobal Perspective. *Environmental Technology & Innovation*, 21, 101290.

Gyawali, M., & Techato, K. (2020). Solid Waste Management and Its Impact on the Environment: A Comprehensive Review. *Journal of Environmental Management*, 262, 110354.

Hahladakis, J. N., & Iacovidou, E. (2020). Soil Pollution: A Hidden Reality. *Environmental Science and Pollution Research*, 27(7), 6717- 6721.

Hassaan, M. A., & El Nemr, A. (2017). Advanced oxidation processes for textile wastewater treatment. *International Journal of Photochemistry and Photobiology*, *2*(3), 85-93.

Junag, R. S., Wu, F. C., Tseng, R. L. (1997) The Ability ofactivated clay for the Adsorption of Dye from Aqueous, *Environmental Technology*, 18, 525-531,.

Khettaf, S., Bouhidel, K. E., Meguellati, N. E. H., Ghodbane, N. E. H., & Bouhelassa, M. (2016). Integrated ion exchange mixed bed with reverse osmosis and nanofiltration for isolation of neutral dissolved organic matter from natural waters. *Water and environment journal*, *30*(3-4), 261-270.

Kim, K. H., Kabir, E., & Jahan, S. A. (2018). Airborne bioaerosols and their impact on human health. *Journal of Environmental sciences*, *67*, 23-35.

Kumar, P. S., Ramalingam, S., & Sathishkumar, K. (2011). Removal of methylene blue dye from aqueous solution by activated carbon prepared from cashew nut shell as a new low-cost adsorbent. *Korean Journal of chemical engineering*, *28*, 149-155.

Landrigan, P. J., Fuller, R., Acosta, N. J., Adeyi, O., Arnold, R., Baldé, A. B., ... & Zhong, M. (2018). The Lancet Commission on pollution and health. *The lancet*, *391*(10119), 462-512.

Li, D., Yan, J., Liu, Z., & Liu, Z. (2016). Adsorption kinetic studies for removal of methylene blue using activated carbon prepared from sugar beet pulp. *International Journal of Environmental Science and Technology*, *13*, 1815-1822.

Maghni, A., Ghelamallah, M., & Benghalem, A. (2017). Sorptive removal of methyl green from aqueous solutions using activated bentonite. *Acta Physica Polonica A*, *132*(3), 448-450.

Pathania, D., Sharma, S., & Singh, P. (2017). Removal of methylene blue by adsorption onto activated carbon developed from Ficus carica bast. *Arabian journal of chemistry*, *10*, S1445-S1451.

Prüss-Ustün, A., Wolf, J., Corvalán, C., Bos, R., & Neira, M. (2016). Preventing disease through healthy environments: a global assessment of the burden of disease from environmental risks. *World Health Organization*.

Rahman, M. A., Amin, S. R., & Alam, A. S. (2012). Removal of methylene blue from waste water using activated carbon prepared from rice husk. *Dhaka University Journal of Science*, *60*(2), 185-189.

Ramakrishna, K.R., Viraraghavan, T. (1997). Dye removal using low-cost adsorbents. *Water Sci. Technol. 36* (2–3) (1997) 189–196.

Sarwar, M. A., Shah, M. T., & Shaheen, N. (2020). Volatile Organic Compounds in the Atmosphere: Sources, Distribution, and Health Implications. *Environmental Geochemistry and Health*, *42*(10), 3027-3047.

Seow, T. W., & Lim, C. K. (2016). Removal of dye by adsorption: a review. *International Journal of Applied Engineering Research*, *11*(4), 2675-2679.

Verma, A. K., Dash, R. R., & Bhunia, P. (2012). A review on chemical coagulation/flocculation technologies for removal of colour from textile wastewaters. *Journal of environmental management*, *93*(1), 154-168.

Scientific Journal for the Faculty of Science-Sirte University Vol. 4, No. 1 (2024) 9-17

Scientific Journal for the Faculty of Science-Sirte University

Journal home page: http://journal.su.edu.ly/index.php/JSFSU/index

DOI: 10.37375/issn.2789-858X

Testing of Vertical Movements and Neotectonics by Using Alluvial Terraces: Study from Wadi Al Kuf, Al Watiyate Region, Al Jabal Al Akhdar, NE Libya

Farag M. El Oshebi, Fares F. Fares and Hamza I. Altweel

Earth Sciences Department, Science Faculty, Benghazi University, Benghazi, Libya.

DOI: https://doi.org/10.37375/sjfssu.v4i1.1805

ARTICLE INFO:

Received: 28 October 2023

Accepted: 18 January 2024

Published: 17 April 2024

Keywords: *Alluvial terraces, Neotectonic, Morphotectonic, Quaternary, Wadi Al Kuf, Al Jabal Al Akhdar, NE Libya.*

A B S T R A C T

Through different periods of the geological era, the Al Jabal Al Akhdar region has faced a number of tectonic events, which mainly had an effect on the geomorphic features of the earth's surface. One of the most notable wadis located in the Al Watiyate Region of Al Jabal Al Akhdar on the lower escarpment is Wadi Al Kuf. Alluvial terraces are dispersed throughout Wadi Al Kuf in various locations and regions. The study of terraces in Wadi Al Kuf revealed an obvious variation in altitude, with some being higher (~ 260 a.m.s.l.) while others abruptly dropped off (~ 145 a.m.s.l.) in levels like behavior, where a set of terraces and surfaces formed both underneath and above the mountain escarpment. Possibly, Wadi Al Kuf alluvial terraces have been assigned and understood as alluvial terraces subjected to neotectonics; in addition, they are supported by the results of one of these neotectonic eras since the alluvial terraces are clarified as non-natural and abnormally arranged. Wadi Al Kuf can be classified as a member of the morphotectonic valley in the Al Jabal Al Akhdar area due to terrace altitude fluctuations. Most previous scientific publications on alluvial terraces in Al Jabal Al Akhdar, for example, Wadi Zazah and Sidi Moussa, and studies carried out by students of the Department of Earth Sciences during graduation projects on Wadi Al Mahboul, Wadi Al Nagar, and Wadi Azzad, revealed that these wadis are still tectonically active. Unfortunately, due to Storm Daniel, which struck part of the mountain of Al Jabal Al Akhdar from Al Marj in the west to Dernah in the east, it removed a large part of the alluvial terraces from the wadis in that area. Geologically, this storm created conditions similar to the devastating debris flow.

1 Introduction

Terrace remains can be found along the banks of valley sides or on the floodplain next to the current river channel in rivers and wadis. However, they also find them in succession to form a staircase. They frequently find them as single terraces. Terraces may be caused by erosion, bedrock that has been planned to create a small-gradient layer that is frequently encased with a thin coating of gravel, or the topmost portion of aggradationsprior to downcutting the preceding flood plains' plane. The condition of the underneath level, or the bottom boundary of potential erosion by waterway incision, determines the gradient of the stream and valley (Selby, 1985; Anketell and Ghellali, 1991; Harvey *et al*., 2005; Robustelli *et al*., 2009; El Oshebi *et al*., 2017; Mather *et al*., 2017; El Oshebi *et al*., 2019). This is the sea's level, the last point. When the base level changes, the gradient of the river's single bed changes, as does the difference in altitude between the river's source and mouth. In order to reassemble older, lengthy river and wadi profiles, as well as to deduce earlier period variations at the underlying level, the

***Corresponding author*: E-mail: farag.issa@uob.edu.ly**

gradients of cut-off flood zones (terraces) can be used. Nevertheless, the development of stream-long profiles may also be influenced by other variables. For instance, because of the control over constrained base levels, gradients may vary across era terraces outside, due to limited variations in deposit delivery or water capacity, or due to variations in run-off basin patterns (Selby, 1985; Rudiger *et al*., 2016; El Oshebi *et al*., 2017; El Oshebi *et al*., 2019).

Terraces of streams and wadis can be found in many types of climatic and geomorphologic environments. Terraces also provide insight into the role of global alluvial and fluvial processes. The terraces could survive as paired or unpaired terrace fragments. If a stream's performance has changed significantly and relatively quickly, such as due to aggravation, paired terraces may appear on both wadi sides if there is an increase in the weight of the silt or if the stream scores into the valley floor. Nevertheless, the formation of a single-paired terrace and the attrition of floodplain deposits on the meander's outer edges result from the flow channel's sideways displacement where the stream starts to meander. Series of terraces. As a result, reveal alongside shifting of the floor and establish adjustments throughout an order of aggradational and downward cutting stages; this is a method that is usually referred to as fill and cut (Selby, 1985; El Oshebi *et al*., 2017; El Oshebi *et al*., 2019).

Because wadi and stream alluvial terraces are mostly constructed of sediment, they are easily damaged by later alluvial and fluvial acts. As a result, a previous floodplain plane is frequently identified as entity terrace fragments, which are just preserved characteristics. Tectonic uplift causes streams to regenerate, which leads to an increased gradient. It is possible to refurbish down wadi gradients of rigid terrace fragments using instrumental height of the fragments of terrace and inspection of the information using elevation-distance illustration (Butzer *et al.*, 1973; Burnett and Schumm, 1983; Selby, 1985; Ruzycki and Paredes, 1996; Colombo *et al.*, 2000; Robustelli *et al.*, 2009; Goswami *et al.*, 2009; Madadi *et al.*, 2016; El Oshebi *et al.*, 2017; Avsin *et al.*, 2019; El Oshebi *et al.*, 2019; Al Musawi *et al.*, 2020).

The evaluation of landform components and the recognition of landforms from various eras may both benefit from altitudinal information. In a strict region, for example, only pieces of past stream terraces can be preserved, making it difficult to categorize and correlate terrace parts from the same time period and to create a terrace chronology fragment extension solely according to field mapping (Hooke *et al.*, 1990; Rowan *et al.*, 2015; Rudiger *et al.*, 2016; Hooke and Oldknow, 2017).

The following goals are prepared for this work:

1) To restructure the terraces distributions in order to show the Quaternary vertical movements in the Wadi Al Kuf region.
2) To provide a timeline of terrace expansion according to field mapping to assist in identifying any neotectonic movement.

2 Tectonic Setting of the Al Jabal Al Akhdar

In northeastern Libya, the Al Jabal Al Akhdar mountain extends over 150,000 km^2. It is bordered to the west and south by the Gulf of Sirt, which is the offshore continuation of the Sirt Rift Complex. It can reach the Marmarica Platform of Egypt's Western Desert to the east. According to El Hawat and Abdulasmad (2004), Cyrenaica is made up of two major tectonic provinces that are divided by the Cyrenaican Fault System (Fig. 1). These are the Cyrenaica Platform to the south and the inverted basin of Cyrenaica in the north, known as Al Jabal Al Akhdar. The Marmarica, Solouq, and Ash-Sheliedima troughs, which are situated to the north of the platform, are two lengthy Tertiary depositional troughs that are found south of the inversion axis. These troughs are split by a raised structural burden that joins with Al Jabal Al Akhdar in the middle and are dipping in relation to their depocenters to the south-east and south-west, as well, along the Cyrenaica Fault System (El Hawat and Abdulasmad, 2004). Jaghboub High, which is to the south, is Cyrenaica Platform's southern extension. It is divided from Al Hameimat Trough, the eastern extension arm of Sirt Basin, by the south Cyrenaica Fault System (Anketell, 1996; El Hawat and Abdulasmad, 2004).

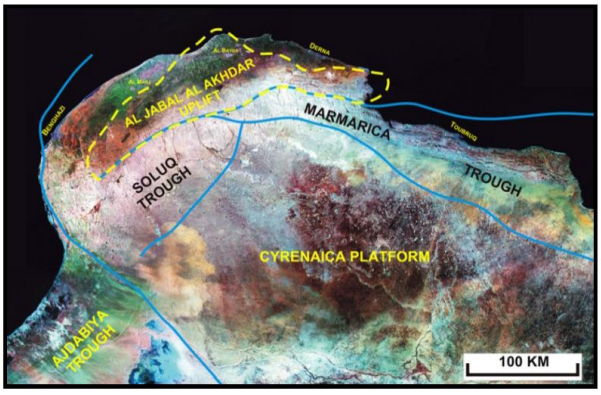

Figure (1) A satellite image illustrates the main tectonic regions of Cyrenaica (from: El Hawat and Abdulasmad, 2004).

The inversion anticlinorium of the Al Jabal Al Akhdar northern boundary is likewise faulted down north of the coast. It spreads out into the sea to the north, forming a

curvy and abrupt continental coastline. An extended, narrow, and deep fault separates the Cyrenaican continental slope from the Mediterranean Ridge (El Hawat and Abdulasmad, 2004). The north Cyrenaica fault system, which extends offshore and parallel to the coast of Cyrenaica, is thought to be the source of this rift (Huguen and Mascle, 2001; El Hawat and Abdulasmad, 2004). A topographical, geological, and geophysical oddity on the coast of northeastern Africa is the Cyrenaican promontory. Identifying Upper Cretaceous inliers at the axis of the anticlinorium's inversion structures is confirmed by the northern Al Jabal Al Akhdar cross-sections and geological map, which also confirm the basin's inversion formations, which were previously sinking (Fig. 2). These structural inliers are located in Al Jabal Al Akhdar's highest topographic regions (El Arnauti and Shelmani, 1985; El Hawat and Shelmani, 1993; El Hawat and Abdulasmad, 2004; Arsenikos *et al.*, 2013).

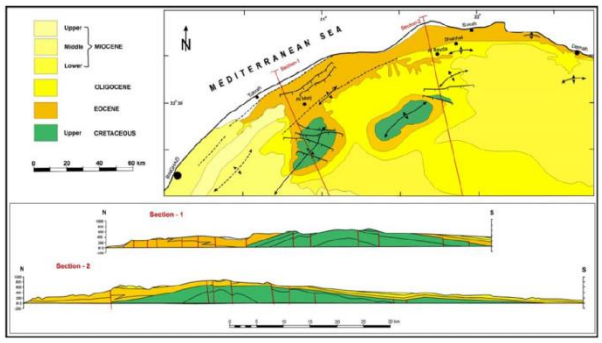

Figure (2) Shows northern Cyrenaica's geologic map and cross sections (from: El Hawat and Shelmani, 1993).

According to El Hawat and Abdulasmad (2004), The North Cyrenaica Basin's inversion during the Upper Cretaceous was primarily caused by compressive forces resulting from the convergence of the African-European and Aegean plates. The stratigraphic record in the northern part of Cyrenaica also reflects this. Since the upper Cretaceous period to the present, there is evidence of recurrent compressive events in the form of unconformities, post-depositional deformation structures, and mass movement of sediments during syndeposition (El Hawat and Abdulasmad, 2004). Surface outcrops from the Cretaceous, Eocene, and Oligocene are frequently found to include large slump structures, slides, and debris flows (El Hawat and Abdulasmad, 2004).

The historical earthquake that has occurred repeatedly devastation of the archaic town of Cyrene, presently known as Shahhat between 262 and 365 A.D., the submersion of the entire harbor complex of the ancient Apollonia, which at least two meters below sea level at this time, and the catastrophic earthquake that occurred more recently that demolished the modern Al Marj city in 1963 serve as evidence of current tectonic activities that have taken place in the Cyrenaica basin. From the inversion of the Upper Cretaceous to the present, Cyrenaica has continued to experience tectonic activity (El Hawat and Abdulasmad, 2004; Arsenikos *et al*., 2013; El Oshebi *et al.*, 2017; El Oshebi *et al*., 2019). In natural conditions, the alluvial terraces are deposited in the middle and bottom streams and are distributed gradually in height from the bottom stream to the top stream. In fact, this happens in the absence of tectonic activity and without fluctuations in alluvial terrace altitudes. In this case, the alluvial terraces were not subjected to any neotectonic movements. However, previous publications about alluvial terraces in the Wadi Zazah region by El Oshebi *et al.* (2017) and the Wadi Sidi Moussa region by El Oshebi *et al.* (2019) and the studies that were carried out by students of the Department of Earth Sciences at the University of Benghazi during their graduation projects For instance, Farag El Oshebi (2007) on the Wadi Al Mahboul region, Bakkar Al Awami (2018) on the Wadi Azzad region, Nasser El Traichi (2020) on the Wadi Al Nagar region, and Abdulmajeed Al Aqibi (2023) on the Wadi Al Jubiyah region in the Al Jabal Al Akhdar region revealed that the alluvial terraces were affected by tectonic movements during the Pleistocene era, and Al Jabal Al Akhdar is still tectonically active. On September 10, 2023, most of the alluvial terraces that were deposited in the Wadis Channel in the area from Al Marj to Dernah were removed due to Storm Daniel. From a geological perspective, this storm provided conditions very similar to the devastating debris flow.

3 Cyclical Terraces Classification

The environment and origin of the earlier floodplain that it characterizes determine the type of cyclical stream terrace built up, specifically depending on whether the terrace plane was sculpted by river deposition, erosion, or a mix of the two. Understanding the chain leading to the terrace requires an accurate classification of the type of cyclic river terrace. Each type of terrace has a geomorphic history that is very distinct from all others, as can be observed in the following description of terrace types (Easterbrook, 1993; El Oshebi *et al*., 2017; El Oshebi *et al.*, 2019).

3.1 Cut in bedrock terraces

Floodplains created by graded rivers cutting through competing rock types are covered in an alluvial layer that is not thicker than the depth of the river's direction. As a result, the terraces contain rock that is faintly veneered among alluvium when the river channel's altered score maintains them as remaining above the active channel (Figs. 3a and 4b). The geomorphic history of these terraces is the easiest to understand of all the terrace types. They are often referred to as cut-in-bedrock terraces (El Oshebi *et al*., 2017).

3.2 Fill terraces

The pieces of past valley floors that have been mixed together to form terraces Alluvium is first added to gorges during aggradation, then a number of stream channels are added to the fill, leaving terraces completely covered with alluvium. Contrary to the cut in bedrock, that has an erosion base in this instance, the terrace plane has a depositional basis. Fill terraces may resemble cut terraces in surface shape and might have comparable gradients, but they're not the same noticeably throughout their history of geomorphology. A cut terrace entails a time of precise flood plain development followed by channel scoring (Figs. 3b and 4a). A fill terrace, on the other hand, entails down cutting, followed by aggradation of filling the wadi, and lastly repaired down cutting to exit the fill plane across the ferocious channel. Therefore, it is essential to distinguish between different types of terraces in order to properly interpret their geomorphic record (El Oshebi *et al*., 2017).

3.3 Cut-in fill terraces

Cut in fill terraces are a combination of previous valley bottoms with alluvium scores and canal incisions. They contrast with fill terraces as their surface has an erosional basis, while the bases of fill terraces are depositional. (Figs. 3c and 4c) describe the distinction. A valley is initially leveled (a), then a gorge is filled and raised (b). The floodplain, built like a cut-in fill terrace, is extended out after the canyon fill, followed by a change in score to level (c) and level (d), departing the gorge. Since the terrace top at (c) is erosion, it differs from a cut-in-bedrock terrace in that it is comparatively carved in alluvium rather than bedrock. Due to the fact that the base of the highest terrace's plane was a deposit, it is important to note that level (b) is a fill terrace (El Oshebi *et al.,* 2017).

3.4 Nested fill terraces

Fill terraces that are nested together are inset and encircled adjacent to each other (Figs. 3d and 4d). They are classified by periods of channel score, but they have a depositional base. For example, as shown in Fig. 3d, the flow is first filled at level (b), then level (a), level (b), level (c), level (d), and finally level (d) is reached by downward cutting to level (c). A weighty back-up towards level (d) is followed by more down-cuts to level (e). As a result, the succession of terraces might resemble its cut-in-fill terraces (Fig. 3c); however, in this case, the entire plane is depositional as opposed to erosion in the base, and the historical geomorphology is notably more intricate (El Oshebi *et al.,* 2017).

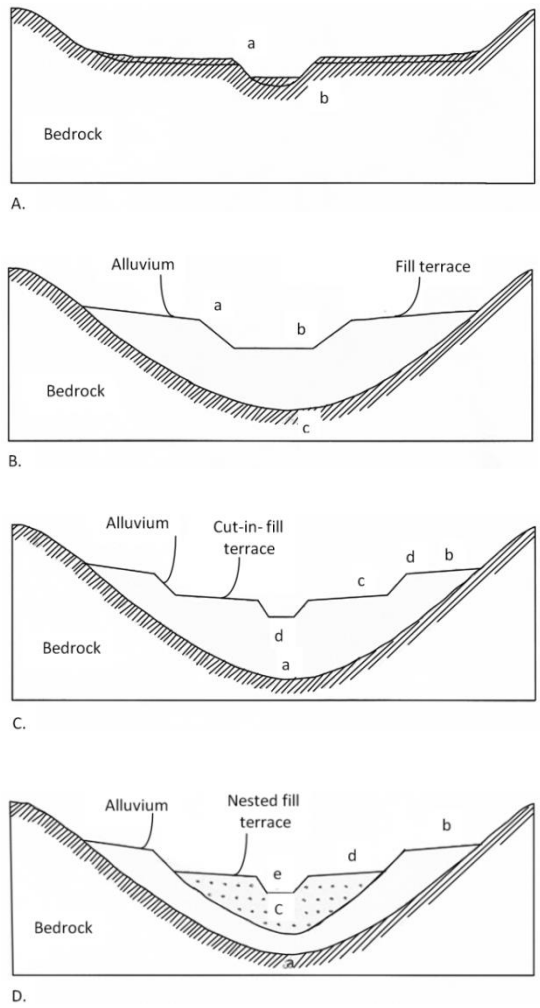

Figure (3) Shows the several kinds of alluvial terraces: (a) bedrock (cut) terrace, (b) fill terrace, (c) cut in fill terrace, and (d) nested fill terrace (from: El Oshebi *et al.*, 2017).

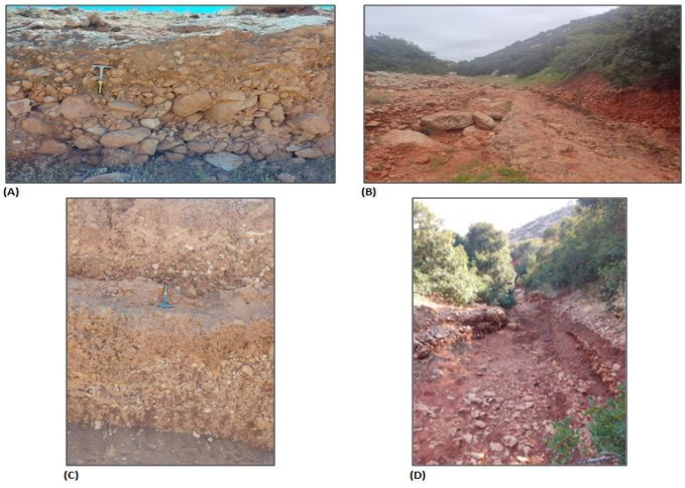

Figure (4) Shows types of alluvial terraces in the Wadi Al Kuf region: (a) fill terrace, (b) bedrock (cut) terrace,(c) cut in fill terrace, and (d) nested fill terrace.

4 Methologies and Materials

The main goal of this work is to compare the directional and altitudinal data of the various alluvial terraces in order to try and rebuild the Quaternary vertical phenomena in the Wadi Al Kuf region. Identification of certain gradient fundamentals in the earth's surface and the behavior of their junction are key considerations for the geomorphological mapping method (Waters, 1958; Savigeor, 1965; Crofts, 1981). In order to ascertain the exact elevation or altitude and change in elevation across distinct landforms, tool leveling, such as using clinometers, Abney levels, or altimeters, is needed. More recently, this has also included using the Global Positioning System (GPS). Fieldwork was done primarily to gather directional and altitudinal data for the group of terrace fragments seen in the Wadi Al Kuf district (elevations were obtained using a GPS gadget called an Etrex device). Throughout the wadi, from the lower to the upper stream, terrace remnants were found at 26 different locations (called measuring stations) (Fig. 5). However, formerly consistent characteristics can be rearranged, gradients identified, and terrace temporal correlations examined by obtaining exact elevation measurements on each terrace fragment (Lowe & Walker, 1984). Additionally, 97 reading joints were measured using a Brunton compass in the Wadi Al Kuf region within the rock-exposed units, including Al Bayda Formation, Al Abraq Formation, Al Faidiyah Formation, Benghazi Formation, and Wadi Al Qattarah Formation (see measured stratigraphic log) (Fig. 6).

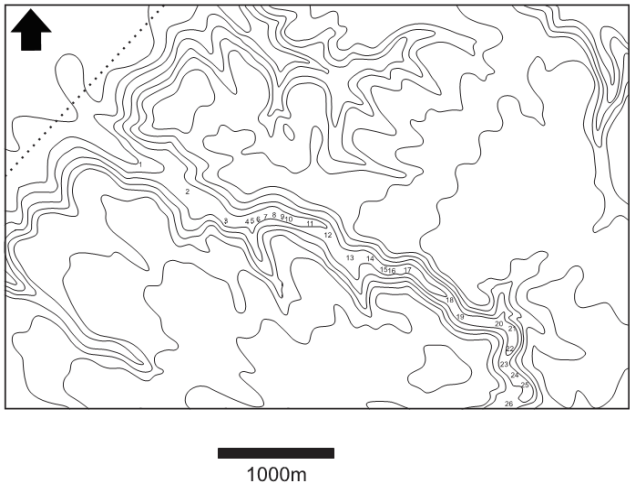

Figure (5) Topographic map of the Wadi Al Kuf region, viewing the locality of stations for determining the direction and elevation of the terrace.

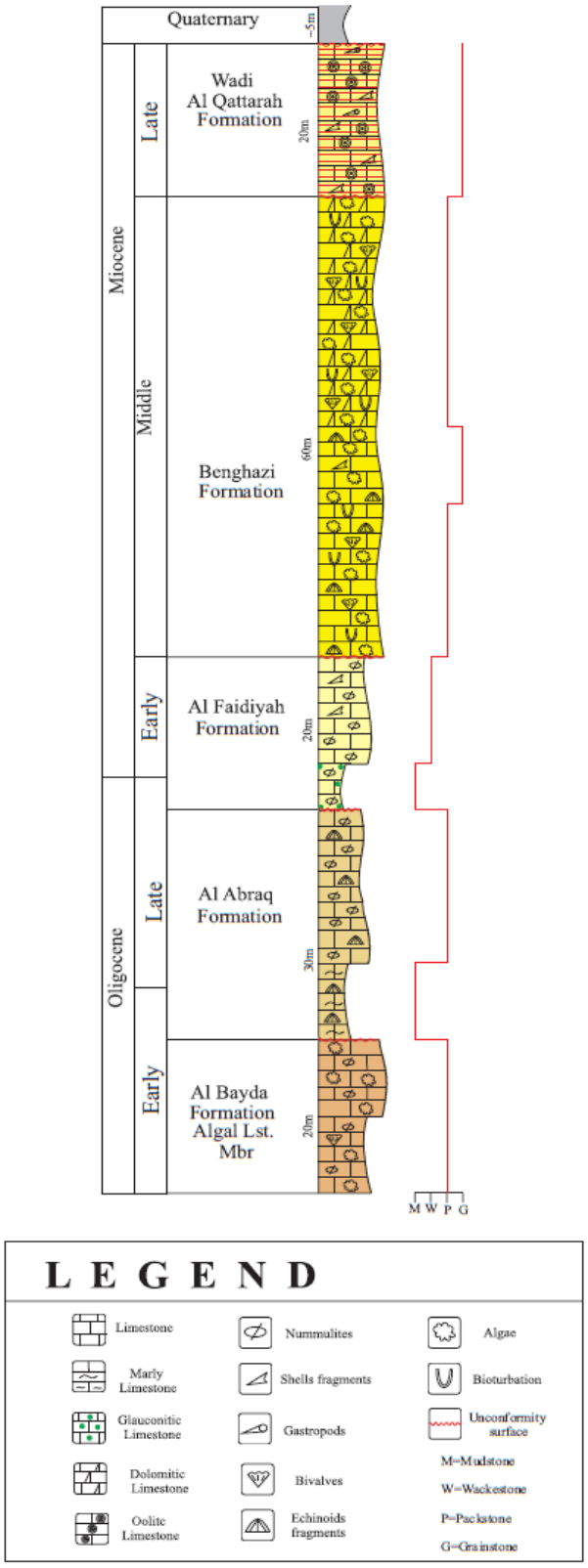

Figure (6) Stratigraphic log showing the exposed rock units in the Wadi Al Kuf area.

5 Location of the Study Area

One of the biggest valleys in the Al Watiyate region of Al Jabal Al Akhdar, northeast Libya, is represented by Wadi Al Kuf (Fig. 7). The study area covers a total area of approximately 15 km^2 and is almost 5 km long in the east-west direction and almost 3 km wide in the north-south direction. It is located nearly 45 kilometers east of Benghazi town and about 10 kilometers south of the Tansulukh area. The research area is a small portion of the initial escarpment of Al Jabal Al Akhdar, which is reached after over 22 kilometers and passes through the Benghazi plain on its way to the Tansulukh checkpoint.

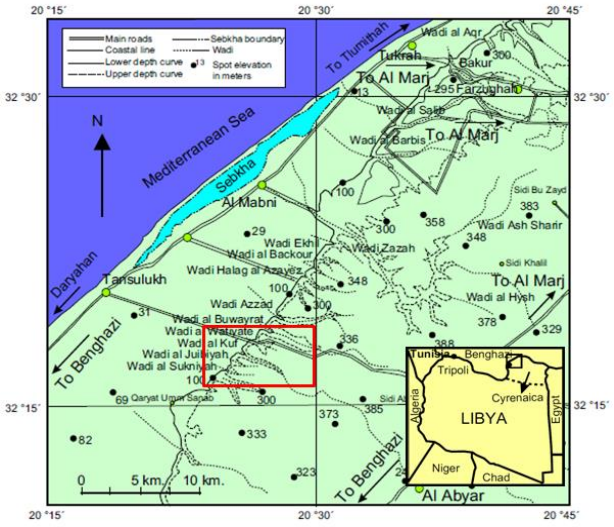

Figure (7) Topographic map of the northwest portion of Al Jabal Al Akhdar seeing the red-highlighted targeted area (modified from: Abdulsamad *et al*., 2009).

6 Interpretation of Results

The relationship between every terrace fragment observed in the remnants of the Wadi Al Kuf region is hypothetical. This is due to the fact that, aside from the directional and altitudinal data, there are insufficient morphostratigraphic verifications. However, the long profile diagram created (Fig. 8) can provide some hints regarding the region's Quaternary and more recent tectonic events.

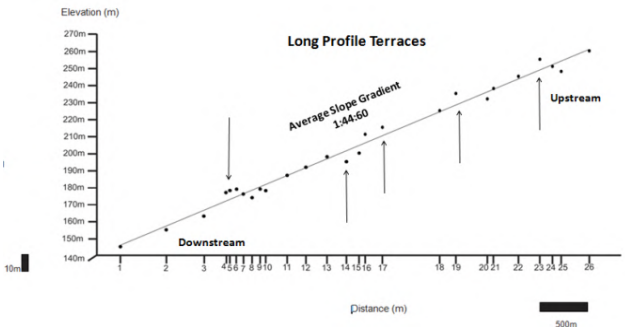

Figure (8) Reconstructed terrace parts' long valley profile was measured in at Wadi Al Kuf region.

The lowest point of the terrace fragment is observed at 145 meters above mean sea level, near the downstream end of Wadi Al Kuf. On the other hand, 260 meters above mean sea level is where the highest terrace fragment is located. A typical slope gradient of 1:44.60 is reached by this offer climb. Additionally, the terrace fragments are observed at significantly higher altitudes along the wadi's long profile in numerous locations; these are anomalous to the typical grade gradient (areas 1–5, Figs. 5 & 8). The most suitable explanation for this condition, given the information, is that the land and the alluvial terraces were raised after they were formed. The marine terraces of Pleistocene times, which are detected at several locations within Al Jabal Al Akhdar mountain, were also produced by the Quaternary tectonic uplift of the region (Desio, 1935; Hey, 1956; El Oshebi *et al.*, 2017; El Oshebi *et al.*, 2019). Additional point in Wadi Al Kuf region is that it has changed its path suddenly everywhere, therefore the alluvial terraces are also oriented differently (Fig. 9) (Tab. 1). Furthermore, as can be seen in (Fig. 10) (Tab. 2), A significant trend can be seen in the terrace fragments' directional data around N80°W that disagrees with the main joint trend identified (N20°E) in the various exposed rock units at Wadi Al Kuf region. The difference of the tectonic periods may be the cause of this heterogeneity between the joints and terrace fragments. Furthermore, it lends credence to the theory that the Wadi Al Kuf region has seen recent tectonic uplifts.

Table (1) The frequency and frequency percentage distribution of the direction of terrace fragments in the Wadi Al Kuf region.

Class interval	NE-SW		NW-SE	
	Frequency	Frequency%	Frequency	Frequency%
0-10	-	-	1	3.84
11-20	1	3.84	2	7.69
21-30	1	3.84	1	3.84
31-40	1	3.84	2	7.69
41-50	1	3.84	3	11.53
51-60	-	-	2	7.69
61-70	-	-	4	15.38
71-80	3	11.53	3	11.53
81-90	-	-	1	3.84

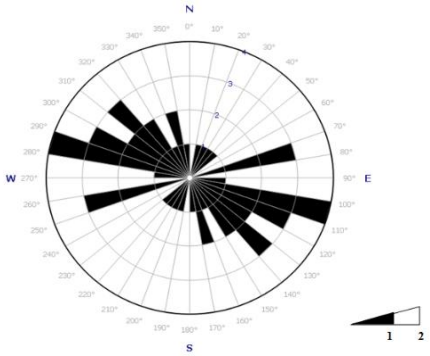

Figure (9) A rose diagram that shows the orientation of 26 terrace fragments in the Wadi Al Kuf region.

Table (2) The direction of joints' frequency and frequency % distribution in the Wadi Al Kuf region.

Class interval	NE-SW		NW-SE	
	Frequency	Frequency%	Frequency	Frequency%
0-10	10	10.3	3	3.09
11-20	14	14.4	2	2.06
21-30	12	12.37	3	3.09
31-40	12	12.37	2	2.06
41-50	10	10.3	2	2.06
51-60	11	11.34	2	2.06
61-70	4	4.12	3	3.09
71-80	4	4.12	1	1.03
81-90	1	1.03	1	1.03

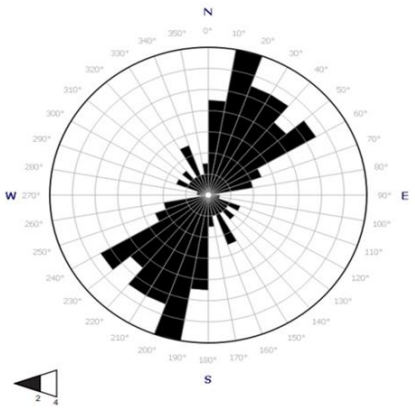

Figure (10) A rose diagram showing the orientation of the 97 joints that were measured in the Wadi Al Kuf region.

7 Discussion

The primary goal of this research was to address issues that are crucial to the construction and development of the Wadi Al Kuf alluvial terraces. In order to provide a thorough and acceptable understanding of the focus region and its terraces, the process of working terraces was traced or pursued down the wadi, calculating terrace altitude and direction. As a result, the elevation at the downstream terraces started at 145 meters above mean sea level and reached roughly 260 meters upstream. Even while moving upstream, they varied at different points. As a result, it is obvious that this method is unusual and has given this study its unique significance and value.

The long profile image shows the relationship between the two parameters by plotting the terraces of Wadi Al Kuf juxtaposed against the horizon. The full set of corresponding locations on the cross-section diagram illustrates the variety from the wadi's lowest height to its highest position, where the terrace heights are described as having a meandering stripe curve. It is possible to divide the section into five loops that go proceed upstream. These cycles or loops indicate expanding or gradation differences, with the differences themselves being additional apparent At the center of the row. Occasionally, terraces head up and become increasingly related, while in other cases, they change.

Based on recently collected data, this study revealed that the Wadi Al Kuf region is still tectonically active. This is because the terraces were deposited during the Quaternary, and their elevation fluctuates from downstream to upstream. Therefore, any variations in the elevation of terraces are not indicative of ancient tectonic possibilities but rather of more recent tectonic movements. Furthermore, the northern part of the Cyrenaica coastal margin exhibits successively far above the ground terraces eroded by waves, featuring Pleistocene calcarenite dunes at the beach left behind in places reaching 150 m above the present sea level, according to El Hawat and Abdulasmad (2004), El Oshebi *et al.* (2017), and El Oshebi *et al.* (2019). The relative Pleistocene eustatic sea level shift was not the main reason for the elevation of these terraces.

8 Conclusion

The key conclusions derived from this study based on the measured terrace fragment altitudinal and directional measurements in the Wadi Al Kuf region are as follows:

1. The Wadi Al Kuf region is distinguished by a morphotectonic valley that was created by tectonic (structural) and geomorphic processes working together.
2. The Wadi Al Kuf region has seen both Quaternary and recent tectonic uplift (neotectonic).
3. Al Jabal Al Akhdar as a whole exhibits tectonic activity and moves like a mobile zone.

Acknowledgements

Special thanks to Prof. Hwaidi Errishi from the Department of Geography at the University of Benghazi for his constructive criticism and recommendations that helped the text. We thank AbdulMajeed Al Aqibi from the Department of Earth Sciences, University of Benghazi, for field assistance for this study.

Conflict of Interest: The authors declare that there are no conflicts of interest.

References

Abdulsamad, E.O., Bu-Argoub, F.M. and Tmalla, A.F.A. (2009) A stratigraphic review of the Eocene to Miocene rock units in the al Jabal al Akhdar, NE Libya. *Marine and petroleum geology*, 26:1228-1239.

Al Musawi, H.A., Abdallah, H.H., and Azzawi, T.M. (2020) Neotectonic activity of segmented alluvial fans alonghemr in south anticline east Iraq. *Iraqi Journal of Science*, 61:2266-2276.

Avsin, N., Vandenberghe, J., Balen, R.V., Kiyak, N.N., and Ozturk, T. (2019) Tectonic and climatic controls on Quaternary fluvial processes and river terrace formation in a Mediterranean setting, the Göksu River, southern Turkey. *Cambridge University press*, 91:533-547.

Anketell, J.M. (1996) Structural history of Sirt basin and its relationship to the Sabratah basin and Cyrenaica platform, northern Libya. In: Geology of Sirt Basin, M.J.Salem, M.T. Busrewil, A.A. Misallati and M.A. Sola (eds.). *Elsevier*, Amsterdam, 3: 57-89.

Anketell, J.M. and Ghellali, S.M. (1991) Quaternary fluvio-aeolian sand/silt and alluvial gravel deposits of northern Libya-event stratigraphy and correlation. *Journal of African Sciences and the Middle East*, 13: 457-469.

Al Aqibi, A. (2023) Geological mapping of the area between Wadi Al Kuf and Wadi Al Jubiyah (sector 1), Deryanah-Al Abyer area, Al Jabal Al Akhdar, NE Libya. Unpublished BSc thesis, University of Benghazi, Benghazi.

Arsenikos, S., de Lamotte, D.F., Rooke, N.C., Mohn, G., Bonneau, M.C and Blanpied C. (2013) Mechanism and timing of tectonic inversion in Cyrenaica (Libya): Integration in the geodynamics of the East Mediterranean. *Tectonophysics*, 608:319-329.

Alwami, B. (2018) Geological mapping of Wadi Azzad area (sector 4), Al Jabal Al Akhdar, NE Libya. Unpublished BSc thesis, University of Benghazi, Benghazi.

Butzer, K.W., Helgren, D.M., Fock, G.J., and Stuckenrath, R. (1973) Alluvial terraces of the lower vaal river, south africa: a reapprusal and reinvestigation. *Journal of Geology*, 81:341-362.

Burnett, A.W., and Schumm, S.A. (1983) Alluvial-River Response to Neotectonic Deformation in Louisiana and Mississippi. *Science*, 222:49-50.

Colombo, F., Busquets, P., Ramos, P., Verges, J., Ragona, D. (2000) Quaternary alluvial terracesin an active tectonic region: the san juan province, argentina. *Journal of South American Earth Sciences*, 13:611-626.

Crofts, R.S. (1981) Mapping techniques in geomorphology, in A.S Goudie (ed), geomorphological techniques. *Allen and Unwin, London and Boston*, 66-75.

Desio, A. (1935) Studig eologicisulla Cirenaica, sul Deserto Libico, sulla Tripolitania e sul Fezzan Oriental. MissioneSecintificadella R. Accd. d'Italia a Cufra (1931), Vol. 1, 480P., 60 fig., 6 Pl., 1 carta geol. scala 1:2,500,000, Roma.

Easterbrook, D.J. (1993) Surface processes and land forms. *Macmillan publishing company*. Newyork, 520 PP.

El Hawat, A.S. and Abdulsamad, E.O. (2004) A field guide to the geology and archaeology of Cyrenaica. In: L. Guerrier, I Rischia and L Serva (eds.). 32nd International Geological Congress, Special Public. Guidebooks & CD-Rom. APAT-It. Agen. Envir. Protct. Tech. Serv. Roma, Vol. 1, PR01-B15, B01, p.1-32.

El Hawat, A.S., and Shelmani, M. A. (1993) Short notes and guide book on the geology of Al Jabal Al Akhdar, Cyrenaica, NE Libya, 70 pp.

El Oshebi, F.M., Badi, A.M., Shaltami, O.S. and Fares, F.F. (2017) Alluvial terraces as a measure of vertical movements and neotectonics: evidences from Wadi Zazah, Al Jabal Al Akhdar, NE Libya. *Journal of Science and Technology*, 6:1 (19-24).

EL Oshebi, F.M., Shaltami, O.R. and Fares, F.F. Al Barghathi1, J.A., El Ogali1, M., Errishi, H., Badi, A.M. (2019) Alluvial terraces as a measure of vertical movements and neotectonics: evidences from Wadi Sidi Moussa, Cyrenaica, NE Libya. *EPH - International Journal of Applied Science*, 1(1): 201-217.

El Oshebi, F.M. (2007) Geology of the area between Wadi Al Mahboul and Wadi Hussein, Ras Al Hilal, Al Jabal Al Akhdar, NE Libya. Unpublished BSc thesis, University of Garyounis, Benghazi.

El Tracichi, N. (2020) Geological investigation of the area between Wadi Kum Al Baghul and Wadi Ehshsis, (sector 3), Tulmithah area, Al Jabal Al Akhdar, NE Libya. Unpublished BSc thesis, University of Benghazi, Benghazi.

Goswami, P.K., Pant, C.C., and Pandey, S. (2009) Tectonic controls on the geomorphic evolution of alluvial fans in the piedmont, zone of ganga plain, utarakhand, india. *Journal of Earth System Society*, 3:245-259.

Harvey, A.M., Mather, A.E., and Stokes, M. (2005) Alluvial fans: geomorphology, sedimentology, dynamics – introduction. A review of alluvial fan research. *Geological Society*, 251:1-7.

Hey, R.W. (1956) The Pleistocene shoreline of Cyrenaica. *Quaternaria Ital.*, 3:139-144, Roma.

Hooke, J.M., Harvey, A.M., Miller, S.Y., and Redmond, C.E. (1990) The chronology and stratigraphy of the alluvial terraces of the river Dane Valley, Cheshire, N.W. England. *Willey*, 15:717-737.

Hooke, J.M., Oldknow, C.J. (2017) Alluvial terraces development and changing landscape connectivity in the great karoo, south Africa. Insights from the wilgerbosch river catchment, sneeuberg. *Geomorphology*, 288:12-38.

Huguen C., and Mascle, J. (2001) La Margie continentalelibyenne, entre 23º30 et 25º30 de longitude est. C.R. Acad. Sci. Paris. *Earth and Planetary Sciences*, 332, p. 553-560.

Jingchun, Y., Lihua, T., Youli, L., and Fengjun, D. (1998) River terraces and neotectonic evolution margin of the qilianshanmountains. *Quaternary Sciences*, 18(3):229-237.

Lowe J.J. and Walker M.J.C. (1984) Reconstructing Quaternary Environments, *ISBN* 0-582- 30070-3.

Mather, A.E., Stokes, M., and Whitfield, E. (2017) River terraces and alluvial fans: the case for an integrated quaternary fluvial archive. *Quaternary Science Reviews*, 166:74-90.

Madadi, A., Mokhtari, D., Shirzadi, H., and Mehrvarz, A. (2016) Neotectonic performance review on alluvial fans, with emphasis on seismic of power fault (case study:northwest slopes of sahand mountain). *Geography and Environmental Hazards*, 18:11-13.

Rowan, J.S., Black, S., Macklin, M.G., Tabner, B.J. and Dore, J. (2015) Quaternary environmental change in Cyrenaica evidenced by U-Th, ESR and OSL dating of coastal alluvial fan sequences. *Cambridge University Press*, 31:5-6.

Robustelli, G., Luca, F., Corbi, F., Pelle, T., Dramis, F., Fubelli, G., Scarciglia, F., Muto, F., and Cugliari, D.

(2009) Alluvial terraces on the lonian coast of northern Calabria, southern italy: implications for tectonic and sea level controls. *Geomorphology*, 106:165-179.

Ruzycki, L., and Paredes, J. (1996) Active tectonic control on alluvial and fluvial deposits of san juan river. Sanjuan, argentina. *ThirdISAG*, 17:733-736.

Rudiger, Z.R., Braucher, R., Novothny, A., Csillag, G., Fodor, L., Molnar, G., Madarasz, B., and Team, A. (2016) Tectonic and climatic control on terrace formation: Coupling in situ produced 10 Be depth profiles and luminescence approach, Danube River, Hungary, Central Europe. *Quaternary Science Reviews*, 131:127-147.

Selby, M.J. (1985) Earth's changing surface. *Clarendonpress*. Oxford.

Savigear, R.A.G. (1965) A technique of morphological mapping. *Ann. Assoc. geogr*., 55: 514-539.

Waters, R.S. (1958) Morphological Mapping. *Geography*, 43: 10-17.

Scientific Journal for the Faculty of Science-Sirte University Vol. 4, No. 1 (2024) 18-29

Scientific Journal for the Faculty of Science-Sirte University

Journal home page: http://journal.su.edu.ly/index.php/JSFSU/index

DOI: 10.37375/issn.2789-858X

Classifying the 1st Year Academic Performance of Nursing Students at Tobruk University via Data Mining with SQL and WEKA Tool

James Neil B. Mendoza, Dorothy G. Buhat-Mendoza

Nursing College, Tobruk University, Libya.

DOI: https://doi.org/10.37375/sjfssu.v4i1.2581

ARTICLE INFO:

Received: 17 January 2024

Accepted: 14 March 2024

Published: 17 April 2024

Keywords: *Classification, Data Mining, Extraction, Preprocess, SQL, WEKA*

A B S T R A C T

Data mining is a tool that can identify hidden patterns affecting academic success. The objective of this research is to investigate and classify the academic performance of first-year nursing students at Tobruk University. This study concentrates on the preliminary stage of data preprocessing and data mining classification. The methodology to classify academic performance includes data acquisition and preprocessing stage using SQL commands to extract student data from the university database and undergo basic cleaning and transformation. Initial classification and data analysis followed using the preprocessed data, further refined by the WEKA data mining tool algorithms including BayesNet, NaiveBayes, JRIP, and J48. Results of the preliminary data distribution and initial classification show that J48 is the most accurate model creator using regular classification (88.6619) and attribute selector (97.8261). Relative to the other three algorithms, J48 also recorded the highest precision, recall, F1 measure, and the lowest error measurement. The recorded Kapa stat of J48 (0.7779 and 0.9599) also proves the significance of the classification result, interpreted as substantial to near-perfect reliability scores respectively, which BayesNet and JRIP also attained. The results reveal that Finals (final exam result) attribute is the biggest factor in determining the descriptive Rating of a student's grade at the university. The created model can serve as a classifier for future test sets and may provide a foundation for further research and model development. Further modification will help discover what factors contribute to student success and what applicable interventions are needed to improve the academic achievement of students in the nursing program.

1 Introduction

Predicting and understanding student academic performance is crucial for educational institutions to improve learning outcomes and student success (Alyahyan & Düştegör, 2020; Cui et al. 2019). In the field of nursing education, ensuring strong academic foundations in the first year sets the stage for future clinical skills development and professional competence. This research focuses on applying data mining techniques to the academic performance (Nahar et al. 2021) of first-year nursing students at Tobruk University. Utilizing a mixed-methods approach, it combines SQL queries for data extraction and transformation (Kumar & Krishnaiah, 2012; Ordonez et al. 2014) with the WEKA data-mining tool for analysis and classification (Han et al. 2006). This paper presents the initial phases of the research, encompassing the preliminary data preprocessing stage (Garcia et al. 2016) and initial classification attempts (Espinosa et al. 2011).

The transition to nursing education marks a pivotal juncture, where aspiring healthcare professionals

Corresponding author: E-mail: james.mendoza@tu.edu.ly

embark on a challenging yet rewarding journey. While academic success paves the way for future competence and patient care (Keshavarzi, 2022), understanding the factors influencing student performance remains crucial for optimizing educational strategies and fostering excellence (Bressane et al. 2023). This study delves into the intricate landscape of academic performance among first-year nursing students at Tobruk University, employing data mining techniques to uncover hidden patterns and predictive insights (Namoun & Alshanqiti, 2020; Villarica, 2020). As such, large data sets can be processed and valuable information can be extracted from simple data using data mining (Feng & Fan, 2024).

Traditionally, student performance assessment relies on summative measures like grade point average (GPA) (Schwab et al. 2018). While these provide valuable snapshots, they often fail to capture the nuanced interplay of factors contributing to academic success (Zughoul et al. 2018). Data mining, with its ability to identify hidden patterns and relationships within large datasets (Roostaee & Meidanshahi, 2023), offers a powerful lens to delve deeper into this intricate landscape (Schwab, 2018). This study leverages the strengths of data mining to explore the complex interplay of academic, demographic, and other possible variables influencing first-year nursing students' performance (Goundar et al. 2022) at Tobruk University.

The first academic year (AY) is considered an important phase of the laying foundation for future success and this investigation concentrates on it. Two powerful tools: SQL for effective data extraction and processing (Mori et al. 2015), and WEKA for powerful data mining algorithms and classification tasks (Aher et al. 2011; Kabakchieva, 2013) will be utilized. This study does not stop at just identifying factors that influence performance. It was desired to use the information gained through data mining for developing focused interventions and educational measures (Barakeh et al., 2024). Through early identification of students likely to have trouble succeeding, the provision of individualized attention and direction, encouragement of their natural ability, and establishment of a solid base for their nursing endeavors. Furthermore, the outcomes of demographic variables can guide initiatives targeted at fostering equity and diversity in Tobruk University's nursing program.

The primary objective of the study is to investigate the academic performance of first-year nursing students at Tobruk University by applying data mining techniques. This data mining study may shed light on the intricate world of academic success. The study sought to reveal hidden patterns and predictive models in an effort of navigating through the academic maze, to guide interventions towards specific targets as future generations of proficient self-assured nurses advanced. The next section is the related study and literature. The materials and methods section follows, describing the data acquisition and preprocessing stage using SQL, where extracted data will be classified and analyzed by the WEKA mining tool. The results of the process performed will be presented and discussed in the data extraction result and data analysis results section.

2 Related Literature and Study

Finding knowledge from a large set of data is difficult to perform. One tool that stands out to analyze hidden patterns from a huge amount of data is data mining. Since it is impractical for data not to be utilized properly (Hussein et al., 2018), data mining procedures will primarily depend on data quality of the sources, requiring preprocessing to obtain dependable knowledge (Espinosa et al. 2011). Data mining is applied to different industries, but one of the emergent sectors is education (Villarica, 2020), as every academic year, a large amount of data is being generated (Gowri et al., 2017). Data mining with its several algorithms for the extraction of patterns and knowledge will aid in better decision-making (Roostaee, & Meidanshahi, 2023).

Before we can use WEKA for classification, data will undergo extraction and cleansing first. Preprocessing involves cleaning, integrating, and transforming extracted data from sources. Preparing a dataset for analysis requires patience and a lot of time since it involves complex SQL queries, joining of tables, and aggregation of columns (Ordonez et al. 2014). These aggregation functions by SQL include SUM, MIN, MAX, COUNT, and AVG to obtain a summary of data (Kumar & Krishnaiah), besides JOIN and conditional queries, which this current study will implement. Preprocessing follows as the accuracy of data mining classification will improve if missing values are attributed (Panda & Adhikari, 2020). Deletion of row and if possible imputation of missing value must be used to complete a data set. A possibility of skewed results may be present when a large set of complex data extracted has an outlier. Outlier discovery in data

mining means finding a pattern in the data set that may deviate from expected behavior (Dash et al., 2023). Generated data are noisy and dirty which is another preprocessing issue. Data cleansing adheres to better data quality making sure data is ready for the analytic phase (Ridzuan & Zainon, 2019). Performing validation and verification will ensure data quality.

After data cleansing, a selection of data mining techniques follows. One of the most useful data mining techniques is classification, a supervised method responsible for identifying previously hidden class labels (Kawade et al., 2020). In their study, they used WEKA to classify the academic performance of students and used the result to make future decision-making. J48 algorithm gains the highest accuracy relative to other methods used in their experiment. Their study used JRIP, NaiveBayes, and BayesNet together with J48 as their classification tool, which the current study will adopt. Another data mining study used WEKA to classify students who are academically good or poor in the government schools of the Vellore district in Tamil, Nadu (Gowri et al., 2017). The current study will try to classify students based on descriptive ratings of failed, passed, good, very good, and excellent. In the paper of Ahmed & Kaber, they also used classification algorithms J48 and JRIP to find the reasons behind the failure of students. They generated the JRIP rule and J48 pruned tree to analyze the result of their study using the data from 1st-year class results from 2017 to 2022 (Ahmed & Kaber, 2022).

The classifier algorithms that are popular among data miners are BayesNet, NaiveBayes, JRIP, and J48. Conditional probabilities are described graph-wise by the Bayesian Network, also known as BayesNet (Baranyi et al., 2019; Hussain et al, 2018). It uses a direct graph with nodes to represent random attributes and conditional dependencies that symbolize arbitrary variables (Almarabeh, 2017). The Bayesian Network improves speed, accuracy, and ease of computation for large databases. On the other hand, Naive Bayes is a simple classifier used for probabilistic learning and it shows great performance in terms of accuracy when attributes are independent (Almarabeh, 2017; Hussain et al, 2018; Pujianto et al. 2017). Data mining commonly uses JRIP, or Repeated Incremental Pruning to Produce Error Reduction, as a rule-based classification algorithm. It is an enhanced variant of RIPPER, or Reduced Error Pruning, renowned for its effectiveness and capacity to produce clear rules (Ahmed & Kabir, 2022; Walia et al. 2020). Finally, the J48 algorithm is an expansion of the ID3 algorithm created by Ross Quinlan. Frequently referred to as a statistical classifier, J48 is used to generate decision trees that are produced by the C4.5 algorithm (Almarabeh, 2017; Mishra et al. 2014).

3 Materials and Methods

The goal of the preliminary preprocessing stage is to clean, integrate, and transform data from sources. The cleansed dataset will then be applied to initial classification algorithms to detect possible associations and predictive models of academic performance. The university database, TUGS-CON Ver. 2 (Mendoza et al., 2017) is the primary source of data. Section 2.1 describes the data acquisition and preprocessing process to gather and prepare data for analysis. Section 2.2 explains the initial classification and data analysis procedure by the WEKA tool as well as the algorithms and metrics to be used.

3.1 Data Acquisition and Preprocessing:

The research utilizes data from the academic records of first-year nursing students at Tobruk University. SQL queries will be used to extract relevant information from the university database, including student demographics, course grades, class standing, and attendance records. The data extraction procedure is explained below.

Figure 1 shows the data extraction process performed in the study. The procedure is explained below:

1. Connect to the database: The researchers will access TUGS-CON Ver. 2 of the College and browse its database.
2. Identify the tables: Database tables containing the relevant data for the research will be specified. For this study, student information (stud_info), course grades (stud_records), and courses (subject_tb) table were selected.
3. Define the query: An SQL query to extract the desired data from the identified tables will be created. SELECT, JOIN, WHERE, GROUP BY, In, and other clauses to filter, combine, and aggregate data according to research needs will be applied.
4. Extract the data: The query will be executed and the result exported as a dataset in a spreadsheet. Results will then be formatted to CSV in preparation for feeding into WEKA. Before feeding, extracted data that are still unclean will undergo a preprocessing procedure.

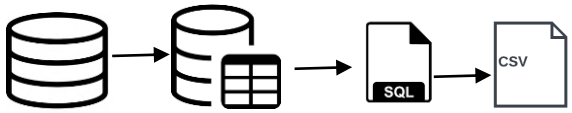

Figure (1) Data Extraction Process

The extracted data undergoes subsequent cleaning and transformation stages. This will be the preprocessing procedures:

1. Imputation and deletion will be used to deal with missing values identified (Panda & Adhikari, 2020).
2. Identification of outliers will be considered for possible influence on the analysis (Dash et al. 2023).
3. Data validation and verification will be performed to rectify data inconsistencies and errors (Ridzuan & Zainon, 2019).
4. The process of feature engineering can be used to develop new features using the existing data (OuahiMariame, 2021).

3.2 Initial Classification and Data Analysis:

Preprocessed data will then be imported into the WEKA software for further analysis and exploration. The descriptive statistics will be computed to determine the distribution of student performance and identify possible influences. Exploratory data analysis techniques will allow us to visualize the relationships between variables and identify patterns.

Selected classification algorithms available in WEKA will be utilized for the initial classifications of experiments. These are BayesNet, NaiveBayes, JRIP, and J48. These algorithms will classify and then try to predict the performance of students based on the features extracted. The created JRIP rule and J48 pruned tree will be presented to identify the main contributor to students' academic performance.

Metrics such as accuracy, precision, recall, and the F1 score will be applied to evaluate every classifier's performance. Kapa stat will be used to gauge the significance of the classification result. Error measurement will include mean absolute error and root mean square error. These metrics will give information on how well each algorithm predicts performance based on the available data.

4 Data Extraction Result

After carefully looking at the tables, we found that the data collected by the system was not as complete as expected. Table stud_info recorded name, control no., gender, and current year level as the only useful information for the study. Table subject_tb has course code, subject, description (if major or minor course), and units (Lecture/theory units, Laboratory Units, and Clinical Units). Table stud_records where students' academic performance was recorded, class standing (Cs, summation of class lecture performance like attendance, quiz, and term exam), Lab/exam (for courses with laboratory), and Finals (final exam). The documented performance however was recorded in summary instead of by category, thus the study can only use Cs as a whole, Lab/exam, and Finals as performance variables. Additional variables include 2nd (reset exam result), and carrier (loading exam result) for students who fail the course after the final exam. A snapshot of the datasheet view of the student's record extracted from the database is shown in Figure 2.

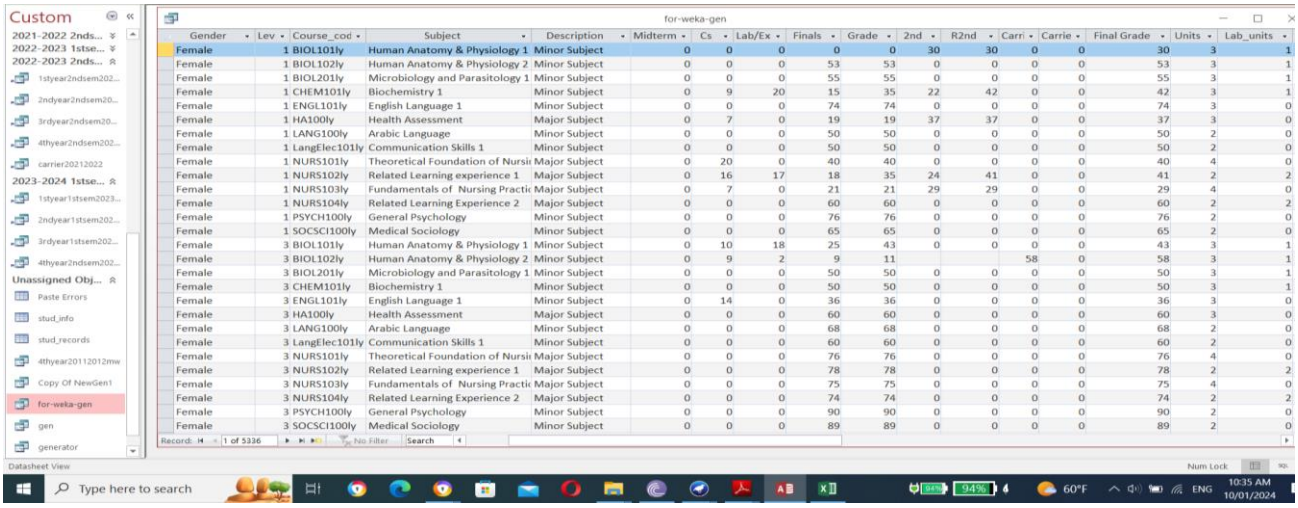

Figure (2) Datasheet view of students' record

The recorded academic performance were noisy and incomplete, a usual suspect for hindering knowledge discovery (Sessa & Syed, 2016). The computation for final grades at the college has different treatments depending on the subject/course description and between theoretical classes and classes with laboratory. Courses described as major (nursing major subject), lecture (theory class), lab (practical or laboratory), or clinical units have a passing rate of 60. All minor (general subject) courses have a passing mark of 50. The grading system and percentage equivalent are shown in Table 1.

Table (1) Grading system and percentage equivalent

Course	Description	CS	Lab Exam	Finals	Clinical	Passing Rate
Lecture (Theory)	Minor	30	0	70	0	50
Lecture (Theory)	Major	30	0	70	0	60
With Lab	Minor	20	20	60	0	50
With Lab	Major	20	40	40	0	60
Clinical	Major	20	0	30	50	60

It is also noteworthy that these were recorded in their summary form instead of raw equivalent. Instead of recording for example Cs=80, Lab=90, and Finals=50 for minor courses and then transmuted, the system shows it recorded instead Cs=16, Lab=18, and Finals=30 with a Grade of 64 for a passing mark. Field Midterm was not used for recording in recent years, instead long quiz that was incorporated with Cs was used. Either task from Cs or midterm was scrapped in the recent school year due to shortened classes and closure from the pandemic and other factors. Figure 3 shows the current Grade computation used in the College of Nursing using SQL's IIf statement.

```
Grade: IIf([lab_units] Or [clinical_units]>0, [Midterm]+ [cs]+[Lab]
+[finals], [midterm]+[cs]+[finals])
```

Figure (3) Grade computation query

Another distinguishing feature of the College's grading system is the recording of a 2nd assessment (reset exam) to replace the result of query Grade. Depending on the subject, lecture courses 2nd assessment results will replace 100% of the student's Final Grade, while courses with lab and clinical units retain their mark. 2nd assessment results will then replace the sum of Finals and Cs. Furthermore, a carrier exam (loading exam) was also given to students who were promoted to the next year's level if the student have only two failing courses after 2nd assessment result. Figure 4 shows the final grade computation with 2nd assessment and carrier (loading exam). There was some school year when even courses with lab were completely replaced by 2nd assessment exam. IIf statements were used to handle carrier, 2nd, and SY in different eras, thus the computation below.

```
Final Grade: IIf([carrier2]<>0,[carrier2], IIf([carrier]<>0,[carrier],
IIf([2nd]=-1,-1,IIf([2nd]=0,[grade], IIf([lab_units]>0 And
[stud_records.SY] >="20162017" Or [stud_records.SY]
<"20132014", [2nd]+[lab],[2nd])))))
```

Figure (4) Final grade computation with 2nd assessment and Carrier Exam (Loading exam)

To capture the core of the 2nd assessment, the researchers created a new query (figure 5) instead of relying on the recorded 2nd (which is only the reset exam result) and computed Final Grade. Computation was recorded in R2nd.

```
R2nd: IIf([2nd]=-1,-1, IIf([2nd]=0,0, IIf([lab_units]>0 And
[stud_records.SY] >="20162017" Or [stud_records.SY]
<"20132014",[2nd]+[lab],[2nd]))
```

Figure (5) Special computation used for courses 2nd Assessment (Reset Exam)

The study will be using the record from the last three (3) school year, 2020-20221, 2021-2022 and 2022-2023. As shown in Figure 6, WHERE clause with an In statement was used to extract the said AY's.

```
WHERE (((stud_records.SY) In
("20202021","20212022","20222023")) AND ((stud_records.sem)
In ("1st","2nd")) AND ((stud_records.code) In ("y1s1","y1s2")))
```

Figure (6) Where and In clause used to extract records from previous three A.Y.

The system produces a final grade status of passing and failing remarks depending on the subject description. For the researcher to create a nominal value better than Status (pass or fail), a Rating query was created to depict a descriptive rating equivalent. Table 2 shows the Final grade equivalent rating and Figure 7 its query.

Table (2) Grading system and percentage equivalent

Final Grade	Course Description	Descriptive Rating equivalent
85 to 100	Both	Excellent
75 to <85	Both	Very Good
65 to <75	Both	Good
60 to <65	Major	Passed or Fair
50 to <65	Minor	Passed or Fair
Below 60	Major	Failed or Poor
Below 50	Minor	Failed or Poor

```
Rating: IIf([Final Grade]>=85,"Excellent", IIf([final grade]>=75,
"Very Good", IIf([final grade]>=65,"Good", IIf(([Final grade]>=50
And ([description]="Minor Subject") Or [final grade]>=50 And
[description]="") Or ([final grade]>=60 And [description]="Major
Subject"),"Passed","Failed"))))
```

Figure (7) Final grade rating

Using the SQL code, the data were extracted and exported to a spreadsheet file. The preprocessing stage then follows. Imputation and deletion were used on missing values. Possible outliers were determined. Validation and verification were performed to rectify data inconsistencies and errors. Feature engineering was utilized to reclassify attributes. A total of 5336 rows of records were gathered in a dataset after preprocessing. There are 316 unique students, 280 were female and 36 were male. A total of 14 courses were also retrieved. The file was then formatted to a CSV file in preparation for data analysis. The next section describes the data analysis result including the classification procedure and algorithms used for this experiment. A sample of dataset extracted from the College's database is shown in Figure 8.

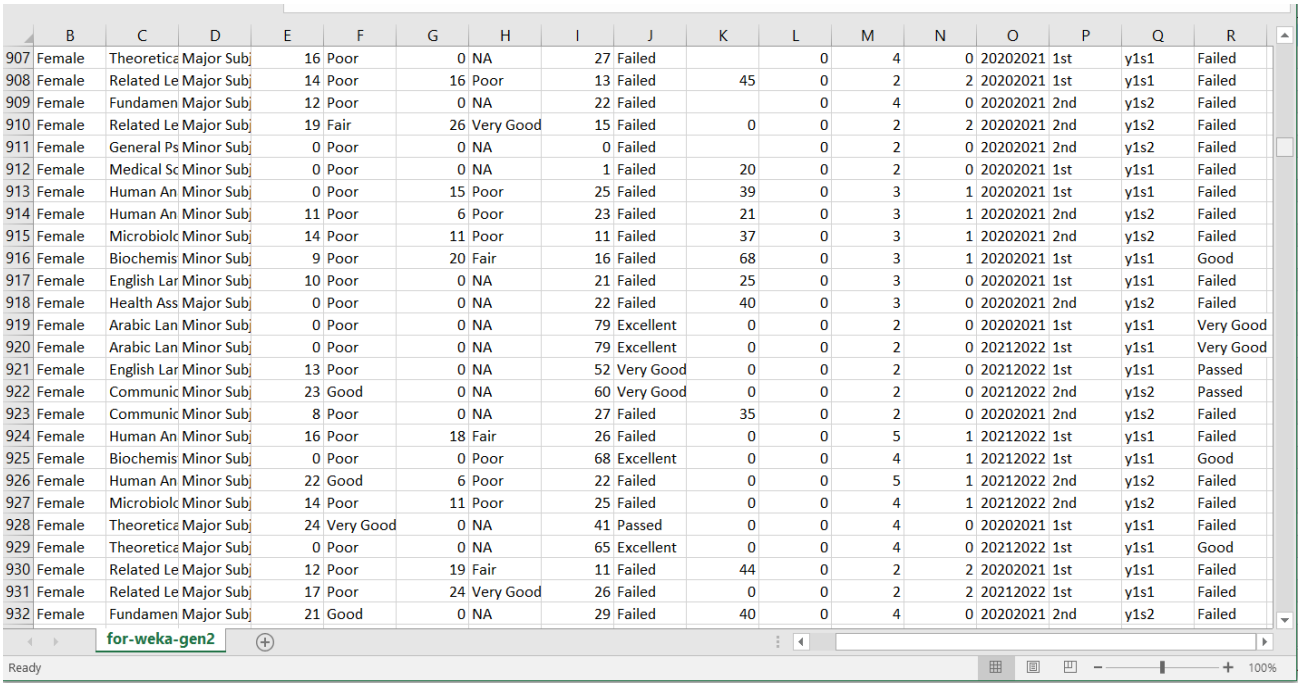

	B	C	D	E	F	G	H	I	J	K	L	M	N	O	P	Q	R
907	Female	Theoretica	Major Subj	16	Poor	0	NA	27	Failed		0	4	0	20202021	1st	y1s1	Failed
908	Female	Related Le	Major Subj	14	Poor	16	Poor	13	Failed	45	0	2	2	20202021	1st	y1s1	Failed
909	Female	Fundamen	Major Subj	12	Poor	0	NA	22	Failed		0	4	0	20202021	2nd	y1s2	Failed
910	Female	Related Le	Major Subj	19	Fair	26	Very Good	15	Failed	0	0	2	2	20202021	2nd	y1s2	Failed
911	Female	General Ps	Minor Subj	0	Poor	0	NA	0	Failed		0	2	0	20202021	2nd	y1s2	Failed
912	Female	Medical Sc	Minor Subj	0	Poor	0	NA	1	Failed	20	0	2	0	20202021	1st	y1s1	Failed
913	Female	Human An	Minor Subj	0	Poor	15	Poor	25	Failed	39	0	3	1	20202021	1st	y1s1	Failed
914	Female	Human An	Minor Subj	11	Poor	6	Poor	23	Failed	21	0	3	1	20202021	2nd	y1s2	Failed
915	Female	Microbiolc	Minor Subj	14	Poor	11	Poor	11	Failed	37	0	3	1	20202021	2nd	y1s2	Failed
916	Female	Biochemis	Minor Subj	9	Poor	20	Fair	16	Failed	68	0	3	1	20202021	1st	y1s1	Good
917	Female	English Lar	Minor Subj	10	Poor	0	NA	21	Failed	25	0	3	0	20202021	1st	y1s1	Failed
918	Female	Health Ass	Major Subj	0	Poor	0	NA	22	Failed	40	0	3	0	20202021	2nd	y1s2	Failed
919	Female	Arabic Lan	Minor Subj	0	Poor	0	NA	79	Excellent	0	0	2	0	20202021	1st	y1s1	Very Good
920	Female	Arabic Lan	Minor Subj	0	Poor	0	NA	79	Excellent	0	0	2	0	20212022	1st	y1s1	Very Good
921	Female	English Lar	Minor Subj	13	Poor	0	NA	52	Very Good	0	0	2	0	20212022	1st	y1s1	Passed
922	Female	Communic	Minor Subj	23	Good	0	NA	60	Very Good	0	0	2	0	20212022	2nd	y1s2	Passed
923	Female	Communic	Minor Subj	8	Poor	0	NA	27	Failed	35	0	2	0	20202021	2nd	y1s2	Failed
924	Female	Human An	Minor Subj	16	Poor	18	Fair	26	Failed	0	0	5	1	20212022	1st	y1s1	Failed
925	Female	Biochemis	Minor Subj	0	Poor	0	Poor	68	Excellent	0	0	4	1	20212022	1st	y1s1	Good
926	Female	Human An	Minor Subj	22	Good	6	Poor	22	Failed	0	0	5	1	20212022	2nd	y1s2	Failed
927	Female	Microbiolc	Minor Subj	14	Poor	11	Poor	25	Failed	0	0	4	1	20212022	2nd	y1s2	Failed
928	Female	Theoretica	Major Subj	24	Very Good	0	NA	41	Passed	0	0	4	0	20202021	1st	y1s1	Failed
929	Female	Theoretica	Major Subj	0	Poor	0	NA	65	Excellent	0	0	4	0	20212022	1st	y1s1	Good
930	Female	Related Le	Major Subj	12	Poor	19	Fair	11	Failed	44	0	2	2	20202021	1st	y1s1	Failed
931	Female	Related Le	Major Subj	17	Poor	24	Very Good	26	Failed	0	0	2	2	20212022	1st	y1s1	Failed
932	Female	Fundamen	Major Subj	21	Good	0	NA	29	Failed	40	0	4	0	20202021	2nd	y1s2	Failed

Figure (8) Sample dataset extracted from the College's database

5 Data Analysis Result

The CSV file created in the data extraction process was then loaded to WEKA ver. 3.8.6 for data classification and analysis using its exploration application. Among the different attributes used, continuous data produced a higher accuracy result compared to attributes with nominal data. The result to be presented in this study will be the regular academic performance of students where attributes include course Description, Cs, Lab, and Finals with Rating as nominal classifier. Table 3 show the comparison of the four classifiers wherein J48 got the highest accuracy (88.6619), best in Kappa,

lowest mean absolute error, and root mean square error, while having 2nd to the highest precision, highest recall, and F1 measurement. On the other hand, NaiveBayes has the lowest accuracy (68.9843) relative to the other algorithms used. Accuracy results do not mean that it is the best tool for the model in data mining. However,

when coupled with other metrics, the result clearly shows J48's supremacy among the four tools. In the similar study of Kawade et al., J48 also displayed the highest accuracy when compared to other tools (Kawade et al. 2020). The model created by BayesNet, JRIP, and J48 recorded a Kappa stat between >=61 to <=80 proving their result is of substantial significance.

Figure 9 shows the JRIP rules created by the experiment, showing Finals as the dominant rule among the students' academic performance. This means that the better the performance in Finals, the nearer its descriptive rating will be classified. Simply put, most students with excellent marks in Finals will have a high probability rating of excellent regardless of their descriptive rating in other performance metrics. JRIP rule also shows that Lab/Exam (lab) and course Description (major or minor) may also contribute to the descriptive rating. Similar to the result of Ahmed & Kabir's experiment, JRIP rules show that the better the result in final major or minor classes, the higher the chance of passing rate expected (Ahmed & Kabir, 2022). A total of nine rules were generated by the model in the current set of attributes. The created JRIP rule model also has a higher chance of classifying higher-rating students than lower-rating ones correctly.

One of the most effective methods for data mining and knowledge discovery is the presentation of decision trees (Bhargava et al., 2013). In the generated J48 pruned tree visualizer (figure 10) Finals appeared as the root (top node) adhering to the fact that the better the result in this attribute the nearer it would be to its descriptive result equivalent or Rating. The tree also created several internal nodes of the said attribute that represent test conditions applied. It shows that marks >49 in Finals have a bigger chance of being classified to its equivalent descriptive rating. Lab/exam also appears to influence marks <=49, however to a lesser extent compared to Finals based on the tree. Both JRIP and J48 classify that attribute Finals will most likely determine the Final grade equivalent descriptive Rating. The nominal attribute Rating is the created leaf node of the tree.

Table (3) Comparison of different classifiers using regular academic performance

Algorithm	Accuracy	Kappa Stat	*MAE	**RMSE	Precision	Recall	F1
BayesNet	83.9393	0.6852	0.0819	0.2357	0.844	0.839	0.833
NaiveBayes	68.9843	0.4272	0.137	0.2957	0.716	0.690	0.682
JRIP	87.8748	0.7581	0.0844	0.2054	0.898	0.879	0.873
J48	88.6619	0.7779	0.0751	0.1931	0.897	0.887	0.882

*Mean Abs Error, **Root mean square error.

```
JRIP rules:
===========

(Finals >= 85) => Rating=Excellent (89.0/0.0)
(Finals >= 75) => Rating=Very Good (124.0/0.0)
(Finals >= 65) => Rating=Good (277.0/1.0)
(Lab/Exam >= 14) and (Finals >= 50) => Rating=Good (17.0/4.0)
(Finals >= 50) and (Description = Minor Subject) => Rating=Passed (686.0/0.0)
(Finals >= 60) => Rating=Passed (161.0/0.0)
(Lab/Exam >= 5) and (Finals >= 31) and (Le-R = Fair) => Rating=Passed (47.0/2.0)
(Description = Minor Subject) and (Finals >= 37) and (Lab/Exam >= 13) => Rating=Passed (29.0/0.0)
 => Rating=Failed (3906.0/640.0)

Number of Rules : 9


Time taken to build model: 0.41 seconds
```

Figure (9) JRIP rules created with regular academic performance

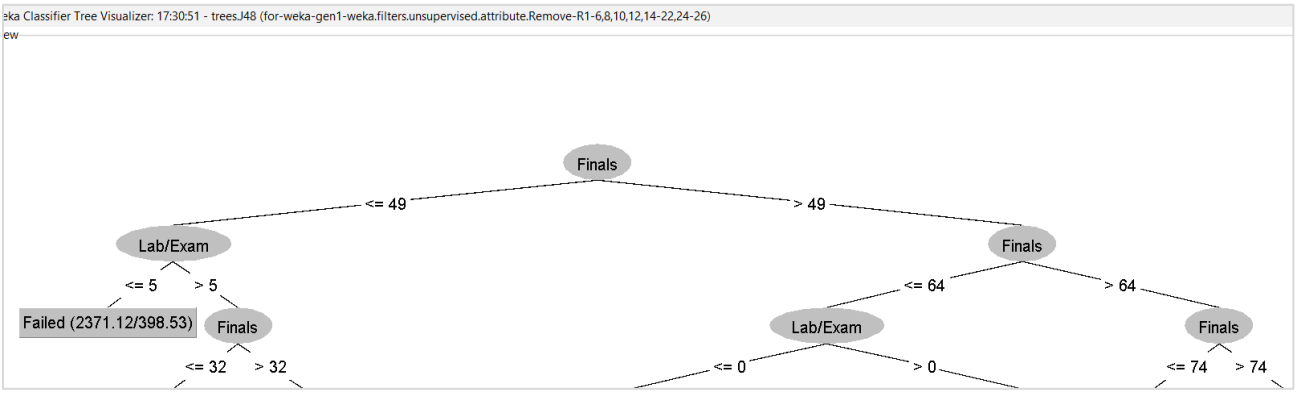

Figure (10) J48 Tree visualizer with regular academic performance (top three levels)

The researchers also used the attribute selector, where WEKA chooses description, Finals, Fe-R (Finals exam descriptive rating), R2nd, and carrier as the best attributes to go along with the Rating. As shown in Table 4, J48 improved and retained the highest accuracy (97.8261), precision, recall, and F1 measure while still having the lowest error stat. The rest of the algorithms vastly improved on their calculation although NaiveBayes remained with the lowest accuracy (79.3853) compared to the rest of the algorithms used. BayesNet, JRIP, and J48 all recorded a KAPA score of >=80, proving the higher reliability of the model, where its significance is interpreted as near perfect. Once again, J48 shows supremacy against the other algorithm using the current set of attributes. The algorithm with a stronger classification and lower error rate was always preferable (Kawade et al., 2020).

Figure 11 shows the JRIP rules created by the experiment, where Finals remained the dominant rule among the students' academic performance. It is the most important attribute in the experiment based on the result. The addition of R2nd also plays a significant part, as it is a result replacer, it mattered considerably in the descriptive Rating result. JRIP rule also shows that Carrier and course Description (major or minor) may contribute to the descriptive rating. The model is created with a total of 14 rules. There are more rules created for this model since there are six attributes selected by the attribute selector compared to the original five attributes selected by the proponents. The higher accuracy and precision of this second JRIP rule model also attributes to its faster creation (0.35 sec) compared to the first set of experiments (0.41 sec).

Likewise in the J48 tree visualizer (figure 12) generated by the WEKA tool, Finals remained as the root of the tree, thus the better the result in this attribute the closer it gets to its descriptive equivalent. R2nd also displays a considerable classification, especially for poorer-performing students. With more attributes compared to the first set of classifications, the J48 pruned tree created more nodes. Metrics like the number of nodes, number of leaves, depth of the tree, and number of attributes used in tree construction define the complexity of a tree (Bhargava et al., 2013).

Table (4) Comparison of different classifiers using an attribute selector

Algorithm	Accuracy	Kappa Stat	*MAE	*RMSE	Precision	Recall	F1
BayesNet	91.9228	0.8489	0.0453	0.1455	0.813	0.919	0.918
NaiveBayes	79.3853	0.5984	0.1069	0.2654	0.799	0.794	0.772
JRIP	97.8073	0.9596	0.0304	0.1024	0.978	0.978	0.978
J48	97.8261	0.9599	0.0171	0.0923	0.979	0.978	0.978

*Mean Abs Error, **Root mean square error

```
JRIP rules:
===========

(Finals >= 85) => Rating=Excellent (89.0/0.0)
(R2nd >= 85) => Rating=Excellent (14.0/0.0)
(Finals >= 75) => Rating=Very Good (124.0/0.0)
(R2nd >= 75) => Rating=Very Good (50.0/0.0)
(Carrier >= 75) => Rating=Very Good (5.0/1.0)
(Finals >= 65) => Rating=Good (277.0/1.0)
(R2nd >= 65) => Rating=Good (85.0/0.0)
(Carrier >= 65) => Rating=Good (6.0/0.0)
(Finals >= 50) and (Description = Minor Subject) => Rating=Passed (703.0/17.0)
(R2nd >= 50) and (Description = Minor Subject) => Rating=Passed (282.0/0.0)
(Finals >= 60) => Rating=Passed (161.0/0.0)
(R2nd >= 60) => Rating=Passed (131.0/0.0)
(Carrier >= 50) => Rating=Passed (45.0/1.0)
 => Rating=Failed (3364.0/97.0)

Number of Rules : 14


Time taken to build model: 0.35 seconds
```

Figure (11) JRIP rules created using an attribute selector

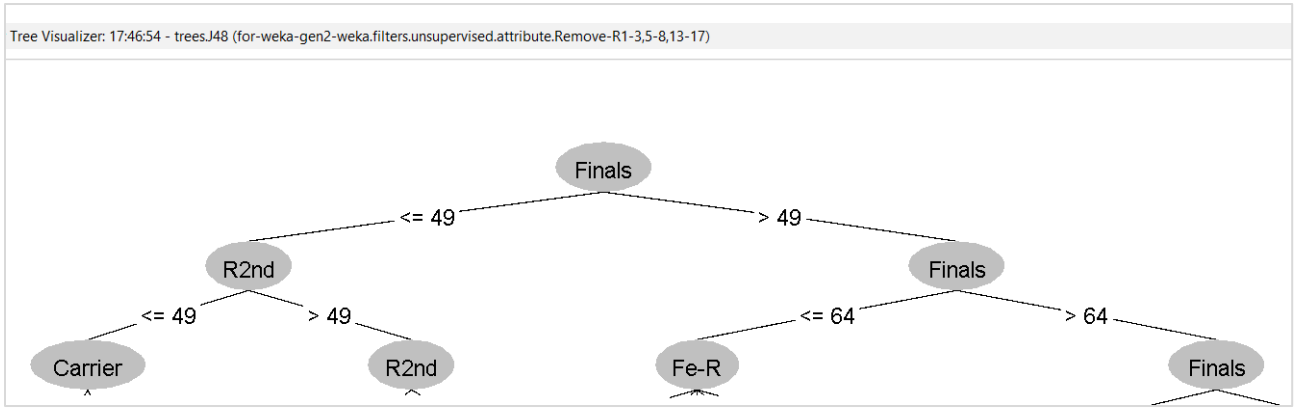

Figure. (12) J48 Tree visualizer using an attribute selector (top three levels)

The preliminary data analysis and initial classification attempts reveal some interesting insights:

- Data distribution: The distribution of different features depends on the data visualization techniques. This implies emerging patterns and relationships to be pursued further.
- Potential influencing factors: The initial analysis shows factors like final exams are predictive of student performance in most courses. There might be other factors contributing to this, but more analysis should be done to validate these relationships and determine other variables affecting them.
- Initial classification results: The analysis of several classification algorithms reveals positive findings. The majority of algorithms obtained accuracy rates over 80% except for NaiveBayes. Nevertheless, these are interim effects, and more fine-tuning as well as cross-validation is needed to evaluate model generalizability and validity.

Due to limited non-academic attributes, the classification algorithm tends to choose academic performance attributes as predictive measures. Despite successfully acquiring and cleaning data in data extraction results, and displaying high accuracy results in data analysis results, further research with additional attributes must be gathered to form a better model. The next section is the study's limitations and recommendations for future work.

6 Limitations and Future Work

This research is currently in its preliminary stages, and some limitations need to be considered:

- Limited data scope: The current analysis is limited to first-year data. Incorporating data from subsequent years may help to paint a broader picture of student performance trajectories.
- Feature selection and engineering: Additional analysis to determine the most pertinent features for prediction and possibly generate new features that can optimize performance is necessary.
- Class imbalance: The distribution of performance grades can be unbalanced and hence there is a need for appropriate treatment to manage this bias in data.

Future research may involve addressing these limitations and further refining the analysis:

- Feature selection and engineering will be performed on the data used for classification.
- Other classification algorithms will be investigated and compared for better performance.
- To verify the generalizability and reliability of developed models, cross-validation methods will be applied.
- The analysis will include data from the subsequent years to track student performance trajectories and long-term academic outcomes.
- Further refinement of classification and predictive models can be achieved by gathering more non-academic performance. Attributes like economic standing, behavior, and other possible factors may affect classification and prediction.

7 Conclusion

Application of the data mining methods promises a great deal in identifying the variables that affect performance scores by students enrolled in nursing studies. As depicted by the algorithms used, Finals attribute is the most important academic performance. However, other attributes may play a significant role in influencing students' Final grades and descriptive ratings. Non-academic factors may also contribute to the result if utilized. The created model may be used as a classification training set for future test sets, although modification and update of attributes are preferable. This study attempts to offer some insights into this area of research by looking at the peculiarities of Tobruk University and tracing patterns that can be used as a starting point for educational interventions, leading students toward success. The preliminary results presented here provide a basis for further analysis and model building, which could lead to a more thorough understanding of academic performance in nursing education at Tobruk University.

Conflict of Interest: The authors declare that there are no conflicts of interest.

References

Aher, S. B., & Lobo, L. M. R. J. (2011, March). Data mining in the educational system using weka. In *International conference on emerging technology trends (ICETT)* (Vol. 3, pp. 20-25).

Ahmed, Md & Kabir, Md. (2022). Analysis of University Students' Performance Using WEKA to Enhance the Education Quality. BAUET Journal. 03. 1-18.

Almarabeh, H. (2017). Analysis of students' performance by using different data mining classifiers. *International Journal of Modern Education and Computer Science*, *9*(8), 9.

Alyahyan, E., & Düştegör, D. (2020). Predicting academic success in higher education: literature review and best practices. *International Journal of Educational Technology in Higher Education*, *17*, 1-21.

Barakeh, A. M., Mezher, M. A., & Alharbi, B. A. (2024). Literature Review for Educational Data Mining Systems—Fahad Bin Sultan University Case Study. In *Artificial Intelligence-Augmented Digital Twins: Transforming Industrial Operations for Innovation and Sustainability* (pp. 435-453). Cham: Springer Nature Switzerland.

Baranyi, M., Gál, K., Molontay, R., & Szabó, M. (2019, November). Modeling students' academic performance using Bayesian networks. In *2019 17th international conference on emerging eLearning technologies and applications (ICETA)* (pp. 42-49). IEEE.

Bhargava, N., Sharma, G., Bhargava, R., & Mathuria, M. (2013). Decision tree analysis on j48 algorithm for data mining. *Proceedings of international journal of advanced research in computer science and software engineering*, *3*(6).

Bressane, A., Zwirn, D., Essiptchouk, A., Saraiva, A. C. V., de Campos Carvalho, F. L., Formiga, J. K. S., & Negri, R. G. (2023). Understanding the role of study strategies and learning disabilities on student academic performance to enhance educational approaches: A proposal using artificial intelligence. *Computers and Education: Artificial Intelligence*, 100196.

Cui, Y., Chen, F., Shiri, A., & Fan, Y. (2019). Predictive analytic models of student success in higher education: A review of methodology. *Information and Learning Sciences*, *120*(3/4), 208-227.

Dash, C. S. K., Behera, A. K., Dehuri, S., & Ghosh, A. (2023). An outliers detection and elimination framework in classification task of data mining. *Decision Analytics Journal*, *6*, 100164.

Espinosa, R., Zubcoff, J., & Mazón, J. N. (2011). A set of experiments to consider data quality criteria in classification techniques for data mining. In *Computational Science and Its Applications-ICCSA 2011: International Conference, Santander, Spain, June 20-23, 2011. Proceedings, Part II 11* (pp. 680-694). Springer Berlin Heidelberg.

Feng, G., & Fan, M. (2024). Research on learning behavior patterns from the perspective of educational data mining: Evaluation, prediction and visualization. *Expert Systems with Applications*, *237*, 121555.

García, S., Luengo, J., & Herrera, F. (2016). Tutorial on practical tips of the most influential data preprocessing algorithms in data mining. *Knowledge-Based Systems*, *98*, 1-29.

Goundar, S., Deb, A., Lal, G., & Naseem, M. (2022). Using online student interactions to predict performance in a first-year computing science course. *Technology, Pedagogy and Education*, *31*(4), 451-469.

Gowri, G. S., Thulasiram, R., & Baburao, M. A. (2017, November). Educational data mining application for estimating students performance in weka environment. In *IOP Conference Series: Materials Science and Engineering* (Vol. 263, No. 3, p. 032002). IOP Publishing.

Han, J., Kamber, M., & Mining, D. (2006). Concepts and techniques. *Morgan kaufmann*, *340*, 94104-3205.

Hussain, S., Dahan, N. A., Ba-Alwib, F. M., & Ribata, N. (2018). Educational data mining and analysis of students' academic performance using WEKA. *Indonesian Journal of Electrical Engineering and Computer Science*, *9*(2), 447-459.

Kabakchieva, D. (2013). Predicting student performance by using data mining methods for classification. *Cybernetics and information technologies*, *13*(1), 61-72.

Kawade, D. R., Oza, K. S., & Naik, P. G. (2020). Student performance classification: A data mining approach. *JIMS8I-International Journal of Information Communication and Computing Technology*, *8*(2), 462-466.

Keshavarzi, M. H., Azandehi, S. K., Koohestani, H. R., Baradaran, H. R., Hayat, A. A., & Ghorbani, A. A. (2022). Exploration the role of a clinical supervisor to improve the professional skills of medical students: a content analysis study. *BMC Medical Education*, *22*(1), 399.

Kumar, V. P., & Krishnaiah, R. V. (2012). Horizontal aggregations in SQL to prepare data sets for data mining analysis. *IOSR Journal of Computer Engineering (IOSRJCE)*, 2278-0661.

Mendoza J., Buhat-Mendoza D., Tan C. (2017). Tobruk University Grading System for College of Nursing Version 2 in Tobruk, Libya. *International Journal for Database Management System (IJDMS)*, Vol. 6, No. 5.

Mishra, T., Kumar, D., & Gupta, S. (2014, February). Mining students' data for prediction performance. In *2014 Fourth International Conference on Advanced Computing & Communication Technologies* (pp. 255-262). IEEE.

Mori, M., Noughi, N., & Cleve, A. (2015). Extracting data manipulation processes from SQL execution traces. In *Information Systems Engineering in Complex Environments: CAiSE Forum 2014, Thessaloniki, Greece, June 16-20, 2014, Selected Extended Papers 26* (pp. 85-101). Springer International Publishing.

Nahar, K., Shova, B. I., Ria, T., Rashid, H. B., & Islam, A. S. (2021). Mining educational data to predict students performance: A comparative study of data mining techniques. *Education and Information Technologies*, *26*(5), 6051-6067.

Namoun, A., & Alshanqiti, A. (2020). Predicting student performance using data mining and learning analytics techniques: A systematic literature review. *Applied Sciences*, *11*(1), 237.

OuahiMariame, S. K. (2021). Feature engineering, mining for predicting student success based on interaction with the virtual learning environment using artificial neural network. *Annals of the Romanian Society for Cell Biology*, *25*(6), 12734-12746.

Ordonez, C., Maabout, S., Matusevich, D. S., & Cabrera, W. (2014). Extending ER models to capture database transformations to build data sets for data mining. *Data & Knowledge Engineering*, 89, 38-54.

Panda, B. S., & Adhikari, R. K. (2020, March). A method for classification of missing values using data mining techniques. In *2020 International Conference on Computer Science, Engineering and Applications (ICCSEA)* (pp. 1-5). IEEE.

Pujianto, U., Azizah, E. N., & Damayanti, A. S. (2017, October). Naive Bayes using to predict students' academic performance at faculty of literature. In *2017 5th International Conference on Electrical, Electronics and Information Engineering (ICEEIE)* (pp. 163-169). IEEE.

Ridzuan, F., & Zainon, W. M. N. W. (2019). A review on data cleansing methods for big data. *Procedia Computer Science*, *161*, 731-738.

Roostaee, M., & Meidanshahi, R. (2023). Hidden Pattern Discovery on Clinical Data: an Approach based on Data Mining Techniques. *Journal of AI and Data Mining*, *11*(3), 343-355.

Schwab, K., Moseley, B., & Dustin, D. (2018). Grading grades as a measure of student learning. *SCHOLE: A Journal of Leisure Studies and Recreation Education*, *33*(2), 87-95.

Sessa, J., & Syed, D. (2016, December). Techniques to deal with missing data. In *2016 5th international conference on electronic devices, systems and applications (ICEDSA)* (pp. 1-4). IEEE.

Villarica, Mia. (2020). Mining Student Academic Performance on ITE subjects using Descriptive Model Approach. *Res. J. Computer and IT Sci* 4. 1-15.

Walia, N., Kumar, M., Nayar, N., & Mehta, G. (2020, April). Student's academic performance prediction in academic using data mining techniques. In Proceedings of the International Conference on Innovative Computing & Communications (ICICC).

Zughoul, O., Momani, F., Almasri, O. H., Zaidan, A. A., Zaidan, B. B., Alsalem, M. A., & Hashim, M. (2018). Comprehensive insights into the criteria of student performance in various educational domains. *IEEE access*, *6*, 73245-73264.

Scientific Journal for the Faculty of Science-Sirte University Vol. 4, No. 1 (2024) 30-35

Scientific Journal for the Faculty of Science-Sirte University

Journal home page: http://journal.su.edu.ly/index.php/JSFSU/index

DOI: 10.37375/issn.2789-858X

Bahr Essalam Gas Wells Production Evaluation Using Theoretical Method

Omar K. H. Aluhwal

Oil & Gas Engineering Department, Bani Waleed University, Bani Waleed, Libya.

DOI: https://doi.org/10.37375/sjfssu.v4i1.1907

ARTICLE INFO:

Received: 07 November 2023

Accepted: 03 December 2023

Published: 17 April 2024

Keywords: *Deliverability test, Flow-After-Flow test, Theoretical method, Gas well forecast*

A B S T R A C T

The production flow phenomenon potential of the Bahr Essalam's natural gas wells surveillance can be determined. However, it is one of the most important challenges for implemented operations to be accomplished at the location. On the other hand, the deliverability test application is a reliable fundamental operation in order to evaluate the reservoir productive capability at the current reservoir conditions. Consequently, the flow-after-flow test has been implemented for three wells of XX-02, XX-14, and XX-15, the pseudo-gas potential and inflow performance relationship have been used to evaluate the test. Therefore, the collected information has been analyzed using theoretical method which is considered an accurate method for the natural gas production flow rate assessment. The data analysis demonstrated that the absolute open flow potentials (AOFP) which mathematically represent the maximum gas flow rate at bottom hole flowing pressure equal to atmospheric pressure for the wells of XX-02, XX-14, and XX-15 are 66.6, 68.97, and 74.5 MMscf/day respectively. Additionally, the prediction of gas production flow rate at bottom hole flowing pressure of 1000 psi for the wells is 63, 65, and 70 MMscf/day respectively. Moreover, the group of IPR curves that belong to three wells depicted no substantially significance change in the delivered gas at the given bottom hole flowing pressure of the reservoir, which provides an average gas flow rate of approximately 41 MM scf/day. In conclusion, the IPR curves are essential study to evaluate the wells capability to deliver the gas to the wells and the gas amount that may actually be delivered up to the separators.

1. Introduction

Therefore, in this paper work, the Flow-After-Flow test will be analyzed using theoretical method to evaluate the Bahr Essalam natural gas field according to obtained data from Mellitah Oil & Gas Company. It is located within Block NC41 in the Mediterranean Sea, approximately 120 km northwest of Tripoli. The offshore gas and condensate field is owned and operated by Mellitah Oil & Gas (MOG), an equal joint venture (JV) between Eni and National Oil Corporation (NOC), a Libyan state-owned oil company. Production started in 2005 as part of the Bahr Essalam Phase I project.

In the natural gas fields, the well testing can be parted into three sections which are transient pressure analysis, production analysis and deliverability analysis. The deliverability testing may be conducted by producing the natural gas well at usually four different gas flow rates (İŞÇAN, 2021). The deliverability conventional back pressure test which known as flow-after-flow test analysis can be used as an analysis technique to define a regular inflow performance relationship (IPR). This practical analysis is a relationship between the bottom hole flowing pressure or tubing well head pressure and natural gas flow rate that may substantially be utilized to

***Corresponding author*: E-mail: springand34@gmail.com**

forecast the gas production rate at any gas reservoir pressure. In other words, the flow-after-flow test run to evaluate the capability of gas well production at a certain reservoir conditions (Brown,1984). Prior to the achievement of gas flow rate, the stabilization of reservoir pressure needs a particular time which is not practical for long period (Lee et. al., 2003), because it is attributed to low permeability reservoir. Therefore, the low permeability gas reservoir can be subjected for deliverability testing such as flow-after-flow test as a result of long time required for reaching reservoir pressure stabilization condition. Additionally, it can be named four-point tests as well. It is carried out by producing the gas well at different stabilized gas flow rates following with measured bottom hole flowing pressure. Usually, conventional flow-after- flow tests are carried out with a succession of increasing flow rates (Smith, 1990). The required time to create the reservoir pressure before the achievement of flow is not practical, because shut in wells leads to reduce the gas production system (Lee et. al., 2003). Rawlins and Schellhardt provided a method to measure the productive capability of the wells. It is a reasonable test that can be conducted to control gas flow rates (Rawlins and Schellhardt, 1935; Smith, 1990). Therefore, this method became standard practice and became known as the conventional multi point or back pressure test. Besides, this practical test is pointed to such the flow-after-flow back pressure test. Moreover, the gas flow rate measurement can be accomplished using an inflow performance formula. This formula could be assessed according to original field data. The theoretical method is used for natural gas production evaluation. It requires extra work that depends on the pseudo-gas potential integral prior to Flow-After-Flow analysis.

In addition, this formula relies on the coefficients A and B of pseudo pressure approach which are essentially independent parameters of the reservoir pressure (Lee, 1982; Ahmed and McKinney, 2011). In addition, it is necessary to mention the most essential phenomena which gas flow rate stabilization. So, it is caused by liquid accumulation in bottom hole, liquid removal or unsteady state action of the gas well. In fact, it is possibly due to a combination of the all previous mentioned phenomena. Typically, previous study by Cullender demonstrated that the stabilization can be achieved. The flowing pressure of the wellhead variation may be no more than a specific number of psia in short duration of about fifteen minutes (Cullender, 1955; Smith, 1990). To evaluate the natural gas well performance, the inflow performance relationship (IPR) curve may be suggested for this purpose. Moreover, the empirical method is one of the most important approach for interpreting and evaluating the deliverability tests analysis of gas wells performance (AL-Attar H and Al-Zuhair, 2009). Consequently, the main target of the deliverability test such as flow after flow test is to foretell the manner in which the gas flow rate is going to decline simultaneously with reservoir pressure depletion (Aluhwal, et. al., 2017). Moreover, absolute open flow potential (AOFP) may be defined as the gas flow rate at which the gas well produces contra a zero-value at sand face. It is impossible to be measured directly but might be procured from deliverability tests. So, it is usually utilized by regulatory authorities as a index in setting maximum allowable production gas flow rate (Nguyen and Sergeev, 2015). The gas well flow performance evaluation of inflow performance relation (IPR) technique was used by Bakyani (Bakyani, et. al., 2018). A case study has been conducted for a gas well to evaluate natural gas production (Igwilo, et. al. 2018). A research study about normalized pseudo variables in gas well testing was carried out in order to estimate well deliverability, skin, permeability, mechanical skin (Meunieur, et. al., 1987). A similar research was run to facilitate the early assessment of natural gas well deliverability in a strong heterogeneity and complex low permeability reservoir (Xi, et. al., 2020; Sergeev et. al., 2017). Therefore, the multipoint back-pressure test results is a very reliable deliverability operation. A limited number of about four points tests are often run for a single gas well (Brar and Aziz, 1978).

2. Methodology

The real data of deliverability test is acquired from the Bahr Essalam gas field. The pseudo gas potential and analytical mode suggested for back pressure test interpretation. The one of the important modes to be used is empirical method for data interpretation.

2.1 Flow-After-Flow Test

Flow-After-Flow test may be named as Back Pressure Test. It can be defined as a simple inflow performance relationship between bottom hole flowing pressure or tubing well head pressure and gas flow rate. Moreover, it could be forecast the production gas flow rate at any given bottom hole pressure. The pressure history and gas flow rate of typical multi point test can be shown in Figure 1. It illustrates a typical sequence of rate varies in

which the gas flow rate increases throughout the test. Besides the test can be run in a reverse sequence as well.

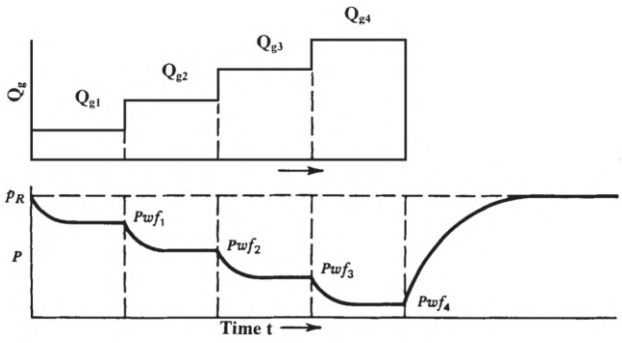

Figure (1) Conventional multi point test (Smith, 1990).

2.2 Collected data

The data of Flow-After-Flow test has been collected from three different gas wells (Well XX-02, Well XX-14 and Well XX-15) that located within Baher Esslam gas field is shown in the Table 1**.** Additionally, the gas sample was collected from this gas reservoir for PVT analysis (hydrocarbon compositions). So, the supplement Table 2 depicts the compositional analysis data. Moreover, the reservoir pressure is 3550 psi, temperature is 279 ^{o}F, 51 ^{o}API condensate, heptane plus P_{pc} and T_{pc} are 352.22 psi and 1012.695 ^{o}R, respectively.

Table (1) Gas test data

Well_XX-02			
Test	P_{wf}, psi	Gas flow rate, scf/D	Q_o, STB/D
1	2890	33,176,354	993
2	2700	38,768,432	1078
3	2460	42,832,109	1183
4	2200	48,043,283	1202
Well_XX-14			
1	2922	31,990,123	1121
2	2650	40,112,879	1163
3	2490	43,123,657	1204
4	2188	49,002,436	1213
Well_XX-15			
1	3030	29,990,102	781
2	2733	39,856,732	793
3	2570	44,109,834	818
4	2311	50,111,232	983

Table (2) Gas compounds

	Mole fraction (Xi)		
	Well No.		
	XX-02	XX-14	XX-15
Comp.	Xi	Xi	Xi
C1	0.714250	0.7269	0.76310
C2	0.041720	0.0409	0.04280
C3	0.027000	0.0194	0.02040
i-C4	0.003700	0.0060	0.00330
n-C4	0.010505	0.0052	0.00260
i-C5	0.001575	0.0027	0.00211
n-C5	0.001230	0.0028	0.00957
C6	0.006940	0.0068	0.00710
C7+	0.019480	0.0191	0.02010
H_2S	0.018460	0.0181	0.01901
N_2	0.029580	0.0290	0.03040
CO_2	0.125560	0.1231	0.07951

2.3 Theoretical Method

The theoretical method is substantially based on the main pseudo steady state inflow performance equation (Lee, 1982; Ahmed and McKinney, 2011) which can be written as following simplified formula:

$$\psi(\bar{P}) - \psi(P_{wf}) = A.Q_g + B.Q_g^2$$

Where A and B are constants, $\psi(P)$ is called pseudo gas potential, psi^2/cp which can be defined at any pressure (P) as the next form:

$$\psi(P) = 2\int_{14.7}^{P} \frac{P}{\mu.z}\, dP$$

Where μ is gas viscosity, cp and z is the gas deviation factor, Q_g stand for gas flow rate, scf/day, P_{wf} is bottom hole flowing pressure, psi, $\bar{P}$ is average reservoir pressure of the drainage area, psi.

2.4 Corrected Gas Flow Rate

The natural gas production flow rates are corrected according to the gas equivalent of the hydrocarbon condensate simplified formula (Cragoe, 1929) which as following:

$$Q_{gc} = Q_g + 3003(1.03 - \gamma_o).Q_{con}$$

Q_{gc} stand for corrected gas flow rate, scf/d, γ_o is liquid condensate specific gravity and Q_{con} liquid condensate rate, STB/day.

3. Inflow Performance Relationship

A plot of gas production flow rate against bottom hole flowing pressure is termed the gas well or reservoir inflow performance relationship (IPR) that proposed as a method of interpretation of flowing and natural gas reservoir potential. Additionally, the absolute open flow potential (AOF) is the major parameter which could be estimated using theoretical approach that common method is used in the natural gas industry.

4. Results and discussion

The theoretical method is considered the best method that used for gas production assessment. It is a reliable method to analyze the back-pressure test in the natural gas industry, because it is more accurate and rigorous than the other methods (Al-Hussainy, *et. al.*, 1966) which is attributed to the pseudo gas potential calculation. Therefore, based on this deduction, the obtained results of deliverability test analysis can be show in Figure 2**.**

The pseudo steady state inflow performance equation that mentioned above demonstrates that the coefficients A and B of pseudo pressure approach for each well are essentially independent variables of the reservoir pressure. These variables can be treated as fixed parameters. A and B might be determined from the individually regression of the straight line for each single gas well.

The obtained results displayed that A is 1.035 and B is 0.00000014567 for Well XX-02 in which A is represent the intercept and B is represent the slope of the fitted line. Secondly, A is 1.861 and B is 0.0000001233 for Well XX-14. Finally, A is 2.4869 and B is 0.00000009587 for Well XX-15. The absolute open flow potential (AOFP) can be calculated from the fitted straight line. AOFP mathematically acts the maximum gas flow rate at bottom hole flowing pressure equal to atmospheric pressure. The AOFPs for the wells of XX-02, XX-14 and XX-15 are 66.6, 68.97 and 74.5 MMscf/day respectively. The pseudo-gas potential ψ(P), at initial reservoir pressure is 714.9 MMpsi^2/cp, because the three wells are located in the same reservoir. Table 3 demonstrates the Pseudo-gas potential results at each pressure data. According to the obtained results, the prediction of gas production flow rate at bottom hole flowing pressure equal to 1000 psi for the well of XX-02, XX-14 and XX-15 are 63, 65 and 70 MMscf/day. Additionally, the inflow performance relationships curves (IPR) for all conducted deliverability tests. It is clearly the IPR curves show no a remarkable significant difference between delivered natural gases for all the wells. It can be noticeable that the average bottom hole flowing pressure of 2595 psi is the average bottom hole flowing pressure of the all wells which reflexes the average gas production flow rate of approximately 41 MM scf/day. This estimated average is obtained from the flow-after-flow test data as displayed in Figure 3. In addition, the Figure 4 illustrates the pseudo gas potential as a function of gas viscosity (μ), cp and gas deviation factor (z) for the natural gas compounds. Finally, it is important to mention that various wells flow-after-flow tests and IPR curves that discussed above are the reliable indicators to assess the pay zone capacity to deliver the natural gas to the wells. Moreover, the test evaluates the capability of the wells to deliver the gas volume to the ground surface at average reservoir pressure of 3550 psi and average flowing bottom hole pressure of 2595 psi.

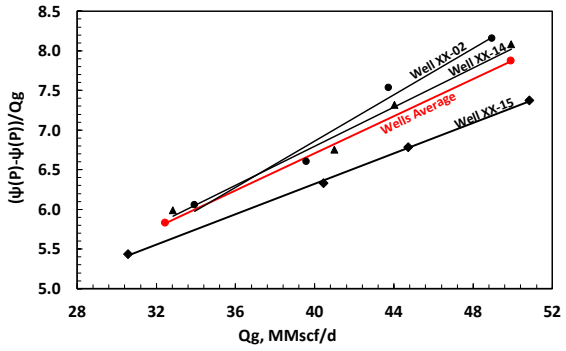

Figure (2) Deliverability test analysis using pseudo gas potential

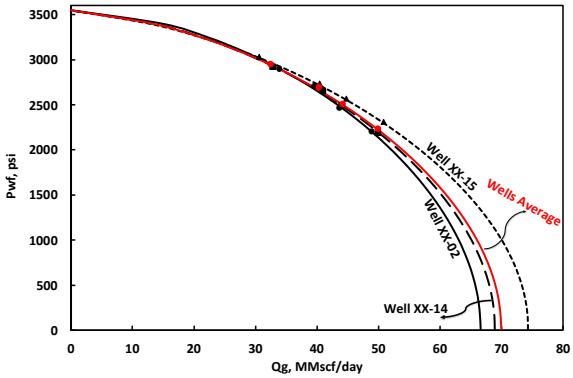

Figure (3) IPR curves for the wells and their average

Table (3) Pseudo-gas potential results

P, psi	Qgc, scf/d	ψ(P), psi^2/cp	[(ψ(P)-ψ(Pwf)]/ Qgc
Well XX-02			
3550	0.000	714,942,893	-
2890	33,935,737	509,463,548	6.0550
2700	39,592,818	453,375,673	6.6064
2460	43,736,792	385,285,164	7.5373
2200	48,962,496	315,630,649	8.1555
Well XX-14			
3550	0.000	715,144,205	-
2922	32,847,393	518,432,228	5.9887
2650	41,002,268	438,123,379	6.7562
2490	44,044,400	392,772,087	7.3193
2188	49,930,061	311,695,307	8.0803
Well XX-15			
3550	0.000	718,202,608	-
3030	30,587,361	551,949,839	5.4353
2733	40,463,168	462,036,687	6.3308
2570	44,735,389	414,734,421	6.7836
2311	50,862,968	343,072,211	7.3753

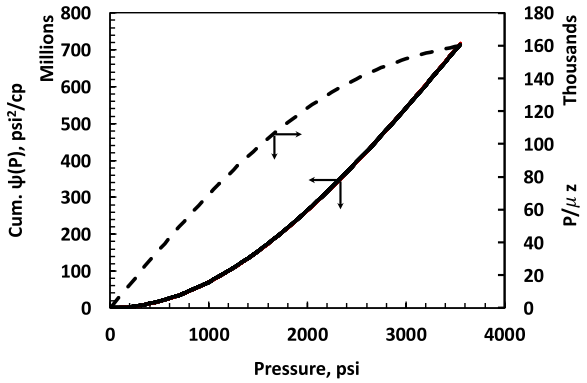

Figure 4: Pseudo-gas potential vs. pressure

5. Conclusion

The flow-after-flow test was analyzed by theoretical method in order to assess the Bahr Essalam's natural gas wells production such as Well XX-02, XX-14 and XX-15. The natural gas production flow rates of these wells are corrected according to the gas equivalent of the hydrocarbon condensate. The main indicator of production potential is the pseudo steady state inflow performance relationship. The analysis has shown that the wells have a productive capability at the current reservoir pressure of 3550 psi and average gas production of 41 MM scf/day at average bottom hole flowing pressure of 2595 psi as can be shown in the average IPR curve of three wells. The forecasting of gas production flow rates of the wells XX-02, XX-14 and XX-15 are 63, 65 and 70 MMscf/day respectively, when the pressure is dropped to1000 psi.

Conflict of Interest: The author declares that there are no conflicts of interest.

References

Ahmed, T., and McKinney, P. (2011). Advanced reservoir engineering. *Elsevier.* Ch. 3 p 190-200.

AL-Attar H and Al-Zuhair S. (2009). A general approach for deliverability calculations of gas wells *Journal of Petroleum Science and Engineering 67*: 97–104.

Al-Hussainy, R., Ramey Jr, H. J., and Crawford, P. B. (1966). The flow of real gases through porous media. *Journal of Petroleum Technology*, *18*(05): 624-636.

Aluhwal, O. K. H., Junin, R. B., and Nasri, N. S. B. (2017). Surfactant Alternating Carbonated Water Injection (SACW) is a New Process for Enhanced Oil Recovery. *Advanced Science Letters*, *23*(9): 9085-9089.

Bakyani, A., A. Rasti, S. Qazvini, and F. Esmaeilzadeh, (2018). Gas condensate wells simulation to optimize well flow performance using tubing equations coupled with ınflow- performance-relation (IPR) curve. *Open Access Library Journal*, *5*(5): 1-17.

Brown, K. E. 1984). The technology of artificial lift methods, Volume 4. *UA: PennWell Publishing Company.*

Brar, G.S., Aziz, K., (1978). Analysis of modified isochronal tests to predict the stabilized deliverability potential of gas wells without using stabilized flow data. *Trans. AIME* 265, 297–304.

Cragoe, C.S. (1929). "Thermodynamic Properties of Petroleum Products," Bureau of Standards, U.S. Dept. of Commerce Miscellaneous Pub. No. 97, 22.

Cullender, M. H. (1955). The Isochronal Performance Method of Determining the Flow Characteristics of Gas Wells. Tran. AIME 204, p. 137.

Igwilo, K., E. Okoro, A. Nwude, A. Mamudu, and C. Onuh, (2018). A review on gas well optimization using production performance models:A case study of horizontal well. Open *Journal of Yangtze Oil and Gas*. ***3***(1): 57-67.

İŞÇAN, A. (2021). Empirical and theoretical analysis of a modified isochronal test in a Caspian region gas reservoir. *International Advanced Researches and Engineering Journal*, *5*(3), 379-386.

Lee, J. (1982). Well Testing. Dallas, TX: Society of Petroleum Engineers of AIME.

Lee, J., Rollins, J.B. and Spivey, J.P. (2003). Pressure Transient Testing., *Richardson TX USA: SPE Textbook Series*

Meunier,D.F., C.S.Kabir, and M.J. Wittmann, (1987). Gas well test analysis: use of normalized pseudovariables. *Eval*. **2**(04): p. 629–636.SPE-13082-PA.

Nguyen T H P and Sergeev V L. (2015). Identification of IPR curve for interpreting gas well deliverability tests *Bulletin of the Tomsk Polytechnic University: Georesources Engineering* 326 12 pp 54–59

Rawlins, E. L., and Schellhardt, M. A. (1935). *Back-pressure data on natural-gas wells and their application to production practices* (Vol. 7). Lord Baltimore Press.

V L Sergeev , Nguyen T H Phuong and A I Krainov, (2017). Adaptive interpretation of gas well deliverability tests with generating data of the IPR curve. *IOP Conf. Series: Journal of Physics: Conf. Series* 803 012136

Smith, R. V. (1990). Practical natural gas engineering. PennWell Publishing Company. 2nd ed. 108-112.

Xi, F., X.Peng, Q. Li, X. Zhao, P. Zhang, and D. Pan. (2020). A new method for evaluating the unstable deliverability of gas wells in gas formation testing phase. *Natural Gas Industry B.* **7**(6): p. 614-623

Scientific Journal for the Faculty of Science-Sirte University Vol. 4, No. 1 (2024) 36-44

Scientific Journal for the Faculty of Science-Sirte University

Journal home page: http://journal.su.edu.ly/index.php/JSFSU/index

DOI: 10.37375/issn.2789-858X

Survey of Plant Species in Cyrene (Campus apollo) Shahat AL-Jabal AL-Akhdar, Libya

Hamida M. Hamad, Ensaf, H. Dakeel, Fatma M. Alwishish, Enas Saed

Botany Department, Science Faculty, Omar AL-Mukhtar University, Libya.

DOI: https://doi.org/10.37375/sjfssu.v4i1.2637

ARTICLE INFO:

Received: 18 February 2024

Accepted: 01 April 2024

Published: 17 April 2024

Keywords: Cyrene, survey, AL-Jabal AL-Akhdar, plant species.

A B S T R A C T

The main objective of this study was to survey plants on the campus of Apollo, located in the Shahat area. The vegetation sampling was carried out between November 2021 to May 2023 with several field trips to the study area, and make a preliminary list dealing with the floristic composition. 194 species belonging to 160 genera and 57 families were recorded, identified in the Herbarium and arranged using the Engler system. Pteridophyta were represented by one species one family, and 4 species 3 families of Gymnosperms, while the remaining 53 families belong to Angiosperms, Dicotyledon were represented by 43 families 154 species and Monocotyledon 10 families 35 species. The most dominant families were Asteraceae (14%), Poaceae family (11%), followed by Fabaceae family (9%). As for life forms, they were classified according to Raunkiaer and were the most dominant as Therophytes (48%), Chamaephytes (15%), and Geophytes (11%).

1 Introduction

Floristic studies are taxonomic examination of a given area's flora or a significant portion of it, including the identification, nomenclature, and documentation of plant species (Keith, 1988; Ilyas *et al.*, 2013). Furthermore, the floristic lists produced by these studies are frequently the only sources of botanical data for a specific region and may provide the foundation for additional in-depth research. For instance, in ecological studies, it can be used to compare the flora of the same habitat at various times or in different habitats (Ferreira *et al.*, 2013; Martínez-Calderón *et al.*, 2017; Bano *et al.*, 2018(. Recently, floristic studies and taxonomy of various ecosystems have also become essential for the conservation of biodiversity (Heywood, 2004). Floristic composition studies are crucial for understanding the range of plants existing in a region as well as having socioeconomic importance. They offer both humans and other species living in that region refuge, food, medical care, and everything else (Shehata & Galal 2015). A variety of floristic studies have been undertaken on the Flora of Libya, for example (Lemaire, 1703). Just 1% of Libya's total land area is made up of the Al-Jabal Al-Akhdar region. It has a width of 50 km and a length of 250 km along the Mediterranean coast. Boulos claims that Al-Jabal Al-Akhdar has over 90% of all the plant species in Libya, making it the most diversified area in terms of vegetation (Boulos, 1972). In northeastern Libya, on the second terrace of Al-Jabal Al-Akhdar, at an altitude of roughly 600 meters, is Cyrene, situated roughly 10 kilometers east of the city of Al-Bayda. Because of its flora, vegetation cover, biodiversity, climate, and ecological significance, the Al-Jabal Al-Akhdar area (in northeastern Libya) was the subject of recent assessments undertaken by local researchers. (Al-Traboulsi and Alaib, 2021; Omar *et al.*, 2021; Mukassabi *et al.*, 2012), still there is a lack of knowledge and data. Al-Jabal Al-Akhdar is a significant area for ecology. The current study aimed to the initial

Corresponding author: E-mail: hameda_h76@yahoo.com

inventory of the types of plants in the region defining them, preparing a list of them, and distributing these plants within groups such as species, genera, and forms different life.

2 Materials and Methods

2.1 Study area

Cyrene is situated on the second terrace of Al-Jabal Al-Akhdar, in the northeast of Libya. It is roughly 10 kilometers east of the city of Al-Bayda. The study area's height ranges from 555 to 578 meters, and it is situated between latitudes 32°49´23.952 ´N and longitude 021°51´11.1888 ´E on the northeastern part of Al Jabal Al-Akhdar. (Figure 1).

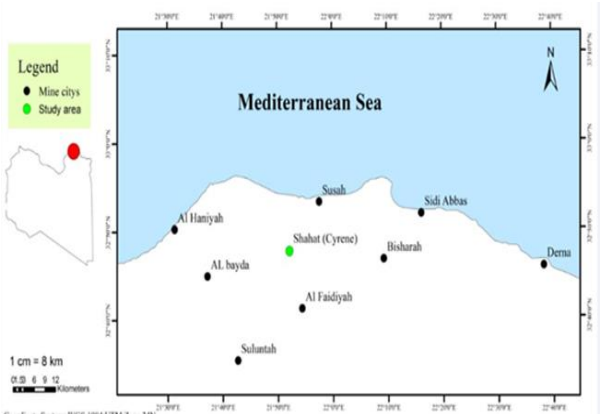

Figure (1) The study area

2.2 Sample collection and Identification

The vegetation sampling was carried out between November 2021 to May 2023 with several field trips to the study area. The specimens were dried for two weeks with presses, they were glued to the herbarium sheet. The plant specimens were identified in the Sylphium herbarium, Department of Botany, College of Science, Omar Al-Mukhtar University, using the Libyan Flora Books. The plant species were arranged and catalogued according to Engler system of classification (Melchoir, 1964), A special file was created for each family, and a serial number for each family was written on the file, according to the Engler system, these files are organized inside the herbarium cabinet, each file according to its own number, and each genus and species contained in the herbarium sheet is also numbered according to its arrangement inside the books of Flora of Libya.

2.3 Climatic data analysis

The region is characterized by a moderate climate with hot winters and dry summers.The average annual rainfall reaches 500 mm. The average annual temperature is 16°C. The information of climatic variables was acquired and gathered from Libyan Public Focus of Meteorology for ten successive years. They were analyzed according to various literatures based on the availability of precipitation and temperatures. A ten-year average show that there is a lot of precipitation, especially in December, January, and February, and that the dry season lasts from June to August. The average maximum temperature was 23 °C, and the average minimum temperature was 15°C. The highest temperatures were recorded in June, July, and August, while the lowest temperatures were recorded during December, January, and February. (Figure 2).

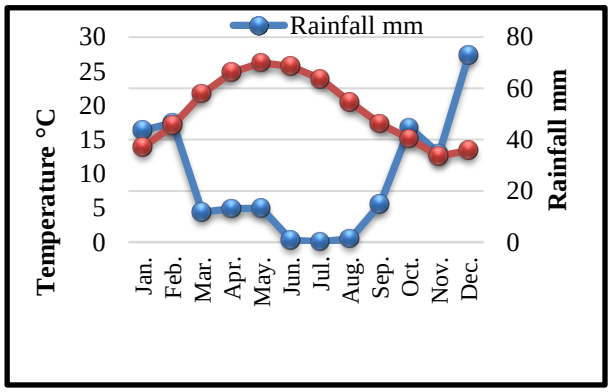

Figure (2) Mean monthly variation of temperatures °C and rainfall (mm) during the period (2010: 2019).

3 Results

The total number of recorded species surveyed in the present study was 194 species, belong to 160 genera and 57 families, they are represented by Pteridophyta 1species 1 family, Gymnosperme 4 species 3 families, Dicotyledone 154 species 43 families and Monocotyledone 35 species 10 families, as shown in (Table1), Families and number of species in each family According to the system Engler.

Table (1) Number of species in each family**.**

No.	Family	Number of species
I.	**Pteridophyta.**	
1	Adiantaceae	1
II.	**Gymnosperms**	
1	Pinaceae	1
2	Cupressaceae	2
3	Epheraceae	1
III.	**Angiosperms**	
a.	**Dicotyledone**	
1	Moraceae	1
2	Urticaceae	2
3	Polygonaceae	5
4	Cactaceae	1
5	Carophyllaceae	1
6	Chenopodiaceae	1
7	Illecebraceae	2
8	Lauraceae	1
9	Ranunculaceae	5
10	Clusiaceae	1
11	Papaveraceae	1
12	Fumariaceae	1
13	Capparaceae	1
14	Brassicaceae	8
15	Resedaceae	2
16	Crassulaceae	1
17	Rosaceae	6
18	Fabaceae	18
19	Caesalpiniaceae	1
20	Mimosaceae	2
21	Oxalidaceae	1
22	Geraniaceae	4
23	Euphorbiaceae	6
24	Anacardiaceae	1
25	Rhamnaceae	3
26	Malvaceae	2
27	Myrtaceae	1
28	Apiaceae	9
29	Primulaceae	2
30	Oleaceae	1
31	Apocynaceae	1
32	Rubiaceae	2
33	Covolvulaceae	1
34	Boraginaceae	7
35	Verbenaceae	1
36	Lamiaceae	10
37	Solanaceae	3
38	Scrophulariaceae	4
39	Caprifoliaceae	2
40	Valerianaceae	2
41	Dipsacaceae	1
42	Campanulaceae	1
43	Asteraceae	28
b.	**Monocotyledone**	
1	Liliaceae	4
2	Alliaceae	1
3	Amaryllidaceae	1
4	Iridaceae	2
5	Poaceae	21
6	Arecaceae	1
7	Araceae	2
8	Lemnaceae	1
9	Cyperaceae	1
10	Orchidaceae	1

Dominant families were Asteraceae (14%) with 28 species, Poaceae (11%) were represented by 21 species,Fabaceae (9%) were represented by 18 species, Lamiaceae (5 %) containing 10 species. The family Apiaceae (5%) containing 9 species. Boraginaceae (4%) represented by 7 species. There were families of 6 species such as Euphorbiaceae and Rosaceae, there were families of 5 species including Ranunculaceae and Polygonaceae, there were families of 4 species represented in Geraniaceae and Liliaceae, there were families containing 3 species represented by Rhamnaceae, Araceae, Scrophulariaceae and Solanaceae, there were families of 2 species such as Caprifoliaceae, Illecebraceae, Iridaceae, Malvaceae and Primulaceae, other families represented by 1 species such as Pinaceae, Papaveraceae and Fumariaceae. (Figure3) and (Table 2)

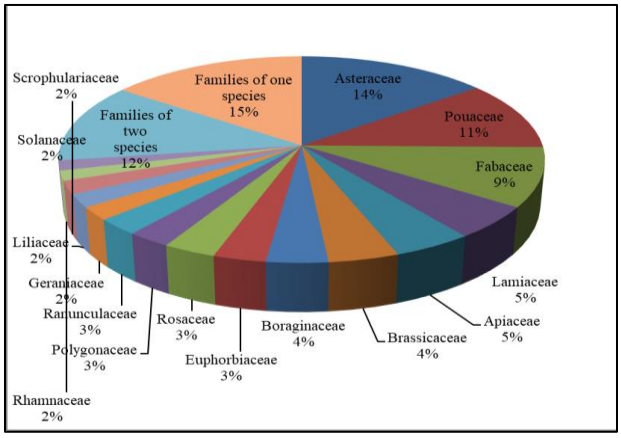

Figure (3) Percentage of species recorded in each family

Table (2) List of plant species in the study area.

No.	Family	Scientific name	Life Forms	Serial number
1	Adiantaceae	*Adiantum capillus-veneris* L.	He	8.1.1
2	Anacardiaceae	*Pistacia lentiscus* L.	Ph	73.1.2
3	Alliaceae	*Allium roseum* L.	G	146.1.5
4	Amaryllidaceae	*Narcissus elegans* (Haw.) Spach.	G	148.2.1
5	Apocynaceae	*Nerium oleander* L.	N. Ph	109.1.1
6	Apiaceae	*Ammi majus* L.	Th	102.24.1
7		*Apium nodiflorum* (L.) Lag	Th	102.21.2
8		*Foeniculum vulgare* Philip Miller.	G	102.15.1
9		*Pimpinella peregrina* L.	Th	102.11.1
10		*Pituranthos denudatus* Viv.	Ch	102.10.2
11		*Scandix pecten-veneris* L.	Th	102.4.2
12		*Smyrnium olusatrum* L.	Ch	102.8.1
13		*Thapsia garganica* L.	Ch	102.33.1
14		*Torilis leptophylla* (L.) Reichb.	Th	102.34.4
15	Araceae	*Arisarum vulgare* Targ. Tozz.	G	155.3.1
16		*Arum cyrenaicum* Hruby.	G	155.1.1
17	Arecaceae	*Phoenix canariensis* Chaub.	Ph	145.1.2
18	Asteraceae	*Anthemis pseudocotula* Boiss.	Th	135.32.4
19		*Bellis sylvestris-cyrenaica* Cyr.	H	135.1.2
20		*Chrysanthemum coronarium* L.	Th	135.40.2
21		*Cicerbita haimanniana* (Ascherson.) Beauverd.	G	135.93.1
22		*Cirsium creticum* (Lam.) D'Urv.	Ch	135.56.2
23		*Conyza aegyptiaca (*L.) Dryander.	Th	135.2.4
24		*Crepis senecioides* Delile.	Th	135.96.6
25		*Cynara cyrenaica* Weiller.	Th	135.61.4
26		*Echinops cyrenaicus* Durand &Barratte.	Th	135.54.3
27		*Evax contracta* Boiss.	Th	135.7.3
28		*Helichrysum stoechas* (L.) Moench.	Ch	135.11.1
29		*Hedypnois rhagadioloides* (L.) F.W Schmidf.	Th	135.79.1
30		*Leontodon tuberosus* L.	G	135.83.3
31		*Notobasis syriaca* (L.) Cass.	Th	135.57.1
32		*Onopordum arenarium* (Desf.) Pomel	Th	135.60.3
33		*O. cyrenaicum* Maire & Weiller.	Th	135.60.4
34		*Pallenis spinosa* (L.) Cass.	H	135.25.1
35		*Phagnalon rupestre* (L.) DC.	Ch	135.13.2
36		*Picris altissima* Delile, Descr.	Th	135.84.4
37		*P. hispanica* (Willd) P.D.Sell	Ch	135.84.6
38		*Ptilostemon gnaphaloides* (Cyr.) Sojak.	Ch	135.58.1
39		*Senecio leucanthemifolius* Poiret.	Th	135.49.2
40		*S. leucophylla* (DC.) Plelser.	--	135.49.
41		*Scolymus hispanicus* L.	Th	135.73.1
42		*Silybum marianum* (L.) Gaertner.	Th	135.62.1
43		*Sonchus oleraceus* L.	Th	135.91.3
44		*Tyrimnus leucographus* (L.) Cass.	Ch	135.59.1
45		*Xanthium spinosum* L.	Th	135.30.1
46	Boraginaceae	*Anchusa hybrida* Ten.	H	116.5.3
47		*Borago officinalis* L.	Th	116.3.1
48		*Cerinthe major* L.	Th	116.13.1
49		*Cynoglossum cheirifolium* L.	Ch	116.17.1

50		*Echium angustifolium* Mill.	Ch	116.12.3
51		*E. sabulicola* Pomel.	Th	116.12.11
52		*Heliotropium europaeum* L.	Th	116.15.7
53	Brassicaceae	*Biscutella didyma* L.	Th	52.32.1
54		*Enarthrocarpus clavatus* Del ex Godr.	Th	52.8.3
55		*E. pterocarpus* (Pers.) DC.	Th	52.8.2
56		*E. strangulatus* Boiss.	Th	52.8.1
57		*Nasturtium officinale* R.Br.	Hy	52.47.1
58		*Raphanus raphanistrum* L.	Th	52.7.1
59		*Sinapis alba* L.	Th	52.3.3
60		*S. flexuosa* Poiret.	Th	52.3.4
61	Cactaceae	*Opuntia ficus-indica* (L.) Mill.	--	37.1.3
62	Caesalpiniaceae	*Ceratonia siliqua* L	Ph	61.1.1
63	Campanulaceae	*Campanula erinus* L.	Th	134.1.2
64	Capparaceae	*Capparis spinosa* L	H	51.1.3
65	Caprifoliaceae	*Lonicera etrusca* Santi.	Ph	131.2.1
66		*Viburnum tinus* L.	Ph	131.1.1
67	Caryophylaceae	*Spergularia marina* (L.) Gariseb.	Th	33.4.2
68	Chenopodiaceae	*Chenopodium vulvaria* L.	Th	35.2.4
69	Clusiaceae	*Hypericum triquetrifolium* Turra.	H	47.1.1
70	Covolvulaceae	*Convolvulus althaeoides* L.	H	113.2.2
71	Crassulaceae	*Umbilicus horizontalis* (Guss.) DC.	G	54.2.3
	Cupressaceae	*Cupressus sempervirens.* *var.horizontalis* (Mill.)Gordon	Ph	15.1.1.b
72		*C. sempervirens* L. *var. Sempervirens*	Ph	15.1.1.a
73		*Thuja orientalis* L	Ph	15.3.1
74	Cyperaceae	*Cyperus alternifolius* L.	G	159.2.4
75	Dipsacaceae	*Scabiosa arenaria* Forskal.	Th	133.2.6
76	Epheraceae	*Ephedra alata* Desf.	Ch	16.1.1
77	Euphorbiaceae	*Andrachne telephioides* L.	H	68.1.1
78		*Euphorbia characias* L.	N. Ph	68.5.26
79		*E. dendroides* L.	Ph	68.5.5
80		*E. peplus* L.	Th	68.5.4
81		*Mercurialis annua* L.	Th	68.3.1
82		*Ricinus communis* L.	Ph	68.4.1
83	Fabaceae	*Anagyris foetida* L.	Ph	60.1.1
84		*Anthyllis tetraphylla* L.	Th	60.20.4
85		*Calicotome villosa* (poir)Link.	N. Ph	60.17.1
86		*Lathyrus aphaca* L.	Th	60.38.12
87		*L. gorgoni* Parl.	Th	60.38.6
88		*Lotus edulis* L.	Th	60.6.2
89		*Medicago lupulina* L.	Ch	60.31.1
90		*M. polymorpha* L.	Th	60.31.13
91		*Melilotus sulcatus* Desf.	Th	60.32.3
92		*Ononis natrix* L.	Ch	60.28.1
93		*O. spinosa* L.	H	60.28.5
94		*Robinia pseudoacaia* L.	Ph	60
95		*Tetragonolobus purpureas* Moench.	Th	60.18.1
96		*Trifolium campestre* Schreb.	Th	60.33.4
97		*T. nigrescens* Viv.	Th	60.33.2
98		*T. tomentosum* L.	Th	60.33.9
99		*Vicia monantha* Retz.	Th	60.34.3
100		*V.sativa* L.	Th	60.34.9
101	Fumariaceae	*Fumaria capreolata* L.	Th	49.1.5

102	Geraniaceae	*Erodium keithii* Guitt.	Th	64.2.11
103		*Geranium molle* L.	Th	64.47
104		*G. robertianum* L.	Th	64.4.2
105		*G. rotundifolium* L.	Th	64.4.6
106	Illecebraceae	*Paronychia arabica* (Linn.) DC.	Th	34.4.4
107		*P. argentea* Lamk.	H	34.4.5
108	Iridaceae	*Iris germanica* L.	G	150.2.1
109		*Romulea bulbocodium* (L.) Seb.	G	150.4.1
110	Lamiaceae	*Ballota pseudo-dictamuns* (L.) Benth.	Ch	119.14.1
111		*Marrubium vulgare* L.	G	119.8.1
112		*Micromeria graeca* (L.) Benth ex Reichenb.	Ch	119.22.4
113		*M. nervosa* (Desf.) Benth.	Ch	119.22.1
114		*Nepeta scordotis* L.	Ch	119.19.2
115		*Origanum cyrenaicum* Beg.	Ch	119.20.3
116		*Phlomis floccosa* D.	N. Ph	119.13.1
117		*Prasium majus* L.	Ch	119.11.1
118		*Rosmarinus officinalis* L.	Ch	119.4.1
119		*Stachys tournefortii* Poiret.	Ch	119.15.1
120	Lauraceae	*Laurus nobilis* L.	Ph	39.1.1
121	Lemnaceae	*Lemna gibba* L.	Hy	156.1.2
122	Liliaceae	*Asparagus aphyllus* L.	G	145.14.2
123		*Bellevalia mauritanica* L.	G	145.11.4
124		*Ornithogalum umbellatum* L.	G	145.10.3
125		*Urginea maritim*a (L.) Baker.	G	145.8.1
126	Malvaceae	*Malva nicaeensis* All.	Th	83.2.4
127		*M. parviflora* L.	Th	83.2 5
128	Mimosaceae	*Acacia farnesiana* (L.) Willd.	Ph	62.1.4
129		*A. cyanophylla* Lindley.	Ph	62.1.5
130	Moraceae	*Ficus carica L.*	Ph	22.2.2
131	Myrtaceae	*Eucalyptus gomphocephala* DC.	Ph	96.4.2
132	Oleaceae	*Olea europaea* L.	Ph	107.1.1
133	Orchidaceae	*Orchis Cyrenaica* Dur. &Barr.	G	163.4.5
134	Oxalidaceae	*Oxalis pes-caprae* L.	G	63.1.2
135	Papaveraceae	*Papaver rhoeas* L.	Th	48.3.4
136	Pinaceae	*Pinus halepensis* Mill.	Ph	14.1.2
137	Polygonaceae	*Polygonum argyrocoleon* Steud.	Th	26.5.3
138		*P. balansae* Boiss.	H	26.5.6
139		*P. equisetiforme* Sibth & Sm.	H	26.5.7
140		*P. patulum* M. Bieb.	Th	26.5.2
141		*Rumex pulcher* L.	Th	26.4.3
	Primulaceae	*Anagallis arvensis* L. *var arvensis*	Th	104.5.2 a
142		*A. arvensis* L. *var caerulea* (L.) Gouan	Th	104.5.2 b
143		*Cyclamen rohlfsianum* Aschers.	G	104.1.1
144	Poaceae	*Avena sterillis* L.	Th	153.37.5
145		*Briza maxima* L.	Th	153.21.2
146		*Bromus alopecuros* Poir.	Th	153.26.7
147		*B. madritensis* L.	Th	153.26.3
148		*Catapodium rigidum* (L.) C.E.Hubbard.	Th	153.9.1
149		*Cynosurus elegans* Desf.	Th	153.19.3
150		*Dactylis glomerata* L.	G	153.16.1
151		*Gastridium scabrum* C. Presl.	Th	153.48.2
152		*Hordeum murinum* L.	Th	153.32.2
153		*Lamarckia aurea* (L.) Moench.	Th	153.20.1
154		*Lolium loliaceum (*Bory et Chaub.)	Th	153.4.4

		Hand.Mazz.		
155		*L. multiflorum* Lam.	Th	153.4.2
156		*Lophochloa salzmanni (*Boiss.) H. Scholz	Th	153.40.2
157		*Melica minuta* L.	H	153.35.1
158		*Phalaris minor* Retz.	Th	153.54.5
159		*Piptatherum miliaceum* (L.) Coss.	H	135.61.1
160		*P. holciforme* (Bieb.) Roem. et Schult.	H	135.61.3
161		*Poa annua* L.	Th	153.18.7
162		*P. trivialis* L.	H	153.18.2
163		*Polypogon semiverticillatus* (Forsk.) Hyl.	H	153.47.3
164		*Trisetaria macrochaeta* (Boiss.) Maire.	Th	153.39.1
165	Urticaceae	*Parietaria judaica* L.	H	23.1.3
166		*Urtica pilulifera* L.	Th	23.2.1
167	Ranunculaceae	*Adonis microcarpa* DC.	Th	40.7.3
168		*Ranunculus asiaticus* L.	G	40.8.12
169		*R. bullatus ssp. cyrenaicus* (Pamp.) Maire.	Ch	40.8.5
170		*R. cyclocarpus* Pamp.	Th	40.8.11
171		*R. trilobus* Desf.	Th	40.8.6
172	Resedaceae	*Reseda alba* L.	Th	53.5.8
173		*R. lutea* L.	Th	53.5.9
174	Rhamnaceae	*Rhamnus alaternus ssp alateinus* L.	N. Ph	80.3.1
175		*R. lyciodes* L.	Ph	80.3.2
176		*R. oleoides* L.	N. Ph	80.3.3
177	Rubiaceae	*Galium aparine* L.	Th	111.4.3
178		*Sherardia arvensis* L.	Th	111.6.1
179	Rosaceae	*Potentilla reptans* L.	Ch	58.9.1
180		*Prumus amygdalus* Batsch.	--	58.2.
181		*Rosa deseglisei* Boreau.	--	58.12.2
182		*Rubus sanctus* Schreber.	N. Ph	58.7.1
183		*Sanguisorba minor* Scop.	H	58.11.9
184		*Sarcopoterium spinosum* (L.) Spach.	Ch	58.10.1
185	Scrophulariaceae	*Kickxia commutata* (Bernh.ex rcichenb.) Fritsch	Th	58.10.1
186		*Scrophularia canina* L.	Ch	122.1.3
187		*Veronica anagallis-aquatica* L.	Ch	122.2.1
188		*Verbascum sinuatum* L.	Ch	122.3.2
189	Solanaceae	*Datura innoxia* Mill.	Ch	120.9.4
190		*Nicotiana glauca* Graham.	N. Ph	120.5.1
191		*Solanum nigrum var nigrum* L.	Th	120.2.2.a
		S. nigrum var villosum L.	Th	120.2.2.b
192	Valerianaceae	*Centranthus calcitrapae* (L.) Dufresne.	Th	132.3.1
193		*Fedia cornucopiae* (L). Gaertner.	Th	132.2.1
194	Verbenaceae	*Verbena officinalis* L.	H	117.2.2

Figure (4) shows the life forms of the recorded species according to Raunkiaer (1934). The recorded species belong to ten different life forms. Therophytes (48%) includes 93 species, and were represented by the largest number of species. Of these were *Borago officinalis* L. *Sinapis alba* L. *Xanthium spinosum* L., *Notobasis syriaca* (L.) Cass., *Evax contracta* Boiss., *Scandix pecten-veneris* L., *Ammi majus* L., *Scabiosa arenaria* Forskal., *Chenopodium vulvaria* L. Chamaephytes has 29 species representing about (15%), among these species were *Onopordum arenarium* (Desf.) Pomel., *Phagnalon rupestre* (L.) DC., *Ephedra alata* Desf.,

Andrachne telephioides L., *Medicago lupulina* L. Geophytes represents about (11%), includes 21 species representing these species were, *Cyperus alternifolius* L., *Allium roseum* L., *Arum cyrenaicum* Hruby., Hemicryptophytes (10%) include 19 species, of these were *Bellis sylvestris-cyrenaica* Cyr., *Anchusa hybrida* Ten., also Phanerophyes (10%)includes 20 species, from these species are *Pinus halepensis* Mill. *Olea europaea* L. Nano-phanerophytes has 8 species representing about (4%), such as *Rhamnus alaternus ssp alateinus* L., Hydrophytes includes 2 species, as for Heleophytes has 1 species .

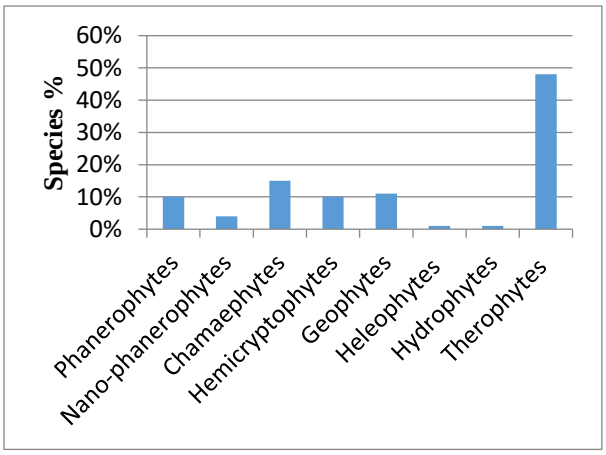

Figure (4) Life forms of the recorded species.

4 Discussion

floristic composition and vegetation analysis studies were becoming increasingly important to provide important critical data for understanding biodiversity and ecosystem functioning in these areas (Heywood, 2004). Since ancient times, Al-Jabal Al-Akhdar has been the focus because of its unique and diverse vegetation (Alzerbi & Alaib, 2017)., which reflects the biological diversity of plant life in a distinct way (Noah, 2014). This was shown by the results of the survey in the study area, which includes 194 species, 160 genera, and 75 families. The Asteraceae was the largest family in the flora of Libya, followed by Poaceae, and Fabaceae (Jafri & El-Gadi, 1977-1993). The survey results showed the dominance of Asteraceae (14%) with 28 species, followed by Poaceae (11%) represented by 21 species, then Fabaceae (9%) represented by 18 species, the results we obtained about these families' dominance were expected given that the study area was within the Mediterranean climate since these families typically dominate the communities in habitats that were influenced by this climate. Furthermore, these families are cosmopolitan in distribution (Mahklouf et al., 2020), and it was noted that there was a similarity in the results with the previous studies in Al-Jabal Al-Akhdar areas such as Al Mansora and Jarjar oma regions (Dahkel, 2014), Boras region (Alzerbi & Alaib., 2017), Al-Agar Valley (Alaib et al., 2017). The results of the survey showed dominance Therophytes (48%) includes 93 species, followed by Chamaephytes, which has 29 species representing about (15%) then Geophytes represent about (11%) including 21 species, and it was noted that there was a similarity in the results with the previous studies (Dahkel,2014) in Al Mansora and Jarjar oma regions , (Omar et al ., 2020) in Wadi Al-Hamar and (El-Darier & El-Mogaspi, 2009) in Al-Jabal Al-Akhdar areas, cold winter in the region may explain why Therophytes were dominant followed by Chamaephytes (Whitaker,1975). study (Mahklouf & Sh-hoob, 2023), also proved that there was a clear positive relationship between Therophytes and the Mediterranean climate because species the Therophytes annual complete their life cycle in a single season and can adapt to high temperatures and the dry summer in The Mediterranean climate which represents the climate of the study area.

5 Conclusion

The floristic composition in Cyrene (campus apollo) ShahatAL-Jabal AL-Akhdar, Libya displayed the presence of 194 plant species belonging to 57 families. The current study aimed to the initial inventory of the types of plants in the region defining them, preparing a list of them, and distributing these plants within groups such as species, genera, and different life forms. The methods developed during the study can be used as a basis for carrying out similar studies and for helping to devise management and conservation programs. In the study area, the major vegetation types, their composition and biodiversity were identified.

Conflict of interest: The authors declare that there are no conflicts of interest

References

Alaib, M. A., El-Sherif, I., & Al-Hamedi, R. I. (2017). Floristic and ecological investigation of Al-Agar Valley in Al-Jabal Al-Akhdar area. *Libya. Sci Appl*, *5*(1), 57-61.

Al-Traboulsi, M., & Alaib, M. A. (2021). A Survey of Medicinal Plants of Wadi Al-Kouf in Al-Jabal Al-Akhdar, Libya. *Natura Croatica: Periodicum Musei Historiae Naturalis Croatici*, *30*(2), 389-404.

Alzerbi, A., & Alaib, M. (2017). Study of vegetation in Sedy Boras region in Al-Jabal Al-Akhdar-Libya. *Journal of Environmental Science and Engineering.;* 1(1), 67–72.

Bano, S., Khan, S. M., Alam, J., Alqarawi, A. A., Abd_Allah, E. F., Ahmad, Z., & Hashem, A. (2018). Eco-Floristic studies of native plants of the Beer Hills along the Indus River in the districts Haripur and Abbottabad, Pakistan. *Saudi journal of biological sciences*, 25(4), 801-810.

Boulos, L. (1972). Our present knowledge on the Flora and vegetation of Libya bibliography. *Webbia*, *26*(2), 365-400.

Dahkel, E. (2014). Habitats and plant diversity of Al Mansora and Jarjar oma regions in Al-Jabal Al-Akhdar – Libya.

El-Darier, S. M., & El-Mogaspi, F. M. (2009). Ethnobotany and relative importance of some endemic plant species at El-Jabal El-Akhdar Region (Libya). *World Journal of Agricultural Sciences*, *5*(3), 353-360.

Ferreira, E. V. R., Prata, A. P. D. N., & Mello, A. A. D. (2013). Floristic list from a caatinga remnant in Poço Verde, Sergipe, Brazil.

Heywood, V. H. (2004). Modern approaches to floristics and their impact on the region of SW Asia. *Turkish Journal of Botany*, *28*(1), 7-16.

Ilyas, M., Qureshi, R., Arshad, M., & Mirza, S. N. (2013). A Preliminary checklist of the vascular flora of Kabal Valley, Swat, Pakistan. *Pak. J. Bot*, 45(2), 605-615.

Jafri, S. M. and El-Gadi, A. A. (Eds) (1977-1993). Flora of Libya. Department, Faculty of Sci., Tripoli Univ., Libya.

Keith, D. A. (1988). Floristic lists of New South Wales (III). *Cunninghamia*, 2(1), 39-73.

Lemaire, (1703) Les antiquites de la cyrenaiqne ouil est aussi question du “seltion” que M. Bonnet areconnu etra le *Phlomis floccosa*.

Mahklouf, M. H., & Sh-hoob, M. (2023). Floristic Study of Al-Orban area in Gharyan District-Libya. *Scientific Journal for Faculty of Science-Sirte University*, *3*(2), 29-43.

Mahklouf, M.H., Shanta, M. B., & El-ahmir, M.S. (2020). Floristic Study of Sedrores Mountains in Gharyan District – Libya. *Journal Of Advanced Zoology*,8(1),1-6.

Martínez-Calderón, V. M., Siqueiros-Delgado, M. E., & Martínez-Ramírez, J. (2017). Checklist of the genus Quercus (Fagaceae) of Aguascalientes, México. *Check List*, 13(1), 2045-2045.

Melchoir, H. A. (1964). *Engler’s syllabus der Pflanzenfamilien*, [12th ed]., part II, Borntraeger, Berlin.

Mukassabi, T. A., Ahmidat, G., Sherif, I. M., & Thomas, P. A. (2012). Checklist and life forms of plant species in contrasting climatic zones of Libya. *Biyolojik Çeşitlilik ve Koruma*, *5*(3), 1-12.

Noah, S. (2014). Geographical distribution of natural vegetation in Al-Jabal Al Akhdar area (Libya). *Scientific Journal of the College of Arts, Omar Al-Mukhtar University*. 28, 1483-1500.

Omar, N., Alaib, M., El-Mghrbi, N., & Alzerbi, A. (2020). Checklist of Flora and Floristic Study of Wadi Al-Hamar Region in Libya. *Journal of Umm Al-Qura University for Applied Science.*; 6 (2), 20-24.

Omar, N., El-Mghrbi, N. G., Rebeh, O. R., Alaib, M. A., & Abdul Hamid, K. A. (2021). Floristic Composition and Plant Diversity of Western Part of Wadi ElEnaghar, Libya. *Species*, *22*(70), 204-217.

Raunkiaer, C. (1934). The life forms of plants and statistical plant geography; being the collected papers of C. Raunkiær. *The life forms of plants and statistical plant geography; being the collected papers of C. Raunkiaer*.

Shehata, H. S., & Galal, T. M. (2015). Factors affecting the distribution and associated species of M alva parviflora in the N ile D elta, E gypt. *Weed Biology and Management*, *15*(1), 42-52.

Whitaker, R. (1975). Communities and ecosystems. Macmillan Co. Coiinc, New York.

Scientific Journal for the Faculty of Science-Sirte University Vol. 4, No. 1 (2024) 45-49

Scientific Journal for the Faculty of Science-Sirte University

Journal home page: http://journal.su.edu.ly/index.php/JSFSU/index

DOI: 10.37375/issn.2789-858X

On Some of Classes of $\mathcal{p}-$ Valent $\beta-$ Uniformly Functions

A. A. Hussain

Mathematics Department, Education Faculty, Sirte University, Libya.

DOI: https://doi.org/10.37375/sjfssu.v4i1.1671

ARTICLE INFO:

Received: 16 September 2023

Accepted: 27 March 2024

Published: 17 April 2024

Keywords: Analytic Functions, $p-$ valent β-Uniformly Functions, $\mathcal{p}$- valent Convex functions.

A B S T R A C T

We focus on the properties of some famous analytical functions. We introduce the classes of *p*- Valent β-uniformly Starlike functions of order α and *p* – Valent β-uniformly Convex functions of order α We come out with new characterization theorems and closure theorems for functions belonging to these classes. Also, we gain radius of p -Valent convexity for functions belonging to the class *p*-valent β-uniformly Convex functions of order α. We insert some notes to explain the evidence of our work.

1 Introduction

The class of analytic functions and $\mathcal{p}$ -valent functions in the open deleted unit disk $\mathbb{U} = \{z \in \mathbb{C}: 0 < |z| < 1\}$ has the form:

$$f(z) = z^{\mathcal{p}} + \sum_{k=1}^{\infty} a_{\mathcal{p}+k} z^{\mathcal{p}+k} (\mathcal{p} \in \mathbb{N}, \mathbb{N} = \{1,2, \dots\}), \qquad (1)$$

represented by $\mathcal{A}(\mathcal{p})$.

We have some notes:

Note 1: $\mathcal{A}(\mathcal{p}) = \mathcal{A}(1)$.

Note 2: If the function $f(z) \in \mathcal{A}(\mathcal{p})$ satisfies the following conditions should be $\mathcal{p}-$valent starlike of order α:

$$Re\left\{\frac{zf'(z)}{f(z)}\right\} > \alpha \ (0 \le \alpha < \mathcal{p}, \mathcal{p} \in \mathbb{N}; z \in \mathbb{U}). \qquad (2)$$

We denote the class of $\mathcal{p} -$ valent starlike functions of order α by $\mathcal{S}_{\mathcal{p}}(\alpha)$.

Note 3: If the function $f(z) \in \mathcal{A}(\mathcal{p})$ satisfies the following conditions, it is called α-order *p*-valent convexity:

$$Re\left\{1 + \frac{z\,f''(z)}{f'(z)}\right\} > \alpha \ (0 \le \alpha < \mathcal{p}, \mathcal{p} \in \mathbb{N}; z \in \mathbb{U}) \quad (3)$$

We denote the class of $\mathcal{p}-$valent convex functions of order α by $\mathcal{K}_{\mathcal{p}}(\alpha)$.

The classes $\mathcal{S}_{\mathcal{p}}(\alpha)$ and $\mathcal{K}_{\mathcal{p}}(\alpha)$ were investigated by (Patil and Thakare, 2011) and (Owa, 1985). Further from (2) and (3), we can see that

$$f(z) \in \mathcal{K}_{\mathcal{p}}(\alpha) \Leftrightarrow \frac{z\,f'(z)}{\mathcal{p}} \in \mathcal{S}_{\mathcal{p}}(\alpha) \ (0 \le \alpha < \mathcal{p}, \mathcal{p} \in \mathbb{N}).$$

For functions $f(z) \in \mathcal{A}$ and $\beta \ge 0$, (Kanas and Wisniowska, 1999& 2000) defined the classes $\beta - \mathcal{UCV}$ and $\beta - \mathcal{ST}$ of $\beta-$unifomly convex and $\beta-$uniformly star like functions, respectively, see (Kanas, 1999) and (Kanas and Srivastava, 2000).

(Marouf, 2009) with $l = 2, m = 1, \alpha_1 = \beta_1$ *and* $\alpha_2 = 1$] and (Salim et al., 2011), with $n = 2$] checked the classes $\beta - \mathcal{S}_{\mathcal{p}}(\alpha)$ and $\beta - \mathcal{K}_{\mathcal{p}}(\alpha)$ for $f(z) \in \mathcal{A}(\mathcal{p})$. $\mathcal{p}-$valent $\beta-$uniformly star like and $\mathcal{p}-$ valent $\beta-$uniformly convex of order $\alpha \ (0 \le \alpha < \mathcal{p})$ are as follows:

Corresponding author: E-mail: aisha84_hussain@yahoo.com

Definition1 (Marouf, 2009 & Salim et al., 2011). *For* $0 \le \alpha < \mathcal{p}, \beta \ge 0, \mathcal{p} \in \mathbb{N}$ *and* $z \in \mathbb{U}$ *, let* $\beta - \mathcal{S}_{\mathcal{p}}(\alpha)$ *be the class of* $f(z) \in \mathcal{A}(\mathcal{p})$ *which satisfy:*

$$Re\left\{\frac{z\,f'(z)}{f(z)} - \alpha\right\} > \beta\left|\frac{z\,f'(z)}{f(z)} - \mathcal{p}\right|. \quad (4)$$

Definition 2 (Marouf, 2009 & Salim et al., 2011). *For* $0 \le \alpha < \mathcal{p}, \beta \ge 0, \mathcal{p} \in \mathbb{N}$ *and* $z \in \mathbb{U}$ *, let* $\beta - \mathcal{K}_{\mathcal{p}}(\alpha)$ *be the class of* $f(z) \in \mathcal{A}(\mathcal{p})$ *which satisfy:*

$$Re\left\{1 + \frac{z\,f''(z)}{f'(z)} - \alpha\right\} > \beta\left|\frac{z\,f''(z)}{f'(z)} - \mathcal{p}\right|. \quad (5)$$

From (4) and (5) we get

$$f(z) \in \beta - \mathcal{K}_{\mathcal{p}}(\alpha) \Leftrightarrow \frac{z\,f'(z)}{\mathcal{p}} \in \beta - \mathcal{S}_{\mathcal{p}}(\alpha).$$

We have noticed: for $\beta = 1$ the above classes were investigated by (Al-Kharsani and Al-Hajiry, 2008).
By taking $\beta = 0$ in (4) and (5), we obtain classes $\mathcal{S}_{\mathcal{p}}(\alpha)$ and $\mathcal{K}_{\mathcal{p}}(\alpha)$ of $\mathcal{p}-$ valence starlike functions of order $(0 \le \alpha < \mathcal{p})$ and $\mathcal{p}-$ valence convex functions of order $\alpha\,(0 \le \alpha < \mathcal{p})$ which were introduced and studied by (Patil and Thakare, 1983) and (Owa, 1983).

Denote by $\mathcal{T}(\mathcal{p})$ the subclass of $\mathcal{A}(\mathcal{p})$ contains functions of the form:

$$f(z) = z^{\mathcal{p}} - \sum_{k=1}^{\infty} a_{\mathcal{p}+k} z^{\mathcal{p}+k} \left(a_{\mathcal{p}+k} \ge 0, \mathcal{p} \in \mathbb{N}\right), \quad (6)$$

and define two further classes:

$$\mathcal{TS}_{\mathcal{p}}(\alpha, \beta) = \beta - \mathcal{S}_{\mathcal{p}}(\alpha) \cap \mathcal{T}(\mathcal{p})$$

and

$$\mathcal{TK}_{\mathcal{p}}(\alpha, \beta) = \beta - \mathcal{K}_{\mathcal{p}}(\alpha) \cap \mathcal{T}(\mathcal{p}).$$

In this paper to prove the main results, we need the next lemmas given by (Marouf ,2009), with $l = 2$, $m = 1, \alpha_1 = \beta_1$ *and* $\alpha_2 = 1$ and (Salim et al.,2011) with $n = 2$.

Lemma1. *See* (Marouf, 2009) and (Salim et al., 2011). *A function* $f(z)$ *in (6) belongs to* $\mathcal{TS}_{\mathcal{p}}(\alpha, \beta)$ *if it satisfies:*

$$\sum_{k=1}^{\infty} [(\mathcal{p} + k)(1 + \beta) - (\alpha + \mathcal{p}\beta)] a_{\mathcal{p}+k} \le \mathcal{p} - \alpha.$$

Lemma2. *See* (Marouf, 2009) and (Salim et al., 2011). *A function* $f(z)$ *in (6) belongs to* $\mathcal{TK}_{\mathcal{p}}(\alpha, \beta)$ *if it satisfies:*

$$\sum_{k=1}^{\infty} \left(\frac{\mathcal{p} + k}{\mathcal{p}}\right) [(\mathcal{p} + k)(1 + \beta) - (\alpha + \mathcal{p}\beta)] a_{\mathcal{p}+k} \le \mathcal{p} - \alpha.$$

Notably, a function $f(z)$ in (6) and belongs to $\mathcal{TS}_{\mathcal{p}}(\alpha, \beta)$. Lemma 1 immediately yields

$$a_{\mathcal{p}+1} \le \frac{\mathcal{p}-\alpha}{(1+\beta)+(\mathcal{p}-\alpha)}, \quad (7)$$

While a function $f(z)$ in (6) which belongs to $\mathcal{TK}_{\mathcal{p}}(\alpha, \beta)$, Lemma 2 immediately yields

$$a_{\mathcal{p}+1} \le \frac{\mathcal{p}(\mathcal{p}-\alpha)}{[(\mathcal{p}+1)(1+\beta)-(\mathcal{p}-\alpha)]}. \quad (8)$$

By taking into account the inequalities (7) and (8), respectively, it seems to be important to introduce two classes, $\mathcal{TS}_{\mathcal{p}}(\alpha, \beta)$ and $\mathcal{TK}_{\mathcal{p}}(\alpha, \beta)$ of uniformly $\mathcal{p}$ −valente functions; $\mathcal{TS}_{\mathcal{p},\gamma}(\alpha, \beta)$ denotes the subclass of $\mathcal{TS}_{\mathcal{p}}(\alpha, \beta)$ contains of functions of the form

$$f(z) = z^{\mathcal{p}} - \frac{(\mathcal{p}-\alpha)\gamma}{[(1+\beta)+(\mathcal{p}-\alpha)]} z^{\mathcal{p}+1} - \sum_{k=2}^{\infty} a_{\mathcal{p}+k} z^{\mathcal{p}+k}, \quad (9)$$

$$a_{\mathcal{p}+k} \ge 0, \mathcal{p} \in \mathbb{N}, 0 \le \alpha < \mathcal{p}, \beta \ge 0, 0 \le \gamma < 1.$$

And $\mathcal{TK}_{\mathcal{p},\gamma}(\alpha, \beta)$ denotes the subclass of $\mathcal{TK}_{\mathcal{p}}(\alpha, \beta)$ consists of functions of the form

$$f(z) = z^{\mathcal{p}} - \frac{\mathcal{p}(\mathcal{p}-\alpha)\gamma}{(\mathcal{p}+1)[(1+\beta)+(\mathcal{p}-\alpha)]} z^{\mathcal{p}+1} - \sum_{k=2}^{\infty} a_{\mathcal{p}+k} z^{\mathcal{p}+k}, \quad (10)$$

$a_{\mathcal{p}+k} \ge 0,\ \mathcal{p} \in \mathbb{N}, 0 \le \alpha < \mathcal{p},\ \beta \ge 0, 0 \le \gamma < 1.$

We note that:
(i) $\mathcal{TS}_{\mathcal{p},\gamma}(\alpha, 0) = \mathcal{T}_{\gamma}^{*}(\mathcal{p}, \alpha,)$ *and* $\mathcal{TK}_{\mathcal{p}}(\alpha, 0) = \mathcal{C}_{\gamma}(\mathcal{p}, \alpha,)$ (see Aouf et al., 2000).

In addition, one can see (Aouf et al., 2016) and (Alharayzeh, and Ghanim 2022).

2 Characterization Theorems for the Classes $\mathcal{TS}_{\mathcal{p},\gamma}(\alpha, \beta)$ and $\mathcal{TK}_{\mathcal{p},\gamma}(\alpha, \beta)$

Throughout our present paper, we assume that:

$$\mathcal{p} \in \mathbb{N}, 0 \le \alpha < \mathcal{p}, 0 \le \gamma < 1 \text{ and } z \in \mathbb{U}.$$

Firstly, we must prove the following theorem.

Theorem1. Suppose that $f(z)$be defined by (9). Then $f(z) \in \mathcal{S}_{p,\gamma}(\alpha,\beta)$ if it satisfies*:*

$$\sum_{k=2}^{\infty}[(p+k)(1+\beta)-(\alpha+p\beta)]a_{p+k} \leq (p-\alpha)(1-\gamma). \quad (11)$$

The above result (11) is conclusive for $f(z)$ of the form

$$f(z) = z^{p} - \frac{(p-\alpha)\gamma}{[(1+\beta)+(p-\alpha)]}z^{p+1} - \frac{(p-\alpha)(1-\gamma)}{[(p+k)(1+\beta)-(\alpha+p\beta)]}z^{p+k}.$$

Proof.

By setting

$$a_{p+1} = \frac{(p-\alpha)\gamma}{[(1+\beta)+(p-\alpha)]}$$

in Lemma1 and simplifying the inequality (7), we arrived at the assertion (11) of Theorem1. ■

If we set

$$a_{p+1} = \frac{p(p-\alpha)\gamma}{(p+1)[(1+\beta)+(p-\alpha)]}$$

in Lemma 2, we similarly get the next theorem.

Theorem 2. Suppose that $f(z)$ is defined by (*10*). Then $f(z) \in \mathcal{TK}_{p}(\alpha,\beta)$ if satisfies:

$$\sum_{k=2}^{\infty}\left(\frac{p+k}{p}\right)[(p+k)(1+\beta)-(\alpha+p\beta)]a_{p+k} \leq (p-\alpha)(1-\gamma).$$

Theorem2 is conclusive for $f(z)$ of the form

$$f(z) = z^{p} - \frac{p(p-\alpha)\gamma}{(p+1)[(1+\beta)+(p-\alpha)]}z^{p+1} - \frac{p(p-\alpha)(1-\gamma)}{[(p+k)(1+\beta)-(\alpha+p\beta)]}z^{p+k}$$

3 Closure Theorems for the $\mathcal{TS}_{p,\gamma}(\alpha,\beta)$ and $\mathcal{TK}_{p,\gamma}(\alpha,\beta)$

The closure theorem for the $\mathcal{TS}_{p,\gamma}(\alpha,\beta)$ is given by next theorem**.**

Theorem 3 . *Let*

$$f_j(z) = z^{p} - \frac{(p-\alpha)\gamma}{[(1+\beta)+(p-\alpha)]}z^{p+1} - \sum_{k=2}^{\infty}a_{p+kj}z^{p+k} \quad (a_{p+kj} \geq 0; j = 1,\dots,m).$$

If $f_j(z) \in \mathcal{TS}_{p,\gamma}(\alpha,\beta)(j=1,\dots,m)$**,** *and the function* $g(z)$ *given by*

$$g(z) = z^{p} - \frac{(p-\alpha)\gamma}{[(1+\beta)+(p-\alpha)]}z^{p+1} - \sum_{k=2}^{\infty}b_{p+k}z^{p+k}$$

with

$$b_{p+k} = \frac{1}{m}\sum_{j=1}^{m}a_{p+kj} \geq 0, \quad (12)$$

then $g(z) \in \mathcal{TS}_{p,\gamma}(\alpha,\beta)$.

Proof: Because $f_j(z) \in \mathcal{TS}_{p,\gamma}(\alpha,\beta)(j=1,\dots,m)$, from Theorem1, we have

$$\sum_{k=2}^{\infty}[(p+k)(1+\beta)-(\alpha+p\beta)]a_{p+kj} \leq (p-\alpha)(1-\gamma)(j=1,\dots,m).$$

Using (12), we get

$$\sum_{k=2}^{\infty}[(p+k)(1+\beta)-(\alpha+p\beta)]b_{p+k}.$$

$$= \sum_{k=2}^{\infty}[(p+k)(1+\beta)-(\alpha+p\beta)]\left(\frac{1}{m}\sum_{j=1}^{m}a_{p+kj}\right)$$

$$= \frac{1}{m}\sum_{j=1}^{m}\left(\sum_{k=2}^{\infty}[(p+k)(1+\beta)-(\alpha+p\beta)]a_{p+kj}\right) \leq (p-\alpha)(1-\gamma).$$

Then by Theorem1, $g(z) \in \mathcal{TS}_{p,\gamma}(\alpha,\beta)$, which completing the proof■

Theorem 4. *Let*

$$f_j(z) = z^{p} - \frac{p(p-\alpha)\gamma}{(p+1)[(1+\beta)+(p-\alpha)]}z^{p+1} - \sum_{k=2}^{\infty}a_{p+kj}z^{p+k} \quad (a_{p+kj} \geq 0; j = 1,\dots,m)$$

If $f_j(z) \in \mathcal{TK}_{p,\gamma}(\alpha,\beta)(j=1,\dots,m)$**,** then $g(z)$ given by

$$g(z) = z^{p} - \frac{p(p-\alpha)\gamma}{(p+1)[(1+\beta)+(p-\alpha)]}z^{p+1} - \sum_{k=2}^{\infty}b_{p+k}z^{p+k}$$

with b_{p+k} defined by *(12)* belongs *to* $\mathcal{TK}_{p,\gamma}(\alpha,\beta)$.

Theorem 5. Let

$$f_{p+1}(z) = z^p - \frac{(p-\alpha)\gamma}{[(1+\beta)+(p-\alpha)]} z^{p+1} \quad (13)$$

and

$$f_{p+k}(z) = z^p - \frac{(p-\alpha)\gamma}{[(1+\beta)+(p-\alpha)]} z^{p+1} - \frac{(p-\alpha)(1-\gamma)}{[(p+k)(1+\beta)-(\alpha+p\beta)]} z^{p+k}. \quad (14)$$

Then $f(z) \in \mathcal{TS}_{p,\gamma}(\alpha,\beta)$ if and only if it has the form

$$f(z) = \sum_{k=1}^{\infty} c_{p+k} f_{p+k}(z) \left(c_{p+k} \geq 0; \sum_{k=1}^{\infty} c_{p+k} = 1 \right). \quad (15)$$

Proof. Suppose that $f(z)$ is given by (15), then from (13) and (14), we find that

$$f(z) = z^p - \frac{(p-\alpha)\gamma}{[(1+\beta)+(p-\alpha)]} z^{p+1} - \sum_{k=2}^{\infty} \frac{(p-\alpha)(1-\gamma)}{[(p+k)(1+\beta)-(\alpha+p\beta)]} c_{p+k} z^{p+k}$$

where

$$c_{p+k} \geq 0, \sum_{k=2}^{\infty} c_{p+k} = 1 - c_{p+1}.$$

Since

$$\sum_{k=2}^{\infty}[(p+k)(1+\beta)-(\alpha+p\beta)] \frac{(p-\alpha)(1-\gamma)}{[(p+k)(1+\beta)-(\alpha+p\beta)]} c_{p+k} = (p-\alpha)(1-\gamma)\sum_{k=2}^{\infty} c_{p+k} = (p-\alpha)(1-\gamma)(1-c_{p+1}) \leq (p-\alpha)(1-\gamma).$$

Then we conclude from Theorem1 that

$f(z) \in \mathcal{TS}_{p,\gamma}(\alpha,\beta)$.

Conversely, assume that $f(z)$ defined by (9) belongs to $\mathcal{TS}_{p,\gamma}(\alpha,\beta)$.

Then from (11), we have

$$a_{p+k} \leq \frac{(p-\alpha)(1-\gamma)}{[(p+k)(1+\beta)-(\alpha+p\beta)]} \ (k \in \mathbb{N} \setminus \{1\}).$$

Setting

$$c_{p+k} = \frac{(p-\alpha)(1-\gamma)}{[(p+k)(1+\beta)-(\alpha+p\beta)]} a_{p+k} \ (k \in \mathbb{N} \setminus \{1\}),$$

and

$$c_{p+1} = 1 - \sum_{k=2}^{\infty} c_{p+k}.$$

Here we come with (15). This completes the proof.

Theorem 6. *Let*

$$f_{p+1}(z) = z^p - \frac{p(p-\alpha)\gamma}{(p+1)[(1+\beta)+(p-\alpha)]} z^{p+1}$$

and

$$f_{p+k}(z) = z^p - \frac{p(p-\alpha)\gamma}{(p+1)[(1+\beta)+(p-\alpha)]} z^{p+1} - \frac{p(p-\alpha)(1-\gamma)}{[(p+k)(1+\beta)-(\alpha+p\beta)]} z^{p+k}$$

Then $f(z) \in \mathcal{KS}_{p,\gamma}(\alpha,\beta)$ if and only if it can be expressed in the form *(15).*

4 The Radius of $p-$ valent Convexity for the Class $\mathcal{TS}_{p,\gamma}(\alpha,\beta)$.

Here, we will prove the next theorem.

Theorem7 . Let $f(z) \in \mathcal{TS}_{p,\gamma}(\alpha,\beta)$, then $f(z)$ *is* $p-$ valent convex function of order

$\delta(0 \leq \delta < p \ in|z| < r_1 = r_1(p,\alpha,\beta,\delta,\gamma),$

where $r_1(p,\alpha,\beta,\delta,\gamma)$ is the largest value *of* r satisfies:

$$\frac{(p+1)(p-\alpha)[(1+\beta)+(p-\delta)]\gamma}{[(1+\beta)+(p-\alpha)]} r + \frac{[(p+k)(1+\beta)+(\delta+p\beta)](p-\alpha)(1-\gamma)}{[(p+k)(1+\beta)-(\alpha+p\beta)]} r^k \leq p(p-\delta)$$

$$(0 \leq \delta < p; p \in \mathbb{N}). \quad (16)$$

The result (16) is conclusive for $f_{p+k}(z)$ *given by (14).*

Proof. It is sufficient to show for $f(z) \in \mathcal{TS}_{p,\gamma}(\alpha,\beta)$, that

$$\left|1 + \frac{zf''(z)}{f'(z)} - p\right| \leq p - \delta, |z| < r_1(p,\alpha,\beta,\delta,\gamma),$$

where $r_1(p,\alpha,\beta,\delta,\gamma)$ is the largest value of r for which the inequality (16) holds true. For $f(z)$ in (9), we have

$$\left|1 + \frac{zf''(z)}{f'(z)} - p\right| \leq \frac{\frac{(p+1)(p-\alpha)\gamma}{[(1+\beta)+(p-\alpha)]} r + \sum_{k=2}^{\infty} k(p+k) a_{p+k} r^k}{p - \frac{(p+1)(p-\alpha)\gamma}{[(1+\beta)+(p-\alpha)]} r + \sum_{k=2}^{\infty}(p+k) a_{p+k} r^k},$$

thus

$$\left|1 + \frac{zf''(z)}{f'(z)} - p\right| \leq p - \delta, |z| < r(p,\alpha,\beta,\delta,\gamma),$$

if and only if

$$\frac{(\mathcal{p}+1)(\mathcal{p}-\alpha)(\mathcal{p}+1-\delta)\gamma}{[(1+\beta)+(\mathcal{p}-\alpha)]}r+$$

$$\sum_{k=2}^{\infty}(\mathcal{p}+k)(\mathcal{p}+k-\delta)a_{\mathcal{p}+k}r^{k}\leq \mathcal{p}(\mathcal{p}-\delta)(0\leq\delta<\mathcal{p}).$$

Since $f(z)\in\mathcal{TS}_{\mathcal{p},\gamma}(\alpha,\beta)$, in view of Theorem1, we may set

$$a_{\mathcal{p}+k}=\frac{(\mathcal{p}-\alpha)(1-\gamma)}{[(\mathcal{p}+k)(1+\beta)-(\alpha+\mathcal{p}\beta)]}c_{\mathcal{p}+k}$$

where

$$c_{\mathcal{p}+k}\geq 0;\sum_{k=2}^{\infty}c_{\mathcal{p}+k}\leq 1.$$

Now, for fixed r, we choose a positive integer number $k_0=k_0(r)$ for which r^k is maximal. Then

$$\sum_{k=2}^{\infty}(\mathcal{p}+k)(\mathcal{p}+k-\delta)a_{\mathcal{p}+k}r^{k}\leq \frac{(\mathcal{p}+k_0)(\mathcal{p}+k_0-\delta)(\mathcal{p}-\alpha)(1-\gamma)}{[(\mathcal{p}+k_0)(1+\beta)-(\alpha+\beta\mathcal{p})]}r^{k_0}.$$

Consequently, $f(z)$ is a $\mathcal{p}-$ valent convex function of the order $\delta(\leq\delta<\mathcal{p})$ *in* $|z|<r_1=r_1(\mathcal{p},\alpha,\beta,\delta,\gamma)$, provided that

$$\frac{(\mathcal{p}+1)(\mathcal{p}-\alpha)(\mathcal{p}+1-\delta)\gamma}{[(1+\beta)+(\mathcal{p}-\alpha)]}r+\frac{(\mathcal{p}+k_0)(\mathcal{p}+k_0-\delta)(\mathcal{p}-\alpha)(1-\gamma)}{[(\mathcal{p}+k_0)(1+\beta)-(\alpha+\beta\mathcal{p})]}r^{k_0}$$

5 Conclusion

In this paper, it has been considered some classes of p-valent β-uniform analytical functions of order α. By selecting different values for each of the parameters p, β, and α and defining new classes of analytic functions, more extent and general results can be obtained for future work.

Conflict of Interest: The author declares that there are no conflicts of interest.

References

Alharayzeh, M. Y. and Ghanim, F. (2022). New Subclass of K-Uniformly Univalent Analytic Functions with Negative Coefficients Defined by Multiplier Transformation, Hindawi journal, 1-6

Al-Kharsani, H. A. and Al-Hajiry, S. S. (2008). A note on certain inequalities for $\mathcal{p}$- valen functions, J. Ineq. Pure Appl. Math., no. 3, Art. 90, 1-6.

Aouf, M. K. Hossen, H. M. and Srivastava, H. M. (2000). Some families of multivalent functions, Comput. Math. Appl.,39-48.

Aouf, M. K. Mostafa, A.O. and Hussain, A. A. (2016). Certain Subclass of p-Valent Uniformly Starlike and Convex Functions Defined by Convolution, Int. J. Open Problems Complex Anal., no. 2, 36-60.

Kanas, S. (1999). Uniformly $\alpha-$ convex functions, Internat. J. Appl. Math., no. 3, 305-310.

Kanas, S and Srivastava, H. M. (2000). Linear operators associated with k-uniformly convex functions, Integral Transform. Spec. Funt., 121-132.

Kanas, S. and Wisniowska, A. (1999). Conic regions and k-uniform convexity, J. Comput. Appl. Math., 327-336.

Kanas, S. and Wisniowska, A. (2000). Conic regions and k-starlike functions, Rev. Roumaine Math. Pures Appl., 647-657.

Marouf, M. S. (2009), A subclass of multivalent uniformly convex functions associated with Dziok-Srivastava linear operator, Int. J. Math. Anal., no. 22, 1087-1100.

Owa, S. (1985). On certain classes of p- valent functions with negative coefficients, Simon Stevin, 385-402.

Patil, B. A. and Thakare, N. K. (1983). On convex and extreme point of $\mathcal{p}$ -valent starlike and convex classes with application, Bull. Math. Soc. Sci. Math. R. S. Roumanie (N. S.) ,no. 75, 145-160.

Salim, T. O. Marouf, M. S. and Shenan, J. M. (2011). A subclass of multivalent uniformly convex functions associated with generalized Sălăgean and Rusheweyh differential operators, Acta Univ. Apulensis, 289-300.

Scientific Journal for the Faculty of Science-Sirte University Vol. 4, No. 1 (2024) 50-58

Scientific Journal for the Faculty of Science-Sirte University

Journal home page: http://journal.su.edu.ly/index.php/JSFSU/index

DOI: 10.37375/issn.2789-858X

Assessing the Drinking Water Quality, and its Commercial Purification Units Efficiency Distributed in Alassaba Municipality- Libya

Salem Irhema S. Irhema[1*] and Adel Almaprok S. Arhouma[2]

[1]*Environmental Sciences Department, Science Faculty, Al-Zintan University, Libya.*
[2]*Chemistry Department, Science Faculty - Alassaba, Gharyan University, Libya.*

DOI: https://doi.org/10.37375/sjfssu.v4i1.2523

ARTICLE INFO:

Received: 18 December 2023

Accepted: 16 February 2024

Published: 17 April 2024

***Keywords*:** *Ground water, Purification technologies, purified water, Water quality.*

A B S T R A C T

The demand for drinking water is increasing daily due to the rising world population, alongside the leakage of water, overuse of groundwater, and occurrence of several pollution issues that led to reducing the quality of groundwater. Consequently, in most countries purifying water technologies have been used to obtain drinkable water. Nationally, Libyans use the purified water extensively in their daily needs. Accordingly, to ensure that our citizen utilize harmless water, the quality of the used water and the efficiency of purification units was assessed by analyzing several physical and chemical characteristics of purified water and raw water supplied to the purification units from some local wells and man-made river (MMR) using recommended standard methods. The study results showed that the quality of purified water is excellent, and the purification process reduced the pH, electro conductivity and the concentration of studied chemical properties significantly to values less than the optimum levels (OL) suggested by the World Health Organization (WHO) and Libyan standards (LS) for drinking water. As a conclusion, the studied purified water may use in the daily needs of human with continuously analytical monitoring.

1 Introduction

Even though, approximately over than 75% of our planet's surface is covered by water, only more less than 1% of this amount is accessible to use by humankind in their daily needs, and with increasing the world population led to raise the demand for drinking water which cause water depletion in some regains and decline the water quality in others (Ighalo et al., 2021). The quality of drinking water is the most important aim that World Health Organization (WHO) emphasised on during the last decades due to appearing of several pollution phenomena such as changing the pH, increasing the levels of some pollutants and other chemical substances in water over than their permissible concentrations, consequently WHO has issued several criteria to adjust drinking water quality. Nowadays, to meet the growing demand of clean drinking water and realise WHO standards many solutions used to encounter this such as sea water distillation or purifying the low-quality fresh water particularly ground water by using various treatment units privately or commercially (Aboraye and Aboraye, 2017; Gabbasa et al., 2020) . These unites may use different technologies to treat drinking water such as reverse osmosis system, boiling, chlorination and solar disinfenction (Malan and Sharma , 2023).

In Libya, groundwater is the main source of drinking water but with unfair use of this source for agriculture, industrial, and municipal activities led to reduce the quality of water, particularly drinking water which

***Corresponding author:* Email: Salemerhima@yahoo.com**

directed to the use of water purifying technologies to obtain palatable water to drink (Ali and Salman, 2021). The used techniques may be beneficial to produce drinking water with high quality if the machine under use has optimal technical characteristics and its filters are replaced in proper time, but if the used system with low manufacture criteria and/or the filters are overused, then the resulted water may be not purified well make it unfavorable for drinking by humankind (Abogussa and Madi, 2012). Unfortunately, people unconcern about the minerals content of purified water and focus only on the taste of water, thus the water quality should be monitored regularly (Ali and Salman, 2021).

Ighalo and Adeniyi, (2020) stated that water quality may be monitored by evaluating some physiochemical and biological characteristics. In this context, several studies investigated the quality of bottled drinking water nationally such as (Al-Keylany et al., 2020; Gabbasa et al., 2020 and Owen and Kamoka, 2019) by estimating several parameters, and to our knowledge there is no study examined the efficiency of the commercial purifying units used to purify water sourced from some local groundwater wells over our country and particularly in Alassaba city, therefore to ensure that the used technologies produce proper drinking water and our nation obtain drinking water with high quality this research aimed at assessing the efficiency of purifying water units by evaluating several physiochemical parameters of water before and after purify it by commercial units distributed in Alassaba Municipality and investigating the quality of drinking purified water by calculating the water quality index (WQI).

2 Methodology

2.1 Sample collection

Fifteenth water samples with triplicates in the volume of 0.5L were collected from several purifying units (10 units) and groundwater wells (5 wells) as sources of raw water to these units, the investigated units and wells distributed in Alassaba Municipality (32.036 N, 12.847 E). Also, one water sample was collected from the man-made river, making a total of 16 samples (48 replicates). These samples were collected on the same day (14 November 2022) and stored in polyethylene bottles, labeled, covered with multi-layered black plastic bags, and kept in a cold place to diminish the effect of environmental conditions till the time of analysis.

2.2 Sample analyses

Rahmanian et al. (2015) reported that several parameters may affect the quality of drinking water that must be determined to justify the water's drinkability including pH, turbidity, electroconductivity (EC), total dissolved solids (TDS), alkalinity, and the levels of Calcium (Ca^{2+}), Chloride (Cl^{-}), Magnesium (Mg^{2+}), Sulphate (SO_4^{2-}), Potassium (K^{+}), Ferric (Fe^{3+}) ions and total hardness (TH), and other several characteristics. Accordingly, the mentioned features were evaluated in the studied samples. The pH was measured by using a pH meter (HANA, model HI 98130), the same machine was used to determine the EC and the turbidity was measured using a turbidity meter (HACH, model 2100P **(**Gabbasa et al., 2020**)** and the other characteristics stated above were determined following the methods reported by APHA, (1995) in the Ras Lanuf oil and gas processing Company's Laboratories.

2.3 Calculating the water quality index (WQI)

According to Verma et al. (2020), WQI has been used to identify the effect of physiochemical parameters individually on the drinking water quality. In this study, the WQI was evaluated following the method described by Oko et al. (2014) and Dhakad et al. (2008) using the equations below.

$$Q = \sum \left(\frac{Ap-Ip}{S-Ip}\right) \times 100 \quad (1)$$

$$WQI = \frac{\sum Qp\ Wp}{\sum Wp} \quad (2)$$

Where Q is the quality of parameters, Ap is the value of the estimated parameter in this study, S is the LS for drinking water, Ip is the ideal value of the determined parameter which is equal to zero for all investigated characteristics except that for pH = 7, and the unit weight (W) was calculated by taking the reciprocal value of S to any studied parameter, separately (Dhakad et al., 2008). As the inhabitants of Alassaba Municipality use the purified water only for drinking and cooking, therefore WQI calculated only for the resulting water from studied units to justify the results and stop on the quality of the used water. The results are presented in Tables 2-10 (look the supplementary data). The resulting data for WQI will justify the used water flowing the instructions that are: if WQI ranged from 0 – 25 the quality of investigated water is excellent, if WQI showed values from 26 – 50 than the water quality is god, and if WQI recorded values from 51

to 75 the quality of examined water is bad, if WQI ranged between 76 – 100 the examined water quality is very bad and if WQI over than 100 thus the studied water is undrinkable (Oko et al., 2014).

2.4 Statistical Analyses

SPSS software version 26 was used to analyse the obtained data and the resulting statistics presented in Table (1) as a mean of 3 replicates ± stander error. To identify if there are differences between the parameter value before and after the purification process for the same sample the independent-sample T-test was run at ($P< 0.05$) after the data tested for normal distribution as the Shapiro-Wilk test confirmed.

3 Results and discussion

The obtained results illustrated in the table (1) and discussed separately as follows:

3.1 pH: The pH value of the purified water ranged between 6.50 ± 0.09 to 7.5 ± 0.17 this means that these waters are weak acid-alkaline water, but the pHs of raw water obtained from studied wells show alkaline characteristics as the pHs recorded 7.60 ± 0.12 to 8.0 ± 0.12 and 7.77 ± 0.09 for MMR water. The purification process reduced the pHs of all investigated samples significantly ($P < 0.05$) related to the input water separately, except the pH of resulted water from U1. The pH reduction of the purified water may be related to the chlorination of row water during the purification process (Gabbasa et al., 2020). Even though, all the pHs of studied water samples were within the recommended value of pH set by WHO and LS for drinking water.

3.2 TDS: The TDS of row water ranged between 755 ± 10 to 1173 ± 15.70 mg L^{1-} as a result, all water samples recorded levels of TDS higher than OL (500 mg L^{1-}) of TDS in drinking water recommended by WHO and LS. The height levels of TDS in water can affect people who suffer from heart and kidney diseases (Memon et al., 2011). On the other hand, the purification process decreased the levels of TDS of resulted in water significantly ($P < 0.05$) in contrast to the TDS of input water as it measured concentrations ranged from 15.73 ± 0.55 to 95.23 ± 3.03 mg L^{1-} which may classify the output of studied units as a super freshwater (Ighalo et al., 2021).

3.3 EC: The ECs of output water showed values ranged from 24.10 ± 1.10 to 193.3 ± 3.90 µS/cm, however the EC of raw water (wells water) ranged between 1110 ± 14.7 to 1725 ± 23.1 µS/cm, and 1610 ± 11 µS/cm in MMR's water. The EC of all purified water except that obtained from U1 and U5 may be classified as a very low saline water, but the U1 and U5 water can be categorised as low saline water. However, Wells and MMR samples are high saline water (Abderahman, 2021). The height values of groundwater EC can be ascribed to the occurrence of several chemical ions that may inter the water from the aquifer's geological compositions (Ali and Salman, 2021) as to the researcher's knowledge, the study cite did not record any pollution phenomenon before. All the analysed water samples recorded ECs lower than the optimum EC in drinking water (1400 and 1500 µS/cm) recommended by LS and WHO, respectively. Except that for water samples collected from W3 and MMR, though, all the wells water samples may be classified as a high saline water (Abderahman, 2021). The purification process reduced the EC of all purified water samples significantly ($P < 0.05$) related to the input water, separately.

3.4 TH: The TH of wells water ranged from 350 ± 10.70 to 720 ± 15.3 mg L^{1-} and were significantly higher ($P < 0.05$) than the TH of units output water that recoded levels between 9.83 ± 0.44 to 30 ± 1.73 mg L^{1-}. All the results of the TH concentrations were lower than the permissible levels of TH recommended by LS and WHO except the samples of water obtained from W3. Even though, the water of Wells and MMR can be classified as very hard water as the levels of TH of them more than 180 mg L^{1-}, while the water purified by unites is soft (Abderahman, 2021).

3.5 Ca^{2+}: The concentration of Ca^{+2} varied in the resulted water from 0.98 ± 0.07 mg L^{-1} to 10.23 ± 0.56 mg L^{-1} which is significantly lower ($P < 0.05$) than the levels of Ca^{+2} in the raw water that recorded levels ranged from 127.7 ± 5.49 mg L^{1-} to 253 ± 18.0 mg L^{-1}. The levels of Ca^{2+} in all studied samples excluding in the water of W3 were lower than its concentration recommended by LS and WHO, but in the resulted water were much lower by approximately more than 10-folds than OL suggested by LS and WHO (72 mg L^{-1}) in drinking water which is critical health issue specially for children by recanting the bone and teeth development (Huaug et al., 2017).

Table (1) The parameters was evaluated for studied samples illustrated as Mean of 3 replicates ± standard error.

Group	Sample Source	Parameters											
		pH	EC	TDS	TH	Ca^{+2}	Cl^{-}	K^{+}	SO_4^{-2}	Alkalinity	Fe^{+3}	Turbidity	Mg^{+2}
		Value	***μ*S/cm**	mg/L	mg/L	mg/L	mg/L	mg/L	mg/L	mg/L	mg/L	**NTU**	**mg/L**
G1	U1	**7.5 ± 0.17a**	**138 ± 4.36a**	**95.23± 3.03 a**	**30 ± 1.73a**	**4.0 ± 0.23a**	**28.27 ± 0.98a**	**1.20± 0.06a**	**11.2 ± 0.52a**	**50.3 ± 3.17a**	**< 0.02**	**< 5**	**4.83 ± 0.43a**
	W1	**7.8 ± 0.12a**	**1110 ± 14.7b**	**755 ± 10b**	**350± 10.70b**	**132 ± 4.04b**	**153 ± 4.91b**	**2.53 ± 0.26b**	**120 ± 4.33b**	**170 ± 6.06b**	**< 0.02**	**< 5**	**0.10 ± 0.01b**
G2	U2	**6.5 ± 0.12a**	**32.57± 2.28a**	**22.1 ± 1.53a**	**19.93± 1.68a**	**3.99 ± 0.34a**	**21.3 ± 0.69a**	**1.03 ± 0.20a**	**2.57± 0.20a**	**43.0 ± 2.52a**	**< 0.02**	**< 5**	**2.43 ± 0.26a**
	W1	**7.8 ± 0.12b**	**1110 ± 14.7b**	**755 ± 10b**	**350± 10.70b**	**132 ± 4.04b**	**153 ± 4.91b**	**2.53 ± 0.26b**	**120 ± 4.33b**	**170 ± 6.06b**	**< 0.02**	**< 5**	**0.10 ± 0.01b**
G3	U3	**6.5 ± 0.06a**	**26.6 ± 0.98 a**	**18.0 ± 0.69a**	**10.0 ± 0.58a**	**1.60 ± 0.09a**	**1.63 ± 0.09a**	**< 1.0**	**< 2.0**	**19.67 ±1.45a**	**< 0.02**	**< 5**	**1.49 ± 0.30a**
	W1	**7.8 ± 0.12b**	**1110 ± 14.7b**	**755 ± 10b**	**350± 10.70b**	**132 ± 4.04b**	**153 ± 4.91b**	**2.53 ± 0.26**	**120 ± 4.33**	**170 ± 6.06b**	**< 0.02**	**< 5**	**0.10 ± 0.01b**
G4	U4	**6.5 ± 0.15a**	**23.1 ±0.78a**	**15.73 ± 0.55a**	**9.83 ±0.73a**	**0.98± 0.07a**	**14.2± 0.21**	**1.10 ± 0.06a**	**< 2.0**	**10.3± 0.88a**	**< 0.02**	**< 5**	**1.78 ± 0.21a**
	W1	**7.8 ± 0.12b**	**1110 ± 14.7b**	**755 ± 10b**	**350± 10.70b**	**132 ± 4.04b**	**153 ± 4.91b**	**2.53 ± 0.26b**	**120 ± 4.33**	**170 ± 6.06b**	**< 0.02**	**< 5**	**0.10 ± 0.01b**
G5	U5	**7.0 ± 0.12a**	**193.3± 3.90 a**	**94.60 ± 2.66a**	**19.83 ± 1.0a**	**7.93 ± 0.41a**	**28.37 ± 2.51a**	**1.23 ± 0.09a**	**12.13± 0.26a**	**20.33 ±2.03a**	**< 0.02**	**< 5**	**0.01± 0.001a**
	W2	**8.0 ± 0.06b**	**1152± 25.4b**	**782 ± 17.30b**	**360 ± 16.2b**	**127.7± 5.49b**	**185.7 ± 7.04b**	**2.10 ± 0.17b**	**110.7 ± 6.06b**	**200 ± 8.37b**	**< 0.02**	**< 5**	**9.47 ± 0.93b**
G6	U6	**7.46± 0.09a**	**55.1 ± 3.72a**	**37.37± 2.51a**	**9.83 ± 0.44a**	**3.97 ± 0.15a**	**14.23 ± 0.43a**	**< 1.0**	**22.03 ± 0.61a**	**20.1± 0.73a**	**< 0.02**	**< 5**	**0.01 ± 0.002a**
	W2	**8.0 ± 0.06b**	**1152± 25.4b**	**782 ± 17.30b**	**360 ± 16.2b**	**127.7± 5.49b**	**185.7 ± 7.04b**	**2.10 ± 0.17**	**110.7 ± 6.06b**	**200 ± 8.37b**	**< 0.02**	**< 5**	**9.47 ± 0.93b**
G7	U7	**6.67 ± 0.09a**	**33.60 ± 2.60a**	**22.80 ± 1.80a**	**10.17± 0.73a**	**4.10 ± 0.26a**	**14.17 ± 0.37a**	**< 1.0**	**2.87 ± 0.20a**	**19.70 ±1.40a**	**< 0.02**	**< 5**	**0.02 ± 0.001a**
	W3	**8.03 ±0.15b**	**1725± 23.1b**	**1173 ± 15.70b**	**720 ± 15.3 b**	**253 ± 18.0b**	**185 ± 3.75b**	**3.80 ± 0.17**	**587± 13.6b**	**170 ± 6.64b**	**< 0.02**	**< 5**	**29.27 ± 1.53b**
G8	U8	**6.50 ± 0.09a**	**24.13 ± 1.70a**	**16.40 ± 1.15a**	**10 ± 0.87a**	**2.50 ± 0.22a**	**21.43 ± 0.38a**	**< 1.0**	**< 2.0**	**20.3 ± 1.45a**	**< 0.02**	**< 5**	**0.94 ± 0.14a**
	W4	**7.60 ± 0.12b**	**1186 ± 21.93b**	**805 ± 14.90b**	**370 ± 8.37b**	**136 ± 3.18b**	**157 ± 6.10b**	**1.70 ± 0.17**	**153 ± 6.06**	**190 ± 6.64b**	**< 0.02**	**< 5**	**7.33 ± 0.54b**
G9	U9	**6.80 ± 0.06a**	**24.10 ± 1.10a**	**16.30 ± 0.75a**	**9.83 ± 0.44a**	**2.16 ± 0.095a**	**10.27 ± 0.15a**	**< 1.0**	**2.47 ± 0.20a**	**10.0 ± 0.58a**	**< 0.02**	**< 5**	**0.94 ± 0.09a**
	W5	**8.0 ± 0.12b**	**1143 ± 14.0b**	**778 ± 9.41b**	**360± 10.68b**	**140 ± 4.19 b**	**163 ± 3.70b**	**2.50 ± 0.17**	**166 ± 7.22b**	**180 ± 6.64b**	**< 0.02**	**< 5**	**7.27 ± 0.61b**
G10	U10	**6.70 ± 0.12a**	**88.20 ± 2.48a**	**60.0 ± 1.67a**	**16.33± 0.88a**	**10.23± 0.56a**	**14.57 ± 0.32a**	**< 1.0**	**5.93 ± 0.64a**	**29.67 ±2.60a**	**< 0.02**	**< 5**	**2.17 ± 0.03a**
	MMR	**7.77± 0.09b**	**1610 ± 11b**	**1096 ± 7.45b**	**374± 6.64b**	**138 ± 3.79b**	**288 ± 7.22b**	**9.37 ± 0.46**	**250 ± 6.64b**	**150 ± 2.61b**	**< 0.02**	**< 5**	**10.73 ± 0.66b**
LS	RL	**6.5-8.5**	**2500**	**1000**	**500**	**200**	**250**	**40**	**400**	**200**	**1.0**	**< 5**	**150**
	OL	**6.5-8.5**	**-**	**500**	**-**	**75**	**150**	**12**	**200**	**-**	**0.03**	**< 5**	**30**
WHO	RL	**6.5-8.5**	**2800**	**1500**	**500**	**200**	**600**	**40**	**400**	**-**	**1.0**	**< 5**	**150**
	OL	**6.5-8.5**	**1500**	**500**		**50**	**200**	**15**	**200**	**-**	**0.3**	**< 5**	**50**

W= well, U= unit, MMR= man-made revie, G= group. LS= Libyan standard, OL= Optimum levels and RL= Recommended levels set by WHO and LS.
The values with different lowercase letters in the same group for each parameter separately are significantly different from each other at $P < 0.05$.

3.6 Cl^-: The levels of chloride ion in the output water ranged from 1.60 ± 0.09 mg L^{-1} to 28.37 ± 2.51 mg L^{1-} which is lower significantly ($P < 0.05$) than chloride levels in the input wells water ranged between 153 ± 4.91 mg L^{1-} to 288 ± 7.22 mg L^{1-}. All the levels of Cl^- in the studied samples except that in MMR (288 ± 7.22 mg L^{1-}) were lower than that suggested by LS and WHO. Even though, the concentrations of Cl^- in the raw water higher than the OL level set by LS and WHO, but was much lower than OL in the resulted water from purification procedure which may affect human body growth due to long-time use of this water as the human body needs Cl^- in the osmotic activity in the external cells and the chloride deficiency may lead to increase blood pH and cause metabolic alkalosis (Tello, 2021).

3.7 K^+: Potassium ion levels were undetectable in resulted water from U3, U6-10 and ranged between 1.03 ± 0.20 mg L^{1-} to 1.20 ± 0.06 mg L^{1-} in resulted water from other units, additionally, in the wells water before purification steps K^+ levels were higher significantly ($P < 0.05$) ranged from 1.70 ± 0.17 mg L^{1-} to 9.37 ± 0.46 mg L^{1-}, as a result showed that all the samples recorded levels of K^+ lower than the acceptable and OL level set by LS and WHO in drinking water.

3.8 SO_4^{2}: The concentration of sulphate ion were undetectable in the samples collected from U3, U4 and U9, on the other hand, its levels in the rest of the samples taken from the rest units ranged from 2.47 ± 0.20 mg L^{1-} to 22.03 ± 0.61 mg L^{1-}. But, in the raw water were significantly higher ($P < 0.05$) than its level in purified water recording levels ranged between 110.7 ± 6.06 mg L^{1-} to 587± 13.6 mg L^{1-}. Only one well (W3) showed levels of SO_4^{2-} higher than that set by LS and WHO (400 mg L^{1-}). The very low levels of sulphate ion in drinking water is a critical health issue as it may decrease the efficiency of immune system and lungs inflammation (Gabbasa et al., 2020).

3.9. Alkalinity: The alkalinity of all studied samples was lower than that set by LS, however, the alkalinity of purified water resulting from all investigated units was significantly ($P < 0.05$) lower than that of water obtained from studied wells and MMR.

3.10 Fe^{3+}: The iron (III) concentrations were undetectable (lower than 0.02 mg L^{1-}) in all collected samples. The presence of Fe^{3+} in water can increase the turbidity and undesirable water test (Gabbasa et al., 2020), the absence of Fe^{3+} in the studied water here may ascribe the low turbidity of all studied samples.

3.11 Mg^{2+}: The purification process reduced the concentrations of Mg^{2+} significantly related to row water except the samples of units 1, 2, 3 and 4 which increased the resulted water content of Mg^{2+} significantly, but to levels much lower than the OL suggested by LS and WHO. The levels of Mg^{2+} in the purified water resulted from U1, U2, U3 and U4 higher than Mg^{2+} concentrations in raw water, this can be ascribed to the filters containing of this metal.

3.12 Turbidity: All the studied water samples recorded turbidity lower than 5 NTU which is lower than that set by LS and WHO, this may be related to the absence of Fe^{3+} in studied samples (Gabbasa et al., 2020).

Generally, the purification process reduced the levels of most investigated parameters in water significantly ($P < 0.05$) to levels greatly less than the acceptable values recommended by WHO and LS. The results of the current study is in line with the results of several national studies that confirmed that the levels of physiochemical properties in the majority of bottled water sold in Libyan markets were in the range of that set by WHO and LS (Al-Keylany et al., 2020; Gabbasa et al., 2020 and Owen and Kamoka, 2019).

The values of WQI of purified drinking water collected from all units (U1-U10) were 11.85, 6.08, 5.97, 6.00, 8.93, 11.50, 6.95, 6.00, 7.69, and 7.18, respectively. This suggests that the quality of purified water is excellent according to the rules stated by Oko et al. (2014). On the other hand, it should be noted that the concentrations of most investigated parameters in purified water are less than the OL set by both WHO and LS which may suggest that the resulting water contains low levels of essential elements to human health, therefore utilizing this water for prolonged may lead to reduce the supply of several nutrients to humans affecting people is health by occurring several health risks such as osteopenia, dental caries and reduce bone development in children (Huang et al., 2018; Huang et al., 2019). Conversely, the water supplied from most studied wells may be used to drink for a short period and under any urgent circumstance as the values of investigated parameters were slightly lower than the higher recommended levels set by LS and WHO, and most of examined characteristics higher than OL. However, the raw water obtained from W3 and MMR must not be used for drinking by inhabitants under any circumstance as the values of some physiochemical parameters exceeded the higher recommended limits set by WHO and LS.

4 Conclusions

The purification procedures reduced the values of pH, EC and the levels of studied chemical parameters to values and levels much lower than the allowable values set by WHO and LS and also to levels less than the OL of these characteristics in drinking water, which highly suggest advising and convince the owners of the purification units in the area of study to select the proper machines and filters with high quality to produce water contain levels of minerals close to OL to ensure that our citizen utilizes water to contain the required concentrations of essential minerals for human body development, furthermore, the purified water quality must be monitored frequently for the water chemical and biological contains.

5 Acknowledgment

I am extremely thankful to the staff of the safety and environmental department, and quality control laboratories in the Ras Lanuf oil and gas processing Company, particularly Abouzid Alfaqi, Abubakr Abdulrahman Bilgasim, Ismail Muhammed Saleh, Ibrahim Al-Asran and Ahamed Al-Laffi for their advice and practical help to analyse the studied sample, also special thankful to Dr**.** Abdulfatah Irhema Salem for his help to edit this work grammatically**.**

Conflict of Interest: The authors declare that there are no conflicts of interest.

References

Abderahman, D. A., 2021. Chemical and physical analyses of bottled water in Duhok governorate. The Academic Journal Of Nawroz Un. – Kurdistan – Iraq, 10 (1), pp., 310 – 317.

Aboraye, R., M. A. and, Aboraye, F. M., 2017. Assessing the quality of surface and ground water of Wadi Kame. The Educational Journal of Al-Margab Un., (11), pp. 143 – 155.

Abogussa, A. M. and Madi, N. A., 2012. Assessment of Microbial and Chemical Contamination in Re-Usable 18 Liter Bottled water Marketed in Tripoli City and its Suburbs. The Libyan Journal of Agriculture, 17 (1-2), pp. 60-67.

Ali, S. M., and Salman, H. Q., 2021. Irrigation water quality (ground water) in some farms of the Hamza agriculture project. Journal Of Marine Science And Environmental Technologies,7(2), pp., A-11 – A-20.

Al-Keylany, A. K., Hassen, T. M., Al-Modey, F. A., 2020. Evaluating the water quality of commercial desalination plants distributed in Sabratha city and its suburbs. Al-qurtas Journal of Humanities and Applied Sciences, 11, pp., 420-432.

APHA: American Public Health Association, Standard Methods: For the Examination of Water and Wastewater, APHA, AWWA, WEF/1995, APHA Publication. 1995.

Dhakad, N.K., Deepak, S. and Choudhary, P., 2008. Water quality index of ground water (GWQI) of Jhabua Town, MP (India). Journal of Environmental Research and Development, 2(3), pp.443-446.

Gabbasa, M. A., Asbany, N. H., Sultan, O. M., 2020. Analysing of chemical and biological properties to evaluate the quality of bottled drinking water in the city of Tripoli, Libya. The University Bulletin – Al-Zawia Un., 22(3), pp., 1 – 19.

Huang, Y., Ma, X., Tan, Y., Wang, L., Wang, J., Lan, L., Qiu, Z., Luo, J., Zeng, H. and Shu, W., 2019. Consumption of very low mineral water is associated with lower bone mineral content in children. The Journal of Nutrition, 149(11), pp.1994-2000.

Huang, Y., Wang, J., Tan, Y., Wang, L., Lin, H., Lan, L., Xiong, Y., Huang, W. and Shu, W., 2018. Low-mineral direct drinking water in school may retard height growth and increase dental caries in schoolchildren in China. Environment international, 115, pp.104-109.

Ighalo, J.O., Adeniyi, A.G. and Marques, G., 2021. Artificial intelligence for surface water quality monitoring and assessment: a systematic literature analysis. Modeling Earth Systems and Environment, 7(2), pp.669-681.

Ighalo, J.O. and Adeniyi, A.G., 2020. A comprehensive review of water quality monitoring and assessment in Nigeria. Chemosphere, 260, p.127569.

Libyan standards of drinking water (No; 82) 2013, The Libyan National Centre for Standardization and Metrology, Tripoli - Libya.

Malan, A. and Sharma, H.R., 2023. Assessment of drinking water quality and various household water treatment practices in rural areas of Northern India. Arabian Journal of Geosciences, 16(1), p.96.

Memon, M., Soomro, M.S., Akhtar, M.S. and Memon, K.S., 2011. Drinking water quality assessment in Southern Sindh (Pakistan). Environmental monitoring and assessment, 177, pp.39-50.

Oko, O.J., Aremu, M.O., Odoh, R., Yebpella, G. and Shenge, G., 2014. Assessment of water quality index of borehole and well water in Wukari Town, Taraba State, Nigeria. Assessment, 4(5), pp.1-9.

Owen, N. A., and Kamoka, H. S., 2019. Study of some physical and chemical properties of some locally bottled water. The journal of sciences- Misrata Un., A special issue for the Third Annual Conference on Theories and Applications of Basic and Life Sciences, held on September 7, 2019, pp., 158 -168.

Rahmanian, N., Ali, S.H.B., Homayoonfard, M., Ali, N.J., Rehan, M., Sadef, Y. and Nizami, A.S., 2015. Analysis of physiochemical parameters to evaluate the drinking water quality in the State of Perak, Malaysia. Journal of Chemistry, pp.1-10.

Tello, Carlos, 2021. Low Chloride Levels (Hypochloremia) Symptoms and Causes. Available at: https://labs.selfdecode.com/blog/low-chloride-levels-hypochloremia/ .[accessed in September 2023. The Journal of Nutrition, 149(11), pp.1994-2000.

Verma, P., Singh, P.K., Sinha, R.R. and Tiwari, A.K., 2020. Assessment of groundwater quality status by using water quality index (WQI) and geographic information system (GIS) approaches: a case study of the Bokaro district, India. Applied Water Science, 10, pp.1-16.

World Health Organization, Drinking Water Guidelines and standard, Geneva, Swizerland, 2002, p.6.

Supplementary data

Table (2) Water quality index of water collected from U_1

Parameter	Mean	LS	Iv	W	Q	QW
pH	7.5	8.5	7	0.1176	33.33	3.92
EC	138	2500	0	0.0004	5.52	0.0022
TDS	95.23	1000	0	0.001	9.523	0.0095
TH	30	500	0	0.002	6	0.012
Ca^{2+}	4	200	0	0.005	2	0.01
Cl^-	28.7	250	0	0.004	11.48	0.046
K^+	1.2	40	0	0.025	3	0.075
SO_4^{2-}	11.2	400	0	0.0025	2.8	0.007
Alkalinity	50.3	200	0	0.005	25.15	0.126
Fe^{3+}	0.02	1.0	0	1	2	2
Turbidity	2.5	5	0	0.2	50	10
Mg^{2+}	4.83	150	0	0.0067	3.22	0.022
∑				1.3692		16.228975
WQI	11.85288855					

Table (3) Water quality index of water collected from U2

Parameter	Mean	LS	Iv	W	Q	QW
pH	6.5	8.5	7	0.1176	-33.33	-3.92
EC	32.57	2500	0	0.0004	1.30	0.00052
TDS	22.1	1000	0	0.001	2.21	0.0022
TH	19.93	500	0	0.002	3.99	0.0080
Ca^{2+}	3.99	200	0	0.005	1.995	0.010
Cl^-	21.3	250	0	0.004	8.52	0.034
K^+	1.03	40	0	0.025	2.575	0.0644
SO_4^{2-}	2.57	400	0	0.0025	0.643	0.0016
Alkalinity	43	200	0	0.005	21.5	0.108
Fe^{3+}	0.02	1.0	0	1	2	2
Turbidity	2.5	5	0	0.2	50	10
Mg^{2+}	2.43	150	0	0.0067	1.62	0.011
∑				1.369		8.31909
WQI	6.075878885					

Table (4) Water quality index of water collected from U3

Parameter	Mean	LS	Iv	W	Q	QW
pH	6.5	8.5	7	0.118	-33.33	-3.92
EC	26.6	2500	0	0.0004	1.064	0.00043
TDS	18	1000	0	0.001	1.8	0.0018
TH	10	500	0	0.002	2	0.004
Ca^{2+}	1.6	200	0	0.005	0.8	0.004
Cl^-	1.63	250	0	0.004	0.652	0.0026
K^+	0.5	40	0	0.025	1.25	0.0313
SO_4^{2-}	1	400	0	0.0025	0.25	0.00063
Alkalinity	19.7	200	0	0.005	9.84	0.049
Fe^{3+}	0.02	1.0	0	1	2	2
Turbidity	2.5	5	0	0.2	50	10
Mg^{2+}	1.49	150	0	0.0067	0.993	0.0067
∑				1.369		8.180538
WQI	5.974685169					

Table (5) Water quality index of water collected from U4

Parameter	Mean	LS	Iv	W	Q	QW
pH	6.5	8.5	7	0.1176	-33.33	-3.92
EC	23.1	2500	0	0.0004	0.924	0.00037
TDS	15.73	1000	0	0.001	1.573	0.0016
TH	9.83	500	0	0.002	1.966	0.0039
Ca^{2+}	0.98	200	0	0.005	0.49	0.0025
Cl^-	14.2	250	0	0.004	5.68	0.023
K^+	1.1	40	0	0.025	2.75	0.070
SO_4^{2-}	1	400	0	0.0025	0.25	0.00063
Alkalinity	10.3	200	0	0.005	5.15	0.026
Fe^{3+}	0.02	1.0	0	1	2	2
Turbidity	2.5	5	0	0.2	50	10
Mg^{2+}	1.78	150	0	0.0067	1.187	0.0080
∑				1.3692		8.2141267
WQI	5.999211					

Table (6) Water quality index of water collected from U5

Parameter	Mean	LS	Iv	W	Q	QW
pH	7	8.5	7	0.1176	0	0
EC	193.3	2500	0	0.0004	7.73	0.0031
TDS	94.6	1000	0	0.001	9.46	0.0095
TH	19.83	500	0	0.002	3.97	0.0079
Ca^{2+}	7.73	200	0	0.005	3.87	0.019
Cl^-	28.37	250	0	0.004	11.35	0.045
K^+	1.23	40	0	0.025	3.075	0.077
SO_4^{2-}	12.13	400	0	0.0025	3.033	0.0076
Alkalinity	20.33	200	0	0.005	10.17	0.051
Fe^{3+}	0.02	1.0	0	1	2	2
Turbidity	2.5	5	0	0.2	50	10
Mg^{2+}	0.01	150	0	0.0067	0.0067	4.47×10^{-5}
∑				1.3692		12.2205
WQI	8.925305081					

Table (7) Water quality index of water collected from U6

Parameter	Mean	LS	Iv	W	Q	QW
pH	7.46	8.5	7	0.1176	30.667	3.606
EC	55.1	2500	0	0.0004	2.204	0.00088
TDS	37.37	1000	0	0.001	3.737	0.0037
TH	9.83	500	0	0.002	1.966	0.0039
Ca^{2+}	3.97	200	0	0.005	1.985	0.0099
Cl^-	14.23	250	0	0.004	5.692	0.0228
K^+	0.5	40	0	0.025	1.25	0.0313
SO_4^{2-}	22.03	400	0	0.0025	5.5075	0.0138
Alkalinity	20.1	200	0	0.005	10.05	0.05025
Fe^{3+}	0.02	1.0	0	1	2	2
Turbidity	2.5	5	0	0.2	50	10
Mg^{2+}	0.01	150	0	0.0067	0.0067	4.47×10^{-5}
∑				1.3692		15.74295702
WQI	11.49792362					

Table (8) Water quality index of water collected from U7

Parameter	Mean	LS	Iv	W	Q	QW
pH	6.67	8.5	7	0.1176	-22	-2.5872
EC	33.6	2500	0	0.0004	1.344	0.00054
TDS	22.8	1000	0	0.001	2.28	0.0023
TH	10.17	500	0	0.002	2.034	0.0041
Ca^{2+}	4.1	200	0	0.005	2.05	0.0103
Cl^-	14.17	250	0	0.004	5.668	0.023
K^+	0.1	40	0	0.025	0.25	0.00625
SO_4^{2-}	2.87	400	0	0.0025	0.7175	0.0018
Alkalinity	19.7	200	0	0.005	9.85	0.0493
Fe^{3+}	0.02	1.0	0	1	2	2
Turbidity	2.5	5	0	0.2	50	10
Mg^{2+}	0.02	150	0	0.0067	0.0133	8.93×10^{-5}
∑				1.3692		9.509990683
WQI	6.945654896					

Table (9) Water quality index of water collected from U8

Parameter	Mean	LS	Iv	W	Q	QW
pH	6.5	8.5	7	0.1176	-33.3	-3.92
EC	24.13	2500	0	0.0004	0.965	0.00039
TDS	16.4	1000	0	0.001	1.64	0.00164
TH	10	500	0	0.002	2	0.004
Ca^{2+}	2.5	200	0	0.005	1.25	0.00625
Cl^-	21.43	250	0	0.004	8.572	0.0343
K^+	0.5	40	0	0.025	1.25	0.03125
SO_4^{2-}	1	400	0	0.0025	0.25	0.000625
Alkalinity	20.3	200	0	0.005	10.15	0.05075
Fe^{3+}	0.02	1.0	0	1	2	2
Turbidity	2.5	5	0	0.2	50	10
Mg^{2+}	0.94	150	0	0.0067	0.627	0.0042
∑				1.3692		8.213387747
WQI	5.998676414					

Table (10) Water quality index of water collected from U9

Parameter	Mean	LS	Iv	W	Q	QW
pH	6.8	8.5	7	0.1176	-13.33	-1.568
EC	24.1	2500	0	0.0004	0.964	0.00039
TDS	16.3	1000	0	0.001	1.63	0.00163
TH	9.83	500	0	0.002	1.966	0.0039
Ca^{2+}	2.16	200	0	0.005	1.08	0.0054
Cl^-	10.27	250	0	0.004	4.108	0.0164
K^+	0.5	40	0	0.025	1.25	0.0313
SO_4^{2-}	2.47	400	0	0.0025	0.6175	0.0015
Alkalinity	10	200	0	0.005	5	0.025
Fe^{3+}	0.02	1.0	0	1	2	2
Turbidity	2.5	5	0	0.2	50	10
Mg^{2+}	0.94	150	0	0.0067	0.6267	0.0042
∑				1.3692		10.521772
WQI	7.684612925					

Table (11) Water quality index of water collected from U10

Parameter	Mean	LS	Iv	W	Q	QW
pH	6.7	8.5	7	0.1176	-20	-2.352
EC	88.2	2500	0	0.0004	3.528	0.0014
TDS	60	1000	0	0.001	6	0.006
TH	16.33	500	0	0.002	3.266	0.0065
Ca^{2+}	10.23	200	0	0.005	5.115	0.0256
Cl^{-}	14.57	250	0	0.004	5.828	0.023
K^{+}	0.5	40	0	0.025	1.25	0.0313
SO_4^{2-}	5.93	400	0	0.0025	1.483	0.0037
Alkalinity	29.67	200	0	0.005	14.84	0.074
Fe^{3+}	0.02	1.0	0	1	2	2
Turbidity	2.5	5	0	0.2	50	10
Mg^{2+}	2.17	150	0	0.0067	1.4467	0.0097
∑				1.3692		9.829654117
WQI	7.18					

Scientific Journal for the Faculty of Science-Sirte University Vol. 4, No. 1 (2024) 59-67

Scientific Journal for the Faculty of Science-Sirte University

Journal home page: http://journal.su.edu.ly/index.php/JSFSU/index

DOI: 10.37375/issn.2789-858X

Exploring the Chemical Components of Porcelain Tiles Commercially available in Benghazi City, Libya

Maysson M. Yaghi [1], Khaled M. Elsherif [2,3] and Majdi A. Abdulhadi [1]

[1]*Chemistry Department, Science Faculty Al-Abyar, Benghazi University, Benghazi, Libya.*
[2]*Libyan Authority for Scientific Research, Tripoli, Libya.*
[3]*Chemistry Department, Science Faculty, Benghazi University, Benghazi, Libya.*

DOI: https://doi.org/10.37375/sjfssu.v4i1.2606

ARTICLE INFO:

Received: 23 January 2024

Accepted: 15 February 2024

Published: 17 April 2024

Keywords: *Porcelain tiles, Chemical composition, Mass percentage, X-Ray Fluorescence Spectrometer, Raw mineral materials*

A B S T R A C T

The objective of this study was to analyze the chemical composition of porcelain tiles by determining their mass percentages. Porcelain tile samples were collected from various markets in Benghazi, Libya, including those from Egypt, India, Spain, and Turkey. The chemical components of the tiles were identified using an X-Ray Fluorescence Spectrometer. The assessment criteria for high-quality raw mineral materials consisted of high representative oxide content, low impurity oxides, and low loss on ignition (LOI). Notably, significant variations were observed in the chemical composition of porcelain tiles. In general, two main formulations were identified: one group characterized by high silica content (45.65% to 48.24%), elevated levels of alumina (11.65% to 11.83%) and alkaline oxides, and low magnesium oxide (MgO); the other group consisted of tiles with low silica content (39.26% to 34.96%), high MgO (1.00%) and alumina content (5.89% to 9.88%), and relatively lower alkaline oxides. The results provided the average mass percentages of different components present in the porcelain tiles. Silica (SiO_2) exhibited a resistant property to melting and shrinkage, accounting for 44.37% of the mass. Alumina (Al_2O_3) played a role in polishing and grinding the tiles, representing 9.85% of the mass. Lime (CaO) contributed to enhancing the tiles' resistance against heat and abrasion, constituting 7.26% of the mass. MgO served as a sintering aid, with a mass percentage of 0.40%. Potassium oxide (K_2O) improved heat resistance, abrasion resistance, and overall appearance of the tiles, accounting for 0.77% of the mass. Sodium oxide (Na_2O) was present at 0.61%. Iron oxide (Fe_2O_3) and titanium oxide (Ti_2O) acted as colored impurities, comprising 2.84% and 0.82% of the mass, respectively. Additionally, calcite ($CaCO_3$) was identified at 11.68%, aiding in the melting and shrinkage process during heating by releasing CO_2.

1 Introduction

Porcelain tile is a highly resistant material that can withstand compact forces and frost, while also exhibiting good durability and low porosity (Amorós et al., 2022). It must adhere to ISO 10545-3 (Alonso et al., 2022), which stipulates a maximum water absorption of 0.5%. For nearly four decades, porcelain tiles have served as exceptional construction materials for walls, floors, pavements, and urban squares (Demarch et al., 2021). The market offers four types of porcelain tile, including glazed and unglazed varieties, as well as polished and unpolished finishes. In addition to their technical performance, aesthetic features play a crucial role in the

***Corresponding author*: E-mail: khaled.elsherif@uob.edu.ly**

decision-making process for end-users. The visual appeal of unglazed porcelain tiles relies heavily on the body colour, while glazed tiles, although the glaze layer covers the body colour, still consider it important, albeit to a lesser extent than unglazed products (Li et al., 2023).

Porcelain tile, which consists of different clay minerals, feldspars, and quartz, is classified as a silicate ceramic material (Berto, 2007). It belongs to the triaxial ceramics category because of the presence of these components. With the rapid progress of the porcelain industry, there is an increasing worry regarding the depletion of clay minerals, which are essential for tile manufacturing. The primary oxide components in porcelain tile are SiO_2 and Al_2O_3, followed by Na_2O, K_2O, CaO, and MgO. Impurities like Fe_2O_3 and TiO_2 are commonly found, and their high concentrations during firing can lead to undesired coloration in an oxidizing atmosphere (Esposito et al., 2005). Therefore, it is crucial to carefully manage the levels of Fe_2O_3 and TiO_2. Traditionally, small quantities of $ZrSiO_4$ have been used to enhance the whiteness of unglazed porcelain tiles (Selli, 2015).

The porcelain tiles exhibit a noticeable range of colors, transitioning from a glossy, vibrant appearance to a more subdued, matte finish. The variation in color can be attributed to several factors. Firstly, it is influenced by the minerals present in the composition of the tiles. These minerals, including ferric oxide (Fe_2O_3) and $CaCO_3$, combine in different proportions to create distinct hues. Additionally, the presence of impurities interacts with the minerals and affects the overall color. Lastly, the atomic bonds within the mineral structure play a significant role in determining how light is absorbed and reflected by the tiles, which in turn impacts the wavelengths perceived by our eyes (Leonelli et al., 2001).

The production process employed for manufacturing porcelain tiles is a well-established and widely used method in the market. It shares similarities with the manufacturing processes of other ceramic tiles. This process comprises three primary stages: (1) the wet milling and homogenization of raw materials, followed by the spray-drying of the resulting suspension; (2) the uniaxial pressing of the spray-dried powder at a pressure of 40-50 MPa, with a moisture content ranging from 5 to 7%; (3) the rapid firing process, lasting 40-60 minutes at temperatures of 1180-1220 °C, to achieve maximum density (De Noni et al., 2010; Njindam et al., 2018). Porcelain tiles are renowned for their exceptional flexural strength, exceeding 35±2 MPa, as well as their low water absorption (<0.5%) and minimal abraded volume (< 175 mm^3). These characteristics make them highly suitable for various applications, both indoors and outdoors, whether as floor or wall tiles (Njoya et al., 2017).

X-ray fluorescence spectrometry (XRF) is an established atomic analytical technique widely used for qualitative and quantitative chemical analysis of environmental samples with diverse compositions. It covers a broad range of elements, spanning from B to U, in atomic number order. XRF provides rapid and non-destructive results, offering sensitivity in the range of 10^{-8} g (depending on the specific element of interest). This makes it highly suitable for various environmental research studies. Its key attributes include its ability to analyze multiple elements simultaneously, its acceptable speed and cost-effectiveness, ease of automation, portability, and the capability to directly analyze solid samples without prior acid digestion. These features have contributed to its maturity as an analytical tool used for routine control in various scenarios, not just limited to traditional industrial applications. XRF can be effectively employed for direct field analysis in agronomy research, on-line analysis of atmospheric particulate matter, remote acquisition of XRF spectral data, and as analytical support in environmental research laboratories (Beckhoff et al., 2006).

This study aims to present a comprehensive analysis of the chemical compositions of porcelain tiles, with the goal of exploring the utilization of untapped mineral resources from Libya. Additionally, it seeks to establish an effective mixture formulation for the successful production of porcelain tiles. The evaluation of these tiles will be conducted in accordance with the ISO 13006 standard. Currently, Libya imports porcelain tiles from Egypt, India, Spain, and Turkey. However, the country possesses abundant raw materials required for manufacturing high-quality porcelain tiles. To assess the chemical properties of porcelain tiles, samples were collected from various locations in Benghazi.

2 Materials and Methods

2.1 Sample collection

A total of 12 porcelain tile products from Egypt, India, Spain, and Turkey were selected to represent the production of these countries. Chemical analyses of the tiles were performed using X-ray fluorescence (XRF) techniques. The major components found in the composition of porcelain tiles, expressed as mass percentages, include SiO_2, CaO, Al_2O_3, Fe_2O_3, Ti_2O, MgO, and K_2O. These samples were carefully chosen to be representative, and they were obtained from various

marketing and selling points. Each sample was labeled with a type designation (P for porcelain) and the corresponding country code (E, I, S, and T) for Egypt, India, Spain, and Turkey, respectively.

2.2 Sample preparation

From each type of porcelain tile, random samples were taken to ensure representativeness. The sample preparation method utilized in this study involved a simple and direct approach using pressed pellets. In general, the samples required minimal preparation; however, it was important to present the materials to the spectrometer in a consistent and uniform manner. For the porcelain tiles, a grinding process was employed to achieve a flat surface, while powders were carefully reduced to a controlled particle size before being pressed into pellets for ease of handling. The porcelain tile samples underwent a drying process in an oven at 100°C for 24 hours to eliminate moisture, after which they were finely crushed to obtain a powder with an average particle diameter of 100 µm. The average particle diameter of 100 µm was measured using a RETSCH woven wire mesh sieve. Subsequently, 10.00 g of the porcelain samples were ground and mixed with 1.00 g of binder before being prepared as pressed pellets. It is important to note that the elemental compositions of the binder used in the study were well known and previously characterized, given the established nature of the experimental setup and the use of the binder in the preparation of pressed pellets. These pellets were placed in suitable sample cups. The straightforward sample preparation method allowed for quick availability of analytical results shortly after the sample was taken. To ensure optimal count rates for various elements, the tube current was optimized and fixed (Sverchkov et al., 2023).

2.3 X-ray fluorescence (XRF) analysis

The S2 PUMA, a compact energy-dispersive X-ray fluorescence (EDXRF) instrument, offers fast and dependable quality control capabilities. It utilizes HighSense™ technology, optimizing beam path geometry to achieve high count rates, reduced measurement times, and improved precision. The measurements were conducted using the Bruker AXS GmbH advice, specifically S2 version 5.0.0, spectraEDX v2.4.2, X-ray fluorescence - Serial-No S2-204420, 220V, 3-50/60 Hz. This instrument is equipped with a 50 W X-ray tube-K230C80 and an XFlash® LE silicon drift detector-A20D800, enabling the determination of chemical components in the porcelain samples. Within a few minutes of sample collection, a single measurement provides analytical results for major components like $CaCO_3$, as well as minor and trace compounds such as Al_2O_3, SiO_2, and Fe_2O_3. The technique offers advantages including programmable measurement conditions for each element, high sensitivity, and low detection limits. The conversion of X-ray intensities into element concentrations is achieved through calibration using reference standards of known compositions.

3 Results and discussion

The primary chemical components found in porcelain tiles are silica (SiO_2), alumina (Al_2O_3), lime (CaO), magnesia (MgO), and sodium and potassium oxides (Na_2O and K_2O). Minor constituents or impurities such as Fe_2O_3 and TiO_2 are also present, and their high concentrations can lead to undesired colors during firing, particularly in an oxidizing atmosphere (Tripati et al., 2017). Therefore, it is important to carefully consider the levels of Fe_2O_3 and TiO_2. Traditionally, a small amount of $ZrSiO_4$ has been used to enhance the whiteness of unglazed porcelain tiles (Hamidalddin, 2020).

The studied oxide ratios exhibited variation within the study samples, with the average concentration order as follows: $SiO_2 > CaCO_3 > CaO \sim Al_2O_3 > Fe_2O_3 > TiO_2 > MgO \sim Na_2O \sim K_2O > Cl > MnO \sim P_2O_3 > SO_3 > MgCO_3$. The levels of oxides in different porcelain samples are presented in Table 1. The SiO_2 percents ranged from 48.28% (Egyptian porcelain) to 34.96% (Indian porcelain), with an average of 44.37±4.05%. Silicon dioxide (SiO_2) was the predominant oxide in all types of porcelain under study, but its concentrations were lower than those reported in previous studies (Sánchez et al., 2010; Gultekin et al., 2017; Montanari et al., 2022). The second most common oxide was $CaCO_3$, followed closely by Al_2O_3 and CaO, with average perecents of 11.68±3.16%, 9.86±1.61%, and 7.26±2.06%, respectively. The remaining oxides were present in proportions below 1% each, while the levels of $MgCO_3$ were below the detection limit.

Table (1) Chemical composition of tested porcelain samples

Parameters (%)	Sample Code											
	PE1	**PE2**	**PE3**	**PI1**	**PI2**	**PI3**	**PS1**	**PS2**	**PS3**	**PT1**	**PT2**	**PT3**
SiO_2	45.65	47.87	48.24	39.26	42.48	34.96	41.92	47.73	47.28	46.67	44.55	45.87
Al_2O_3	9.68	11.65	11.83	9.77	10.28	5.89	8.60	10.83	10.28	11,43	9.72	9.88
Fe_2O_3	2.03	4.95	3.21	2.45	2.90	2.01	2.23	2.23	2.41	3.56	2.51	3.55
CaO	5.07	5.75	5.67	5.71	5.48	8.94	10.24	6.80	5.13	8.86	9.34	10.12
MgO	0.47	0.00	0.00	0.00	0.70	0.90	1.00	0.00	0.00	0.63	0.45	0.68
Na_2O	0.66	0.62	0.65	0.55	0.62	0.63	0.58	0.65	0.66	0.61	0.59	0.55
K_2O	0.20	0.75	0.65	0.87	0.75	0.93	1.18	0.64	0.40	1.26	0.99	0.56
TiO_2	0.86	0.85	0.88	0.83	0.85	0.76	0.70	0.81	0.82	0.86	0.79	0.88
MnO	0.02	0.02	0.02	0.02	0.02	0.02	0.01	0.02	0.01	0.03	0.02	0.02
P_2O_5	0.08	0.06	0.10	0.07	0.06	0.09	0.08	0.08	0.07	0.05	0.08	0.08
SO_3	0.00	0.003	0.005	0.00	0.00	0.01	0.01	0.01	0.00	0.01	0.01	0.01
$CaCO_3$	9.05	10.27	10.98	10.19	9.79	15.97	18.28	12.17	9.15	7.64	14.78	11.92
$MgCO_3$	0.00	0.00	0.00	0.00	0.00	0.00	0.00	0.00	0.00	0.00	0.00	0.00
Cl	0.15	0.15	0.15	0.15	0.15	0.15	0.15	0.15	0.15	0.15	0.15	0.15

P: Porcelain, E: Egypt, I: India, S: Spanish, T: Turkey

The composition of porcelain tiles reveals silicon oxide (SiO_2) as the predominant component, accounting for a significant portion of the tile's mass, ranging from 34.96% to 48.20%. This information is visually depicted in Figure 1. Additionally, small quantities of aluminum oxide (Al_2O_3) are present, comprising approximately 5.89% to 11.83% of the tile's mass as shown in Figure 2. The provided data reveals clear differences in the ratio of Al_2O_3 (alumina) compared to SiO_2 (silica) among the samples. These variations indicate distinct disparities in the composition of the two elements throughout the samples. The higher proportions of Al_2O_3 suggest a stronger presence of alumina, while the range of SiO_2 percentages indicates a wider distribution of silica content. These findings highlight the contrasting nature of the two elements and emphasize the importance of considering their individual ratios in further analyses or investigations. The Figure 3 provide a graphical representation of the calcium oxide (CaO) values, which range from 5.07% to 10.24%. The prominence of silicon oxide as the major component in porcelain tiles is crucial to their structural integrity and durability. SiO_2, commonly known as silica, is a key building block in ceramics due to its high melting point and its ability to form strong bonds with other elements. Its presence ensures that the tiles possess the necessary strength and resistance to withstand various stresses and impacts.

The inclusion of aluminum oxide within the composition of the tiles contributes to their aesthetic appeal and performance characteristics. Al_2O_3 acts as a fluxing agent during the firing process, enabling the tiles to achieve their desired shape and preventing excessive shrinkage. Moreover, aluminum oxide imparts certain desirable properties to the tiles, such as enhanced hardness and resistance to wear and abrasion (Dondi et al., 2005).

The calcium oxide content, as indicated in Figure 3, plays a crucial role in the final properties of the porcelain tiles. CaO acts as a flux in the ceramic composition, lowering the melting point and facilitating the verification process during firing. This results in a denser and more impervious tile surface, enhancing its resistance to moisture, staining, and chemical damage. Understanding the composition and distribution of these components within the porcelain tiles provides valuable insights into their physical characteristics, performance, and potential applications. By carefully controlling the proportions of silicon oxide, aluminum oxide, and calcium oxide, manufacturers can tailor the properties of the tiles to meet specific requirements, such as strength, durability, and aesthetic preferences (Cheng et al., 2012).

Figure (1) silicon oxide SiO_2 (mass%) of the porcelain tile samples

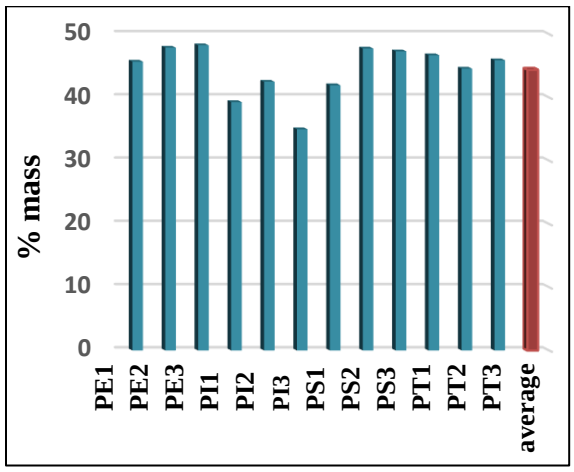

Figure (2) Aluminum oxide Al_2O_3 (mass%) of the porcelain tile samples

Figure 3 depicts the presence of minute quantities of certain constituents in porcelain tiles. These include traces of magnesium oxide (MgO), with concentrations ranging from 0.00% to 1.00% of the tile's mass. It is worth noting that the maximum concentration of MgO detected does not exceed 1.00% of the total mass. The presence of MgO in porcelain tiles can have several implications for their properties and performance. Magnesium oxide acts as a flux during the firing process, aiding in the vitrification and densification of the tiles. It can contribute to the overall strength and durability of the tiles, enhancing their resistance to cracking and structural failure. Additionally, the presence of MgO can influence the thermal expansion characteristics of the tiles, allowing them to withstand thermal stresses and temperature fluctuations without compromising their integrity. Furthermore, Figure 4 also demonstrates the presence of sodium oxide (Na_2O) and potassium oxide (K_2O) in the porcelain tiles. The concentrations of Na_2O range from 0.55% to 0.66% of the tile's mass, while K_2O concentrations range from 0.20% to 1.26%. The inclusion of Na_2O and K_2O in the tile composition can serve various purposes. These oxides act as fluxes and can lower the melting point of the ceramic mixture. This facilitates the sintering process during firing, allowing for the formation of a dense and well-consolidated tile structure. Additionally, Na_2O and K_2O can influence the viscosity of the liquid phase during firing, affecting the flow and leveling behavior of the glazes used on the tiles. This can result in improved surface quality and better adhesion of the glaze. The careful control and understanding of these minor constituents, such as MgO, Na_2O, and K_2O, in the composition of porcelain tiles are essential for achieving desired properties and ensuring consistent quality. Manufacturers can fine-tune the levels of these constituents to optimize various aspects of the tiles, such as strength, thermal stability, and glaze performance, ultimately delivering high-quality products to meet the diverse needs of architects, designers, and end-users (Martín et al., 2010; Pérez et al., 2012).

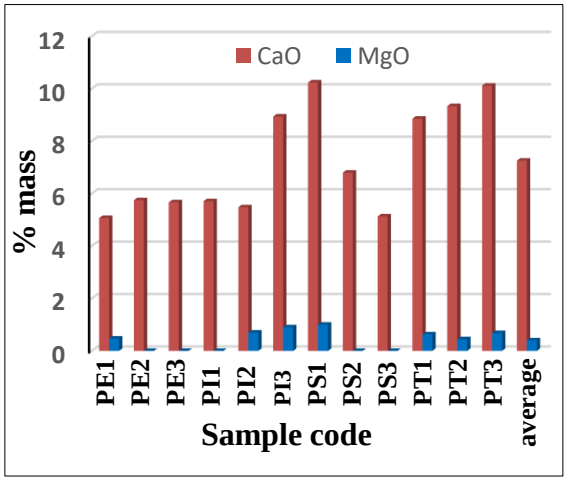

Figure (3) Calcium oxide CaO + Magnesium oxide MgO (mass%) of the porcelain tile samples

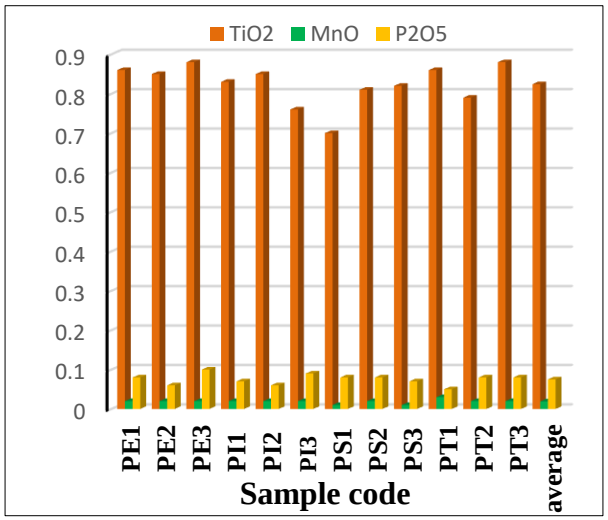

Figure (4) Potassium oxide K_2O + Sodium oxide NaO_2 (mass%) of the porcelain tile samples

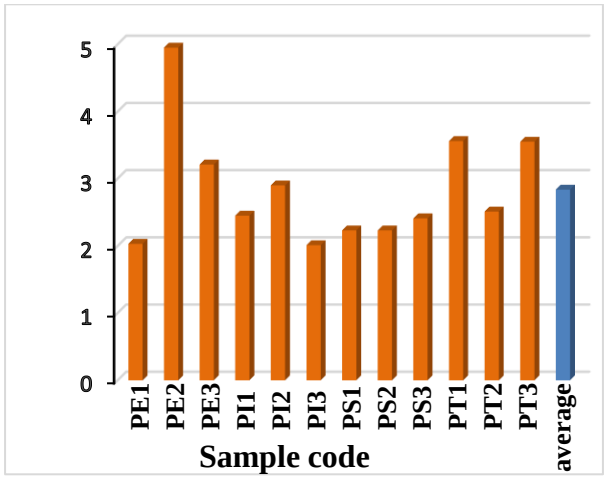

Figure (5) (Fe_2O_3 mass%) of the porcelain tile samples

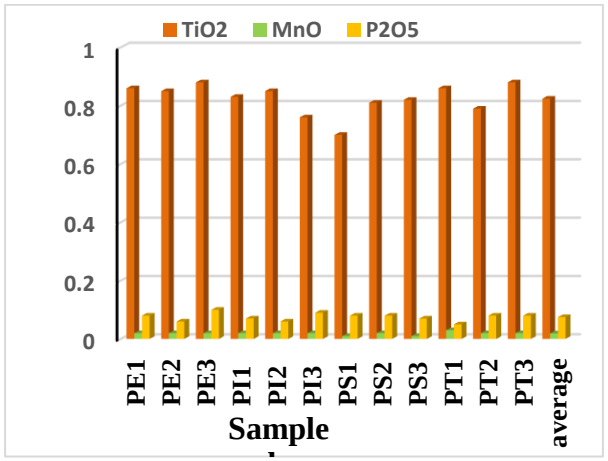

Figure (6) (P_2O_3 + TiO_2 + MnO - mass%) for all the porcelain tile samples

Figures 5 and 6 reveal the presence of minor constituents or impurities in the samples of porcelain tiles. These constituents include iron oxide (Fe_2O_3), titanium dioxide (TiO_2), and phosphorus trioxide (P_2O_3), detected in small amounts within the tiles. The measured values for Fe_2O_3 range from 2.01% to 4.95% of the tile's mass, while TiO2 concentrations fall between 0.70% and 0.88%. Additionally, P_2O_3 concentrations range from 0.05% to 0.10%. The detection of these minor constituents or impurities in porcelain tiles can have significant implications for their physical and chemical properties. Fe_2O_3, also known as iron(III) oxide or ferric oxide, is responsible for the reddish or brownish hues observed in some tiles. Its presence can add warmth and depth to the color palette of the tiles, offering a range of earthy tones. However, excessive amounts of Fe_2O_3 can affect the overall color consistency and may lead to undesirable variations in the final appearance of the tiles. TiO_2, or titanium dioxide, is a versatile compound that plays a crucial role in the ceramic industry. It acts as an opacifier, imparting brightness and opacity to the glazes used on porcelain tiles. TiO_2 can enhance the whiteness and brilliance of the glaze, improving the overall aesthetic appeal of the tiles. Additionally, it contributes to the tiles' resistance to UV radiation and provides durability against fading or discoloration over time. P_2O_3, or phosphorus trioxide, is a less commonly encountered constituent in porcelain tiles. Its presence may be attributed to impurities in the raw materials or as a deliberate addition for specific purposes. Phosphorus compounds can exhibit unique properties; such as flame retardancy or the ability to enhance certain glaze effects. However, its concentration is typically low in porcelain tiles, and its influence on the overall properties is relatively minor (Kamseu et al., 2007; Ferrari et al., 2006).

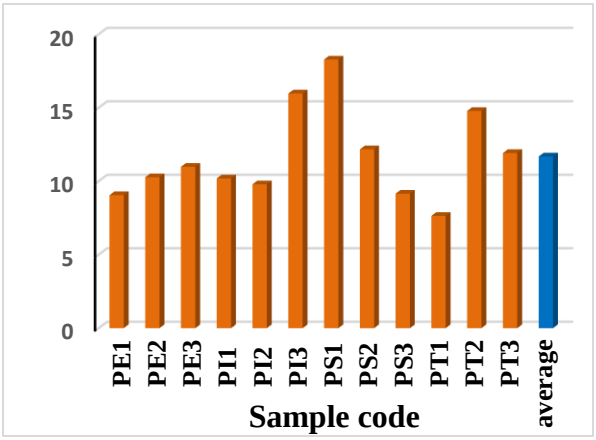

Figure (7) Calcite ($CaCO_3$ mass%) of the porcelain tile samples

Calcium carbonate is an affordable building material known for its primary physical characteristic: a white, odorless powder composed of colorless crystals that are nearly insoluble in water. In today's industrial and commercial applications, calcium carbonate is widely utilized as a mineral material. Its presence significantly enhances the stability of various building materials such as cement, bricks, and adhesives. The analysis of the samples revealed substantial levels of calcite as shown in Figure 7, which is the crystalline form of calcium carbonate ($CaCO_3$). In porcelain tiles with high silica content, the calcite content ranged from 7.64% to 12.17% of the tile's mass. Conversely, in porcelain tiles with low silica content, the calcite content varied from 9.05% to 18.28%. Examining the data presented in Table 1, we observe a consistent $CaCO_3$/CaO ratio across most samples, approximately 1.79. However, there were a few exceptions. Samples PE3, PT1, PT2, and PT3 exhibited ratios of 1.94, 0.89, 1.58, and 1.18, respectively. The $CaCO_3$/CaO ratio is of particular interest as it provides insights into the composition and behavior of the porcelain tiles. This ratio reflects the proportion of calcium carbonate to calcium oxide, both of which play vital roles in the properties and performance of the tiles. A consistent ratio suggests a balanced and controlled manufacturing process, ensuring the desired characteristics of the tiles. However, the deviations observed in certain samples indicate potential variations in the production process or the presence of additional factors that influenced the composition (Esposito et al., 2005; Bragança et al., 2011).

Based on the recorded results in Table 1, the samples can be categorized into two groups based on their silica content and other oxides:

1. Tiles with high silica content (>46% by mass), ranging from 46.67% to 48.20%. These tiles are rich in Al_2O_3 (>10% by mass) and have low concentrations of alkaline oxides (<1.4% by mass), except for sample PT1, which had a concentration of 1.87% by mass. The alkaline-earth oxides (CaO) ranged from 5.67% to 8.86% by mass, and MgO was absent except for sample PT1, which had a concentration of 0.63% by mass. The Al_2O_3/SiO_2 ratio falls within the range of 0.22-0.24, with most samples in this group having a ratio of 0.24.
2. Tiles with low silica content (<46% by mass), ranging from 34.96% to 45.86%. These tiles have higher concentrations of alkaline oxides (>1.4% by mass), except for samples PE1 and PT3, which had concentrations of 0.86% and 1.11% by mass, respectively. They also have lower amounts of Al_2O_3 (<10% by mass) and alkaline-earth oxides (CaO ranging from 5.07% to 10.24% by mass, and MgO ranging from 0.47% to 1.00% by mass). The Al_2O_3/SiO_2 ratio consistently remains equal to or below 0.22 in this group.

4 Conclusion

X-ray fluorescence (XRF) techniques were employed to determine the mass percentages of chemical components in twelve different samples of porcelain tiles collected from various markets in Benghazi city. The results revealed that percaline samples exhibited high mass percentages of quartz (SiO_2) and trace amounts of various metal oxides, including Al_2O_3, CaO, MgO, K_2O, Na_2O, Fe_2O_3, Ti_2O, P_2O_5, and MnO. Overall, there were no significant variations observed in the content of these metal oxides. The average mass percentages of silica (SiO_2), alumina (Al_2O_3), CaO, MgO, K_2O, Na_2O, Fe_2O_3, and Ti_2O were determined as 44.37%, 9.85%, 7.26%, 0.40%, 0.77%, 0.61%, 2.84%, and 0.82%, respectively. The average content of calcite ($CaCO_3$) was found to be 11.68%. From a scientific and economic perspective, it is more advantageous to use a smaller variety of raw minerals in the composition of porcelain tiles. This approach simplifies the analysis process and reduces the complexity associated with a larger number of components. However, from an engineering application standpoint, a diverse range of raw minerals in the formulation of porcelain tiles is preferable. By utilizing multiple types of minerals, the content of each mineral can be reduced. This allows for potential substitutions of similar minerals, while maintaining almost unchanged product properties. Consequently, this approach significantly mitigates the limitations associated with the availability of specific mineral resources.

Conflict of Interest: The authors declare that there are no conflicts of interest.

References

Alonso De la Garza, D.A.; Guzmán, A.M.; Gómez, C.; Martínez, D.I.; & Elizondo, N. (2022). Influence of Al_2O_3 and SiO_2 nanoparticles addition on the microstructure and mechano-physical properties of ceramic tiles. Ceramics International, 48, 12712–12720. https://doi.org/10.1016/j.ceramint.2022.01.140

Amorós, J.L.; Blasco, E.; Moreno, A., Feliu, C. (2022). Kinetics of the transformations occurring during the

firing process of an industrial spray-Dried porcelain stoneware body. Ceramics International, 48, 17611–17620. https://doi.org/10.1016/j.ceramint.2022.03.031

Beckhoff, B.; Kanngießer habil, B.; Langhoff, N.; Wedell, R.; Wolff, H. (Eds.). (2006). Handbook of Practical X-Ray Fluorescence Analysis. Berlin, Heidelberg: Springer Berlin Heidelberg. https://doi.org/10.1007/978-3-540-36722-2

Berto, A.M. (2007). Ceramic tiles: Above and beyond traditional applications. Journal of the European Ceramic Society, 27, 1607-1613. https://doi.org/10.1016/j.jeurceramsoc.2006.04.146

Bragança, S.R.; Lengler, H.C.M.; Bergmann, C.P. (2011). Spodumene-bearing rock as flux for triaxial ceramic bodies. Advances in Applied Ceramics, 110(5-6), 293-300. https://doi.org/10.1179/1743676111Y.0000000018

Cheng, X.; Ke, S.; Wang, Q.; Wang, H.; Shui, A.; Liu, P. (2012). Characterization of transparent glaze for single-crystalline anorthite porcelain. Ceramics International, 38, 4901-4908. https://doi.org/10.1016/j.ceramint.2012.02.081

De Noni Jr., A.; Hotza, D.; Soler, V.C.; Vilches, E.S. (2010). Influence of composition on mechanical behaviour of porcelain tile. part I: microstructural characterization and developed phases after firing. Materials Science & Engineering A, 527(7-8), 1730-1735. https://doi.org/10.1016/j.msea.2009.10.057

Demarch, A.; Waterkemper, A.; Pasini, D.; Ruzza, S.; Montedo, O.R.; & Angioletto, E. (2021). Effects of roughness parameters on slip resistance for different methods used to determine the coefficient of friction for ceramic floor tiles. Ceramics International, 47, 24281–24286. https://doi.org/10.1016/j.ceramint.2021.05.139.

Dondi, M.; Ercolani, G.; Guarini, G.; Melandri, C.; Raimondo, M.; Rocha e Almendra, E.; & Cavalcante, P.M.T. (2005). The role of surface microstructure on the resistance to stains of porcelain stoneware tiles. Journal of the European Ceramic Society, 25, 357-365. https://doi.org/10.1016/j.jeurceramsoc.2004.01.017

Esposito, L.; Tucci, A.; & Naldi, D. (2005). The reliability of polished porcelain stoneware tiles. Journal of the European Ceramic Society, 25, 1487-1498. https://doi.org/10.1016/j.jeurceramsoc.2004.05.030

Esposito, L.; Salem, A.; Tucci, A.; Gualtieri, A.; & Jazayeri, S.H. (2005). The use of nepheline-syenite in a body mix for porcelain stoneware tiles. Ceramics International, 31(2), 233-240. https://doi.org/10.1016/j.ceramint.2004.05.006

Ferrari, S.; Gualtieri, A. F. (2006). The use of illitic clays in the production of stoneware tile ceramics. Applied Clay Science, 32, 73-81. https://doi.org/10.1016/j.clay.2005.10.001

Gultekin, E.E.; Topates, G.; & Kurama, S. (2017). The effects of sintering temperature on phase and pore evolution in porcelain tiles. Ceramics International, 43(14), 11511-11515. https://doi.org/10.1016/j.ceramint.2017.06.024

Hamidalddin, S.H.Q. (2020). A Study of Chemical, Mineral Compositions (of Some Metals) and Natural Radioactivity in Porcelain and Ceramic Dinner Ware. Journal of Geoscience and Environment Protection, 8(11), 209-221. https://doi.org/10.4236/gep.2020.811014

Kamseu, E.; Leonelli, C.; Boccaccini, D. N.; Veronesi, P.; Miselli, P.; Pellacani, G.; Melo, U. C. (2007). Characterisation of porcelain compositions using two china clays from Cameroon. Ceramics International, 33(5), 851-857. https://doi.org/10.1016/j.ceramint.2006.01.025

Zhong, X.; Cao, L.; Huang, J.; Liu, Y.; Shen, X.; Wang, Q.; Li, X.; Wang, Yan, H.; D.; Ji, T. (2023). Enhanced mechanical properties of porcelain ceramic tile/Kevlar fabric composite with bio-inspired shell-like structure. International Journal of Applied Ceramic Technology, 20(5), 3073-3081. https://doi.org/10.1111/ijac.14413

Li, K.; Cordeiro, E.d.S.; De Noni, A. Jr. (2023). Comparison between Mullite-Based and Anorthite-Based Porcelain Tiles: A Review. Eng, 4(3), 2153-2166. https://doi.org/10.3390/eng4030123

Martín, J.; De la Torre, A.G.; Aranda, M.A.; Rincón, J.M.; & Romero, M. (2010). Evolution with temperature of crystalline and amorphous phases in porcelain stoneware. Journal of the American Ceramic Society, 92, 229-234. https://doi.org/10.1111/j.1551-2916.2008.02862.x

Montanari, R., Murakami, N., De Bonis, A., Colomban, P., Alberghina, M. F., Grifa, C., Izzo, F., Morra, V., Pelosi, C., & Schiavone, S. (2022). The early porcelain kilns of Arita: Identification of raw materials and their use from the 17th to the 19th century. Open Ceramics, 9, 100217. https://doi.org/10.1016/j.oceram.2021.100217

Njindam, O.; Njoya, D.; Mache, J.; Mouafon, M.; Messan, A.; & Njopwouo, D. (2018). Effect of glass powder on the technological properties and microstructure of clay mixture for porcelain stoneware tiles manufacture. Construction and Building Materials, 170, 512-519. https://doi.org/10.1016/j.conbuildmat.2018.03.069

Njoya, D.; Tadjuidje, F.; Ndzana, E.; Pountouonchi, A.; Tessier-Doyen, N.; % LecomteNana, G. (2017). Effect of flux content and heating rate on the microstructure and technological properties of mayouom (western-Cameroon) kaolinite clay based ceramics. Journal of Asian Ceramic Societies, 5(4), 422-426. https://doi.org/10.1016/j.jascer.2017.09.004

Pérez, J.M.; Rincón, J.M.; & Romero, M. (2012). Effect of moulding pressure on microstructure and technological properties of porcelain stoneware. Ceramics International, 38, 317-332. https://doi.org/10.1016/j.ceramint.2011.07.009

Sánchez, E.; García-Ten, J.; Sanz, V.; & Moreno, A. (2010). Porcelain tile: Almost 30 years of steady scientific-technological evolution. Ceramics International, 36, 831-845. https://doi.org/10.1016/j.ceramint.2009.11.016

Selli, N.T. (2015). Development of anorthite based white porcelain stoneware tile compositions. Ceramics International, 41, 7790-7795. https://doi.org/10.1016/j.ceramint.2015.02.112

Sverchkov, I.P.; Gembitskaya, I.M.; Povarov, V.G.; Chukaeva, M.A. (2023). Method of reference samples preparation for X-ray fluorescence analysis. Talanta, 252, 123820. https://doi.org/10.1016/j.talanta.2022.123820

Tripati, S.; Parthiban, G.; Pattan, J.N.; & Menezes, A. (2017). Chemical composition and provenance of Chinese porcelain shards recovered from Old Goa, west coast of India. Journal of Archaeological Science: Reports, 14, 467-478. https://doi.org/10.1016/j.jasrep.2017.06.002

Scientific Journal for the Faculty of Science-Sirte University Vol. 4, No. 1 (2024) 68-74

Scientific Journal for the Faculty of Science-Sirte University

Journal home page: http://journal.su.edu.ly/index.php/JSFSU/index

DOI: 10.37375/issn.2789-858X

Iterative Processes Methods for Solving Boundary Value Problem for the Caputo Fractional Differential Equations

Mufeedah M. S. Ahmed

Mathematic Department, Art & Science Kasr Khiar Faculty, Elmergib University, Khums, Libya.

DOI: https://doi.org/10.37375/sjfssu.v4i1.2598

ARTICLE INFO:

Received: 19 January 2024

Accepted: 26 March 2024

Published: 17 April 2024

Keywords: *Iterative processes methods, Caputo Fractional Differential equations with boundary conditions.*

A B S T R A C T

In this article, we introduce a study of approximate solutions for the Caputo fractional differential equations with boundary conditions in Banach space. We transformed given equations into equivalent integral equations for the construction of contraction mapping and other compact mapping, both of which allow for the proof of the existence of a solution. The ultimate goal of this study is to present a comparison of the speed convergence of the approximate solutions of Caputo Fractional differential equations obtained by using the processes repetitiveness of the Picard, Mann, Picard-Mann hybrid, Picard-Krasnoselskii hybrid, and Ishikawa methods to the general solutions.

1 Introduction

The study of the iterative processes for fractional differential equations to find approximating solutions is an active area of research. However, the exact or approximate analytical solutions are preferable for the boundary value problems because they permit the investigation of the qualitative properties of the appropriate control systems. The Picard iterative method is one of the simplest iteration methods to approximate the solution of fixed-point equations for fractional differential equations involving nonlinear contractive operators.

(Chidume et al., 2013; Chidume, 2014) introduced a study on the Picard iteration process and Krasnoselskii-type sequences. (Berinde, 2004) introduced a study on convergence for iterative methods and showed that the Picard iteration converges more rapidly than the Mann iteration. (Berinde et al., 2005) proved the Krasnoselskij iteration was speedily convergent for approximating fixed points in Banach spaces. The authors (Abdeljawad et al., 2020; Ghiura, 2021) published a study on the speed of convergence for iterative methods and explained in their results whether the convergence is strong or weak for a class of mappings. The existence and uniqueness of the solutions for the nonlinear fractional differential equation boundary value problem considered by the authors (Furati & Tatar, 2005; Lyons et al., 2017; Wang et al., 2014; Zhang, 2006).

2 Preliminaries

Let A be a real Banach space, and $M \neq \phi$ be a convex subset of A. Let $F : M \to M$ be a mapping, then F is said to be non-expansive mapping if:

$$\|Fx_1 - Fx_2\| \leq \|x_1 - x_2\| \quad \forall\ x_1, x_2 \in M \qquad (2.1)$$

and contraction mapping if:

$$\|Fx_1 - Fx_2\| \leq \rho\|x_1 - x_2\| \quad \forall\ x_1, x_2 \in M\ , \rho \in (0,1) \qquad (2.2)$$

***Corresponding author*: E-mail:** mmahmad@elmergib.edu.ly

Now, we define the Picard method (Picard, 1890) as the follows, let $x_0 \in M$ and $\{x_i\} \subset M$

$$x_{i+1} = Fx_i, \qquad i = 0,1,... \tag{2.3}$$

Let $\{\eta_i\}_{i=0}^{\infty}$ be a sequence in $(0,1)$ for $u_0 \in M$, then the Mann iterative method defined by the sequence $\{u_i\} \subset M$ (Mann, 1953):

$$u_{i+1} = (1-\eta_i)u_i + \eta_i Fu_i \quad, i = 0,1,... \tag{2.4}$$

Let $\{y_i\} \subset M$, the Krasnoselskii iteration method defined by (Krasnoselskii, 1955):

$$y_{i+1} = (1-\kappa)y_i + \kappa Fy_i \quad, i = 0,1,... \tag{2.5}$$

where $\kappa \in (0,1)$ is real a constant and $y_0 \in M$.

(Khan, 2013) presented the Picard-Mann hybrid method, which is given by the sequence $\{v_i\} \subset M$ as follows:

$$\begin{aligned} v_{i+1} &= Fy_i, \\ y_i &= (1-\eta_i)v_i + \eta_i Fv_i, \quad i = 0,1,... \end{aligned} \tag{2.6}$$

where $\{\eta_i\}_{i=0}^{\infty}$ are appropriately chosen sequences in $(0,1)$ and $v_0 \in M$.

(Okeke & Abbas, 2017) introduced a study on the Picard-Krasnoselskii hybrid iterative process. This iterative process is given by the sequence $\{x'_i\} \subset M$ as follows:

$$\begin{aligned} x'_{i+1} &= Fy_i, \\ y_i &= (1-\kappa)x_i + \kappa Fx_i, \quad i = 0,1,... \end{aligned} \tag{2.7}$$

where $\kappa \in (0,1)$ and $x_0 \in M$.

The Ishikawa iterative process is defined by the sequence $\{v_i\} \subset F$ as follows (Ishikawa, 1974):

$$\begin{aligned} w_{i+1} &= (1-\eta_i)w_i + \eta_i Fy_i, \\ y_i &= (1-\xi_i)w_i + \xi_i Fw_i, \quad i = 0,1,... \end{aligned} \tag{2.8}$$

where $\{\eta_i\}_{i=0}^{\infty}, \{\xi_i\}_{i=0}^{\infty}$ are appropriately chosen sequences in $(0,1)$ and $w_0 \in M$.

Definition 2.1. Let $\{a_i\}_{i=0}^{\infty}, \{b_i\}_{i=0}^{\infty} \in [0,\infty)$ converge to ℓ_1 and ℓ_2 respectively. Assume that there exists the following limit:

$$\lim_{i\to\infty}\left|\frac{a_i + \ell_1}{b_i + \ell_2}\right| = l$$

1- If $l = 0$, then a_i converges more rapidly to ℓ_1 than b_i to ℓ_2.
2- If $0 < l < \infty$, then a_i and b_i converge at the same rate.

Definition 2.2. Suppose that the iteration sequences $\{x_i\}_{i=0}^{\infty}$ and $\{y_i\}_{i=0}^{\infty}$ both converge to a fixed point q. Let $\{a_i\}, \{b_i\} \in \Re^+$, such that:

$$\|x_i - q\| \le a_i \ , \forall\ i \in \aleph,$$
$$\|y_i - q\| \le b_i \ , \forall\ i \in \aleph,$$

where a_i and b_i are converging to 0. If a_i converges faster than b_i, then $\{x_i\}$ is said to converge faster than $\{y_i\}$ to q.

Definition 2.3. If $\{x_i\}_{i=0}^{\infty}$ and $\{y_i\}_{i=0}^{\infty}$ are iteration sequences that converge to the unique fixed point q of F, then $\{x_i\}$ converges faster than $\{y_i\}$, if

$$\lim_{i\to\infty}\left\|\frac{x_i - q}{y_i - q}\right\| = 0$$

Lemma 2.1. (Şoltuz & Otrocol, 2007)

Let $\{s_i\}_{i=1}^{\infty} \in \Re^+$ which satisfies: $s_{i+1} \le (1-\delta_i)s_i$, if $\{\delta_i\}_{i=1}^{\infty} \in (0,1)$ and $\sum_{i=1}^{\infty}\delta_i = \infty$, then $s_i \to 0$ as $i \to \infty$.

Lemma 2.2. (Osilike & Aniagbosor, 2000)

Let $\{s_i\}_{i=1}^{\infty}, \{\delta_i\}_{i=1}^{\infty}$ and $\{\sigma_i\}_{i=1}^{\infty}$ be sequences in $\Re^+$ which satisfies the inequality:

$$s_{i+1} \le (1+\delta_i)s_{i+1} + \sigma_i \ , \qquad \forall\ i \ge 1. \tag{2.9}$$

If $\sum_{i=1}^{\infty}\delta_i < \infty$ and $\sum_{i=1}^{\infty}\sigma_i < \infty$, then $s_i \to 0$ as $i \to \infty$.

3 Fractional calculus

Fractional calculus has operations of integration and differentiation of fractional order, and the theory of fractional differential equations has affected many authors in mathematics, physics, and engineering. In this section, we will review some fundamental definitions and lemmas concerning fractional calculus operators (Diethelm & Ford, 2010; Kilbas et al., 2006):

Definition 3.1. Let $\alpha > 0$ and $g : \Re^+ \to \Re$ be a function, the left and right RLF integral operators I_{a+}^{α} and I_{b-}^{α} of order $\alpha \in \Re^+$ of g are defined by:

$$I_{b-}^{\alpha} g(t) = D_{b+}^{-\alpha} g(t) = \frac{1}{\Gamma(\alpha)} \int_t^b (\tau - t)^{\alpha-1} g(\tau) d\tau, t \in [a,b) \subset \Re^+ \quad (3.1)$$

$$I_{a+}^{\alpha} g(t) = D_{a+}^{-\alpha} g(t) = \frac{1}{\Gamma(\alpha)} \int_a^t (t - \tau)^{\alpha-1} g(\tau) d\tau, t \in (a,b] \subset \Re^+ \quad (3.2)$$

respectively, where $\Gamma(.)$ is defined by $\Gamma(\alpha) = \int_0^{\infty} t^{\alpha-1} e^{-t} dt$.

Definition 3.2. Let $\alpha \in \Re^+$, $0 < \alpha < 1$, the left and right RLF derivative of g are defined by:

$$D_{a+}^{\alpha} g(t) := DI_{a+}^{1-\alpha} g(t), \quad \forall t \in (a,b] \quad (3.3)$$

$$D_{b-}^{\alpha} g(t) := -DI_{b-}^{1-\alpha} g(t), \quad \forall t \in [a,b) \quad (3.4)$$

The following properties are held for fractional integrals and derivatives:-

1- $D_{a+}^{\nu} I_{a+}^{\alpha} g(t) = I_{a+}^{\alpha-\nu} g(t)$ and $D_{b-}^{\nu} I_{b-}^{\alpha} g(t) = I_{b-}^{\alpha-\nu} g(t)$ if $\alpha, \nu \in \Re^+$.

2- $D^{-\alpha} D^{-\nu} g(t) = I^{\alpha+\nu} g(t) = D^{-\alpha-\nu} g(t)$, $\alpha, \nu > 0$.

3- $I^{\alpha} I^{\nu} g(t) = I^{\nu} I^{\alpha} g(t)$

4- $I^{\alpha} D^{\alpha} g(t) = g(t), 0 < \alpha < 1$, $g \in C[a,b]$, and $D^{\alpha} g(t) \in C(a,b) \cap L(a,b)$.

5- $I^{\alpha} t^{\nu} = \frac{\Gamma(\nu+1)}{\Gamma(\nu-\alpha+1)} t^{\nu-\alpha}$, $\alpha \geq 0, \nu > -1$

Definition 3.3. The Caputo derivative of order α for a function $g : \Re^+ \to \Re$ is given by:

$${}^{C}D_{0^+}^{\alpha} g(t) = \frac{1}{\Gamma(\upsilon - \alpha)} \int_0^t (t - \varsigma)^{\upsilon-\alpha-1} g^{(\upsilon)}(\varsigma) d\varsigma \quad (3.5)$$

where $\upsilon \in \aleph$ with $\upsilon - 1 < \alpha < \upsilon$.

4 Main Results

We will employ iterative processes (2.3), (2.4),(2.6), (2.7), and (2.8) to find the approximate solutions of the fractional differential equations. We consider Caputo's fractional differential equation with boundary conditions:

$$\begin{aligned} {}^{c}D_{a+}^{\alpha} u(t) &= \varphi(t, u(t)), \quad t \in \Im \\ u(a) &= u_a, \quad u(b) = u_b \end{aligned} \quad (4.1)$$

where $0 < \alpha \leq 1, u(t) \in C(\Im, \Re)$ and $\left(C(\Im, \Re), \| \|_{\infty}\right)$ is Banach space, where $\left\| u - u^* \right\|_{\infty} = \sup_{t \in \Im} \left| u(t) - u^*(t) \right|$, consequently, φ is a continuous function from $I \times \Re$ to $\Re$, and there exists a constant $L > 0$ such that $\left| \varphi(t,u) - \varphi(t,u^*) \right| \leq L \left| u - u^* \right|$, $\forall t \in \Im, u, u^* \in C(\Im, \Re)$, L is a Lipschitzian constant.

Lemma 4.1. Assume that $\varphi : \Im \times \Re \to \Re$ is a continuous function, then the fractional differential equation of boundary value problem (4.1) has a unique solution:

$$u(t) = u(a) + \frac{1}{\Gamma(\alpha)} \int_a^t (t - \tau)^{\alpha-1} \varphi(\tau, u(\tau)) d\tau, \quad (4.2)$$

in $C(\Im, \Re)$ and the sequence of successive approximations $\{u_i\}$ defined by:

$$u_{i+1}(t) = u_0(a) + \frac{1}{\Gamma(\alpha)} \int_a^t (t - \tau)^{\alpha-1} \varphi(\tau, u_i(\tau)) d\tau, \; t \in \Im, i \geq 0$$

converges to u as $m \to \infty$.

Lemma 4.2. Assume $\varphi(t, u(t))$ is a continuous function on $\Im \times \Re$. Then $u(t) \in C(\Im, \Re)$ is a solution of the BVP (4.1) if and only if $u(t)$ is a solution of (4.2).

Lemma 4.3. Suppose that $\varphi(t, u(t))$ is a continuous on $\Im \times \Re$, and define the mapping F from $C(\Im, \Re)$ into itself by:

$$Fu(t) = u(a) + \frac{1}{\Gamma(\alpha)} \int_a^t (t - \tau)^{\alpha-1} \varphi(\tau, u(\tau)) d\tau$$

Then F is a completely continuous.

Proof. For any $u \in C(\Im, \Re)$ from definition of $Fu(t)$ and lemma (4.1), we have $Fu \in C(\Im, \Re)$ and $Fu(t) \geq 0$, $t \in \Im$. Hence $F(C(\Im, \Re)) \subset C(\Im, \Re)$. Since $\varphi(t, u(t)) \in C(\Im \times \Re)$ the continuity of F is obvious. Now, let $\Omega_{\varepsilon} \subset C(\Im, \Re)$ be bounded; where $\Omega_{\varepsilon} = \{u \in C(\Im, \Re) : \|u\|_{\infty} < \varepsilon\}$, let $M = \max_{t \in \Im} \left| \varphi(t, u(t)) \right|$, then for that $u \in \Omega_{\varepsilon}$, from the lemma (4.1), we have

$$\begin{aligned} \left| Fu(t) \right| &\leq \left| u(a) \right| + \frac{1}{\Gamma(\alpha)} \int_a^t \left| (t - \tau)^{\alpha-1} \right| \left| \varphi(\tau, u(\tau)) \right| d\tau \\ &\leq \left| u_a \right| + \frac{M (t - a)^{\alpha}}{\Gamma(\alpha + 1)} \end{aligned} \quad (4.3)$$

Hence, $F(\Omega_{\varepsilon})$ is bounded. Let $t_1, t_2 \in \Im, t_1 < t_2$, and $u \in \Omega_{\varepsilon}$. Then:

$$\begin{aligned} \left| Fu(t_1) - Fu(t_2) \right| &= \left| \frac{1}{\Gamma(\alpha)} \int_a^{t_1} (t - \tau)^{\alpha-1} \varphi(\tau, u(\tau)) d\tau - \frac{1}{\Gamma(\alpha)} \int_a^{t_2} (t - \tau)^{\alpha-1} \varphi(\tau, u(\tau)) d\tau \right| \\ &\leq \frac{1}{\Gamma(\alpha)} \int_{t_1}^{t_2} (t - \tau)^{\alpha-1} \left| \varphi(\tau, u(\tau)) \right| d\tau \\ &\leq \frac{M}{\Gamma(\alpha + 1)} \left[\chi_1 - \chi_2 \right] \end{aligned} \quad (4.4)$$

where $\chi_j = (t - t_j)^{\alpha}, j = 1,2$, the Arzela-Ascoli theorem guarantees that $F(\Omega_{\varepsilon})$ is relatively compact, which means that F is compact. Thus, F is completely continuous.

Theorem 4.2. Assume that $\varphi(t,u(t))$ is a given and satisfied the following conditions:

($\boldsymbol{H_1}$) the function $\varphi:\Im\times\Re\to\Re$ is a continuous.
($\boldsymbol{H_2}$) There exist $0<L<1$ such that:
$|\varphi(t,u)-\varphi(t,u^*)|\le L|u-u^*|$, for any $t\in\Im$, $u,u^*\in C(\Im,\Re)$.
($\boldsymbol{H_3}$) $L\dfrac{(t-a)^\alpha}{\Gamma(\alpha+1)}<1$.

Then eq.(4.1) has a unique solution q in $C(\Im,\Re)$, and the Picard iteration is a converging to q.

Theorem 4.3. Assume that $\varphi(t,u(t))\in(C(\Im\times\Re,\Re))$ is a given, and satisfied condition ($\boldsymbol{H_1}$)-($\boldsymbol{H_3}$). Then the problem (4.1) has a unique solution q in $C(\Im,\Re)$ and the Mann iterative process converges to q.

Proof : Let a sequence $\{u_i\}$ generated by the iteration (2.4). Now, we define F as the form:

$$Fu(t)=u_a+\frac{1}{\Gamma(\alpha)}\int_a^t(t-\tau)^{\alpha-1}\varphi(\tau,u(\tau)d\tau,\quad t\in\Im \tag{4.5}$$

So, for each $t\in\Im, i=0,1,...$, we have:

$$\begin{aligned}\|u_{i+1}-q\|_\infty&=\|(1-\eta_i)(u_i-q)+\lambda_i(Fu_i-q)\|_\infty\\&=(1-\eta_i)\|u_i-q\|_\infty+\eta_i\sup_{t\in\Im}|Fu_i(t)-Fq(t)|\\&=(1-\eta_i)\|u_i-q\|_\infty+\frac{\eta_i}{\Gamma(\alpha)}\sup_{t\in\Im}\left|\int_a^t(t-\tau)^{\alpha-1}|\varphi(\tau,u_i(\tau))-\varphi(\tau,q(\tau))|d\tau\right|\end{aligned}$$

$$\begin{aligned}\|u_{i+1}-q\|_\infty&\le(1-\eta_i)\|u_n-q\|_\infty+\frac{L\eta_i}{\Gamma(\alpha)}\int_a^t(t-\tau)^{\alpha-1}\sup_{t\in\Im}|u_n(\tau)-q(\tau)|d\tau\\&\le[(1-\eta_i)+L\eta_i\frac{(t-a)^\alpha}{\Gamma(\alpha+1)}]\|u_i-q\|_\infty.\end{aligned}\tag{4.6}$$

Since $(1-\eta_i)+\dfrac{L\eta_i(t-a)^\alpha}{\Gamma(\alpha+1)}<1$, hence, the conditions stipulated by Lemma 2.1. have been fulfilled, and consequently, $u_i\to p$ as $i\to\infty$ according to Banach's fixed point theorem (Chipot, 2011, Granas & Dugundji, 2003), the operator F has a unique fixed point, which implies that eq.(4.1) has a unique solution q in $C(\Im,\Re)$.

Theorem 4.3. Assume that $\varphi(t,u(t))\in(C(\Im\times\Re,\Re))$ is a given and satisfied condition ($\boldsymbol{H_1}$)-($\boldsymbol{H_3}$). Then eq.(4.1) has a unique solution q in $C(\Im,\Re)$ and the iteration process (2.6) converges to q.

Proof: Let $\{v_i\}$ generated by the Picard-Mann hybrid process (2.6), and define F as:

$$Fv(t)=v(a)+\frac{1}{\Gamma(\alpha)}\int_a^t(t-\tau)^{\alpha-1}\varphi(\tau,v(\tau)d\tau,\quad t\in\Im$$

Thus, for each $t\in\Im, i=0,1,...$

$$\begin{aligned}\|y_i-q\|_\infty&=\|(1-\eta_i)(v_i-q)+\eta_i(Fv_i-q)\|_\infty\\&=(1-\eta_i)\|v_i-q\|_\infty+\eta_i\sup_{t\in\Im}|Fv_i(t)-Fq(t)|\\&=(1-\eta_i)\|v_i-q\|_\infty+\frac{\eta_i}{\Gamma(\alpha)}\sup_{t\in\Im}\left|\int_a^t(t-\tau)^{\alpha-1}|\varphi(\tau,v_i(\tau))-\varphi(\tau,q(\tau))|d\tau\right|\\&\le[(1-\eta_i)+\frac{L\eta_i}{\Gamma(\alpha+1)}(t-a)^\alpha]\|v_i-q\|_\infty.\end{aligned}\tag{4.7}$$

Using (2.6), (2.2) and (4.7), we obtain the follow:

$$\begin{aligned}\|v_{i+1}-q\|_\infty&=\|Fy_i-Fq\|_\infty=\sup_{t\in\Im}|Fy_i(t)-Fq(t)|\\&\le\rho\|y_n-q\|_\infty\\&\le\rho[(1-\eta_i)+\frac{L\eta_i}{\Gamma(\alpha+1)}(t-a)^\alpha]\|v_i-q\|_\infty\end{aligned}\tag{4.8}$$

since $(1-\eta_i)+\dfrac{L\eta_i}{\Gamma(\alpha+1)}(t-a)^\alpha<1, 0<\rho<1$, therefore, from Lemma 2.1. we have: $v_i\to q$ as $i\to\infty$ and according to Banach's Theorem, the operator F has a unique fixed point, which is a unique solution for eq. (4.1) in $C(\Im,\Re)$.

Theorem 4.4. Assume that $\varphi\in(C(\Im\times\Re,\Re))$ is a given and satisfied condition ($\boldsymbol{H_1}$)-($\boldsymbol{H_3}$). Then problem (4.1) has a unique solution q in $C(\Im,\Re)$, and the iteration process (2.7) converging to q.

Proof: Let $\{x_i\}$ generated by the Picard-Krasnoselskii hybrid iteration (2.7) and the operator F define by:

$$Fx'(t)=x'(a)+\frac{1}{\Gamma(\alpha)}\int_a^t(t-\tau)^{\alpha-1}\varphi(\tau,x(\tau)d\tau,\tag{4.9}$$

subsequently, for each $t\in\Im, i=0,1,...$:

$$\begin{aligned}\|y_i-q\|_\infty&\le(1-\kappa)\|x'_n-q\|_\infty+\kappa\|Fx'_i-Tq\|_\infty\\&=(1-\kappa)\|x'_i-q\|_\infty+\kappa\sup_{t\in\Im}|Fx'_i(t)-Fq(t)|\\&=(1-\kappa)\|x'_i-q\|_\infty+\frac{\kappa}{\Gamma(\alpha)}\sup_{t\in\Im}\left|\int_a^t(t-\tau)^{\alpha-1}[\varphi(\tau,x'_i(\tau))-\varphi(\tau,q(\tau))]d\tau\right|\\&\le(1-\kappa)\|x'_i-q\|_\infty+\frac{L\kappa}{\Gamma(\alpha)}\int_a^t(t-\tau)^{\alpha-1}\|x'_i-q\|_\infty d\tau\end{aligned}\tag{4.10}$$

$$\|y_i-q\|_\infty\le[(1-\kappa)+\frac{L\kappa}{\Gamma(\alpha+1)}(t-a)^\alpha]\|x'_i-q\|_\infty.\tag{4.11}$$

By use (2.7), (2.2) and (4.11) we get the follow:

$$\begin{aligned}\|x'_{i+1}-q\|_\infty&=\|Fy_n-Fq\|_\infty=\sup_{t\in\Im}|Fy_i-Fq|\\&\le\rho\|y_n-q\|_\infty\\&\le\rho[(1-\kappa)+\frac{L\kappa}{\Gamma(\alpha+1)}(t-a)^\alpha]\|x'_i-q\|_\infty.\end{aligned}\tag{4.12}$$

Since $(1-\kappa)+\dfrac{L\kappa}{\Gamma(\alpha+1)}(t-a)^\alpha<1$ and $\rho\in(0,1)$, then the

of Lemma 2.1. are satisfied, which implies that $x'_i \to q$ as $i \to \infty$ and by applying Banach's theory, it follows that F has a unique fixed point, which means that q is a unique solution for eq.(4.1) in $C(\Im, \Re)$.

Theorem 4.5. Assume that $\varphi \in (C(\Im \times \Re, \Re))$ is a given, and satisfied condition (***H*₁**)-(***H*₃**), then eq.(4.1) has a unique solution q in $C(\Im, \Re)$ and the Ishikawa iterative process (2.8) converges to q.

Proof : Let a sequence $\{w_i\}$ generated by the Ishikawa process (2.8). Now, we define the operator F as:

$$Fw(t) = w(a) + \frac{1}{\Gamma(\alpha)} \int_a^t (t-\tau)^{\alpha-1} \varphi(\tau, w(\tau)) d\tau, \quad t \in \Im \tag{4.13}$$

for each $t \in \Im, i = 0,1,...$ we have:

$$\begin{aligned} \|y_i - q\|_\infty &= \|(1-\xi_i)(w_i - p) + \xi_i (Fw_i - q)\|_\infty \\ &\le (1-\xi_i)\|w_i - q\|_\infty + \xi_i \sup_{t \in I} |Fw_i(t) - Fq(t)| \\ &\le [(1-\xi_i) + \frac{L\xi_i}{\Gamma(\alpha+1)}(t-a)^\alpha] \|w_i - q\|_\infty . \end{aligned} \tag{4.14}$$

Consequently, from (2.8), (2.2) and (4.14) we obtain the following:

$$\begin{aligned} \|w_{i+1} - q\|_\infty &= \|(1-\eta_i) w_n + \eta_i F y_i - q\|_\infty \\ &\le (1-\eta_i)\|w_i - p\|_\infty + \eta_i \rho \|y_i - q\|_\infty \\ &\le (1-\eta_i)\|w_i - p\|_\infty + \eta_i \rho [(1-\xi_i) + L\xi_i \frac{(t-a)^\alpha}{\Gamma(\alpha+1)}] \|w_i - q\|_\infty \\ &\le \left(1 - \eta_i [1 - \rho[(1-\xi_i) + \frac{L\xi_i}{\Gamma(\alpha+1)}(t-a)^\alpha]\right) \|w_i - q\|_\infty \\ &\le \left(1 - \eta_i [1 - \rho[(1-\xi_i (1 - \frac{L}{\Gamma(\alpha+1)}(t-a)^\alpha]\right) \|w_n - q\|_\infty \end{aligned} \tag{4.15}$$

since $1 - \eta_i [1 - \rho[(1-\xi_i (1 - \frac{L}{\Gamma(\alpha+1)}(t-a)^\alpha] < 1$, so $w_n \to q$, through the Banach's Theorem we get $q \in fixd(F)$, and conclude that the eq.(4.1) has a unique solution q in $C(\Im, \Re)$.

Now, we are in a position to give the following proposition for the comparison between the previous iterative processes.

Proposition 4.1 Let $M \neq \phi$ be a bounded and closed convex subset of Banach space A, the mapping F from M into itself is a contraction, assume that each processe: (2.3),(2.4),(2.6),(2.7) and (2.8) converges to the same fixed point of F, where $\{\eta_i\}_{i=0}^\infty, \{\xi_i\}_{i=0}^\infty$ are sequences in the interval $(0,1)$ such that:

$0 < \gamma \le \eta_i, \xi_i < 1$ for all $i \ge 0$ and for some $\gamma \ge 0$, $\kappa \in (0,1)$. Then the Picard-Mann hybrid iteration (2.6) converges faster than the other iterations.

Proof: Suppose that $q \in fixd(F)$, and given that F is a contraction mapping from (2.2) and Picard iteration (2.3) we have:

$$\begin{aligned} \|x_{i+1} - p\|_\infty &= \|Fx_i - q\|_\infty \\ &\le \rho \|x_i - q\|_\infty \\ &\vdots \\ &\le \rho^i \|x_1 - q\|_\infty \end{aligned} \tag{4.16}$$

Let:

$$a_i = \rho^i \|x_1 - q\|_\infty \tag{4.17}$$

So, from (2.2) and the Mann iteration (2.4),we have:

$$\begin{aligned} \|u_{i+1} - q\|_\infty &= \|(1-\eta_i)(u_i - p) + \eta_i (Fu_i - q)\|_\infty \\ &= (1-(1-\rho)\eta_i)\|u_i - q\|_\infty \\ &\le (1-(1-\rho)\gamma)\|u_i - q\|_\infty \\ &\vdots \\ &\le (1-(1-\rho)\gamma)^i \|u_1 - q\|_\infty \end{aligned} \tag{4.18}$$

Let:

$$b_i = (1-(1-\rho)\gamma)^i \|u_1 - q\|_\infty \tag{4.19}$$

By using (2.2)and (2.6), we obtain:

$$\begin{aligned} \|v_{i+1} - q\|_\infty &= \|Fy_i - q\|_\infty \\ &\le \rho \|y_i - q\|_\infty \\ &\le \rho \left[(1-\eta_i)\|v_i - q\|_\infty + \rho\eta_i \|v_i - q\|_\infty\right] \\ &= \rho(1-(1-\rho)\eta_i)\|v_i - q\|_\infty \\ &\le \rho(1-(1-\rho)\gamma)\|v_i - q\|_\infty \\ &\vdots \\ &\le \rho^i (1-(1-\rho)\gamma)^i \|v_1 - q\|_\infty \end{aligned} \tag{4.20}$$

Put:

$$c_i = \rho^i (1-(1-\rho)\gamma)^i \|v_1 - q\|_\infty \tag{4.21}$$

By using (2.2) and eq. (2.7), we obtain:

$$\begin{aligned} \|x'_{i+1} - q\|_\infty &= \|Fy_i - q\|_\infty \le \rho \|y_i - q\|_\infty \\ &\le \rho \|(1-\kappa)(x'_i - q) + \kappa(Fx'_i - q)\|_\infty \\ &= \rho(1-(1-\rho)\kappa)\|x'_i - q\|_\infty \\ &\vdots \\ &\le \rho^i (1-(1-\rho)\kappa)^i \|x'_1 - q\|_\infty \end{aligned} \tag{4.22}$$

Since $0 < \kappa < 1$, then for $i \ge 0$ we have $1-(1-\rho)\kappa < 1$

Put:

$$d_i = \rho^i \|x'_1 - q\|_\infty \tag{4.23}$$

Now, from (2.2) and the Ishikawa iteration (2.6), it follows that:

$$\begin{aligned}\|y_i - q\|_\infty &= \|(1-\xi_i)w_n + \xi_i F w_i - p\|_\infty \\ &\le (1-\xi_i)\|w_i - q\|_\infty + \xi_i \rho \|w_i - q\|_\infty \\ &\le [(1-\xi_i) + \rho\xi_i]\|w_i - q\|_\infty \end{aligned} \quad (4.24)$$

From (2.2), (2.6), and (4.24), we obtain that

$$\begin{aligned}\|w_{i+1} - q\|_\infty &= \|(1-\eta_i)(w_i - q) + \eta_i (Fy_i - q)\|_\infty \\ &\le (1-\eta_i)\|w_i - q\|_\infty + \rho\eta_i [(1-\xi_i) + \xi_i \rho]\|w_i - q\|_\infty \\ &\le (1-\eta_i + \rho\eta_i [(1-\xi_i) + \xi_i \rho])\|w_i - q\|_\infty \\ &\le (1-\eta_i(1-\rho) - \rho\eta_i\xi_i(1-\rho))\|w_i - q\|_\infty \\ &\vdots \\ &\le (1-\gamma(1-\rho) - \rho\gamma^2(1-\rho))^i \|w_1 - q\|_\infty \end{aligned} \quad (4.25)$$

for $i \ge 0$. Since $0 \le \gamma \le \eta_i, \xi_i \le 1$, then for $i \ge 0$ we have: $1-\eta_i(1-\rho) - \rho\eta_i\xi_i(1-\rho) \le 1-\gamma(1-\rho) - \rho\gamma^2(1-\rho) < 1$

Put:

$$e_i = \|w_1 - p\|_\infty \quad (4.26)$$

We now compare the convergence of the Picard-Mann hybrid iteration process (2.6) as follows:

Firstly, we calculated the convergence rate between the Picard-Mann hybrid and iterations (2.3), we obtained:

$$\frac{c_i}{a_i} = \frac{(1-(1-\rho)\gamma)^i \|v_1 - q\|_\infty}{\|x_1 - q\|_\infty} \to 0 \ as \quad i \to \infty \quad (4.27)$$

Secondly, we calculate the convergence rate between the iterative process (2.6) and Mann iteration methods:

$$\frac{c_i}{b_i} = \rho^i \frac{\|v_1 - q\|_\infty}{\|u_1 - q\|_\infty} \to 0 \ as \quad i \to \infty \quad (4.28)$$

Thirdly, we computed the convergence rate between the iterative process (2.6) and the Picard-Krasnoselskii hybrid iteration process:

$$\frac{c_i}{d_i} = (1-(1-\rho)\gamma)^i \frac{\|v_1 - q\|_\infty}{\|x'_1 - q\|_\infty} \to 0 \ as \quad i \to \infty \quad (4.29)$$

Finally, we calculated the convergence rate between the iterative process (2.6) and the Ishikawa iteration process:

$$\frac{c_i}{e_i} = \frac{\rho^i (1-(1-\rho)\gamma)^i \|v_1 - q\|_\infty}{\|w_1 - q\|_\infty} \to 0 \ as \quad i \to \infty \quad (4.30)$$

Consequently, we conclude from (4.27), (4.28), (4.29), (4.30) that the speed convergence of $\{v_i\}_{i=1}^\infty$ to q is better than both $\{x_i\}_{i=1}^\infty, \{u_i\}_{i=1}^\infty, \{x'_i\}_{i=1}^\infty$ and $\{w_i\}_{i=1}^\infty$.

5 Illustrative Example

We introduce the following example to illustrate the previous comparison in the proposition:

Example 1. we consider Caputo Fractional differential equation for $\alpha = 1/2$ with conditions:

$$\begin{cases} {}^C D^\alpha_{a=0} u(t) = Exp(-t)u(t), & t \in [0,1] \\ u(0) = 1, \ {}^C D^\alpha u(0) = 1 \end{cases}$$

where $\kappa = 1/3$ and $\{\eta_i\}_{i=0}^\infty = \{10^{-2i}\}_{i=0}^\infty, \{\beta_i\}_{i=0}^\infty = \{1/2^{(i+1)!}\}_{i=0}^\infty$.

it's clear that: $\Phi = Exp(-t)u(t) \in (C([0,1]\times\Re,\Re))$ was satisfied the conditions (***H*₁**)-(***H*₃**), further, for each $t \in [0,1]$ and $u, u^* \in \Re$, we get:

$$|\Phi(t,u) - \Phi(t,u^*)| = |e^{-t}| |u - u^*| \le |u - u^*|$$

The following tables show that the Picard-Mann hybrid iterative is better convergent than all other processes to the exact solution.

t_i	Exact	Picard	Mann	Krasnoselskii
0.	1.	1.	1.	1.
0.1	1.10517	1.33396	1.00334	1.33396
0.2	1.2214	1.44243	1.00442	1.44243
0.3	1.34986	1.50807	1.00508	1.5080
0.4	1.49182	1.5506	1.00551	1.5506
0.5	1.64872	1.57829	1.00578	1.57829
0.6	1.82212	1.59567	1.00596	1.59567
0.7	2.01375	1.60559	1.00606	1.60559
0.8	2.22554	1.60995	1.0061	1.60995
0.9	2.4596	1.61014	1.0061	1.61014
1.	2.71828	1.60716	1.00607	1.60716

Table 1

t_i	Picard–Mann	Picard- Krasnoselskii.	Ishikawa
0.	1.	1.	1.
0.1	1.45199	1.38855	1.00404
0.2	1.6859	1.56505	1.00595
0.3	1.87722	1.70443	1.00748
0.4	2.04333	1.82354	1.00878
0.5	2.19135	1.92904	1.00995
0.6	2.32523	2.02443	1.011
0.7	2.44748	2.11187	1.01196
0.8	2.55992	2.19281	1.01285
0.9	2.6639	2.26828	1.01367
1.	2.7605	2.33909	1.01444

Table 2

Acknowledgments

We thank the anonymous referees for their time spent reviewing our paper and carefully reading it to give valuable feedback to improve the quality of this article.

Conflict of Interest: The author declares that there are no conflicts of interest.

REFRENCES

Abdeljawad, T.; Ullah K., Ahmad, J. (2020): "On Picard–Krasnoselskii hybrid iteration process in Banach spaces." Jour. of Mathematics, 2020, 1-5.

Berinde, V.(2004): "Picard iteration converges faster than Mann iteration for class of quasi-contractive operators." Fixed Point Theory and Appl., 2004, 1-9.

Berinde, V., Mădălina, B. (2005): "The fastest Krasnose-lskij iteration for approximating fixed points of strictly pseudo-contractive mappings." Carpathian Journal of Mathematics, 13-20.

Chipot, M. (2011): Handbook of differential Equations: Stationary Partial Differential Equations. Elsevier.

Chidume, C.E., Chidume, C.O., Djitté, N., Minjibir, M.S. (2013,January): "Convergence theorems for fixed points of multivalued strictly pseudo contractive mappings in Hilbert spaces." Abstract Appl. Anal., (vol. 2013), Hindawi.

Chidume, C.E. (2014): "Strong convergence and stability of Picard iteration sequences for a general class of contractive-type mappings." Fixed Point Theory Appl., 2014, 1-10.

Chidume, C.E. (2014): "Picard iteration process for a general class of contractive mappings." Journal of the Nigerian Mathematical Society, 33(1-3), 19-23.

Diethelm, K., Ford, N.J. (2010): "The analysis of fractional differential equations." Lect. Notes in Mathematic, 2004.

Furati, K. M., Tatar, N. E. (2005): "Power-type estimates for a nonlinear fractional differential equation." Nonlinear Analysis: Theory Methods & Applications, 62(6), 1025-1036.

Granas, A., Dugundji, J. (2003): "Fixed point theory." (vol. 14), New York: Springer.

Ghiura, A. (2021): "Convergence of modified Picard-Mann hybrid iteration process for nearly nonexpansive mappings." *arXiv preprint arXiv:* 2101.04567.

Ishikawa, S. (1974): "Fixed points by a new iteration method." Proceedings of the American Math. Society, 44(1), 147-150.

Krasnoselskii, M.A. (1955): "Two observations about the method of successive approximations." Uspekhi Matematicheskikh Nauk, 10(1), 123-127.

Kilbas, A.A., Srivastava, H.M., Trujillo, J.J. (2006): "Theory and applications of fractional differential equations." (Vol. 204), Elsevier.

Khan, S. H. (2013): "A Picard-Mann hybrid iterative process." Fixed Point Theory and Applications, 2013, 1-10.

Lyons, R., Vatsala A. S., Chiquet, R. A. (2017): "Picard's iterative method for Caputo fractional differential equations with numerical results." Mathematics, 5(4), 65.

Mann, W. R. (1953): "Mean value methods in iteration." Proceedings of the American Math. Society 4(3) 506-510.

Osilike, M.O., Aniagbosor, S.C. (2000): "Weak and strong convergence theorems for fixed points of asymptotically nonexpensive mappings." Math. and Comp. Modelling 32(10), 1181-1191.

Okeke, G. A., Abbas, M. (2017): "A solution of delay differential equations via Picard–Krasnoselskii hybrid iterative process." Arabian Journal of Mathematics, (6), 21-29.

Picard, E. (1890): "Memoire sur la theorie des equations aux derivees partielles et la methode des approximations successives." Jour. Mathematic Pures Appl. (6), 145–210.

Wang, J., Feckan, M., Zhou, Y. (2014): "Weakly Picard operators method for modifed fractional iterative functional differential equations." Fixed Point Theory 15(1), 297-310.

Şoltuz, Ş.M., Otrocol, D. (2007) "Classical results via Mann-Ishikawa iteration." Revue d'analyse numérique et de théorie de l'approximation, 36(2), 193-197.

Zhang, S. (2006): "Positive solutions for boundary-value problems of nonlinear fractional differential equations." Electronic Journal of Differential Equations (EJDE) [electronic only], 2006, Paper-No.

Scientific Journal for the Faculty of Science-Sirte University
Journal home page: http://journal.su.edu.ly/index.php/JSFSU/index
DOI: 10.37375/issn.2789-858X

Spectrophotometric Determination of 5-Hydroxymethylfurfural in Honey Samples from Al-Marj City in Libya using White Method

Amani Abdugadar

Chemistry Department, Benghazi University, Arts and Sciences Al-Marj College, Al-Marj, Libya.

DOI: https://doi.org/10.37375/sjfssu.v4i1.2572

ARTICLE INFO:

Received: 16 January 2024

Accepted: 06 March 2024

Published: 17 April 2024

Keywords: *Honey, 5-hydroxymethylfurfural (HMF), spectrophotometric determination, White method, quantification.*

A B S T R A C T

5-hydroxymethylfurfural (HMF) content was determined as a parameter for honey quality for three Sidr honey samples from Al-Marj city in Libya. In this study, the spectrophotometric quantification of HMF in honey was performed using White method which is one of the most accurate and recommended official methods. The honey samples were obtained from three different farms that distribute honey to most of the retail centers across the city. The aim of this study was to determine HMF concentration in samples from this geographical region to provide some data for future studies. HMF can be considered one of the most important parameters for honey testing and its concentration can predict if heat was used in any stage of honey production. All samples showed normal HMF concentrations indicating good honey quality, good storage conditions, and no possible adulteration nor heating. The preparation of a full report for the honey quality in this region is recommended.

1. Introduction

Honey is a natural sweet material that is created by honeybees. Bees collect nectar from flowers, and for further processing, bees combine it with substances of their own and finally store it in the honeycomb to ripen (Codex Alimentarius Commission). Honey testing is essential for the assessment of its quality and authenticity worldwide during consumption and purchase using several methods; these methods are utilized to determine the chemical composition of honey as well as its biological activity (Żak & Wilczyńska, 2023). Diastase number and 5-hydroxymethylfurfural are the most frequent parameters tested for honey quality (Sakač & Sak-Bosnar, 2012; White, 1994).

5-(hydroxymethyl-)furan-2-carbaldehyde, or 5-Hydroxymethylfurfural (HMF) is a heterocyclic aldehyde formed by dehydration reactions of reducing sugars, mainly fructose in acidic medium. Its concentration is usually expressed in milligrams per kilogram, and it is naturally present even in fresh honey but in low concentrations. HMF is formed as a result of non-enzymatic dehydration of glycans (caramelization) during storage or as a Maillard reaction byproduct during thermal honey treatment (Capuano & Fogliano 2011; Silva et al., 2016; Veríssimo et al., 2017).

HMF could also be found in other foodstuff including pastries, beverages, caramel solution, and coffee. In general, HMF could be used as a parameter and a special marker compound for quality for a wide range of processed fruits and food products (Capuano & Fogliano 2011; Rada-Mendoza et al., 2002; Rada-Mendoza et al., 2004; Cristina 2010). Inappropriate storage conditions including the type of storing containers and moisture contribute to HMF formation. High HMF content in honey may also indicate the

***Corresponding author*: E-mail: amani.atiyalla@uob.edu.ly**

addition of syrups or another kind of sugars. Therefore, The HMF content is regarded as a measure of the freshness of honey as well as proof of its quality, which can be impacted by heat treatment, storage conditions, or sugar factors including storage conditions, heat-treatment or adulteration with sugars (Tosun 2013 & Veríssimo et al., 2017).

HMF is quantified in honey due to its potential harmful effects on human health since it is carcinogenic substance (Abraham et al., 2011; Janzowski et al., 2000; Teixidó et al., 2006). HMF can be rapidly absorbed from the gastrointestinal tract in our bodies, and at high concentrations HMF is cytotoxic with LD_{50} of 3.1 g/kg body weight in rats and with a dietary intake of 1.6 mg per person a day (Capuano & Fogliano 2011, Veríssimo et al., 2017). According to the Codex Alimentarius Commission, honey HMF content after processing should not exceed 40 mg/kg, and for honey coming from regions with tropical temperatures 80 mg/kg is the limit.

There are three methods to quantify HMF in honey using UV or UV-VIS detectors recommended by The International Honey Commission (IHC); two of them are conventional spectrophotometric techniques (White and Winckler methods), and the third is using high performance liquid chromatography (HPLC method) (Bogdanov, 2009; Zappala et al., 2005). The UV-VIS spectrophotometric determination of HMF in honey by White is based on reacting HMF with the bisulfite anion (HSO_3^-) (Teixidó et al., 2011; White, 1979). The White method gave more accurate HMF values when compared to Winckler method and gave almost identical HMF concentrations to the ones determined by HPLC. The White method also uses low-cost reagents compared to HPLC and is considered a greener alternative to Winckler's (Bogdanov, 2009).

The current study aimed to investigate whether heat was utilized in any stage of honey production in Al-Marj, Libya. Heat could lower the quality of honey by producing Maillard by-products such as HMF or affecting enzymes that are naturally present in honey. In acidic solutions like honey, heat could elevate the level of HMF. In this study, HMF concentration was quantified spectrophotometrically using the conventional, and most recommended official method developed by White. Other honey-quality parameters such as the enzyme levels (diastase and invertase) were not the focus of the study since if heat was used, the enzymes would be affected. The purpose of this study was to quantify HMF in honey samples from this geographical region to provide some data for future studies. The importance of this data is to highlight cities for honey export.

2. Materials and Methods

The current study used White's method to determine the concentration of HMF in three honey samples obtained from different random farms across Al-Marj city, Libya; these Sidr honey samples were collected and analyzed before the flood that happened in the region in 2023 (UNICEF, 2023). The determination of HMF content in this study was based on the determination of UV absorbance of HMF of "White honey sample" against a reference sample at 284 nm where HMF should absorb. The interference of other components present in honey at this wavelength was avoided by subtracting the difference between the absorbances of a clear aqueous honey solution (i.e., after the addition of deproteinating agents) and the same solution after the addition of bisulfite. HMF content is then calculated after subtraction of the background absorbance at 336 nm (White, 1979; Bogdanov, 2009).

2.1. Preparing the Reagents

For White method, solutions of 15% potassium ferrocyanide (Carrez solution I), 30% zinc acetate (Carrez solution II), and 0.2% sodium bisulfite were prepared in volumetric flasks and renewed daily. Carrez solution I was prepared by dissolving 15.0 g of potassium hexacyanoferrate(II), $K_4Fe(CN)_6 \cdot 3H_2O$ in water and made the volume up to 100. mL. Carrez solution II was then prepared by diluting 30.0 g of zinc acetate dihydrate, $Zn(CH_3.COO)_2.2H_2O$ and then made up to 100. mL. Finally, Sodium bisulfite solution 0.20 g/100.0 g was prepared by dissolving 0.20 g of solid sodium hydrogen sulfite $NaHSO_3$ in water and then diluted to 100 mL (White 1979; Bogdanov, 2009).

2.2. Equipment

Double-beam spectrophotometer operating in a wavelength range including 284 and 336 nm is needed to measure the absorbance of the sample solution since the absorbance of HMF is from 250-330 (the maximum is 284). In this study, spectrophotometer (Cecil Aquarius CE 7400) was used, and the cuvette was a 1-cm quartz cell. Vortex mixer was used to homogenize the honey samples.

2.3. Sample preparation and procedures

For each sample, five grams of honey were weighed into a beaker and dissolved in about 20 mL distilled water, and then transferred quantitatively into a 50 mL volumetric flask. The solution afterward was homogenized and 0.5 mL of Carrez solution I and 0.5 mL of Carrez solution II were added. Finally, the flask was filled to the mark with distilled water. The solution was filtered through general-purpose filter paper so the precipitated proteins in honey have no contribution to the UV-VIS absorbance leaving only HMF absorbance; 5.0 mL of the filtrate was then pipetted in each of two test tubes. 5.0 mL of water was added to one of the test tubes (the sample solution), and 5.0 mL of 0.2% sodium bisulfite solution was added to the other (the reference solution or White solution). The absorbance reading was measured using the spectrophotometer at 284 nm (for the maximum HMF absorbance) and then at 336 nm. According to White, about 94% of the HMF absorbance band at 284 nm was reduced by the presence of the bisulfite indicating the reaction between the two compounds (White, 1979 & Bogdanov, 2009).

3. Results and Discussion

Following the White method, the UV-VIS absorbance of a clarified honey solution (sample) was determined against a reference solution of the same honey sample after the destruction of the 284 nm chromophore of HMF by its reaction with the bisulfite. This way the background absorbance of honey was not included leaving only HMF absorbance in the sample. The difference between sample absorbance (without bisulfite) and the reference (with bisulfite) indicated the absorbance of HMF. Thus, the difference absorbance eliminated the contribution of other honey constituents. The HMF was then quantified using its literature absorptivity value. The absorbance of the bisulfite is negligible at 336 nm, and it is about 0.014 at 284 nm. According to White, the absorbance values then were placed in the official formula developed by White (see Equation 1 below). Where: A_{284} and A_{336} are the absorbance values at 284 nm and 336 nm respectively, and m is the sample mass of 5.0 g. The factor 149.7 was calculated by (126/16830) x (1000/10) x (1000/5). Where: 16830 is HMF molar absorptivity at wavelength of 284 nm, 1000 is the conversion factor from grams of sample to milligrams, and 5 is the honey mass (White, 1979).

$$HMF(mg/kg) = (A_{284} - A_{336})\, x149.7\, x\, \frac{5}{m} \quad \textbf{(1)}$$

Table 1 below shows the absorbance values for the three honey samples with their corresponding HMF concentration that were calculated using Equation 1. For honey samples 1, 2, and 3, the HMF concentrations were 26.65, 10.93, and 28.00 mg/kg respectively. The three samples collected randomly from different nearby farms from Al-Marj city in Libya were good-quality honey samples and fulfilled the European standards for honey. Maillard reaction products such as HMF depend directly on the processing temperature (White, 1979; Cristina et al, 2010). This concludes that the three honey samples were not exposed to any kind of heat treatment during processing. Since HMF levels were normal, heat was not used, and other parameters of honey quality such as diastase number and invertase levels would not be a concern for this study.

Table (1) Absorbance values for honey samples with the corresponding HMF values.

Honey sample	Absorbance at 284	Absorbance at 336	HMF content in mg/kg
1	**0.248**	**0.07**	**26.65**
2	**0.223**	**0.15**	**10.93**
3	**0.327**	**0.04**	**28.00**

4. Recommendation and Future Work

HPLC is used today for measuring HMF levels in food products. However, it is considered an expensive technique and that is the reason why the White method is still on top of conventional spectrophotometric methods for HMF quantification. Development of a safe, quick and reliable technique for measuring HMF content is still needed. Using more environmental-friendly chelating agents to deproteinize honey, as a replacement for Carrez solutions, is a possibility for a better quantification of HMF in honey without producing chemical waste. The chemical waste produced by White method limits its utilization in educational settings including graduation projects and as a biochemistry laboratory experiment. The replacement of Carrez solutions would make White method one of the recommended biochemistry laboratory experiments for science major and premedical college students since it uses a real, inartificial sample (honey). That would have an impact on students' learning experience and would better prepare them for their career. The modification of White's method

recommended by Okibe et al., can only be used in industry but not for educational purposes since Carrez solutions were replaced with corrosive, strong acid, the perchloric acid (Okibe, et al., 2020; Perchloric acid. SDS, 2023). For a greener quantification of HMF, the development of a more benign method is still needed since the White method utilizes reagents that could be replaced. In addition, including more parameters in the future to generate a full, intensive honey-quality report should be considered; these parameters include ash content, moisture, acidity, conductivity, and enzyme levels.

5. Conclusion

HMF levels were normal for honey samples that were obtained from the main distributors from Al-Marj city in Libya using the official White method. The significance of this research was providing insights into this geographical region and testing the main indicator for overheating honey. The focus was whether heat was used in any stage of honey production in these farms. HMF was the main heat-byproduct that naturally present in honey, but its health issues emerge at high concentrations. If honey was heated in any stage, other parameters would be affected as well including diastase number and invertase levels. Since the main heat-byproduct is HMF, the current study focused on the determination of its concentrations to provide data regarding this particular region to support further scientific research.

Conflict of Interest: The author declares that there are no conflicts of interest.

References

Abraham, K., Gürtler, R., Berg, K., Heinemeyer, G., Lampen, A., & Appel, K. E. (2011). Toxicology and risk assessment of 5-hydroxymethylfurfural in food. *Molecular Nutrition Food Research, 55*(5), 667–678. https://doi.org/10.1002/mnfr.201000564.

Bogdanov, S. (2009). Harmonised methods of the European Honey Commission. Retrieved from: http://www.ihc-platform.net/ihcmethods2009.pdf.

Codex Alimentarius Commission. Standard for honey (CXS 12-1981). Report of the forty-fifth session of the Codex Committee on sugar, amended in 2019, 2022. Retrieved from: https://www.fao.org/3/i0842e/i0842e20.pdf

Capuano, E., & Fogliano, V. (2011). Acrylamide and 5-hydroxymethylfurfural (HMF): A review on metabolism, toxicity, occurrence in food a mitigation strategies. *LWT– Food Science and Technology, 44*(4), 793–810. https://doi.org/10.1016/j.lwt.2010.11.002.

Cristina, D. A., Seiquer, I., Haro, A., Castellano, R., & Navarro, M. P. (2010). Development of the Maillard reaction in foods cooked by different techniques: Intake of Maillard-derived compounds. *Food Chemistry, 122* (1),145-153.

Janzowski, C., Glaab, V., Samimi, E., Schlatter, J., & Eisenbrand, G. (2000). 5-Hydroxymethylfurfural: Assessment of mutagenicity, DNA-damaging potential and reactivity towards cellular glutathione. *Food and Chemical Toxicology, 38*(9), 801–809. https://doi.org/10.1016/S0278-6915(00)00070-3.

Maeda, I. C., Sampaio, A. N. C. E., Flores Caron, E. F., Nardy, J. F., Oliveira, S. C., Pereira, J. G., & Martins, O. A. (2023). Spectrophotometry of Winkler and White's official methods for the determination of hydroxymethylfurfural in bee honey. *Brazilian Journal of Food Technology, 26*. https://doi.org/10.1590/1981-6723.13322

Veríssimo, M. I. S., Gamelas, J. A. F., Evtuguin, D. V., Gomes, M. T. S. R. Determination of 5-hydroxymethylfurfural in honey, using headspace-solid-phase microextraction coupled with a polyoxometalate-coated piezoelectric quartz crystal. (2017). *Food Chemistry*, 220, 420-426. https://doi.org/10.1016/j.foodchem.2016.09.204

Okibe, F. G., Shallangwa, G.A. & Usman, I. (2020). Modification of White Method for Quantitative Evaluation of 5-hydroxymethylfurfural in Honey. *Communication in Physical Sciences, 5*(1), 34-41.

Perchloric acid. SDS (2023). Sigma Aldrich [online: 311421]. Retrieved from: https://www.sigmaaldrich.com/LY/en/sds/aldrich/311421?userType=undefined (accessed January 31, 2024).

Rada-Mendoza, M. M., Olano, A., & Villamiel, M. (2002). Determination of hydroxymethylfurfural in commercial jams and in fruit-based infant foods. *Food Chemistry, 79*(4). 513-516. https://doi.org/10.1016/S0308-8146(02)00217-0.

Rada-Mendoza, M. M., Sanz, M. L., Olano, A., & Villamiel, M. (2004). Formation of hydroxymethylfurfural and furosine during the storage of jams and fruit-based infant foods. *Food Chemistry, 85*(4). 605-609. https://doi.org/10.1016/j.foodchem.2003.07.002.

Sakač, N., & Sak-Bosnar, M. (2012). A rapid method for the determination of honey diastase activity. *Talanta, 93*, 135–138. https://doi.org/10.1016/j.talanta.2012.01.063

Silva, P. M., Gauche, C., Gonzaga, L. V., & Costa, A. C. O. (2016). Honey: Chemical composition, stability and authenticity. *Food Chemistry, 196*(1), 309–323. https://doi.org/10.1016/j.foodchem.2015.09.051.

Teixidó, E., Santos, F. J., Puignou, L., & Galcetan, M. T. (2006). Analysis of 5-hydroxymethylfurfural in food by gas chromatography–mass spectrometry. *Journal of Chromatography A, 1135*, 85–90. https://doi.org/10.1016/j.chroma.2006.09.023.

Tosun, M. (2013). Detection of adulteration in honey samples added various sugar syrups with $^{13}C/^{12}C$ isotope ratio analysis method. *Food Chemistry, 138*(2-3), 1629–1632. https://doi.org/10.1016/j.foodchem.2012.11.068.

UNICEF. (2023). Devastating floods in Libya: Two months after massive storm, families are still reeling. Retrieved from: https://www.unicef.org/emergencies/devastating-flooding-libya

White, J. W. (1979). Spectrophotometric Method for Hydroxymethylfurfural in Honey. *Journal of the Association of Official Analytical Chemists*, *62*, 509.

White, J. W. (1994). The Role of HMF and Diastase Assays in Honey Quality Evaluation, *Bee World*, *75*(3), 104-117. https://doi.org/10.1080/0005772X.1994.11099213.

Zappala, M., Fallico, B., Arena, E., & Verzera, A. (2005). Methods for the determination of HMF in honey: a comparison. *Food Control, 16*, 273–277. https://doi.org/10.1016/j.foodcont.2004.03.006

Żak, N., & Wilczyńska, A. (2023). The Importance of Testing the Quality and Authenticity of Food Products: The Example of Honey. *Foods, 12*(17), 3210. Retrieved from: https://doi.org/10.3390/foods12173210.

Scientific Journal for the Faculty of Science-Sirte University Vol. 4, No. 1 (2024) 80-88

Scientific Journal for the Faculty of Science-Sirte University

Journal home page: http://journal.su.edu.ly/index.php/JSFSU/index

DOI: 10.37375/issn.2789-858X

Building Recommender Systems with Machine Learning and Data Mining Techniques

Yousuf A. Maneetah, Suhil M. Elsibai, Ali A. Bouras, Ahmed H. Alhabbh, Fathia Elbadri

Computer Science Department, Benghazi University, Benghazi, Libya.

DOI: https://doi.org/10.37375/sjfssu.v4i1.2677

ARTICLE INFO:

Received: 19 January 2024

Accepted: 06 April 2024

Published: 17 April 2024

Keywords: *Recommender systems, dataset, Content-based filtering, Collaborative filtering, hybrid filtering.*

A B S T R A C T

The current study presents a unique use of machine learning algorithms for developing a recommendation system. Recommender systems are often employed in a wide range of industries, including e-commerce, entertainment, and search engines. Recommender systems are algorithms that utilize user preferences and behavior to recommend relevant objects, such as movies, books, goods, or songs. This article examines the many characteristics and features of different methodologies used in recommendation systems, with an emphasis on filtering and prioritizing important information to serve as a compass for searches. When recommender engines properly recommend individualized content or items, they provide businesses with a competitive advantage over rivals and generate considerable income. This study investigates content-based filtering, which suggests things with comparable attributes to those that a user previously liked. It also investigates hybrid filtering, which combines content-based and collaborative filtering techniques (using user-item interaction data) to solve issues such as the cold start problem (little user data) and data sparsity (few user-item interactions). The installed recommender systems that use content-based and hybrid filtering approaches produce promising individualized suggestions. Content-based filtering is particularly effective at proposing comparable goods, but hybrid filtering provides a more diversified and accurate suggestion pool by including user preferences. Content-based filtering has limits owing to data sparsity, which hybrid filtering addresses. This article discovered that the suggested technique uses content-based filtering when applied to small to medium-sized datasets. However, hybrid filtering is used when the dataset is vast and sparse.

1 Introduction

Recommender systems (RSs) aim to provide meaningful suggestions to consumers based on their preferences, such as suggesting books on Amazon or movies on Netflix. Recommendation systems (RSs) use domain-specific data. For example, Netflix keeps user ratings for movies in a huge table, which allows the algorithm to create suggestions based on this information. There are several recommendation algorithms, each having advantages and disadvantages. Combining these techniques typically results in enhanced performance.

The current study investigates several recommendation approaches, examining their data sources and the algorithms that process that data. RSs are collaborative filters that look for similarities between users. Collaborative filtering is based on previous user-item interactions maintained in a "user-item interactions matrix" (Reddy et al., 2023). In order to improve suggestion diversity and personalization, this study presents a direct comparison of content-based and hybrid approaches, goes deeper into sparsity mitigation strategies, and examines user demographics and implicit feedback data.

***Corresponding author*: E-mail:** yousuf.maneetah@uob.edu.ly

Problem statement

Do various domains, such as e-commerce, entertainment, and scientific libraries require reliable and accurate recommendation engines? The objective is to deliver users trustworthy and pertinent recommendations while taking into account their interests and behavior. In order to boost user satisfaction and recommendation system effectiveness, the main focus is on evaluating various recommendation techniques, data sources, and algorithms.

Research questions

1. What are the different recommendation methods used in various domains, and how do they utilize data sources?
2. How do collaborative filtering and content-based filtering contribute to the performance of recommendation engines?
3. What are the strengths and weaknesses of different recommendation algorithms?

Aiming to analyze, compare, and evaluate different aspects of recommendation systems, including methods, data sources, algorithms, and their impact on user behavior and organizational outcomes. Literature reviews on methods of recommender systems with their challenges and limitations are specified in Section 2, methodology is specified in Section 3, and results obtained and conclusion are shown in Sections 4 and 5.

2 Literature Review

2.1 Related Work

Supermarkets (RS): IBM researchers developed a recommender system to be integrated with Smart Pad. It was created as an online shopper's personal assistant (Zahrawi et al., 2021).A different study focuses on using cosine similarity and the TF-IDF algorithm to a content-based filtering strategy. It investigates how to extract keywords and combine keywords with genres to suggest movies. Performance evaluation criteria, including f1-score, accuracy, and recall, are used, and the Movie Lens dataset, which is accessible to the public, is utilized. The results of the experiment show that the relevance and accuracy of the movie recommendation system have limits. In particular, it is discovered that the content-based filtering approach with TF-IDF and cosine similarity, in addition to keyword extraction utilizing the sclera library, is less successful in producing pertinent movie suggestions (Permana et al., 2023). Recommendation systems, which are extensively utilized in a variety of industries including e-commerce, entertainment, and search engines, are developed using machine learning techniques. Recommender systems make use of algorithms to offer consumers recommendations for related goods, music, movies, and books. As a useful tool for directing user queries, the article examines several strategies and characteristics used in recommendation systems to filter and prioritize content (Zahrawi et al., 2021). In order to forecast user preferences for movie genres and their rating behavior, the study offers a unique method that makes use of psycholinguistic variables collected from social media interactions. It creates links between ideals and personality through conversations on Twitter and IMDb. The research contrasts these strategies with conventional approaches and finds that the combined models perform better than single models based only on personality or values. Using information from Flexible, the research looks at Netflix, the most widely used on-demand broadcasting network worldwide. The authors used the TF-IDF and cosine similarity algorithms to create a recommendation system after analyzing 7,787 distinct data. Although the system has flaws, the authors think it has potential for future features because of the analysis's insights about Netflix's content patterns (Chiny et al., 2022). In order to help readers choose the next book to read, this study presents a hybrid recommendation system. The study evaluates the suggested algorithm's efficacy using the LitRec dataset and focuses on book and author suggestions within a hybrid recommendation framework. Two item-based collaborative filtering algorithms are combined in the hybrid technique to predict books and authors based on user preferences. The booklist that results from extending the author predictions is combined with the original book predictions. Moreover, the best book recommendations are generated using the given booklist. The author illustrates how author recommendations can enhance total book recommendations through a series of studies (Vaz et al., 2021). In the context of e-commerce businesses, recommendation systems (RS) are discussed in this study with a particular emphasis on book recommendation systems utilized by sites such as Amazon and Barnes & Noble. Products are suggested by RS software depending on a user's preferences or previous purchases. In RS, lists of items that are similar

to the user's preferences are often generated through the use of collaborative filtering (CF). However, CF has issues with sparsity, scalability, and cold start issues, which affects how accurate the recommendations are. The research suggests employing collaborative filtering with Jacquard similarity (JS) to generate recommendations that are more accurate in order to address these issues. When two books are paired together, JS creates an index by dividing the total number of users who have rated each book separately by the ratio of common users who have rated both books. Better recommendations are indicated by higher JS indices, and recommended books with high JS indices are given priority in the list (Rana et al., 2019). Group Lens Research at the University of Minnesota maintains the Movie Lens dataset website. When a new user joins Movie Lens, it suggests some of the most well-known movies for them to evaluate. Movie Lens makes individualized predictions for movies you are likely to appreciate based on your movie ratings. It also assists you in avoiding movies that might not suit your tastes. The user is given recommendations for other movies based on these ratings. Moreover, Movie Lens generates customized suggestions through collaborative filtering using these ratings (Khan et al., 2020).

2.2 Recommendation Systems

The recommendation system provides product recommendations based on user preferences, history, and information in order to obtain desired products (Dong et al., 2022; Attalariq et al., 2023). Collaborative filtering and content-based filtering are two extensively used strategies for developing recommendation systems. Collaborative filtering is a technique for evaluating and predicting items based on the opinions and similarities of other users. On the other hand, content-based filtering is a technique for recommending a product based on the availability of similar material (Ko et al., 2022).

2.2.1 Collaborative filtering

Collaborative filtering is a popular approach in recommender systems for making tailored recommendations. It is based on the idea that people who have had similar preferences in the past are more likely to have similar choices again. The technique entails examining user behavior and item evaluations to identify trends and similarities. There are two main techniques for collaborative filtering: user-based and item-based. User-based filtering compares people based on their prior behavior and ratings, locating those who rated products similarly to the target user. It then suggests things that comparable people have enjoyed or rated highly. Item-based filtering, on the other hand, uses user ratings to determine similarities between things, detecting objects that have been rated similarly by users. It offers things that are comparable to those that the target user has previously rated or liked. Collaborative filtering can be improved using matrix factorization techniques such as singular value decomposition (SVD). These strategies minimize the complexity of the rating matrix, revealing latent variables or characteristics that represent the underlying patterns in user-item interactions (Reddy et al., 2023).

2.2.2 Content-Based Filtering

Content-based filtering is a type of recommendation system that uses data or information about consumers' interests based on previous interactions. Content-based filtering algorithms seek to recommend items by comparing their resemblance to those that previous users have rated highly. The most appropriate things are then recommended by comparing the similarity of the items previously assessed by the user to other items in the collection. Several algorithms are widely employed in content-based recommendation systems. These include TF-IDF (Term Frequency-Inverse Document Frequency), which calculates the importance of words in a film's description or synopsis, and cosine similarity, which measures the similarity between films based on their input for content-based recommendation systems that include various film-related features, as illustrated in Figure 1. This includes a variety of data kinds, including textual data like film titles, genres, synopses, and user-generated tags, as well as graphic elements like film posters and even audio features like soundtracks. However, in this study, the author will concentrate on the movie domain, including aspects such as genres, keywords, and a mix of both. The combination of genre and keyword refers to the merger of both aspects via a concatenation process. Content-based systems can use these inputs to capture unique film attributes and generate recommendations according to the user's preferences and interests (Permana et al., 2023).

i . TF-IDF :

The acronym TF-IDF stands for Term Frequency Inverse Document Frequency of Records. TF-IDF determines the significance of a word inside a document. The TF-IDF value of a word reflects its level of categorization inside the document. A greater score

for a term indicates its significance in the paper (Ko et al., 2022). According to the above description, TF-IDF is determined using equation (1) as follows:

$$tfi\,df_i = tf_i \times idf_i \quad (1)$$

tf_i (Term Frequency of a term in a document) represents the number of times a term appears in a given document. It measures the importance or frequency of the term within the document. idf_i (Inverse Document Frequency of a term) represents the inverse document frequency of a term across the entire corpus or collection of documents. It measures the rarity or uniqueness of the term in the entire collection (Rani et al., 2021).

ii . *Cosine Similarity*

Cosine similarity is an algorithm for calculating the similarity between a desired collection of data and a provided set of data. It compares two documents based on size differences and computes the cosine angle between the two vectors in a multidimensional space. In this work, the authors use cosine similarity as a computational metric to detect the presence or absence of certain phrases in an item. Recommendations are then generated based on the degree of similarity between the relevant item and the active item connected with a certain user. The likelihood of recommending an item to a user improves with increased levels of resemblance to the active item. Cosine similarity necessitates converting the dataset's data items as vectors, which allows for complete vector-based analysis and comparison. This technique makes it easier to provide efficient and correct suggestions in the research setting (Yunanda et al., 2022). Based on the preceding description, cosine similarity is calculated using the following formula:

$$Cos(x,y) = \frac{x\,.\,y}{\|x\| * \|y\|} \quad (2)$$

The formula $Cos\ (x, y)$ calculates the cosine similarity between x and y. x is the vector acquired from the TF-IDF calculation on the active item, and y is the vector received from the TF-IDF calculation on the reference item. $\|x\|$ represents the unit length of vector x, and $\|y\|$ represents the unit length of vector y.

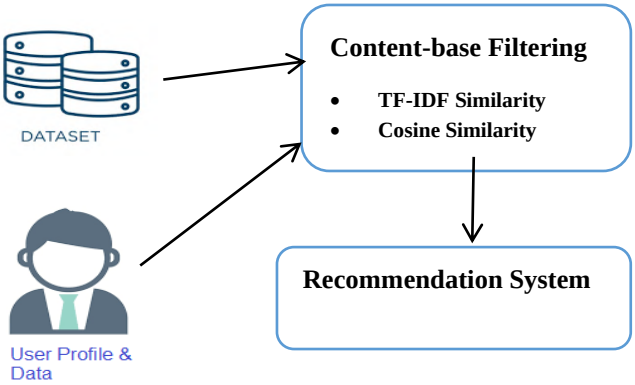

Figure (1) Content-Based Filtering Recommended System Model.

2.2.3 Hybrid Filtering

A hybrid recommender system combines many methods, such as collaborative filtering, content-based filtering, and other approaches, to capitalize on their particular strengths while mitigating their limitations. A hybrid recommender system uses numerous methodologies to deliver more accurate and diversified recommendations, hence enhancing the recommendation engine's overall effectiveness. The hybrid technique enables a more extensive examination of user preferences and item features, resulting in higher suggestion quality.

i. Singular Value Decomposition

Singular Value Decomposition (SVD) is a technique used in the creation of model-based collaborative filtering (CF) recommendation systems. This technique is one of several methods to the matrix factorization method. In this approach, the author has a list of users, things, and user ratings, which are often represented as a user-item rating matrix. Based on this, the SVD algorithm calculates the latent factor and generates suggestions using the user-item matrix.

$$\boldsymbol{A = U \cdot S \cdot VT} \quad (3)$$

The matrix decomposes into three additional matrices, as shown below: $\boldsymbol{M}$ is a $m\ x\ n$ utility matrix, U is a $m\ x\ m$ orthogonal matrix, S is a $r\ x\ r$ diagonal matrix, and VT is a $r\ x\ n$ matrix arising from the orthogonal matrix. Thus, matrix U represents users with latent factors; matrix VT represents objects with latent factors; and the diagonal matrix S is the singular value. Figure 2 depicts this process clearly.

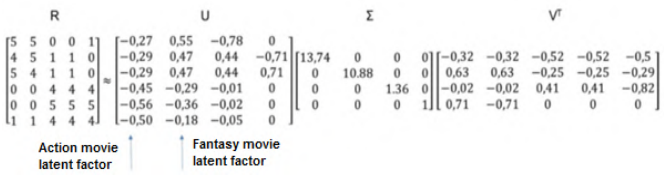

Figure (2) Singular Value Decomposition example (Baesens et al., 2020).

In this study, the authors employ the appropriate singular vector to achieve item-based collaborative filtering. Item-based CF with SVD computes item similarity using SVD vectors and generates recommendations based on user-item interaction. This strategy is efficient in dealing with huge datasets and has the ability to provide correct suggestions by exploiting the latent characteristics recorded by singular value decomposition (SVD), as shown in Figure 3. The matrix has several *k* latent components for each item (Attalariq et al., 2023).

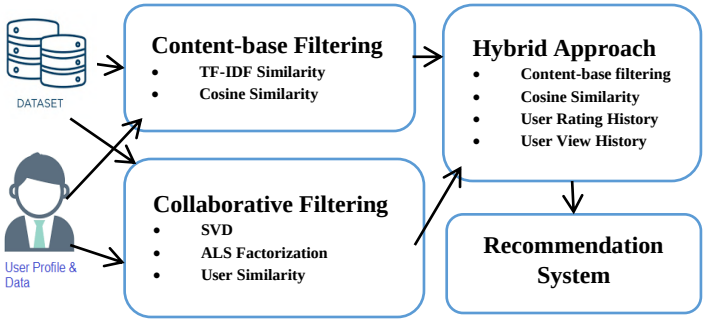

Figure (3) Hybrid Filtering recommended system model.

2.2.4 Challenges and Limitations

i. Cold Start Problem:

For new users, encourage them to evaluate certain things or submit initial preferences so that data may be collected for individualized suggestions. Use the ratings of other users with comparable demographics to generate first suggestions to new users. Regarding new items: Encourage consumers to review and offer comments on new products in order to gather data for recommendations. Collect ratings from a small portion of the community before spreading to the complete community.

ii. Data Sparsity Problem:

Content-based techniques, which depend on item content rather than user evaluations, can assist to alleviate data scarcity. Investigate strategies such as matrix factorization or neighborhood-based algorithms for identifying successful neighbors and making suggestions based on their scores.

iii. Scalability:

Optimize enormous dataset processing time by removing unused data or using scalable techniques and distributed computing technologies. Use techniques such as parallel processing or distributed computing to address the computational complexity of massive datasets.

iv. Dynamic and Evolving Preferences:

User preferences might change over time; therefore recommender systems must adapt and deliver recommendations that match users' changing interests. Tracking and comprehending these changes presents problems for the system. The cold start problem, data sparsity, scalability, and changeable preferences are key problems for recommender systems. To solve these issues, options include requesting users for initial ratings, reusing comparable data, reducing data sparsity, controlling computational complexity with optimization approaches, and reacting to changing user preferences, which necessitate continual knowledge and tracking (Ankam., 2016).

3 Proposed Methodology

Recommendation engines must be arranged a certain way because they are usually built using big datasets. This paper aims to introduce several forms of reinforcement learning (RS) and demonstrate a methodical approach to developing a Python recommendation system. Due to the extensive usage of linear algebra, a fully evolved recommendation system is resource and math-intensive. Content-based and hybrid filtering are the two types of recommender engines that are most often used. The proposed system is done with the following configurations:

- Intel R CoreTMi3-2330 M 2.20 GHz 4 GB RAM 32-bit Windows 7 Home Premium. The experiments are carried out on the dataset files using the Python language version 3.8.6 using several libraries: sklearn, numpy, pandas, and scipy.
- Deploying two types of recommendation systems (RS):
  i. Content-base filtering techniques.
  ii. Hybrid filtering techniques using singular value decomposition.

3.1 Datasets

Movie Lens is an established movie recommendation dataset that is utilized extensively in recommender system research and development. It was built by the

University of Minnesota's Group Lens research group and has been updated and maintained on a regular basis over time. Movie Lens databases include detailed information on movies, ratings, and user preferences. Recommendation engines are generally built using Movie Lens datasets, which include 100,873 rows and 5 columns (user_id, item_id, rating, timestamp, and title), representing 610 users x 9,724 movies and 5,931,640 ratings.

3.2 Applying the system

In this part, the authors will develop two different types of recommender engines. Let's begin with simple RS content-based screening. Table 1 shows the samples from each dataset for enhanced understanding.

i. Content-Based Filtering

Datasets are well-organized and devoid of missing values. Using a content-based filtering approach on the movie lens dataset.

- Load Movie Lens dataset. Load the dataset with movie information, such as names, genres, and descriptions.
- Preprocess data: Clean and preprocess data as needed. This may include deleting unneeded columns or dealing with missing values.
- TF-IDF vectorization. Use a TF-IDF vectorization approach, such as the sklearn library's TfidfVectorizer, to convert movie descriptions or genres into numerical vectors.
- Create a TfidfVectorizer and provide any necessary settings, such as stop words or n-grams. Fit the vectorizer to movie descriptions or genres to learn language and calculate IDF weights. Transform the movie descriptions or genres into TF-IDF vectors using the fitted vectorizer, as indicated in Table 1.

Table (1) The result of the Cosine Similarity Calculation

title	Toy Story (1995)	...	Andrew Dice Clay: Dice Rules (1991)
title		...	
Toy Story (1995)	1.000000	...	0.267586
Jumanji (1995)	0.813578	...	0.000000
Grumpier Old Men (1995)	0.152769	...	0.570915
Waiting to Exhale (1995)	0.135135	...	0.505015
Father of the Bride Part II (1995)	0.267586	...	1.000000
...	...	...	...
Black Butler: Book of the Atlantic (2017)	0.680258	...	0.318581
No Game No Life: Zero (2017)	0.755891	...	0.354002
Flint (2017)	0.000000	...	0.000000
Bungo Stray Dogs: Dead Apple (2018)	0.421037	...	0.000000
Andrew Dice Clay: Dice Rules (1991)	0.267586	...	1.000000

[9742 rows x 9742 columns]

- Use sklearn's cosine similarity function to calculate pairwise cosine similarity between movie TF-IDF vectors. The cosine similarity function returns a similarity matrix in which each member indicates the content similarity of two movies.

ii. Hybrid filtering techniques using singular value decomposition

Using a hybrid filtering technique on the Movie Lens dataset.

- Load Movie Lens dataset. Load the dataset with movie ratings and other pertinent data, such as user IDs, movie IDs, and ratings.
- Preprocess data: Clean and preprocess data as needed. This might include deleting extraneous columns, addressing missing numbers, or standardizing the ratings.

-Separate the dataset into training and test sets. Divide the dataset into two parts: a training set for developing the recommendation models, and a test set for assessment. Create the user-item matrix. Create a user-item matrix, with rows representing people and columns representing movies. The matrix should contain user ratings for movies.

- The matrix should be sparse, with missing values reflecting unrated movies by users, as illustrated in Figure 4.

-To apply Singular Value Decomposition (SVD), a matrix factorization technique, the user-item matrix is divided into three matrices: U, Σ, and V^T.

U stands for user embedding, Σ is a diagonal matrix with singular values, and V^T represents movie embedding. Determine the amount of latent components to keep depending on your needs and domain expertise.

Table (2) The result of SVD Calculation with Five Priorities

```
[[ 0.0921447   0.00082937 -0.01089745 -0.06167385 -0.05555415]
 [-0.00149426 -0.01334201 -0.00442345  0.01773772 -0.0058663 ]
 [ 0.00738945  0.00196068  0.00171517 -0.00206861 -0.00135323]
 ...
 [ 0.04676093  0.08402888 -0.00976291 -0.01184704 -0.11611442]
 [-0.00806337  0.00138157 -0.03974124 -0.01378463 -0.00757944]
 [ 0.15783851  0.01658204  0.09267536  0.20218445 -0.13886488]]
 [  0.         170.42250831   0.           0.           0.
 [  0.           0.         191.1508762    0.           0.
 [  0.           0.           0.         231.23661142   0.
 [  0.           0.           0.           0.         534.41989777]]
   1.40608836e-04 -7.26189695e-04]
 [-1.68374052e-03  5.06728557e-02  3.74528571e-02 ... -4.90112220e-05
  -4.90112220e-05 -8.94587287e-04]
 [-7.84438842e-02 -5.68447103e-02 -1.80051145e-02 ...  8.71093879e-05
   8.71093879e-05 -1.22833344e-04]
 [-2.75911949e-02 -2.06662722e-03 -2.47146155e-02 ...  5.97586244e-04
   5.97586244e-04  1.27236200e-03]
 [-7.04498985e-02 -3.85393459e-02 -1.59129220e-02 ... -6.46836073e-05
  -6.46836073e-05 -2.71729303e-04]]
```

- Collaborative Filtering: Apply the SVD factors (U, Σ, V^T) to anticipate missing ratings in the user-item matrix. To forecast ratings for all user-movie pairs, utilize the dot product of the user embedding (U) and movie embedding (V^T). Adjust the anticipated ratings as needed, such as scaling them between certain ranges or rounding them to a specified accuracy. TABLE 2 illustrates this procedure visually.

Content-Based Filtering: To calculate similarity scores between movies, use content-based filtering techniques such as TF-IDF vectorization on movie attributes such as descriptions or genres. Create movie suggestions based on the similarity scores and user preferences.

- Combine recommendations: Combine expected ratings from collaborative and content-based filtering. Assign weights to each suggestion source depending on its significance or efficacy.

Create final recommendations: Combine the suggestions from collaborative and content-based filtering by computing the weighted average or using other fusion techniques. Sort the final recommendation ratings in descending order to get the top N suggested movies for each user.

4 Results and Discussion

The suggested system, which employs both content-based and hybrid filtering algorithms, has demonstrated encouraging results in terms of generating accurate and tailored suggestions. The system overcame issues including cold start, sparsity, and scalability by integrating the qualities of both systems. Present the results obtained by using content-based filtering based on item title similarities. The results of using the hybrid filtering approach, which combines content-based and collaborative filtering, demonstrate the benefit of combining both strategies to maximize their complementary strengths and produce better suggestions. The preceding dataset included 100,873 rows and 5 columns. The authors discovered that the majority of films get zero ratings using explanatory data analysis. That makes sense because most people see renowned or major popular movies, which will have a lot of reviews or ratings, as illustrated in Figure 4.

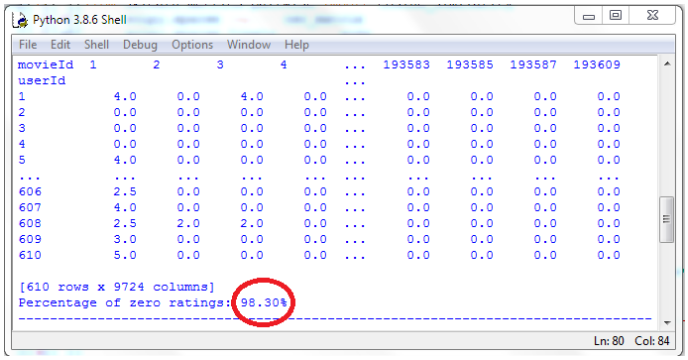

Figure (4) The user-item matrix.

The matrix has around 5,931,640 cells, with a sparsity level of approximately 98.3%. Finally, to improve prediction, the authors built the recommender engine employing memory-based calculation of the Cosine Similarity model-based CF using SVD. Content-based filtering using TF-IDF offers advantages such as independence from user data: Content-based filtering is not primarily reliant on user information or previous interactions. It can provide recommendations even for new or cold-start users with little or no prior experience with the system. Overcoming the Cold Start Problem: By depending on item attributes, content-based filtering can address the Cold Start problem in situations when there is minimal user data available. It can provide recommendations based on item similarities and user preferences derived from item characteristics. Limited Discovery of New Interests: Content-based filtering is mostly focused on item attributes that correspond to the user's existing choices. As a result, it may have limited capacity to discover and propose goods that do not align with the user's defined interests. Dependency on item metadata: Content-based filtering is strongly reliant on precise and detailed item metadata, such as descriptions or genres. If the item metadata is insufficient, incorrect, or does not reflect the item's genuine features, the quality of suggestions suffers. One disadvantage of content-based filtering is its inclination to promote items that are similar to those with which the user has previously engaged, resulting in a lack of diversity in recommendations. This can lead to a lack of diversity in recommendations, thereby narrowing the available item space. Content-based filtering confronts difficulties when proposing new or recently introduced items with insufficient user interactions or features. With little data to examine, it may struggle to make reliable suggestions for these things. Hybrid filtering using SVD provides several advantages, including enhanced recommendation. Accuracy: By combining the advantages of content-based and collaborative filtering, hybrid filtering can improve suggestion accuracy. Content-based filtering focuses on item attributes, whereas collaborative filtering takes into account user-item interactions, resulting in more precise and tailored suggestions. Collaborative filtering can address data sparsity concerns by exploiting user-item interactions. Even if a user has limited interaction or novel items have low ratings, collaborative filtering can still provide suggestions based on the behavior of comparable individuals or objects. Hybrid filtering can help both new users and new goods overcome cold start issues.

Content-based filtering can provide recommendations to new users based on item features, whereas collaborative filtering can make suggestions based on user-item interactions. Either has a downside, such as complexity or computational Cost: Implementing and maintaining a hybrid filtering system might be more difficult and expensive than using separate filtering approaches. The integration of content-based and collaborative filtering required increased processing and storage capacity. Model Selection and Parameter Tuning: Hybrid filtering entails choosing appropriate models and adjusting parameters for both content-based and collaborative filters. Determining the best mix of tactics and striking the correct balance between them may be difficult and requires experience. Cold Start for New Users and Products: While hybrid filtering can help to alleviate cold start issues, it may still have difficulty offering correct suggestions for completely new users or objects with insufficient data or features. The authors discovered that the suggested technique, when applied to small to medium-sized datasets, employs content-based filtering. However, when the dataset is vast and sparse, hybrid filtering is used. This strategy improves speed while also addressing scalability and data sparsity problems. The researchers' findings emphasize the recommendation system's flexibility to dataset features, successfully employing either content-based or hybrid filtering strategies to improve suggestion accuracy and overcome restrictions caused by dataset size and sparsity.

5 Conclusion and future work

This study investigates and presents several types of techniques usually used in the development of recommender engines, including content-based and hybrid filters. These techniques have been effectively utilized in a variety of areas, including financial services and popular platforms such as Netflix and Amazon. Throughout our investigation, the authors discussed and utilized content-based filtering algorithms that use item title similarities to provide meaningful suggestions. Furthermore, the author's explored hybrid filtering, which combines content-based and collaborative filtering techniques. This hybrid technique utilized into consideration additionally comparable item names but also user rating profiles to improve suggestion accuracy and customization. In addition to describing these strategies, the author has looked at some of the frequent issues found in recommender systems. Content-based filtering was used to solve the cold start problem, which occurs when there is minimal user or item data. The collaborative filtering strategy, which leverages the aggregate behavior of comparable users or objects, was used to reduce sparsity in user-item interactions. The authors also looked at scalability issues, because recommender systems must efficiently manage big datasets and rising user bases. Overall, the strategies investigated by the authors have shown helpful in producing accurate and tailored suggestions across a variety of disciplines. Using content-based and hybrid filtering, recommender engines can provide significant insights and improve user experiences. To ensure the long-term effectiveness and performance of recommender systems in real-world applications, certain difficulties such as cold start, sparsity, and scalability must be properly addressed. In the future, we hope to investigate approaches for reducing data sparsity, a recurrent difficulty in collaborative filtering. This involves looking at matrix factorization techniques such as singular value decomposition (SVD) and neighborhood-based algorithms to increase recommendation accuracy with minimal data. Furthermore, we will look into ways to increase suggestion diversity while keeping personalization. This might entail combining user demographics or implicit feedback data (browsing history, clicks, etc.) to discover larger user interests and hidden preferences. Finally, to analyze the scalability and generalizability of recommender systems, we will test their performance on larger and more varied datasets, evaluating features such as recommendation time and performance as the amount of data expands.

Conflict of Interest: The authors declare that there are no conflicts of interest.

References

Deldjoo, Y., Nazary, F., Ramisa, A., Mcauley, J., Pellegrini, G., Bellogin, A., & Noia, T. D. (2023). A review of modern fashion recommender systems. ACM Computing Surveys, 56(4), 1-37.

Reddy, S. V. G., Putchakayala Meher Sowjanya, A. P. K. R., Sai, B., Saketh, L. Y. K., & Reddy, K. V. A. (2023). MOVIE RECOMMENDATION SYSTEM USING COLLABORATIVE FILTERING.

Zahrawi, M., & Mohammad, A. (2021). Implementing recommender systems using machine learning and knowledge discovery tools. Knowledge-Based Engineering and Sciences, 2(2), 44-53.

Permana, A. H. J. P. J., & Wibowo, A. T. (2023). Movie Recommendation System Based on Synopsis Using Content-Based Filtering with TF-IDF and Cosine Similarity. International Journal on Information and Communication Technology (IJoICT), 9(2), 1-14.

Khan, E. M., Mukta, M. S. H., Ali, M. E., & Mahmud, J. (2020). Predicting users' movie preference and rating behavior from personality and values. ACM Transactions on Interactive Intelligent Systems (TiiS), 10(3), 1-25.

Chiny, M., Chihab, M., Bencharef, O., & Chihab, Y. (2022). Netflix Recommendation System based on TF-IDF and Cosine Similarity Algorithms. no. Bml, 15-20.

Vaz, P. C., Martins de Matos, D., Martins, B., & Calado, P. (2012, June). Improving a hybrid literary book recommendation system through author ranking. In Proceedings of the 12th ACM/IEEE-CS joint conference on Digital Libraries (pp. 387-388).

Rana, A., & Deeba, K. (2019, November). Online book recommendation system using collaborative filtering (with Jaccard similarity). In Journal of Physics: Conference Series (Vol. 1362, No. 1, p. 012130). IOP Publishing.

Dong, Z., Wang, Z., Xu, J., Tang, R., & Wen, J. (2022). A brief history of recommender systems. arXiv preprint arXiv:2209.01860.

Ko, H., Lee, S., Park, Y., & Choi, A. (2022). A survey of recommendation systems: recommendation models, techniques, and application fields. Electronics, 11(1), 141

Rani, U., & Bidhan, K. (2021). Comparative assessment of extractive summarization: textrank tf-idf and lda. Journal of Scientific Research, 65(1), 304-311.

Yunanda, G., Nurjanah, D., & Meliana, S. (2022). Recommendation system from microsoft news data using TF-IDF and cosine similarity methods. Building of Informatics, Technology and Science (BITS), 4(1), 277-284.

Attalariq, M., & Baizal, Z. K. A. (2023). Chatbot-Based Book Recommender System Using Singular Value Decomposition. Journal of Information System Research (JOSH), 4(4), 1293-1301.

Ankam, V. (2016). Big data analytics. Packt Publishing Ltd.

Baesens, B., & vanden Broucke, S. (2020, February 24). Singular Value Decomposition in Recommender Systems.DataMiningApps.https://www.dataminingapps.com/2020/02/singular-value-decomposition-in-recommender-systems/

Scientific Journal for the Faculty of Science-Sirte University Vol. 4, No. 1 (2024) 89-97

Scientific Journal for the Faculty of Science-Sirte University

Journal home page: http://journal.su.edu.ly/index.php/JSFSU/index

DOI: 10.37375/issn.2789-858X

Isolation and Identification of Pectobacterium Bacteria in Al Bayda, Aljabal Alakhdar, Causing Soft Rot on Potato Plants

Hosnia A. A. Bofarwa

Botany Department, Science Faculty, Omar Al-Mukhtar University, Al-Bayda –Libya.

DOI: https://doi.org/10.37375/sjfssu.v4i1.2658

ARTICLE INFO:

Received: 03 March 2024

Accepted: 10 April 2024

Published: 17 April 2024

Keywords: (*Pectobacterium*, Potatoes, Disease, Soft Rot, Antibiotics) .

A B S T R A C T

This study sought to identify and characterize the bacteria causing soft rot disease in potatoes in a few Al-Bayda markets. It also sought to determine the pathogenicity of the bacteria and assess their susceptibility to various antibiotics and biochemical tests. From tubers afflicted with soft rot disease and from all samples taken from a few farms and shops in the Al-Bayda marketplaces, a bacterial isolate was obtained. The ability of the bacterial isolate to cause the illness was demonstrated by the pathogenicity test conducted on potato slices. The bacteria were identified as Pectobacterium based on the outcomes of phenotypic and biochemical tests. A test revealed some antibiotic sensitivity. The study's findings demonstrated that, with the exception of the antibiotic tetracyclin, all tested antibiotics are harmful to Pectobacterium, albeit to varied degrees. However, the antibiotic was Erythromycine, at varied degrees. One of the best antibiotics since it prevents erythromycine from being made An region with an average diameter of 3 cm is where bacteria proliferate. Amoxicilline, an antibiotic, was brought with them. It came in second place in terms of effectiveness because the antibiotic Tetracyclin had no harmful effects on the bacteria and the average diameter of the area surrounding the disc containing it free of bacterial growth was 1.5 cm.

1 Introduction

The potato crop Solanum tuberosum, L. is the third most consumed food crop globally and the fourth most strategic crop after wheat, corn, and rice (AL-Razaq et al., 2018; Shayaa and Hussein, 2019). . It is classified as a member of the Solanaceae family. Potato tubers are not only indirectly used in the processing industry, but are also directly consumed as nutrition for humans and animals. after dehydration or freezing (Boras et al., 2006). In light of the challenges the world faces due to rapid population growth and food supply challenges, the Food and Agriculture Organization of the United Nations strongly advocates potato as a key crop for food security. Furthermore, the potato plant is considered one of the most important vegetable crops in the world, as it represents an energy-rich food source and a source of nutrients. It is rich in nutrients such as carbohydrates, sugars, proteins, amino acids, organic acids, minerals and fiber. It is an excellent source of several vitamins, the most important of which are C and B (Alaee, 2018).

Potatoes contain a variety of chemicals that support activity. Antioxidants Hellmann et al. (2021), Suareza et al. (2020), Akrimi et al. (2020), the potato crop ranks fourth, after wheat, corn and rice, and is also very important and forms a large part of the Libyan diet. In 2010, the potato cultivation area in Libya exceeded 15,000 hectares. This year the country's potato production is about 290,000 tons, with a yield of about 19.3 tons per hectare. The areas east and south of Tripoli are important potato production areas due to their favorable soil composition and temperature (Souad

Corresponding author: **E-mail:** Hosnia.bofarwa@omu.edu.ly

Al-Bandaqo 2014). Many bacterial, fungal, viral and nematode diseases can affect potatoes. One of the most serious diseases is bacterial soft rot, caused by the pathogenic bacterium Fruitbacter carotobacter. Infection starts in the field and spreads rapidly during tuber transportation and storage (Youdkes et al., 2020), resulting in heavy agricultural losses (Guttman et al., 2021). Since soft rot is prevalent in both tropical and temperate climates, it is one of the most significant bacterial diseases that harm a wide variety of plants, including members of the Solanaceae family, which includes potatoes and many other crops. It is a disease that harms plants both in the field and in storage, leading to major losses (Motyka et al., 2021).

The genus Pectobacterium is a member of the family Enterobacteriaceae. It is one of the most important families in charge of soft rot in economically important crops like corn, tomatoes, and potatoes, according to Oulghazi et al. (2021). Moreover, the main culprit behind black leg illness is a genus of Pectobacterium called Dickeya (Werra et al., 2020). Pectobacterium bacteria l infections also cause soft rot in a variety of crops (Fan et al., 2020, Koh et al., 2012). Plant tissue components can be destroyed by it due to the action of enzymes that break down plant cell walls (Lee et al., 2013, Li et al., 2018, Giovannoni et al., 2020). According to Paul et al. (2020), the activity of these enzymes released by these bacteria that cause the breakdown of cell walls is what causes soft rot illness. Plant cell wall-degrading enzymes (PCWDEs), like pectinases, are the wall-degrading enzymes released by these bacteria. In addition to cellulases, hemicellulases, and proteinases. In order to cause disease symptoms, these bacteria require specific environmental conditions, such as humidity and the availability of nutrients that are gotten through wounds or naturally occurring plant holes. Once within the plant, they embed themselves in the interstitial spaces or vascular tissues, where they produce an enzyme. as per Colmer et al. (2009) and Paul et al. (2020), who disintegrate the cell wall of plants.

Given the significance of soft rot on potatoes and its extensive spread in the city of Al-Bayda as a result of the paucity of research on this illness, the study's objective is to identify and isolate the bacteria that cause the condition.

2 Materials and Methods

2.1 Gather samples, isolate the pathogen, and purify it

Pathogen Isolation and purification

In the fall of 2023, samples of potato tubers exhibiting soft rot symptoms were gathered from Al-Bayda local markets. With a few minor adjustments, the methodology of Doololbeldieva et al. (2016) was used to isolate the pathogen. Selected potato tubers exhibiting signs of soft rot disease were taken from the Al-Bayda local markets and cleaned under running tap water to eliminate dust. After that, it was surface sterilized for three minutes using sodium hypochlorite NaCl (chlorine 5%, concentration 2%). Next, after removing the potato's outer peel with 10 ml of sterilized normal saline, washed three times with sterile distilled water to remove the sterile substance, and mashed using a ceramic mortar. (0.85% NaCl). Using a sterile carrier loop, a portion of the bacterial suspension was collected, and the planing procedure was used to inoculate the NA medium. After that, the inoculation-treated dishes were kept in the incubator for a whole day at 28 °C. Using a sterile loop, a piece of the developing bacteria was transferred to Nutrient Agar medium, where it was striped to create single colonies and cultured for 24 hours under the same circumstances. Fig (1).

2.2 Examining the isolate of bacteria that is causing the soft rot on potatoes for pathogenicity

2.2.1 Examining potato slices for pathogenicity

To test for pathogenicity, the tubers that were as healthy, regular, and constant in size as feasible were chosen. After repeatedly washing them with water to get rid of dust, they were surface sterilized for three minutes with NaCl (5% chlorine) (2% concentration), and then they were repeatedly cleaned with sterile distilled water. They cut the tubers. The potatoes were sanitized and then sliced into uniform pieces that were about 10 mm thick. Using a sterile cork drill with a 5 mm diameter, a hole was drilled in the center of each slice, which was then put in sterile Petri plates (with sterile filter paper placed underneath). At 24 hours old, all of the bacteria under investigation were put into the holes. microliter/hole (610 colony-forming units/ml) including six slides per isolate, each kept in its own plate. After inoculating the slides, the dishes were kept in an

incubator set at 28 °C for six days to monitor the infection's progress Fig (2).

2.3 Phenotypic and biochemical testing

2.3.1 3.1- Bacterial isolate's microscopic and phenotypic features:

After the bacteria were cultured on NA media for 24 hours, smears were made on slides. After clean glass was stained with Gram staining, it was viewed using an optical microscope with an objective lens set to 100 x magnification. This allowed researchers to record the morphology, aggregations, and interactions between the bacterial cells and the dye .Table 1. in addition to the type, color, and form of the bacterial colonies' development on NA medium. Properties embraced the diagnostic standards that Schaad (1988) and Holt et al. (1994) mentioned.

2.3.2 Capacity to grow in certain media with differential cultures.

2.3.2.1 Dextrose-Yeast Extract CaCO3 Medium

To make the YDC medium, mix 1000 milliliters of sterile distilled water with 10 grams of yeast extract, 20 grams of dextrose, 20 grams of calcium carbonate, and 15 grams of agar. In one liter of hot distilled water, dissolve the aforementioned elements, and thoroughly mix the mixture with a Vortex mixer. Adjust the pH to 7.2 and incubate for 20 minutes at 121 degrees Celsius and 15 pounds per square inch of pressure. Transfer the medium into sterile plates and introduce the studied bacterial isolates into them. The plates were incubated for seventy-two hours at a temperature of 28 °C. Krieg and Dobereiner (1984), Schaad et al. (2001), and Wilson et al. (1967) all documented the type of growth that occurred on this medium.

2.3.2.2 Kings Medium (KB)

Add 20.0 g of peptone, 2.5 g of 4HPO2K, 6.0 g of O2.7H4MgSO, 15.0 g of agar, and 15 ml of glycerol to 1000 ml of distilled water to prepare the medium. After dissolving the medium's ingredients in hot distilled water and adjusting the pH to 7.2, the autoclave was sterilized for 20 minutes at 121 degrees Celsius and 15 pounds per square inch of pressure. The planned approach was used to inoculate the medium with the bacterial isolate under investigation after it had been poured into dishes. For seventy-two hours, bacterial cultures were cultured at 28 °C (Schaad et al., 2001). Table (2).

2.3.3 Biochemical assays for the investigated bacterial isolate:

2.3.3.1 Catalase test:

The bacterial growth on NA media was given a few drops of a 3% aqueous solution of hydrogen peroxide (H2O2) at the 24-hour mark, as the development of gas bubbles after a few seconds indicated a positive test (2000, MacFaddin, Winn et al., 2006).

2.3.3.2 Oxidase test:

A portion of the bacterial growth was transferred to the area of the filter paper saturated with the reagent and gently rubbed with a stick after several drops of the reagent Tetramethyl-P-phenylendiamine dihydrochlorie (made by adding 1 g of the listed substance to 100 ml of sterile distilled water) were placed on the paper. Wooden, the test is positive if the violet color appears within ten seconds (MacFaddin, 2000).

2.3.3.3 Growth test at 35°C :-

After preparing and sterilizing NA medium in an incubator for 20 minutes at 121 degrees Celsius and 15 pounds per hour of pressure, the medium was inoculated using 24-hour-old bacterial colonies and incubated for 48 hours at 35 degrees Celsius for observation. Expansion or Absence Scchad 1980.

2.3.3.4 Growth test in a medium containing 5% NaCL

After preparing 100 milliliters of NA medium and adding five percent sodium chloride to it, autoclave it for twenty minutes at 121 degrees Celsius and 15 pounds per hour of pressure. Following that, it was injected with 24-hour-old B. teria colonies and let to incubate for 24 hours at 28±2°C in order to observe it. Development or not (Schaad et al. (2001).

2.4 Pectobacterium sensitivity to specific antibiotics:

The working methodology:

1- Readyed a test tube with three milliliters of distilled sterile water in it.

2- To adequately mix the bacteria in the container containing bacteria in water, equal amounts of bacterial growth were poured into a tube using a sterile transfer needle (loop). The needle was then placed on top of the container and shaken several times.

3- The Hilton Muller's surface is contaminated with microorganisms, and Cotton Swab publishes the information by covering the entire surface of the center—not just the bust.

4- After the inoculated dishes were in the incubator for two hours at 28 °C, they were taken out and placed near the flame using sterile tongs. I then added three disc containers to each dish and repeated the process with different antibiotics spaced equally apart. Set aside three discs for each antibiotic and place the dishes in the incubator at the same temperature.

5- Following two days of good bacterial growth on the medium, all the dishes were taken out and the diameter of the empty circle around each disc—where the bacteria could not grow was measured.

6- The disk will be measured (by millimeter) using thementioned and comparing ruler to ascertain the degree of resistance if a transparent loop forms around it. Table (4) and Fig (3). Tetracyclin, Amoxicillin, and Erythromycin are the medications that.

3 Results

3.1 1. Gather samples and separate disease-causing bacteria

From every sample taken from the local markets in the city of Al-Bayda, where the growth first emerged, a bacterial isolate linked to the soft rot illness on potatoes was identified. Bacteria were cultured on NA culture media for 12 hours, and individual colonies were identified after 24 hours of incubation at 28°C. The colonies had a smooth, convex surface, a cream to white color, and regular, flawless edges.

Figure (1) (a and b) demonstrating the gathering of samples exhibiting disease symptoms; (c) demonstrating the emergence of cream-colored to brilliant white bacterial growths following isolation, 24 hours of culture in Na medium, and 28-degree Celsius incubatio

3.2 Evaluating the pathogenic potential of different microorganisms linked to soft rot illness

3.2.1 A test for pathogenicity using potato slices

The results of the pathogenicity test on potato slices showed that the studied bacterial isolate has the ability to cause rot disease on potato slices and the appearance of distinctive symptoms, the most important of which is tissue decomposition and the emission of unpleasant odors due to bacterial activity.

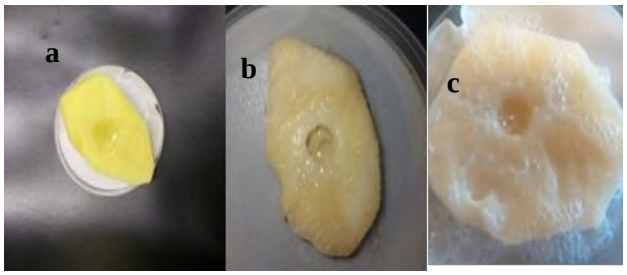

Figure (2) Effects *Pectobacterium* of potato slices, a. Control , b and c Symptoms of tissue decomposition and the emission of unpleasant odors appear a result of bacterial activity

3.1- Evaluations both biochemical and phenotypic

3.1.1- Microscopic and morphological features of the bacterial isolates being examined:

Table (1) shows the results obtained from studying the phenotypic and microscopic characteristics of bacteria isolated from potato tubers and stems infected with potato soft rot disease:

Table (1) Microscopic and phenotypic characteristics of the bacteria under study

Adjective	Notes
Reaction with Gram stain	Negative
Cell shape	Short rod
Cell assembly	Most of them are solitary and some are clustered
Color and shape of colonies on NA medium	Creamy to shiny white, round, with regular, perfect, convex edges

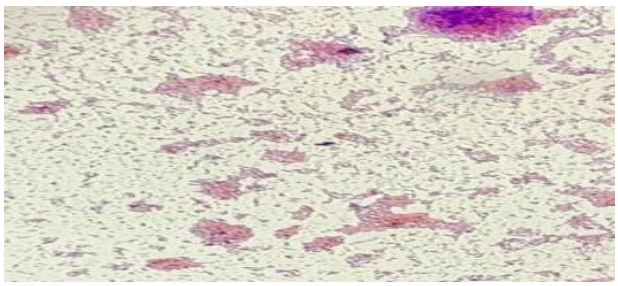

Reaction with Gram stain:- Negative

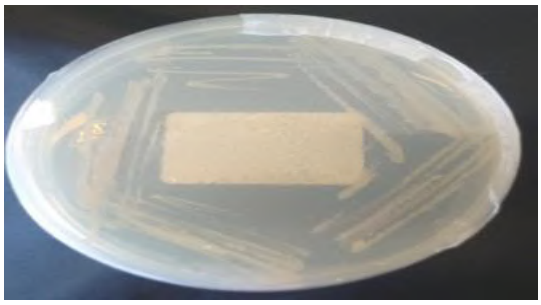

Color and shape:- Creamy to shiny white, round, with regular, perfect, convex edges

3.1.2 - Growth ability in some differential culture media

Table (2) shows the nature of growth of the bacterial isolates under study and the characteristics of the colonies growing on some selective and differential media.

The agricultural medium	Notes
Nature of growth on YDC medium	Colonies are yellow to cream, convex, shiny, circular with a perfect edge
Nature of growth on Kings Medium (KB)	White to cream colonies with a round, convex, opaque entire edge

3.1.3- Biochemical tests for the bacterial isolates under study:

Table (3) shows the overall results of the biochemical tests obtained for the bacterial isolates under study that are associated with soft rot disease on potatoes

Biochemical tests	**Results**
Catalase	**+**
Oxidase	**-**
growth at temperature 35 °C	**+**
Growth in a medium containing 5% sodium chloride +	**+**

(+) Positive test result

(-) Negative test result

4- Sensitivity of *Pectobacterium* to some antibiotics :

The study's findings demonstrated that, with the exception of the antibiotic tetracyclin, all tested antibiotics are harmful to *Pectobacterium*, albeit to varied degrees. However, erythromycine was the antibiotic to varied degrees. One of the best antibiotics since it prevents erythromycine from being made An region with an average diameter of three centimeters is where bacteria proliferate. Table Four: Amoxicilline, an antibiotic, was brought with them. It came in second place in terms of effectiveness because the antibiotic Tetracyclin had no harmful effects on the bacteria and the average diameter of the area surrounding the disc containing it free of bacterial growth was 1.5 cm. Figure (3)

Table (4): Effect of various antibiotics against *Pectobacterium* isolate

Antibiotics	**Diameter of growth-free zone/cm**			
	Duplicates			**the average**
Erythromycine	**3**	**2**	**2**	**3**
Amoxicilline	**1.5**	**1.0**	**0.6**	**1.5**
Tetracyclin	**0**	**0**	**0**	**0**

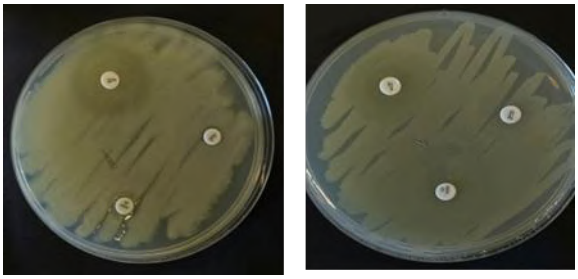

Figure (3) Effect of various antibiotics against Pectobacterium isolate

4 Discussion

According to Dees et al. (2017), the Pectobacterium genus is a member of the Enterobacteriaceae family. According to Oulghazi et al. (2021) it is one of the most significant families responsible for soft rot in economically significant crops including corn, tomatoes, and potatoes. Furthermore, black leg illness is primarily caused by the genera Dickeya and Pectobacterium (Werra et al., 2020). Pectobacterium bacterial infections induce soft rot in a variety of crops and generate large-scale economic losses globally (Fan et al., 2020; Koh et al., 2012). It is capable of destroying plant tissue components through the activity of plant cell wall-degrading enzymes (Lee et al., 2013; Li et al., 2018; Giovannoni et al., 2020). Paul et al. (2020) indicated that soft rot disease occurs as a direct result of the activity of these enzymes, which Secreted by these

bacteria, which leads to the decomposition of cell walls, these wall-degrading enzymes secreted by these bacteria are called (PCWDEs), such as Pectinases , Cellulases, Hemicellulases and Proteinases. These bacteria need certain environmental factors, such humidity, and the availability of nutrients that are obtained through wounds or natural plant holes in order to create illness symptoms. They enter the plant and become embedded in the vascular tissues or interstitial spaces, where they manufacture an enzyme. which (Colmer et al., 2009 and Paul et al., 2020) break down the plant cell wall. The pathogenicity test on potato slices revealed its results. It demonstrated that the investigated bacterial isolate can induce potato slice rot illness and manifest many symptoms, the most significant of which are tissue degradation and malodorous emissions due to bacterial activity. These outcomes agree with the research conducted by Zhou (2019) and Goszczynska et al. (2000).

Based on variations in the metabolic activity of various bacteria, biochemical tests are performed to identify different species of bacteria (Schaad et al., 2001). The ability to use specific compounds, produce specific enzymes differently in different species, and have diverse metabolisms all aid in the identification of different species. According to Schaad et al. (2001), Terta et al. (2013), and Li et al. (2020), this kind of testing helps. Phenotypic differences cannot differentiate one type of bacteria from another based solely on appearance, so they cannot be used to make a diagnosis in the case of bacteria. the arrangement and size of bacteria because many different types of bacteria have the same sizes and shapes. The findings demonstrated that the bacteria were round, cream to bright white, gram-negative, short rod-shaped, and found singly or in colonies. These characteristics are in line with the descriptions of P. given in Holt et al. (1994), Schad (2001), Perombilon (2006), Galilei et al. (2009), and Olgazi et al. (2021). Perfect, convex, and regular edges. These outcomes align with Thus, in the end, the primary method for identifying bacteria is based on variations in their metabolic activities (Ztruk et al., 2018). According to Terta et al. (2013) and Agyemang et al. (2021), 2020), each type of bacteria has a unique set of metabolic activities that set it apart from all other types. These biochemical fingerprints are characteristics that are controlled by bacterial enzymes, which can be divided into two categories: those that operate outside of bacterial cells and are primarily in charge of producing cellular energy from simple substances required for cell survival and function, as well as those that work inside bacterial cells Bacterial cells produce enzymes into their surroundings that break down complex molecules with a high molecular weight, such proteins, carbohydrates, and fats, which are too big to fit through a cell membrane. Bacterial bacteria, this is because to their complex makeup, such as lipids, or their huge size, such as proteins and carbohydrates (Kraepiel and Barny 2016). Additionally, the bacteria tested positive for catalase and negative for oxidase. As it was grown on media containing 5% sodium chloride, bacteria also grew on NA medium kept at 35°C. These results were in line with those of Gasik et al. (2014) and Ramadan and Al-Mashhadani (2006). Additionally, bacteria developed on the examined electoral media, with the following outcomes. It agrees with findings from other research on Pectobacterum growth in a few selective media (Holt and Krieg, 1984; Terta et al., 2010; Ravari Baghaee et al., 2011).

The bacterial ribosome is made up of the S50 unit and the 30S unit. A number of antibiotics block the function of ribosomes. Any of these can be impacted by antibodies. Antibodies Aminoglycosides bind to a certain type of ribosome to function. Glycosidic linkages bind complex sugars together to form substances known as aminoglycosides. Tetracyclines, for example, have a different molecular nucleus than streptomycin or deoxystreptidine because the latter inhibits the 30S unit. Daniel Robert (1988).

Three major classes of antibiotics, including chloramphenicol, block the 50S subunit. The broad-spectrum bacterial inhibitor, like erythromycin, inhibits both Gram-positive and Gram-negative bacteria. Manzer J. (1989) The study's findings demonstrated that, with the exception of the antibiotic tetracyclin, all tested antibiotics are harmful to Pectobacterium, albeit to varied degrees. However, in different amounts, the antibiotic was Erythromycin One of the best antibiotics since it prevents erythromycine from being made An region that has an average diameter of 3 cm is where bacteria proliferate. The investigated antibiotics' effects varied. Where the bacteria were exposed to the antibiotic Erythromycine Extremely successful while the medication Amoxicilline was It had a moderate impact. Tetracyclin, an antibiotic, was ineffective in this regard. This discrepancy can result from the tested antibiotics' varied interactions with the contents or parts of the bacterial cell wall. The findings of Khalil et al. (2021) and Maha Raouf Al-Saad (1980) suggest that

certain antibiotics impede the processes of protein synthesis and amino acid metabolism, whereas other antibiotics impede cell division or the action of enzymes that attach peptide side chains to the peptidoglycan portion of the cell wall.

Acknowledgements

Firstly, thanks and merciful to god Sincere thanks and deep a ppreciation are extended to **Dr. Soad M. Omar** Associate prof. of Microbiology , Faculty of Science, Omar AL-Mukhtar University for the support and guidance and facilities provided for the completion of this work, valuable advice, continuous help throughout the investigation and preparation of and putting the research in its final form.

Great thanks are also to all staff of Botany Department, Faculty of Science, Omar AL-Mukhtar University, for help and using the Microbiology lab facilety advices

Conflict of interest: The author declares that there are no conflicts of interest.

References

Abd AL-Razaq, A. H., Wafaa, A. H., & Mohammed, M. M. (2018). Production of potato under soilless culture. Int. J. Agricult. Stat. Sci, 14(1), 299-310.

Shayaa, A. H., & Hussein, W. A. (2019). Effect of neem leaves extract and organic fertilizer in the productivity and quality of two potato cultivars. The Iraqi Journal of Agricultural Science, 50(1), 275-285.

Bouras, M., Abu Turabi, B., & Al Basit, I. (2006). Production of vegetable crops. The theoretical part.

Alaee, S. (2018). Air pollution and infertility–a letter to editor. J of Environ Treat Tech, 6(4), 72-3.

Akrimi, R., Hajlaoui, H., Rizzo, V., Muratore, G., & Mhamdi, M. (2020). Agronomical traits, phenolic compounds and antioxidant activity in raw and cooked potato tubers growing under saline conditions. Journal of the Science of Food and Agriculture, 100(9), 3719-3728.

Suárez, S., Mu, T., Sun, H., & Añón, M. C. (2020). Antioxidant activity, nutritional, and phenolic composition of sweet potato leaves as affected by harvesting period. International Journal of Food Properties, 23(1), 178-188.

Hellmann, H., Goyer, A., & Navarre, D. A. (2021). Antioxidants in potatoes: A functional view on one of the major food crops worldwide. Molecules, 26(9), 2446.

Guttman, Y., Joshi, J. R., Chriker, N., Khadka, N., Kleiman, M., Reznik, N., ... & Yedidia, I. (2021). Ecological adaptations influence the susceptibility of plants in the genus Zantedeschia to soft rot Pectobacterium spp. Horticulture Research, 8.

Youdkes, D., Helman, Y., Burdman, S., Matan, O., & Jurkevitch, E. (2020). Potential control of potato soft rot disease by the obligate predators Bdellovibrio and like organisms. Applied and Environmental Microbiology, 86(6), e02543-19.

Motyka-Pomagruk, A., Zoledowska, S., Sledz, W., & Lojkowska, E. (2021). The occurrence of bacteria from different species of Pectobacteriaceae on seed potato plantations in Poland. European Journal of Plant Pathology, 159, 309-325.

Li, L., Yuan, L., Shi, Y., Xie, X., Chai, A., Wang, Q., & Li, B. (2019). Comparative genomic analysis of Pectobacterium carotovorum subsp. brasiliense SX309 provides novel insights into its genetic and phenotypic features. BMC genomics, 20(1), 1-17.

Voronina, M. V., Kabanova, A. P., Shneider, M. M., Korzhenkov, A. A., Toschakov, S. V., Miroshnikov, K. K., ... & Ignatov, A. N. (2019). First report of Pectobacterium carotovorum subsp. brasiliense causing blackleg and stem rot disease of potato in Russia. Plant Disease, 103(2), 364-364.

Mantsebo, C. C., Mazarura, U., Goss, M., & Ngadze, E. (2014). The epidemiology of Pectobacterium and Dickeya species and the role of calcium in postharvest soft rot infection of potato (Solanum tuberosum) caused by the pathogens: A review. African Journal of Agricultural Research, 9(19), 1509-1515.

Waldee, E. L. (1942). Comparative studies of some peritrichous phytopathogenic bacteria. Iowa State University.Skerman, V. B. D.; McGowan, V. and Sneath, P. H. A. (1980). Approved Lists of Bacterial Names. International Journal of Systematic Bacteriology, 30:225-420.

Portier, P., Pédron, J., Taghouti, G., Fischer-Le Saux, M., Caullireau, E., Bertrand, C., ... & Barny, M. A. (2019). Elevation of Pectobacterium carotovorum subsp. odoriferum to species level as Pectobacterium odoriferum sp. nov., proposal of Pectobacterium brasiliense sp. nov. and Pectobacterium actinidiae sp. nov., emended description of Pectobacterium carotovorum and description of Pectobacterium versatile sp. nov., isolated from streams and symptoms on diverse plants. International journal of systematic and evolutionary microbiology, 69(10), 3207-3216.

Dees, M. W., Lysøe, E., Rossmann, S., Perminow, J., & Brurberg, M. B. (2017). Pectobacterium polaris sp. nov., isolated from potato (Solanum tuberosum). International journal of systematic and evolutionary microbiology, 67(12), 5222-5229.

Oulghazi, S., Sarfraz, S., Zaczek-Moczydłowska, M. A., Khayi, S., Ed-Dra, A., Lekbach, Y., ... & Faure, D. (2021). Pectobacterium brasiliense: Genomics, host range and disease management. Microorganisms, 9(1), 106.

de Werra, P., Kopp, C., Häberli, M., Stöcker, I., Keil, A., Debonneville, C., ... & Keiser, A. (2020). Monitoring potato seed lots to control blackleg in fields in Switzerland and southern Germany. Plant Pathology, 69(7), 1331-1346.

Fan, J., Ma, L., Zhao, C., Yan, J., Che, S., Zhou, Z., ... & Hu, B. (2020). Transcriptome of Pectobacterium carotovorum subsp. carotovorum PccS1 infected in calla plants in vivo highlights a spatiotemporal expression pattern of genes related to virulence, adaptation, and host response. Molecular plant pathology, 21(6), 871-891.

Lee, D. H., Lim, J. A., Lee, J., Roh, E., Jung, K., Choi, M., ... & Heu, S. (2013). Characterization of genes required for the pathogenicity of Pectobacterium carotovorum subsp. carotovorum Pcc21 in Chinese cabbage. Microbiology, 159(Pt 7), 1487.

Giovannoni, M., Gramegna, G., Benedetti, M., & Mattei, B. (2020). Industrial use of cell wall degrading enzymes: the fine line between production strategy and economic feasibility. Frontiers in Bioengineering and Biotechnology, 8, 356.

Agyemang, P. A., Kabir, M. N., Kersey, C. M., & Dumenyo, C. K. (2020). The bacterial soft rot pathogens, Pectobacterium carotovorum and P. atrosepticum, respond to different classes of virulence-inducing host chemical signals. Horticulturae, 6(1), 13.

Collmer, A., Schneider, D. J., & Lindeberg, M. (2009). Lifestyles of the effector rich: genome-enabled characterization of bacterial plant pathogens. Plant physiology, 150(4), 1623-1630.

Doolotkeldieva, T., Bobusheva, S., & Suleymankisi, A. (2016). Biological control of Erwinia carotovora ssp. carotovora by Streptomyces species. Advances in Microbiology, 6(02), 104.

Bergey, D. H. (1994). Bergey's manual of determinative bacteriology. Lippincott Williams & Wilkins.

Schaad, N. W. (1988). Identification schemes. Laboratory guide of identification of plant pathogenic bacteria. 2nd ed. American Phytopathological Society. Press, USA, 1-15.

Schaad, N. W., Jones, J. B., & Chun, W. (2001). Laboratory guide for the identification of plant pathogenic bacteria (No. Ed. 3). American Phytopathological society (APS press).

Schaad, N. W., Jones, J. B., & Chun, W. (2001). Laboratory guide for the identification of plant pathogenic bacteria (No. Ed. 3). American Phytopathological society (APS press).

Wilson, E. E., Zeitoun, F. M., & Fredrickson, D. L. (1967). Bacterial phloem canker, a new disease of Persian walnut trees. Phytopathology, 57, 618-21.

Krieg, N. R. & Dobereiner., J. (1984) . Bergey´s Manual of Systematic Bacteriology , Wilkins , Baltimore – London.

MacFaddin, J.E. (2000). Individual biochemical test for identification of medical bacteria. 3th ed . Lippincott Williams Wilkins.London.

Win, W. C., Allen, S. D., Janda, W. M., Koneman, E. W., Procop, G. W., Schreckenberger, P. C., & Woods, G. (2006). Color Atlas and Textbook of Diagnostic Microbiology. 6 [sup] th ed.

Khalil, K. A., Fatima, M. M. & Intisar, M. Q. (2021). Studies on the Bacteria Erwinia carotovora (Jones) Holland which is causative in mushy decay of Potato . Journal of Science, No. 2

Daniel R. (1988). Basics of plant diseases, translated by Ibrahim Gamal El-Din, Kamal Jalal Mahmoud, Abdel-Rahman Hassan, and Ahmed Zaki. Arab Publishing and Distribution House - Arab Republic of Egypt.

Manzer, J. (1989) Basics of plant diseases, translated by Al-Taher Al-Sadiq Al-Ghazali. National Authority for Scientific Research - Libyan Jamahiriya.

de Werra, P., Kopp, C., Häberli, M., Stöcker, I., Keil, A., Debonneville, C., ... & Keiser, A. (2020). Monitoring potato seed lots to control blackleg in fields in Switzerland and southern Germany. Plant Pathology, 69(7), 1331-1346.

Koh, Y. J., Kim, G. H., Lee, Y. S., Sohn, S. H., Koh, H. S., Kwon, S., ... & Jung, J. S. (2012). Pectobacterium carotovorum subsp. actinidiae subsp. nov., a new bacterial pathogen causing canker-like symptoms in yellow kiwifruit, Actinidia chinensis. New Zealand Journal of Crop and Horticultural Science, 40(4), 269-279.

Li, X., Ma, Y., Liang, S., Tian, Y., Yin, S., Xie, S., & Xie, H. (2018). Comparative genomics of 84 Pectobacterium genomes reveals the variations related to a pathogenic lifestyle. BMC genomics, 19, 1-22.

Goszczynska, T., Serfontein, J. J., & Serfontein, S. (2000). Introduction to practical phytobacteriology (No. 589.9/G682). Safrinet.

Zhou, X., Liu, Y., Huang, J., Liu, Q., Sun, J., Cai, X., ... & Miao, W. (2019). High temperatures affect the hypersensitive reaction, disease resistance and gene expression induced by a novel harpin HpaG-Xcm. Scientific Reports, 9(1), 990.

Terta, M., Azelmat, S., M'hand, R. A., Achbani, E. H., Barakate, M., Bouteau, F., & Ennaji, M. M. (2012). Molecular typing of Pectobacterium carotovorum

isolated from potato tuber soft rot in Morocco. Annals of microbiology, 62, 1411-1417.

Perombelon, M. C. M. (2006). The Prokaryotes. Second Edition. pp: 2899- 2921.

Gallelli, M. F., Blatter, M. C., & Castillo, V. (2010). A comparative study by age and gender of the pituitary adenoma and ACTH and α-MSH secretion in dogs with pituitary-dependent hyperadrenocorticism. Research in Veterinary Science, 88(1), 33-40.

Oulghazi, S., Sarfraz, S., Zaczek-Moczydłowska, M. A., Khayi, S., Ed-Dra, A., Lekbach, Y., ... & Faure, D. (2021). Pectobacterium brasiliense: Genomics, host range and disease management. Microorganisms, 9(1), 106.

Agyemang, P. A., Kabir, M. N., Kersey, C. M., & Dumenyo, C. K. (2020). The bacterial soft rot pathogens, Pectobacterium carotovorum and P. atrosepticum, respond to different classes of

virulence-inducing host chemical signals. Horticulturae, 6(1), 13.

Kraepiel, Y., & Barny, M. A. (2016). Gram-negative phytopathogenic bacteria, all hemibiotrophs after all?. Molecular plant pathology, 17(3), 313.

Ramadan, M. N. & Zahraa, S. A. (2006). Isolation and identification of black leg disease bacteria in potatoes. Al-Rafidain Science Journal, 17 (11): 193 – 203.

Gašić, K., Gavrilović, V., Dolovac, N., Trkulja, N., Živković, S., Ristić, D., & Obradović, A. (2014). Pectobacterium carotovorum subsp. carotovorum-the causal agent of broccoli soft rot in Serbia. Pesticidi i fitomedicina, 29(4), 249-255.

Bergey, D. H. (1994). Bergey's manual of determinative bacteriology. Lippincott Williams & Wilkins.

Ravari, A. K., Othman, I. B., & Ibrahim, Z. B. (2011). Finite element analysis of bolted column base connection without and with stiffeners. Int. J. Phys. Sci, 6(1), 1-7.

Duan HM, Ma YC, Liu RR, Li Q, Yang Y, Song J (2018) Effect of combined waterlogging and salinity stresses on euhalophyte Suaeda glauca. Plant Physiol. Biochem.127:231-237. https://doi.org/10.1016/j.plaphy.2018.03.030

Scientific Journal for the Faculty of Science-Sirte University Vol. 4, No. 1 (2024) 98-108

Scientific Journal for the Faculty of Science-Sirte University

Journal home page: http://journal.su.edu.ly/index.php/JSFSU/index

DOI: 10.37375/issn.2789-858X

Application of Cloud Point in Spectrophotometric Determination of Drugs, Overview

Lamya A. Sarsam[1] and Theia'a N. Al-Sabha[2]

[1]*New and Renewable Energies Department, College of Science, Mosul University, Mosul, Iraq.*
[2]*Chemistry Department, Al-Noor University College, Mosul, Iraq.*

DOI: https://doi.org/10.37375/sjfssu.v4i1.1798

ARTICLE INFO:

Received: 22 November 2023

Accepted: 14 January 2024

Published: 17 April 2024

Keywords: *Cloud point, drugs, surfactant, spectrophotometry, Solid-phase extraction*

A B S T R A C T

The technique known as "cloud point extraction," or CPE, involves removing organic and inorganic compounds from chemical or biological systems using safe extractants such as non-ionic surfactants. These extractants have a tendency to separate out of the bulk solution and form clouds when heated to significant temperatures, and the capacity of the surfactants in the aforementioned procedure to concentrate these compounds is well established. The simplicity and speed of the CPE approach get a lot of attention, and the extraction process improves the experimental settings by varying the temperature, surfactant concentration, type of electrolyte, acidity function, and extraction duration. The so-called surfactant-rich phase and the surfactant aqueous phase separate into phases as a result of the surfactant. The cloud point temperature is the result of comparing the greatest temperature with the crucial temperature. It will be the material to be examined is then highly concentrated, with a high preconcentration factor. This article explains the application of CPE method for determination of various medicines utilizing various reactions.

Introduction

In 1978, Watanabe and Tanak (Watanabe & Tanaka, 1978) introduced the CPE technique as a green extraction, which is used as a surfactant agent (Ghasemi, & Kaykhaii, 2016). An analytical method with tremendous potential to increase detection limits is separation and pre-concentration. There are many advantages to using CPE as a pre-concentration process. Some of the features include speed, safety, and low cost. CPE is a simple method that concentrates a wide range of analytes with excellent recoveries and high concentration factors. Results with CPE are equivalent to those acquired using other methods of separation. Therefore, species that interact with the micellar system can be extracted and preprocessed from concentrated solutions either directly (usually through hydrophobic organic compounds) or indirectly through the necessary derivatization reactions (e.g., metal ions after reaction with appropriate hydrophobic ligands).

CPE is divided into three steps: The first three stages are the solubilization of the analyte into micellar aggregates, clouding, and phase separation for analysis.

A surfactant solution swiftly separates into two different phases when heated to a critical temperature. One phase is a surfactant-rich phase, whereas the other phase contains surfactant at a concentration below or equal to the critical micelle concentration (Ojeda & Rojas, 2009). Hydrophobic molecules that were previously confined to micelles in solution are liberated during the surfactant-rich phase.

This impact is noticeable, especially for polyoxymethylene surfactants. The two ethylene oxide fragments in the micelle, which when hydrated repel one another at low temperatures and attract one another at higher degrees due to dehydration, are responsible for

***Corresponding author*: E-mail:** lamyasarsam@uomosul.edu.iq

this phenomenon. The theory and related applications of this extraordinary separation technique have been discussed in various reviews (McLntire & Dorsey, 1990; Hinze & Pramauro, 1993; Sanz-Medel et al., 1999; Quina & Hinze, 1999; Stalikas, 2002; Rubio& Pérez-Bendito, 2003; Ferrera et al., 2004; Burguera& Burguera, 2004; Paleologos et al., 2005). And reports on its use in metal determination (Bezerra et al., 2005; Silva et al., 2006).

CPE has been promoted as a desirable substitute for liquid-liquid extraction in recent times. This method is based on the finding that most nonionic surfactants, when heated to their cloud point temperature (Watanabe & Tanaka, 1978), form micelles in aqueous solution and turn cloudy.

In order to separate the two phases, the aqueous supernatant phase and the surfactant-rich phase, in CPE, the appropriate experimental conditions must be met, with the surfactant concentrated near the critical micelle concentration. As a result, temperature change causes two-phase separation in zwitterionic and non-ionic surfactant solutions, In contrast, other factors (such as pH, the addition of an ionic salt, or the presence of an organic solvent) result in two-phase separation in ionic surfactant solutions. Parameters that produce phase separation can limit the types of compounds that can be extracted.

As a result, weakly basic drugs (such as Adrenaline, Codeine, and Atropine) which are ionized in low pH solutions, cannot be analyzed using acidic solutions, while thermo labile chemicals (such as vitamins) cannot be analyzed using CPE at high temperatures. Fig. 1 illustrates the actions needed in each of the five crucial CPE periods (Madej, 2009): (I) treating the sample with a surfactant, (II) keeping the temperature at a tolerable level for a while, (III) centrifuging, (IV) removing the supernatant and (V) correctly handling the surfactant-rich phase.

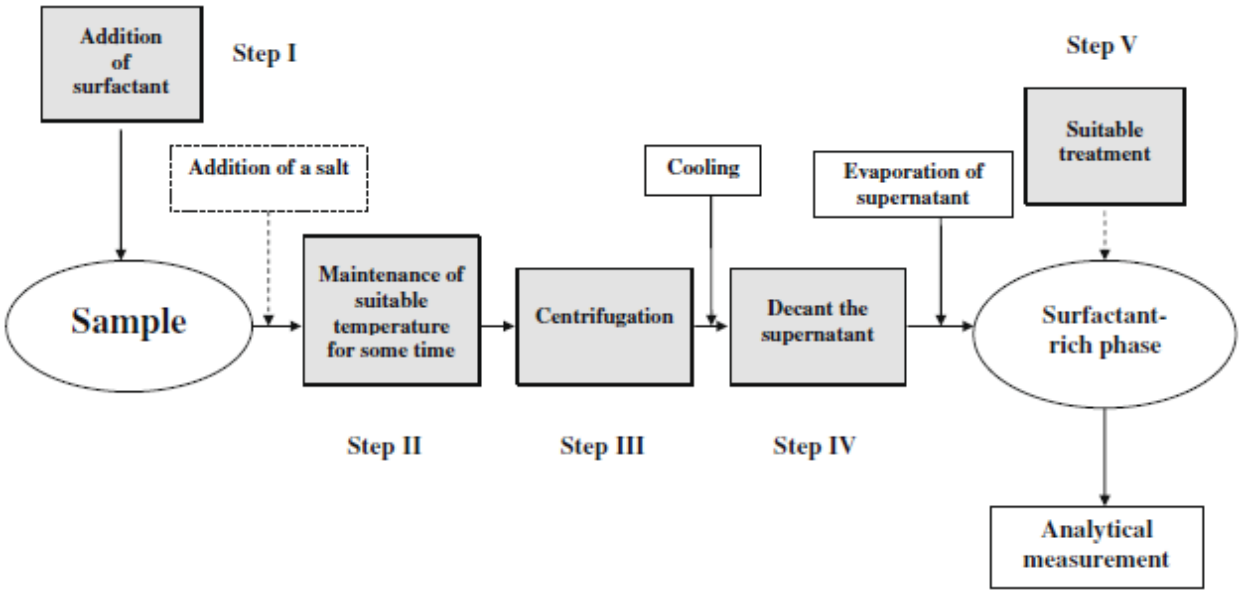

Figure (1) Five key steps in cloud–point extraction (CPE).

If these techniques don't work, you'll need to perform additional cleanup (such as solid-phase extraction (SPE) of the extract being studied) or switch to another detection method.

Ionic strength, temperature, and the kind and concentration of the surfactant are the three most important key variables. When developing a CPE approach, these considerations must be taken into account.

The acidity of the sample solution, similar to liquid-liquid extraction (LLE), is one of the most important factors controlling how well the analyte partitions in the concentrated surfactant-rich phase. The efficiency of maximum extraction of ionized species has been achieved at pH values where the uncharged form of the sample predominates. In micelle-mediated extraction, various surfactants can be used. The three types of surfactants that are most frequently utilized are anionic, double-ionic, and non-ionic.

In general, the effectiveness of CPE increases with the introduction of more hydrophobic surfactants and hydrophobic analytes. The surfactant amount present in the sample solution is an important additional factor

affecting the CPE effectiveness of CPE. The recommended range for surfactant concentrations is a pretty narrow band. As the final surfactant volume increases, it is seen that the analytical signal degrades over the optimal range. However, analytical accuracy and reproducibility deteriorate if surfactant concentration is dropped below the values that are recommended.

Dehydration happens when the temperature rises, and the surfactant-rich phase's volume decreases. Researches have indicated that during CPE, two phases, a micelle-rich phase and a water micelle phase, must be maintained for a certain amount of time and at temperatures higher than the cloud point temperature.

. Using ionic compounds creates a repulsive electrostatic effect. This can be explained by the fact that increasing ionic strength usually promotes phase separation and improves recovery. The effect of ionic strength on biological fluids is particularly significant (Madej, 2009).

Spectrophotometry is the most popular and enticing approach since it is simple and less `expensive to use than other instrumental processes (BİŞGİN, 2018).

The measurement of dyes using spectrophotometry can be difficult because of the low dye concentrations and matrix interference in real samples (Bişgin & Narin, 2015). As a result, many analytical methods such as dispersive liquid-liquid microextraction (DLLME), CPE (Karatepe & Soylak, 2017; Pourreza & Zareian, 2009) and others are combined with UV-Vis spectroscopy (Bazregar, et al., 2018).

Solid-phase extraction (SPE) (Yu & Fan, 2016). Has been developed to identify food dyes. For the identification and quantification of trace hazardous chemicals in diverse matrixes, such as dyes and heavy metal ions, CPE, a separation, purification, and enrichment approach, has been widely used (Li, et al., 2017; Nambiar et al., 2017). Phase separation makes it possible to observe two stages in CPE (Shi et al., 2004). The crucial temperature over which the surfactant-containing solution turns turbid and divides into two phases is known as the cloud point temperature. First, the target analyte is present in very small quantities in the surfactant-rich phase. The diluted aqueous phase is at the second stage and has a large volume (Lemos et al., 2007).

The spectrophotometric technique combined with CPE offers appealing qualities in regular examinations of metals and chemical compounds in various matrices as an alternative to using the pricy instruments mentioned above (Surme et al., 2007; Candir et al., 2008; Khammas et al., 2014; Khammas et al., 2013).

The unaided eye is the best tool for finding cloud patches. It is especially suitable when the appearance of the solution changes quickly and noticeably. The cloud point temperature is the point at which a solution begins to get clouded (cloud). However, since eye observation is subject to observer error, especially if the cloudiness is increasing, its assessment is essentially arbitrary (Pincemaille, et al., 2018).

In compliance with standard CPE technique, an aqueous two-phase system known as "ATPS" is utilized. In order to create a surfactant-rich phase containing the target analyte, a PEG-based aqueous solution containing a surfactant or mixture of surfactants was heated and centrifuged.

. In this study, temperature-induced cloud point extraction (TICPE) and a new methodology were used to extract, separate, or elevate flavonoids from *Euonymus alatus* (see Figure 2). To do this, flavonoids were extracted from euonymus by ultrasonically-assisted extraction (UAE) using PEG-water as a homogeneous media system (Mai et al., 2020).

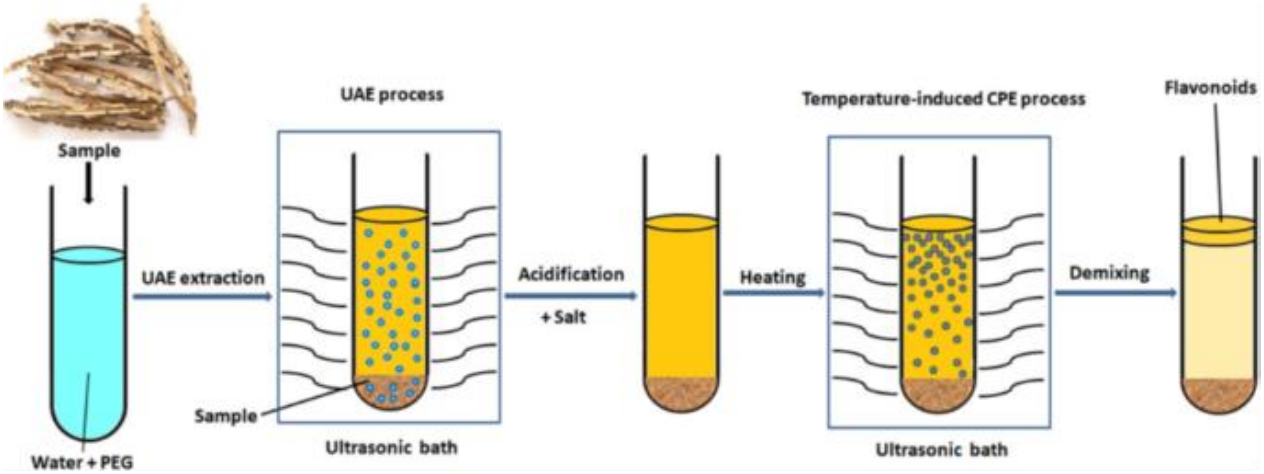

Figure (1) elevate flavonoids from Euonymus alatus.

The CPE method has gradually replaced the conventional liquid-liquid extraction process as the standard. Instead of using harmful organic solvents, CPE uses very small amounts of non-hazardous surfactants.

, it is far healthier and more environmentally sustainable than other kinds of separation processes. CPE is an appealing method that lowers exposure and solvent consumption, which reduces disposal costs and the amount of time required for the pre-concentration of metal ions following the production of sparsely water-soluble complexes (Akl et al., 2021).

To deal with these problems, the micro-cloud point extraction (MCPE) method was put out. The advantages of CPE are maintained, however, MCPE completely does away with the water bath stage and increases the amount of dangerous chemical solvents utilized from a few mL to a few 10 L. They make MCPE an efficient, inexpensive, and ecologically friendly process (Ghasemi & Kaykhaii 2015).

Advantage of CPE

Comparing CPE to conventional liquid-liquid extraction, there are a number of benefits. Water is used in CPE instead of a lot of hazardous and combustible organic solvents, which are used in standard solvent extraction. The capacity of surfactant to reduce analyte losses as a result of its adsorption onto the container can also raise the pre-concentration factors and recovery efficiency of CPE.

Rence Metal ions have been separated and pre-concentrated in a variety of substances employing CPE prior to their detection by analytical techniques.

The new online deployment of CPE into an FIA system has considerable benefits because it does away with all manual work (Ojeda & Rojas, 2009).

The CPE technique (green method) has become the best extraction method due to its advantages over other extraction techniques, including its simplicity, safety, affordability, good recovery, high enrichment factor, minimal need for organic solvents, and capacity to extract a range of chemicals and metals, as well as its ease of use and high efficiency (Kaykhaii & Ghasemi 2016).

Specifically in the extraction and pre-concentration processes, analytical procedures are increasingly using micelles and surfactants. CPE is an environmentally friendly extraction technique when compared to other liquid-liquid extraction techniques. The use of minute amounts of extracted solvents or surfactants in place of toxic organic solvents allowed for the development of CPE-safer procedures and the measurement of a variety of analytes, including organic (Katsoyannos et al., 2012).,inorganic (Shariati & Golshekan, 2014)., and nano-compounds (Majedi & Kelly 2012). Additionally, less solvent is being consumed, which reduces extraction times and costs (Abdullah, 2017). Medicinal substances have been extracted and identified using CPE from a range of matrixes.

Tabrizi proposed employing cloud point extraction and spectrofluorimetry as a quick and efficient method to evaluate thiamine levels in human urine. Thiochrome is produced by oxidizing thiamine with ferricyanide, and it is subsequently extracted into Triton X-114 micelles for spectrofluorimetric analysis. (Tabrizi, 2006). To measure paracetamol using spectrophotometry, cloud point extraction (CPE) was used (PCT). The process is based on the acidic hydrolysis of PCT to PAP, which is then combined with tetrahydroxy-calix [4] arene (CAL4) and an oxidizing agent (KIO_4) to produce a blue-colored product at room temperature. Following formation, the PAP-CAL4 blue dye was captured in Triton X-114's surfactant micelles and detected at 590 nm (Filik, et al., 2006).

According to Khammas (Khammas, 2009), the CPE methodology offers various advantages to those using extraction/preconcentration in analytical chemistry and research. These advantages include robustness, low cost, excellent extraction efficiency, and the ability to use a novel, exciting green chemistry process. Additionally, the ability to conduct online analysis using the majority of instrumental approaches will create a desirable alternative in the field of automated separation techniques. Even though there have been numerous developments in linking CPE with instrumental approaches, it is clear that there will be even more advancements in this field of study during the coming years. To fully comprehend the operation of the parameters governing the behavior of micelle-mediated extraction, additional theoretical foundations about the process of separation and preconcentration are also required.

By creating a charge transfer-ion pair complex with bromothymol blue in an acetate buffer medium, codeine was identified. Triton X-114 was used to extract the compound, and an absorbance measurement at 430 nm was taken **(**Mashhadizadeh & Jafari, 2010).

In an acidic solution, trifluoperazine hydrochloride (TFPH) formed a colored complex with vanadium (V-TFPH), which was then extracted by the surfactant Triton X-114 and spectrophotometrically quantified at a wavelength of 476 nm (Khammas & Rashid, 2015).

In a dilute acidic medium, norfloxacin reacts with Fe(III) ions to form a colored hydrophobic (Fe(III)-NOR) complex. This complex is first extracted as a mediated extractant in micelles of Triton X-114. This is done after NOR and Fe(III) ions are separately measured by spectrophotometry at 432 nm (Khammas, & mubdir, 2015).

Aspirin was extracted and preconcentrated using Triton X-114, a non-ionic surfactant, in the presence of HNO3. At 305 nm, the absorbance of this mixture was measured in comparison to a blank (Kaykhaii, & Ghasemi, 2016).

Amoxicillin and Metoclopramide hydrochloride concentrations in medicines were determined using a method that was provided. The method involves the reaction of diazotized Metoclopramide and Amoxicillin in an alkaline medium to produce an orange-colored and water-soluble product that is readily extractable from micelles in nonionic surfactant (Triton X-114). The two drugs are measured consecutively at 479 nm (Khammas, & Abdulkareem, 2016).

Using spectrophotometry, the three different cephalosporin classes of Cefotaxime (CFX), Ceftriaxone (CFT), and Cefepime (CFM) were identified. The procedures involved creating an azo dye by reacting diazonium salts of CFT, CFX, and CFM with phenol, resorcinol, and α-naphthol in a basic solution. The resulting compounds were then extracted using Triton X-114 and measured at 545, 500, and 515 nm, respectively (Hassan & Al-Rubaiaw, 2017).

Following diazotization and coupling with o-aminobenzoic to produce azo dye, lamotrigine was identified. After that, Tritone X-114 was used to extract the substance, and its absorbance was measured at 424 nm (Dhahir & Mahdi, 2017).

In an acetate buffer media with a pH of 3.5, bromophenol blue and vardenafil HCl formed an ion pair combination. The complex was extracted using Triton X-114, and the surfactant-rich phase from that extraction was diluted with methanol before its absorbance at 420 nm was measured (Hafez, 2017).

Using the cloud point extraction (CPE) methodology, a spectrophotometric approach for clonazepam (CLO) determination in pharmaceutical dosage forms was described. The procedure uses Triton X-114 as a surfactant to recover the product from the oxidative coupling between reduced CLO and phloroglucinol (PHG), which is then measured at 543 nm (Abdullah, 2017).

For the measurement of catecholamine medications (Hassan & Al-hraishawi, 2017) established batch and cloud point spectrophotometric approaches. Cloud-point extraction technique to get the most analytical data and to obviate any potential measurement interference. The batch approach depends on diazotizing 2-aminothiazole and combining it with Dopamine or Adrenaline. The violet-colored dye with Adrenaline has λ_{max} at 565 nm, and the faint violet-colored dye with Dopamine at 555nm. The UV-visible spectrophotometry measures the separation and preconcentration of violet dye in the cloud point extraction procedure. Analytical results obtained from the batch method show that the concentration ranges for dopamine and adrenaline are 1.0-12.5 and 1.0-17.5 µg/ml, respectively, with molar absorptivity values of 1.7 x 104 and 5.51 ×105 l.mol-1.cm-1, Sandell's sensitivity values of 0.0175 and 0.061 µg/cm2, limit of detection of 0.043 and 0.038 µg/ml, and RSDs of 0.65% and 0.91%, respectively. With molar absorptivity values of 4.8×104 and 1.8×105 l.mol-1.cm-1 for dopamine and adrenaline, respectively, the concentration range for the CPE method was 0.25 to 5.0 µg ml-1. Sandell's sensitivity values were 6.1 × 10-3 and 0.01 µg/cm2, and the limits of detection were 0.019 and 0.025 µg/ml, RSD is 0.307 and 0.445, and recovery% were 100.03% and 99.93% respectively. The measurement enrichment factors for Dopamine and Adrenaline are 2.71, and 2.46, as well as the preconcentration factor was 25. Adrenaline and Dopamine measurement in conventional medications and urine using the two approaches was successful alongside catecholamine. Additionally, the cloud-point extraction method was used to invest the colored dye result from the aforementioned reaction in order to collect the most analytical data and to obviate any potential measurement influence. These techniques have been used successfully to estimate catecholamine molecules in medicines and urine.

For the determination of vitamins B1 (thiamine) and B2 (riboflavin) utilizing cloud point extraction-HPLC technology, trace levels based on cloud point extraction were disclosed. The method is based on the complex formation between each vitamin and Ag (I) ions that were removed to nonionic surfactant phase cetyl pyridinium chloride (CPC) in the presence of KNO_3, Tergitol, and Genapol (Ulusoy & Akçay, 2018).

After being diazotized and combined with 4-tert-butylphenol and 2-NPT in a basic medium, cefdinir was identified. Triton X-114 was used to remove the azo dyes, and the measurements for each reagent were made at 490 and 535 nm, respectively (Hassan & Mizher, 2018).

A cloud point extraction approach and a spectrophotometric method are both used to determine the presence of sulphadimidine sodium in Trtion X-114. The procedure involved diazotizing the medication Sulphdimidine Sodium, combining it with α-naphthol in the basic medium to produce an orange-colored product, and then extracting it using a surfactant to measure it at 473 nm (Dhahir et al., 2019).

Streptomycin Sulfate was measured using the cloud point extraction method with Trtion X-114. The procedure involved creating an Ag+1 chelating complex at pH 12 and measuring it at 404 nm (Dhahir & Mohammed, 2019).

Three spectrophotometric techniques have been proposed for the determination of salbutamol and methyldopa (Abood et al., 2019). The first method involved the oxidation of Methyldopa by ferric nitrate and then coupling with thiosemicarbazide, yielding a

dark green colored product with an absorbance maximum at 460 nm. In the presence of potassium iodide and sodium hydroxide, salbutamol undergoes a coupling reaction with 4-nitrophenyl hydrazine to produce a violet-colored substance with a maximum 530 nm absorbance. Beer's law is seen between 1 and 50 µg/ml with Sandall's sensitivity of (0.039, 0.073), and molar absorptivity of 0.536×10^4 and 0.327×10^4 $l.mol^{-1}.cm^{-1}$ for Methyldopa and Salbutamol, respectively. The second technique is CPE for estimating the traces of the above medicines that result from the same reaction. This technique allows for accurate drug assessment under the best experimental circumstances, with maximal absorption at 470 and 535 nm, respectively. For Methyldopa and Salbutamol, the concentration range was between 0.25 and 6 µg/ml, the molar absorptivity values were 0.510×10^5 and 0.483×10^5 respectively, and the enrichment factor was between 9.51 and 14.72. The third method is based on using flow injection analysis (FIA) depending on measuring the absorption signal for products produced by the above reaction to determine the phenolic drug content. The stability of the product's color was also studied. The active material for Salbutamol and Methyldopa was detected at maximum wavelengths of 460 and 530nm for each respectively. A total flow injection of 1.5 ml/min was pumped. The provided approaches were successfully used in this case to determine the presence of Salbutamol and Methyldopa in pharmaceutical formulations.

Recently**,** three spectrophotometric methods for the determination of the Cefixime drug have been created (Abood et al., 2019). In method (I), NH_2 in Cefixime was diazotized and coupled with bisphenol A in a basic medium, producing an orange-colored product that had a maximum absorbance at 490 nm. Beer's Law followed the concentration range of 1 to 50 µg/ ml with a limit of detection of 0.157 µg/ml, and the molar absorptivity was 0.866×10^4 $l.mol^{-1}.cm^{-1}$. In method (II), CPE was used to pre-concentrate the Cefixime azo dye for trace amounts. The azo dye was measured at λ_{max} 500 nm. A calibration plot had a molar absorptivity of 0.961×10^5 $l.mol^{-1}.cm^{-1}$, and the concentration ranged from 0.25 to 6 µg/ml. Method (III) was based on the above reaction using FIA and the absorbance of the diazotized orange-colored product was measured at 490 nm.

A rapid and effective cloud point spectrophotometric method was used to quantify the concentrations of salbutamol and methyldopa in both pure and pharmaceutical formulations. The process relied on the ion-pair complex formed with eosin Y dye. The extraction of complexes was driven to Triton X-114 surfactant and measured at 558 and 564 nm for the above drugs respectively (Shihab & Al-Sabha2020).

A rapid and precise approach for enriching and identifying Oxymetazoline (OMZ) in its pharmaceutical matrix was proposed by Wahdan et-al, (Wahdan et al., 2021) using the CPE methodology. The diazotization of OMZ and coupling with metoclopramide in a basic medium is the basis of the procedure. Triton X-114 surfactant was used to extract the azo dye product, which was then measured at 510 nm.

Al-Ward et-al developed a sensitive and exact reaction for the batch and cloud point extraction (CPE) methods of determining vancomycin hydrochloride. The first approach is based on the reaction of diazotized dapsone with vancomycin HCl (VAN) in a basic media, which forms azo dye. By using Triton X-114, a nonionic surfactant, and the cloud point extraction approach (second method), the sensitivity of this reaction was increased. After being removed into the surfactant-rich phase, the azo dye was diluted in ethanol and spectrophotometrically measured at λ_{max} 446 nm. Both batch and CPE procedures (with and without extraction) were used to study the reaction, and a straightforward comparison of the two developed methods was performed. A thorough examination has been done of the factors influencing the extraction process and the approaches' sensitivity. For both batch and CPE methods, the linearity of the calibration curves fell between 3 and 50 and 0.5 and 25 µg.mL-1, respectively, with detection limits of 0.806 and 0.214 µg.mL-1 for VAN. For the two approaches, the relative standard deviation (R.S.D.%) percentage was superior to 2.54% and 2.83%, respectively. Assaying VAN in commercial injection has proven to be an effective use of the suggested methodologies (Al-ward et al., 2023).

The pure form of mesalazine (MEZ) and its medicinal formulation were identified, and a rapid and accurate cloud point spectrophotometric method was proposed. The technique relied on the interaction of mesalazine with brilliant green dye (B.G.), which is extracted with triton x-114 and measured at 361 nm, to generate a yellow ion-pair complex. The experimental conditions for phase separation were optimized. With a precision (RSD) of 1.26, an average recovery % of 100.82, a molar absorptivity of 3.914×10^4 L.mol-1.cm-1, and a concentration range of 0.3 to 3.5 g mL^{-1}, Beer's law was observed. the method was successful in identifying MEZ in its pharmaceutical forms (Jabar et al., 2023). However; applications of the CPE technique for the determination of drugs are described in Table (1).

Table (1) Applications of the CPE technique for the determination of drugs is described

Reference number	Analyte	λmax nm	Linear range	Surfactant	Molar absorptivity $L.mol^{-1}.cm^{-1}$	RSD %	Application
Tabrizi, 2006	Thiamine	438	2.5-1000 $ng.mL^{-1}$	Triton x-114		2.42	Human urine
Filik et al., 2006	p-aminophenol (PAP)	590	1.5-12 $mg.mL^{-1}$	Triton x-114		2.15	Tablets and blood samples
Mashhadizadeh & Jafari, 2010	Codeine	430	100-700 $ng.mL^{-1}$	Triton x-114		2.15	Tablets and blood samples
Al-Khammas & Rashid, 2015	Trifluoperazine hydrochloride (TFPH)	476	0.5-10 $\mu g\ mL^{-1}$	Triton x-114		0.48-3.40	Pharmaceuticals and the spiked serum samples
Al-Khammas & Mubdir, 2015	Norfloxacin (NOR)	432	2.5-125 $\mu g.mL^{-1}$	Triton x-114		0.04-0.66	Biological and pharmaceutical samples
Kaykhaii & Ghasemi, 2016	Aspirin	305	0.05–2 $mg.L^{-1}$	Triton x-114			Pharmaceuticals
Khammas & Abdulkareem 2016	AMX and MCP	479	0.3-3.0 $\mu g\ mL^{-1}$	Triton x-114		2.35-10.8 and 0.20-3.43	Pharmaceuticals
Hassan & Al-Rubaiawi, 2017	ceftriaxone (CFT), cefotaxime (CFX), and cefepime (CFM)	545, 500, and 515	1 of 2.5 to 62.5 $mg.\ L^{-1}$	Triton x-114			Pure and pharmaceutical formulations
Dhahir & Mahdi, 2017	Lamotrigine drug	424	0.5–18 $\mu g\ mL^{-1}$	Triton x-114	2.88×10^{3}	1.62–3.04	
Hafez and et al., 2017	vardenafil HCl (VARD)	420	0.1-2.0 $\mu g\ mL^{-1}$	Triton x-114		1.80	Tablets
Abdullah, 2017	Clonazepam (CLO)	543	0.3-25 $\mu g.mL^{-1}$	Triton x-114		2.5	Tablets
Jasim et al., 2017	catecholamine	565	1.0 – 17.5 $\mu g.mL^{-1}$	Triton x-114	4.8×10^{4}	0.307	Urine and drugs
Ulusoy & Akçay, 2018	vitamins B1 (thiamin) and B2 (riboflavin)		4 - 400 , 1-500 $ng.mL^{-1}$	Triton x-114		2.90 and 2.20	Baby foods, milk, and cereals.
Hassan & Mizher, 2018	cefdinir (CFD), cephalosporin species	490, 535	3-100 $\mu g.mL^{-1}$	Triton x-114	0.6129×10^{4}, 0.3361×10^{4}		Commercial formulation
Dhahir et al., 2019	sulphadimidine sodium (SDMS)	473	1-12 $\mu g.mL^{-1}$	Triton x-114		1.3-5.28	pharmaceutical dose
Saadiyah et al., 2019	Streptomycin Sulfate	404	2.5-30 $\mu g.\ mL^{-1}$	Triton x-114		good	Some Pharmaceuticals
Abood et al., 2019	Methyldopa and Salbutamol	460, 530	1-50 $\mu g.mL^{-1}$	Triton x-114	0.536×10^{4}, 0.327×10^{4}		Pharmaceutical preparation.
Abood et al., 2019	Cefixime	490	1-50 $\mu g.mL^{-1}$	Triton x-114	0.866×10^{4}		Bulk drug and pharmaceutical formulations

Shihab et al., 2022	Salbutamol Sulphate and Methyldopa	558, 564	0.1-20, 0.3-10 $\mu g.mL^{-1}$	Triton x-114	4.0×10^4, 5.7×10^4	<1.6 >0.3	Pharmaceutical preparations.
Whdan et al., 2021	Oxymetazoline	510	0.05-17.0 $\mu g.mL^{-1}$	Triton x-114	2.7×10^4	4.48	Commercial nasals
Al-ward et al., 2022	Vancomycin Hydrochloride	446	0.5-25 $\mu g.mL^{-1}$	Triton x-114	7.2071×10^4	2.83	Commercial injections
Jabar et al., 2023	Mesalazine	361	0.3 – 3.5 $\mu g.mL^{-1}$	Triton x-114	3.914×10^4	1.26	Pharmaceutical preparations

The table above clarifies the uses of different types of spectrophotometric methods and chromatography for the determination of drugs by cloud point extraction (CPE) using Triton x-114 as a surfactant and they give good results. That means CPE is a suitable technique to increase detection limits in separation and pre-concentration.

Conclusions

This review describes the cloud point extraction (CPE) technique as an environmentally friendly analytical technique, providing a simple, rapid, inexpensive, and method for preconcentrating and separating trace amounts of substances in aqueous solutions suitable for extraction. CPE is a cost-effective analytical tool. Also; the potential benefits of established technique include time savings, reduction in the amount of reagents used, and minimization of analyst effort.

Acknowledgments

The Department of New and Renewable Energies, College of Science, University of Mosul, is greatly appreciated by the authors for providing the facilities necessary for this effort to be successful.

Conflict of interest: The authors certify that there are no conflicts of interest.

References

AAAbdullah, H. H. (2017). Cloud-point extraction and spectrophotometric determination of clonazepam in pharmaceutical dosage forms. Bulletin of the Chemical Society of Ethiopia, 31(3), 373-382. http://dx.doi.org/10.4314/bcse.v31i3.2

Abood, N. K., Hassan, M. J. M., & Al-Da'amy, M. A. (2019). Spectrophotometric determination methyldopa and salbutamol by oxidative coupling, cloud point and flow injection in pharmaceutical formulations. *International Journal of Drug Delivery Technology*, *9*(2), 182-192. https://doi.org/10.25258/ijddt.9.2.11

Akl, M. A., AL-Rabasi, A., & Molouk, A. F. (2021). Cloud point extraction and FAAS determination of copper (II) at trace level in environmental samples using N-benzamido-N'-benzoylthiocarbamide and CTAB. Egyptian Journal of Chemistry, 64(1), 313-322. https://doi.org/10.21608/ejchem.2020.36387.2752

Al-ward, H. S. A. W., Al-Abachi, M. Q., & Ahmed, M. R. (2023). Spectrophotometric Analysis of Vancomycin Hydrochloride in Pure and Pharmaceutical Injections via Batch and Cloud Point Extraction Techniques. *Baghdad Science Journal*, *20*(2), 0245-0245.

Bazregar, M., Rajabi, M., Yamini, Y., Arghavani-Beydokhti, S., & Asghari, A. (2018). Centrifugeless dispersive liquid-liquid microextraction based on salting-out phenomenon followed by high performance liquid chromatography for determination of Sudan dyes in different species. *Food chemistry*, *244*, 1–6. https://doi.org/10.1016/j.foodchem.2017.10.006

Bezerra, M. D. A., Arruda, M. A. Z., & Ferreira, S. L. C. (2005). Cloud point extraction as a procedure of separation and pre-concentration for metal determination using spectroanalytical techniques: a review. Applied Spectroscopy Reviews, *40*(4), 269-299. https://doi.org/10.1080/05704920500230880

BİŞGİN, A. T. (2018). Cloud point extraction and spectrophotometric determination of Allura red (E129) in foodstuffs. *Journal of the Institute of Science and Technology*, *8*(4), 239-246. https://doi.org/10.21597/jist.397479

Bişgin, A. T., Uçan, M., & Narin, İ. (2015). Comparison of column solid-phase extraction procedures for spectrophotometric determination of E129 (Allura red) in foodstuff, pharmaceutical, and energy drink samples. *Journal of AOAC International*, *98*(4), 946-952. https://doi.org/10.5740/jaoacint.14-222

Burguera, J. L., & Burguera, M. (2004). Analytical applications of organized assemblies for on-line spectrometric determinations: present and future. *Talanta*, *64*(5), 1099-1108. https://doi.org/10.1016/j.talanta.2004.02.046

Candir, S., Narin, I., & Soylak, M. (2008). Ligandless cloud point extraction of Cr (III), Pb (II), Cu (II), Ni (II), Bi (III), and Cd (II) ions in environmental samples with Tween 80 and flame atomic absorption spectrometric determination. *Talanta*, *77*(1), 289-293. https://doi.org/10.1016/j.talanta.2008.06.024

Dhahir, S. A., & Mohammed, N. J. (2019). Micro Spectrophotometric Determination Streptomycin Sulfate by Cloud point Extraction in pure form and pharmaceutical preparation. *Journal of Pharmaceutical Sciences and Research*, *11*(4), 1621-1628.

Dhahir, S. A., Kadhim, E. A., & AL-Gani, R. H. A. (2019). Micro Spectrophotometric Determination and Cloud Point Extraction of Sulphadimidine Sodium in Pure form and Pharmaceutical Drug. *Baghdad Science Journal*, *16*(2), 332-344. https://doi.org/10.21123/bsj.2019.16.2.0332

Ferrera, Z. S., Sanz, C. P., Santana, C. M., & Rodrıguez, J. J. S. (2004). The use of micellar systems in the extraction and pre-concentration of organic pollutants in environmental samples. *TrAC Trends in Analytical Chemistry*, *23*(7), 469-479. https://doi.org/10.1016/S0165-9936(04)00732-0

Filik, H., Şener, İ., Cekiç, S. D., Kiliç, E., & Apak, R. (2006). Spectrophotometric determination of paracetamol in urine with tetrahydroxycalix [4] arene as a coupling reagent and preconcentration with Triton X-114 using cloud point extraction. *Chemical and Pharmaceutical Bulletin*, *54*(6), 891-896. https://doi.org/10.1248/cpb.54.891

Ghasemi, E., & Kaykhaii, M. (2015). Developing a new micro cloud point extraction method for simultaneous preconcentration and spectrophotometric determination of uranium and vanadium in brine. Analytical Sciences, 31(5), 407-411. https://doi.org/10.2116/analsci.31.407

Ghasemi, E., & Kaykhaii, M. (2016). Application of a novel micro-cloud point extraction for preconcentration and spectrophotometric determination of azo dyes. *Journal of the Brazilian Chemical Society*, *27*, 1521-1526. https://doi.org/10.5935/0103-5053.20160030

Hafez, E. M. (2017). Ragaa El Shiekh, Alaa S Amin, Ayman A Gouda,'Cloud point extraction of vardenafil HCl from pharmaceutical formulations prior to spectrophotometric determination. *International Journal of Research in Pharmacy and Pharmaceutical Sciences*, *2*(5), 3-10.

Hassan, M. J. M., & Al-hraishawi, T. J. (2017). Batch and Cloud Point Extraction Spectrophotometric Methods for the Determination of Two Types Catecholamine Drugs. *International Journal of Chem Tech Research*, *10*, 756-768.

Hassan, M. J. M., & Mizher, O. Q. (2018). New spectrophotometric estimation and cloud point extraction of cefdinir. *Baghdad Science Journal*, *15*(4), 0425-0425. https://doi.org/10.21123/bsj.2018.15.4.0425

Heidarizadi, E., & Tabaraki, R. (2016). Simultaneous spectrophotometric determination of synthetic dyes in food samples after cloud point extraction using multiple response optimizations. *Talanta*, *148*, 237–246. https://doi.org/10.1016/j.talanta.2015.10.075

Hinze, W. L., & Pramauro, E. (1993). A critical review of surfactant-mediated phase separations (cloud-point extractions): theory and applications. *Critical Reviews in Analytical Chemistry*, *24*(2), 133-177. https://doi.org/10.1080/10408349308048821

Jabar, f. M., ismael, s. O. and Al-sabha, Th. N.,, (2023). Extractive cloud point spectrophotometric determination of mesalazine using brilliant green dye. *Journal of Duhok University*, *26*(1), 61-71. https://doi.org/10.26682/sjuod.2023.26.1.7.

kais Abood, N., Hassan, M. J. M., & Muneer, A. (2019). Determination of Cefixime Using Batch, Cloud Point Extraction and Flow Injection as New Spectrophotometric Methods. *Al-Mustansiriyah Journal of Science*, 30(3), 28-37. https://doi.org/10.23851/mjs.v30i3.648

Karatepe, A., AKALIN, Ç., & Soylak, M. (2017). Spectrophotometric determination of carmoisine after cloud point extraction using Triton X-114. *Turkish Journal of Chemistry*, *41*(2), 256-262. http://doi.org/10.3906/kim-1606-45

Katsoyannos, E., Gortzi, O., Chatzilazarou, A., Athanasiadis, V., Tsaknis, J., & Lalas, S. (2012). Evaluation of the suitability of low hazard surfactants for the separation of phenols and carotenoids from red-flesh orange juice and olive mill wastewater using cloud point extraction. Journal of separation science, 35(19), 2665-2670. https://doi.org/10.1002/jssc.201200356.

Kaykhaii, M., & Ghasemi, E. (2016). Micro-cloud point extraction for preconcentration of Aspirin in commercial tablets prior to spectrophotometric determination. Journal of Analytical Chemistry, 71, 844-848.

Khammas, Z. A. (2009). Recent Trends for Separation and Preconcentration in Metal Ions and Organic Compounds Analysis after Clould-Point Methodology: Developments and Analytical Applications--A review. *Eurasian Journal of Analytical Chemistry*, *4*(1). https://www.researchgate.net/profile/Zuhair-

Khammas, Z. A., & Abdulkareem, H. M. (2016). A new visible spectrophotometric approach for mutual determination of amoxicillin and metoclopramide hydrochloride in pharmaceuticals after cloud point extraction. *Science*, *4*(5), 66-76. https://doi.org/ 10.11648/j.sjac.20160405.12

Khammas, z. A., & mubdir, n. S. (2015). Cloud point extraction spectrophotometric method for mutual determination of norfloxacin and iron (III) in human

serum and drug formulations. *Chemical Science*, *4*(2), 483-497. https://doi.org/10.7598/cst2015.990

Khammas, Z. A., Jawad, S. K., & Ali, I. R. (2013). A new spectrophotometric determination of chromium (VI) as Cr_2O_7-after cloud-point extraction using a laboratory-made organic reagent. *Global Journal of Science Frontier Research Chemistry*, *13*(8), 9-19.

Khammas, Z. A., Jawad, S. K., & Ali, I. R. (2014). A new approach for extraction and determination of manganese in environmental samples using cloud-point extraction coupled with spectrophotometry. *Chemical Science Transactions*, *3*(1), 255-267. https://doi.org/10.7598/cst2014.505

Lemos, V. A., da França, R. S., & Moreira, B. O. (2007). Cloud point extraction for Co and Ni determination in water samples by flame atomic absorption spectrometry. *Separation and Purification Technology*, *54*(3), 349-354. https://doi.org/10.1016/j.seppur.2006.10.004

Li, X., Song, N., Feng, W., & Jia, Q. (2017). Cloud point extraction of rare earths and zinc using 1, 10-phenanthroline and Triton X-114 coupled with microwave plasma torch-atomic emission spectrometry. *Analytical Methods*, *9*(36), 5333-5338.
https://doi.org/10.1039/C7AY00421D

Madej, K. (2009). Microwave-assisted and cloud-point extraction in determination of drugs and other bioactive compounds. *TrAC Trends in Analytical Chemistry*, *28*(4), 436-446. https://doi.org/10.4155/bio-2018-0160

Mai, X., Liu, Y., Tang, X., Wang, L., Lin, Y., Zeng, H., & Li, P. (2020). Sequential extraction and enrichment of flavonoids from Euonymus alatus by ultrasonic-assisted polyethylene glycol-based extraction coupled to temperature-induced cloud point extraction. Ultrasonics Sonochemistry, 66, 105073.
https://doi.org/10.1016/j.ultsonch.2020.105073

Majedi, S. M., Lee, H. K., & Kelly, B. C. (2012). Chemometric analytical approach for the cloud point extraction and inductively coupled plasma mass spectrometric determination of zinc oxide nanoparticles in water samples. Analytical chemistry, 84(15), 6546-6552. https://doi.org/10.1021/ac300833t.

Mashhadizadeh, M. H., & Jafari, L. (2010). Cloud point extraction and spectrophotometric determination of codeine in pharmaceutical and biological samples. *Journal of the Iranian Chemical Society*, *7*, 678-684.

McLntire, G. L., & Dorsey, J. G. (1990). Micelles in analytical chemistry. *Critical Reviews in Analytical Chemistry*, *21*(4), 257-278.
https://doi.org/10.1080/10408349008051631

Mohammed Jasim M. Hassan and Marwah Sabbar Falih Al-Rubaiaw, (2017), "Cloud Point Extraction Spectrophotometric Method for Determination of Three Types of Cephalosporin via Diazotization Reactions with Different Reagents", *Br. J. Anal. Chem.*, *4*(17), 24-36.

Nambiar, A. P., Sanyal, M., & Shrivastav, P. S. (2017). Performance evaluation and thermodynamic studies for the simultaneous cloud point extraction of erythrosine and tartrazine using mixed micelles in food samples. *Food Analytical Methods*, *10*, 3471-3480. https://doi.org/10.1007/s12161-017-0923-1.

Ojeda, C. B., & Rojas, F. S. (2009). Separation and preconcentration by a cloud point extraction procedure for determination of metals: an overview. *Analytical and Bioanalytical Chemistry*, *394*, 759-782.

Paleologos, E. K., Giokas, D. L., & Karayannis, M. I. (2005). Micelle-mediated separation and cloud-point extraction. *TrAC Trends in Analytical Chemistry*, *24*(5), 426-436.
https://doi.org/10.1016/j.trac.2005.01.013

Pincemaille, J., Banc, A., Chauveau, E., Fromental, J. M., Ramos, L., Morel, M. H., & Menut, P. (2018). Methods for screening cloud point temperatures. *Food Biophysics*, 13, 422-431.
https://doi.org/10.1007/s11483-018-9548-1

Pourreza, N., & Zareian, M. (2009). Determination of Orange II in food samples after cloud point extraction using mixed micelles. *Journal of Hazardous Materials*, *165*(1-3), 1124-1127.
https://doi.org/10.1016/j.jhazmat.2008.10.132

Quina, F. H., & Hinze, W. L. (1999). Surfactant-mediated cloud point extractions: an environmentally benign alternative separation approach. *Industrial & Engineering Chemistry Research*, *38*(11), 4150-4168. https://doi.org/10.1021/ie980389n

Rubio, S., & Pérez-Bendito, D. (2003). Supramolecular assemblies for extracting organic compounds. *TrAC Trends in Analytical Chemistry*, *22*(7), 470-485.
https://doi.org/10.1016/S0165-9936(03)00706-4

Saadiyah Ahmed Dhahir and, Shatha Mahdi ,(2017), Spectrophotometric Determination and Cloud point Extraction of Lamotrigine Drug in Pure Form and Pharmaceutical preparation", Review Article, World *Journal of Pharmacy and Pharmaceutical Science*, *6*(5), 78-104.

Sanz-Medel, A., Gonzalez, E. B., & Fernandez-Sanchez, M. L. (1999). Organised surfactant assemblies in analytical atomic spectrometry. *Spectrochimica Acta Part B: Atomic Spectroscopy*, *54*(2), 251-287.

Shariati, S., & Golshekan, M. (2014). Optimization of cloud point extraction of copper with neocuproine from aqueous solutions using Taguchi fractional factorial

design. Journal of Analytical Chemistry, 69, 248-254.

Shi, Z., He, J., & Chang, W. (2004). Micelle-mediated extraction of tanshinones from Salvia miltiorrhiza bunge with analysis by high-performance liquid chromatography. *Talanta*, *64*(2), 401-407. https://doi.org/10.1016/j.talanta.2004.03.001

Shihab, A. I., & Al-Sabha, N. T. (2020). Application of cloud point method for spectrophotometric determination of Salbutamol sulphate and Methyldopa. *Pak. J. Anal. Environ. Chem*, *21*(1), 10-18. https://doi.org/10.21743/pjaec/2020.06.02

Silva, M. F., Cerutti, E. S., & Martinez, L. D. (2006). Coupling cloud point extraction to instrumental detection systems for metal analysis. *Microchimica Acta*, 155, 349-364.

Stalikas, C. D. (2002). Micelle-mediated extraction as a tool for separation and preconcentration in metal analysis. *TrAC Trends in Analytical Chemistry*, *21*(5), 343-355. https://doi.org/10.1016/S0165-9936(02)00502-2

Surme, Y., Narin, I., Soylak, M., Yuruk, H., & Dogan, M. (2007). Cloud point extraction procedure for flame atomic absorption spectrometric determination of lead (II) in sediment and water samples. *Microchimica Acta*, *157*, 193-199.

Tabrizi, A. B. (2006). A cloud point extraction-spectrofluorimetric method for determination of thiamine in urine. *Bulletin-Korean Chemical Society*, *27*(10), 1604.

Ulusoy, S., & Akçay, M. (2018). Simultaneous determination of vitamins B1 and B2 in food samples by modified cloud point extraction method and HPLC-DAD. *Food analytical methods*, *11*(1), 260-269. https://doi.org/10.1007/s12161-017-0996-x.

Wahdan, K., Alnedawi, Z., Hassan, A. M., Hadi, H., & Shabana, A. (2021). Cloud Point Pre-concentration with Spectrophotometric De-tection for Determination of Oxymetazoline in Pharmaceuti-cal Formulations.

Watanabe, H., & Tanaka, H. (1978). A non-ionic surfactant as a new solvent for liquid—liquid extraction of zinc (II) with 1-(2-pyridylazo)-2-naphthol. *Talanta*, *25*(10), 585-589. https://doi.org/10.1016/0039-9140(78)80151-9.

Yu, Y., & Fan, Z. (2016). Determination of rhodamine B in beverages using a polystyrene-coated magnetite nanocomposite for magnetic solid phase extraction. *Analytical Letters*, *49*(12), 1835-1846. https://doi.org/10.1080/00032719.2015.1124112.

Zuhair, A. A. , Khammas, Rana Abbas Rashid, (2015)." Mutual Determination of Trifluoperazine Hydrochloride and Vanadium (V) Ions in Real Matrices by Visible Spectrophotometry after Cloud Point Extraction. Science *Journal of Analytical Chemistry*, *3*(5), 61-70. https://doi.org/10.11648/j.sjac.20150305.14.

Scientific Journal for the Faculty of Science-Sirte University Vol. 4, No. 1 (2024) 109-116

Scientific Journal for the Faculty of Science-Sirte University

Journal home page: http://journal.su.edu.ly/index.php/JSFSU/index

DOI: 10.37375/issn.2789-858X

Effect of Exogenous Application of Nicotinic Acid on Genotypes of durum wheat (*Triticum aestivum* L.) under salt stress.

Sami M. salih* and Ahmed A. Abdulrraziq

Biology Department, Education Faculty, Omar Al-Mukhtar University, Al-Bayda, Libya.

DOI: https://doi.org/10.37375/sjfssu.v4i1.2680

ARTICLE INFO:

Received: 18 March 2024

Accepted: 12 April 2024

Published: 17 April 2024

Keywords: *Triticum aestivum* L, Salinity tolerance, Seawater Irrigation, Wheat genotypes, Nicotinic acid.

A B S T R A C T

Two experiments were conducted (laboratory and pot). The laboratory experiment represented the tolerance of ten durum wheat genotypes (ACSAD) to levels (20, 30, 40%) of seawater. The pot experiment evaluated the efficiency of foliar spraying of nicotinic acid for three election genotypes of durum wheat (ACSAD 1671, 1711, and 1765), Under seawater levels (20, 30%). The results of the laboratory experiment showed that revealed significant ($p < 0.05$) differences in the genotypes' response to salinity, the genotypes' (1671, 1711and 1765), were superior in recording the best average germination percentage and seedling length compared to the other genotypes. The results of the pot experiment showed, after 80 days of sowing, under seawater irrigation conditions, decreases in (Plant height, Leaf area /plant, Spike length, number of spikes/plant, number of grains/spike, chlorophyll a, chlorophyll b, carotenoids, and total pigments) of the three durum wheat genotypes (ACSAD), compared to control. In contrast, foliar application of Nicotinic acid led to a significant decrease in a negative effect resulting from salinity for all vegetative growth parameters and the contents of photosynthetic pigments, especially with low concentrations of seawater. The (1671) genotype performed better than the (1711and 1765) genotypes in concern to high averages for all studied traits, under salinity and spraying with Nicotinic acid.

1 Introduction

Today agriculture faces challenges of high saltwater intrusion levels along coastal areas, which ruins the efficiency and quality of the cultivation of wheat crops, due to Sea level rise (Yanagi, 2024). This increases the salt concentration in the soil, causing Salt stress for wheat crops (Salih *et al*., 2023). Through many negative reactions, represented by an osmotic stress, ionic imbalance, oxidative stress, membrane disorganization, reduction of cell division, and finally increased accumulation of reactive oxygen species (Ain *et al*., 2024). To address the problem of changing climate conditions on crop growth, studies have dealt with the use of genotypes that can withstand abiotic stress (Cabusora, 2024). For example, the results of a study conducted on 40 genotypes of bread wheat at the germination stage under salinity conditions indicated, that only three genotypes were salt-tolerant (Ahmed *et al*., 2024). Wheat genotypes adapt to climatic conditions changes, especially salinity, through reduced formation of oxygen species (ROS) by antioxidants (AOS), consisting of a complex of enzymes, which works to protect cells from salinity damage (Kononenko *et al*., 2023). Furthermore, the role of osmolytes in quenching free radicals, regulating osmotic and ion homeostasis, and regulating phytohormones (Choudhary *et al*., 2023). Nicotinic acid (NA) or vitamin B3 known as (niacin) of the water-soluble vitamins (Çatak and Yaman, 2019). Contributes to the biosynthesis of the enzymatic conjugates (NAD, NADP), Which has a role in giving cells plasticity to the response of plants to environmental conditions (Noctor *et*

**Corresponding author*: E-mail: sami.mohammed@omu.edu.ly

al., 2011; Gasperi *et al*., 2019), addition, as DNA repair or post-translational modification of proteins (Gakière *et al*., 2018). The height of fresh weight and bulb dry weight of onion during salt stress was observed to be increased by foliar application of nicotinic acid and tryptophan (Hussein *et a*l., 2014). Also, (Farooq *et al*., 2022), reported the potential of barley to tolerate water stress through foliar treatments with nicotinic acid. Consequently, this study aims to test the effect of irrigation with different seawater levels on the tolerance of ten durum wheat genotypes in a dish experiment and follow-up of salt-resistant genotypes in pot experiments through foliar application Nicotinic acid under seawater irrigation conditions.

2 Materials and Methods

2.1 Plant material and experimental setup:

The laboratory study was conducted in the Department of Biology/Faculty of Education at Omar AlMukhtar University. The experiment was conducted on ten genotypes of durum wheat, which included ACSAD (1595, 1651, 1671, 1695, 1697, 1711, 1729, 1735, 1747, and 1765). They were obtained from the Arab Center for the Studies of Arid Zones and Dry Lands ACSAD. They were soaked in 1% Sodium hypochlorite solution for 3 minutes for sterilization, and washed with distilled water.

2.2 Preparation of seawater dilutions:

Five seawater dilution treatments were used in the experimen:

1- tap water (control).

2- 20% seawater + 80% tap water (20% seawater).

3- 30% seawater + 70% tap water (30% seawater).

4- 40% seawater + 60% tap water (40% seawater).

2.3 Seed germination:

The petri dishes were filled with 20 seeds and were lined with two Whatman No.1 filter papers and incubated at room temperature. Each treatment was repeated three times. The dishes were subjected to daily observation for 10 days and follow-up on germination in terms of addition of saline solution to the treated dishes. Distilled water was added to control as needed for each dish. The filter papers were changed once every two days to prevent salt accumulation due to evaporation, germination was calculated by recording the number of germinated seeds in all treatments starting from the second day, which the first germination occurred, germination criterion is the appearance of radical outside seed cover. At the end of the experiment, the final results of the following qualities:

- Germination percentage (PG %) = the number of germinated seeds / total number of seeds cultured × 100 (Salih *et al*., 2023).
- Seedling lengths (cm): The seedling lengths were taken using a graduated ruler, and the averages were calculated by taking 5 seedlings from each plate.

2.4 Pots Experiment:

Three salt-tolerant genotypes of durum wheat were used, ACSAD (1671, 1711, and 1765), according to the results of the laboratory experiment. The pot experiment was carried out inside under greenhouse conditions, the soil samples were sterilized at (90ºC for 48 h). Five kg of sterilized clay-sandy soil were put into pots, a ratio of 2:1 (weight to weight). Ten seeds of durum wheat were sown in each pot. Before the transactions take place, the quantity of seedlings is decreased to five per pot. After two weeks of planting, the saltwater irrigation began. and grown under greenhouse conditions of 54 pots, for 80 days of sowing. and with no chemical fertilizers. The experiment was set up in a completely random arrangement with six treatments and three repetitions as follows:

- T_1 without Salinity or spraying (control).
- T_2 20% Seawater (Sw).
- T_3 30% Seawater (Sw).
- T_4 Spraying of Nicotinic acid (NA) 75ppm without Salinity.
- T_5 Spraying NA75ppm+ 20% Sw.T_6 Spraying NA75ppm+ 30% Sw.

The application of nicotinic acid was carried out through foliar spraying thrice, the first, second and third sprays were done 30, 45 and 60 days after sowing, respectively. At the end of the experiment took final results of the following qualities:

Plant height and spike length (cm) were measured using a graduated ruler in three replicates, and the averages were calculated.

The number of spikes per plant and the number of grains per spike.

Leaf area / Plant (cm^2) according to (Mokhtarpour *et al*., 2010).

Photosynthetic pigments (chlorophyll a, b, and carotenoids) were determined spectrophotometrically according to (Metzner *et al*.,1965).

Statistical Analysis:

The study experience was created using the complete random design (CRD). The statistical analysis was done using the Minitab 17 program and ANOVA variance analysis tables. The averages were compared using Tukey's test at P <0.05.

3 Results

3.1 Laboratory experiment:

Effect of different concentrations of seawater on germination percentage and seedling length in the laboratory :

The results presented in Tables (1 and 2), represented the effect of seawater irrigation levels (20, 30 and 40%) of ten ACSAD durum wheat genotypes, on the germination percentage and seedling length after 10 days of germination. Significant differences have been recorded in the germination percentage of tested genotypes. The lowest averages were for ACSAD genotypes (1697, 1729 and 1747), from 100% for the control to (53.25, 55.00 and 56.50 %), respectively. According to the findings, the germination percentage of all genotypes was not affected at a concentration of seawater of 20% but decreased at a concentration of 30%. while a concentration of 40% seawater suppressed all seed growth for all wheat genotypes except ACSAD (1671, 1711 and 1765) by (20, 20 and 36%) respectively. Moreover, the results showed a decrease in the average seedling length of ten wheat genotypes. The highest average seedling length was recorded (8.00, 8.52 and 8.30cm), for ACSAD (1671, 1711 and 1765) respectively. In contrast, there are no significant differences in seedling length between the rest of the wheat genotypes. In general, all tested concentrations of seawater significantly reduced seedling lengths.

Table (1) Effect of different concentrations of seawater on seed germination (%) of wheat genotypes.

Genotypes	Seawater Concentration %				Genotypes average
	Control	20	30	40	
A1595	100	100	36	0	59.00 bc
A1651	100	100	50	0	62.50 bc
A1671	100	100	100	20	80.00 a
A1695	100	100	40	0	60.00 bc
A1697	100	100	13	0	53.25 c
A1711	100	100	80	20	75.00 ab
A1729	100	100	20	0	55.00 c
A1735	100	100	40	0	60.00 bc
A1747	100	100	26	0	56.50 c
A1765	100	100	100	36	84.00 a

Table (2) Effect of different concentrations of seawater on seedling length of wheat genotypes.

Genotypes	Seawater Concentration %				Genotypes average
	Control	20	30	40	
A1595	10.8	6.4	3.6	0	5.20 b
A1651	11.2	8.5	3.2	0	5.72 b
A1671	14.5	10.0	7.0	0.5	8.00 a
A1695	12.0	8.0	3.2	0	5.80 b
A1697	11.0	7.5	2.5	0	5.25 b
A1711	14.0	11.0	8.3	0.8	8.52 a
A1729	9.7	7.0	2.0	0	4.67 b
A1735	10.9	9.5	4.1	0	6.12 b
A1747	10.0	7.0	2.0	0	4.75 b
A1765	13.8	11.5	7.0	9.0	8.30 a

3.2 Pots Experiment:

Effect of different concentrations of seawater on some morphological and photosynthetic pigment parameters of the three-durum wheat genotypes (ACSAD).

Current work is shown in tables (3 and 4) an effect of seawater irrigation levels (0, 20, and 30%) on some morphological and photosynthetic pigment parameters of wheat genotypes after 80 days of sowing. The results showed that irrigation with seawater 20% caused a significantly decrease ($p<0.05$) in (plant height, leaf area /plant, spike length, No of spikes/plant, No. of grains/spike, chlorophyll a, chlorophyll b, carotenoids, and total pigments), for all genotypes from (100%) of the control to (84.03, 87.16, 88.33, 75.47, 81.27,81.31, 86.14, 71.69 and 82.02%), for ACSAD 1671, and (76.39, 76.23, 74.13, 71.73, 63.90, 80.86, 83.87, 62.50 and 82.41%), for ACSAD 1711, and (79.89, 79.20, 81.66, 71.42, 75.95, 83.94, 84.37, 65.38 and 82.43%) for ACSAD 1765, respectively. In addition, genotypes grown under a seawater concentration of 30% exhibited significantly lower performance in all previously studied parameters compared to control (100%), to (63.02, 59.24,

61.66, 56.60, 65.77, 51.26, 77.71, 49.05 and 61.23%), for ACSAD 1671, (42.61, 47.33, 51.72, 56.52, 44.96, 51.26, 77.71, 49.05 and 61.23%), for ACSAD 1711, and (54.98, 55.24, 48.33, 53.57, 61.73, 50.52, 75.62, 48.07 and 57.09%) for ACSAD 1765, respectively. The ACSAD 1671 genotype exhibited the highest averages for all studied parameters under Salt stress conditions, whereas the ACSAD 1711 genotype exhibited the lowest averages.

Effect of foliar application of Nicotinic acid on some morphological and physiological characteristics of three wheat genotypes (ACSAD), under seawater irrigation levels.

The data presented in Tables (3 and 4) show the effect of foliar application of nicotinic acid on some morphological and photosynthetic pigment parameters for three genotypes of wheat (ACSAD), under seawater irrigation levels after 80 days of sowing. The results showed a significant increase in plant height for the three genotypes (ACSAD 1671, 1711 and 1765) by (17.31, 22.45, and 15.81%), leaf area /plant, (11.51, 10.94 and 11.09%), spike length, (5.00, 12.07 and 8.34%), the number of spikes/plant, (30.19, 15.22 and 5.36%), the number of grains/spike, (16.06, 16.57 and 14.21%), Chlorophyll a,(27.52, 13.21 and 21.58%), Chlorophyll b, (12.65, 13.54 and 5.63%), carotenoids, (13.21, 12.50 and 17.31%), and Total pigments, (22.04, 10.96 and 16.89%), respectively of treatment (T5), compared to (T2). As indicated by the treatment (T6) indicated a clear increase in plant height for the three genotypes (ACSAD 1671, 1711 and 1765) by (10.25, 18.81, and 12.20%), leaf area /plant, (8.49, 8.68 and 6.54%), spike length, (13.34, 8.62 and 18.33%), the number of spikes/plant, (18.87, 15.21 and 17.85%), the number of grains/spike, (13.37, 34.32 and 12.58%), Chlorophyll a,(25.76, 3.24 and 22.90%), Chlorophyll b, (10.24, 9.67 and 6.88%), carotenoids, (11.32, 10.42 and 7.69%), and total pigments, (17.30, 3.84 and 17.23), respectively compared to (T3).

Table (3) The effect of Nicotinic acid on the morphological characteristics of election genotypes of ACSAD wheat under different levels of salinity.

Genotypes	Con	Plant height		Leaf area /plant		Spike length		No. of spikes/plant		No. of grains/spike	
		(cm)	%	(cm^2)	%	(cm)	%	number	%	number	%
A1671	T_1	59.5 cd	100	53.0 b	100	6.0 abc	100	5.30 abc	100	62.33 bc	100
	T_2	50.0 h	84.03	46.2 e	87.16	5.3 abcde	88.33	4.00 bcde	75.47	50.66 f	81.27
	T_3	37.5 l	63.02	31.4 h	59.24	3.7 defg	61.66	3.00 de	56.60	41.00 h	65.77
	T_4	68.2 a	115.20	61.5 a	116.03	6.4 a	106.66	6.60 a	124.52	67.00 a	107.49
	T_5	60.3 c	101.34	52.3 bcd	98.67	5.6 abcd	93.33	5.60 ab	105.66	60.67 cd	97.33
	T_6	43.6 j	73.27	35.9 g	67.73	4.5 abcdefg	75.00	4.00 bcde	75.47	49.33 g	79.14
Genotype average		**53.18**		**46.71**		**5.25**		**4.75**		**55.16**	
A1711	T_1	52.1 g	100	50.7 cd	100	5.8 abc	100	4.60 abcde	100	56.33 e	100
	T_2	39.8 k	76.39	38.5 f	76.23	4.3 bcdefg	74.13	3.30 bcde	71.73	36.00 ij	63.90
	T_3	22.2 n	42.61	24.0 j	47.33	3.0 fg	51.72	2.60 e	56.52	25.33 k	44.96
	T_4	57.3 ef	109.98	52.9 bc	104.33	6.0 abc	103.44	5.00 abcd	108.69	59.00 d	104.73
	T_5	51.5 gh	98.84	44.2 e	87.17	5.0 abcdef	86.20	4.00 bcde	86.95	45.33 g	80.47
	T_6	32.0 m	61.42	28.4 i	56.01	3.5 efg	60.34	3.30 cde	71.73	34.66 j	79.28
Genotype average		**42.48**		**39.78**		**4.60**		**3.80**		**42.77**	
A1765	T_1	58.2 de	100	50.5 cd	100	6.0 abc	100	5.60 ab	100	61.00 bcd	100
	T_2	46.5 i	79.89	40.0 f	79.20	4.9 abcdefg	81.66	4.00 bcde	71.42	46.33 g	75.95
	T_3	32.0 m	54.98	27.9 i	55.24	2.9 g	48.33	3.00 de	53.57	37.66 i	61.73
	T_4	64.3 b	110.17	54.5 b	107.92	6.1 ab	101.66	6.00 ab	107.14	63.33 b	103.81
	T_5	55.7 f	95.70	45.6 e	90.29	5.4 abcde	90.00	4.30 bcde	76.78	55.00 e	90.16
	T_6	39.1 kl	67.18	31.2 h	61.78	4.0 cdefg	66.66	4.00 bcde	71.42	45.33 g	74.31
Genotype average		**49.30**		**41.61**		**4.88**		**4.58**		**51.44**	

Table (4) The effect of Nicotinic acid on photosynthetic Pigment of election genotypes of ACSAD wheat under different levels of salinity.

Genotypes	Con	Chlorophyll a		Chlorophyll b		Carotenoids		Total pigments	
		mg/ g	%	mg/ g	%	mg/ g	%	mg/ g	%
A1671	T_1	3.96 abcd	100	1.66 ab	100	0.53 abc	100	6.15 de	100
	T_2	3.22 abcd	81.31	1.43 abc	86.14	0.38 abcde	71.69	5.03 gh	82.02
	T_3	2.03 cd	51.26	1.29 bc	77.71	0.26 de	49.05	3.58 j	61.23
	T_4	5.04 a	127.27	1.87 a	112.65	0.62 a	116.98	7.53 a	122.43
	T_5	4.31 ab	108.83	1.64 ab	98.79	0.45 abcd	84.90	6.40 cd	104.06
	T_6	3.05 abcd	77.02	1.46 abc	87.95	0.32 cde	60.37	4.83 hi	78.53
Genotype average		**3.60**		**1.55**		**0.42**		**5.58**	
A1711	T_1	3.71 abcd	100	1.55 abc	100	0.48 abcd	100	5.74 ef	100
	T_2	3.00 abcd	80.86	1.30 bc	83.87	0.30 cde	62.50	4.60 hi	82.41
	T_3	2.06 cd	55.52	1.05 c	67.74	0.20 e	41.66	3.31	59.29
	T_4	4.53 ab	122.10	1.60 ab	103.22	0.53 abc	110.41	6.66 bc	116.02
	T_5	3.49 abcd	94.07	1.51 abc	97.41	0.36 bcde	75.00	5.36 fg	93.37
	T_6	2.18 cd	58.76	1.20 bc	77.41	0.25 de	52.08	3.63 j	63.13
Genotype average		**3.16**		**1.36**		**0.35**		**4.88**	
A1765	T_1	3.80 abcd	100	1.60 ab	100	0.52 abc	100	5.92 e	100
	T_2	3.19 abcd	83.94	1.35 abc	84.37	0.34 bcde	65.38	4.88 h	82.43
	T_3	1.92 d	50.52	1.21 bc	75.62	0.25 de	48.07	3.38 j	57.09
	T_4	4.74 ab	124.73	1.71 ab	106.87	0.58 ab	111.53	7.03 b	118.75
	T_5	4.01 abc	105.52	1.44 abc	90.00	0.43 abcd	82.69	5.88 e	99.32
	T_6	2.79 bcd	73.42	1.32 bc	82.5	0.29 cde	55.76	4.40 i	74.32
Genotype average		**3.40**		**1.43**		**0.40**		**5.24**	

4 Discussion

Wheat plays a crucial role in ensuring global food and nutritional security production. However, soil salinity poses a significant environmental, that hampers productivity and quality (El Sabagh *et al*., 2021). Nevertheless, the detrimental impacts of salinity can be alleviated by identifying genotypes that are tolerant to salinity (Salih *et al*.,2023). Therefore, this study was conducted with two experiments (laboratory - pots), To find out the impact of irrigation with seawater at the concentrations (20, 30 and 40%) on the tolerance of ten ACSAD durum wheat genotypes at the early seedling stage (laboratory experiment). According to the results of this experiment, the effect of foliar application of Nicotinic acid was evaluated for three salt-tolerant genotypes (ACSAD 1671, 1711 and 1765), under seawater salinity conditions at the concentrations 20 and 30% (pot experiment). Results indicated this study, laboratory experiment revealed significant differences when ($P<0.05$) in reducing average germination percentage, and seedling length in wheat genotypes compared to control. Differences in germination rates were documented between wheat genotypes based on their tolerance to salinity (Ramadan *et al*.,2023; Khanishova *et a*l., 2024). Hmissi *et al* (2023) outlined that the primary factor hindering germination in low-salinity conditions is the osmotic effect, while the toxic impact of sodium ions is observed in high-salinity environments. The negative effect of salinity attributed to Increased Na+ disorganizing ionic balance in cells, disturbs cell division, genetic circuits and protein synthesis machinery of plants, It also higher cellular membrane damage, and alters the nutrient level (Sarkar and Sadhukhan, 2023). Likewise, (Sghayar *et al* 2023) stated that Na+ accumulation in wheat seedling tissues significantly impaired carbohydrate and protein mobilization by inhibiting amylase and protease enzymes. The ACSAD (1765, 1671 and 1711) genotypes scored the highest average germination percentage (84.00, 80.00 and 75.00%), respectively. On the other hand, she exhibited significantly greater seedling length than other genotypes. Observed by (Mahboob *et al*., 2023) Differences between genotypes in salt tolerance are a polygenic trait controlled by multiple genes. Wheat's salt tolerance mechanisms include osmoregulation and scavenging reactive oxygen species. These mechanisms are supported by accumulated compounds such as sugars, polyhydric alcohols, amino acids, and quaternary ammonium compounds (Slama *et al*., 2015). Moreover, plants possess both enzymic and non-enzymatic mechanisms for scavenging ROS, through the antioxidant defense system (Singh, 2022). It was observed that increased salinity from 30 to 40% Sw

significantly affected the initial growth traits. After the laboratory experiment, the germination data results of the laboratory experiment categorize ACSAD durum wheat genotypes into tolerant genotypes (1671, 1711 and 1765), moderate (1595, 1651, 1695 and 1735), and sensitive (1697, 1729 and 1747). Results of the pot experiment showed significant ($P < 0.05$) decreases in vegetative growth parameters and the contents of photosynthetic pigments, of the three-durum wheat genotypes (ACSAD), under seawater irrigation conditions, after 80 days of sowing. The harmful effect of saline stress was clear, especially in a concentration (30% Sw), which recorded the largest rates of decline in general. Similar findings were reported for wheat under seawater irrigation conditions by (Nassar *et al*., 2020; Bashasha *et al*., 2021; Elfanah *et al*., 2023). In another study, Stojšin et al (2023) reported that a decrease in plant height, spike length, and number of grains per spike was significant under the effect of salinity, for 27 wheat genotypes. The higher level of salts causes cell damage, reactive oxygen species (ROS) generation increased rate of lipid peroxidation, inhibiting apical growth, and inhibiting protein synthesis, (Alharbi *et al*., 2022). The detrimental effects of salt stress on photosynthetic pigments were reported in studies on wheat (Salih and Abdulrraziq, 2023). The reduction in photosynthetic pigment parameters under salinity could be due to osmotic stress limits CO_2 fixation in the leaves by stomatal closure, downregulation of the Calvin cycle, as well as increased proteolytic enzymes chlorophyllase responsible for the degradation of chlorophyll, and decreased activity of ribulose bisphosphate (Kwon *et al*.,2019; Sharma *et al*., 2020). The results of the data analysis showed that foliar application of Nicotinic acid alleviated the adverse effects of salinity levels in all morphological and the contents of photosynthetic pigments Parameters of wheat, compared to the untreated plant. Our results are consistent with many studies that showed Vitamin treatment successfully increases the productivity of crops (Khudair *et al*., 2019; Al-Jboory *et al*., 2022). The results are similar to (Farooq *et al*., 2022), who suggested the foliar application of Nicotinic acid increases plant height, leaf area, and the number of leaves. also increases stomatal conductance, improves cell wall integration and enzymatic activities, and increases photosynthetic and transpiration rates. These results agree with those published by (Yaseen *et al*., 2017) on the effects of vitamins on plant species organogenesis in vitro. The (1671) genotype performed better than the (1711 and 1765) genotypes in concern to high averages for all studied traits, under salinity and spraying with Nicotinic acid. foliar application of Nicotinic acid reduced salt stress and increased wheat growth through an increase in the levels of IAA, GA3, and cytokinins, and a decrease in ABA content (El-Bassiouny, 2005). Reduces the damage caused by cell membrane lipid peroxidation and improves plants' antioxidant capacity, contributing to cell osmotic regulation, and ROS detoxification according to (Chi *et al*., 2021). In addition, Nicotinic acid is required by plants for synthesizing the amino acids and also helps in carbohydrate metabolism (Tomar *et al*., 2018). Nicotinic acid counteract the formation of DNA strand breaks caused by oxidative stress, and prevent cell leakage and glutathione depletion caused by oxidative stress (Berglund et al., 2017).

5 Conclusion

The laboratory experiment showed that the genotypes (1671, 1711and 1765), were superior in recording the best average germination percentage and seedling length compared to the other genotypes, Under different seawater levels. Also, the pot experiment showed, under seawater irrigation conditions, decreases in all vegetative growth parameters and the contents of photosynthetic pigments, of the three durum wheat genotypes (ACSAD1671, 1711and 1765), foliar application of Nicotinic acid led to a significant decrease in a negative effect resulting from salinity. The (1671) genotype performed better than the (1711 and 1765) genotypes in concern to high averages for all studied traits, under salinity and spraying with Nicotinic acid.

Conflict of interest: The authors declare that there are no conflicts of interest

References

Ahmed, H. G. M. D., Zeng, Y., Yang, X., Faisal, A., Fatima, N., Ullah, A., Hussain, G. S., Iftikhar, M., and Anwar, M. R. (2024). Heritability and Genotypic Association Among Seedling Attribute Against Salinity Stress Tolerance in Wheat Genotypes for Sustainable Food Security. Journal of Crop Health, 1-13.

Ain, Q. U., Hussain, H. A., Zhang, Q., Kamal, F., Charagh, S., Imran, A., Hussain, S., and Bibi, H. (2024). Deciphering the Role of Nanoparticles in Stimulating Drought and Salinity Tolerance in Plants: Recent Insights and Perspective. Journal of Plant Growth Regulation, 1-26.

Alharbi, K., Al-Osaimi, A. A., & Alghamdi, B. A. (2022). Sodium chloride (NaCl)-induced physiological alteration and oxidative stress generation in *Pisum sativum* (L.): A toxicity assessment. ACS omega, 7(24), 20819-20832.

Al-Jboory, W. S. H., & Al-Sharea, A. O. E. (2022). Study the effect of spraying of Vitamin B3 and the amino acid Glycine and their overlap on some growth indicators of *Apium graveolens* L. Bulletin of National Institute of Health Sciences, 140(1), 1185-1199.

Bashasha, J. A., El-Mugrbi, W. S., & Imryed, Y. F. (2021). Effect of magnetic treatment in improve growth of three wheat cultivars irrigated with seawater. Multidiscip. Sci. Adv. Technol, 1, 24-32.

Berglund, T., Wallström, A., Nguyen, T. V., Laurell, C., & Ohlsson, A. B. (2017). Nicotinamide; antioxidative and DNA hypomethylation effects in plant cells. Plant Physiology and Biochemistry, 118, 551-560.

Cabusora, C. C. (2024). Developing climate-resilient crops: adaptation to abiotic stress-affected areas. Technology in Agronomy, (tia-0024-0002), 1-12.

Çatak, J., & Yaman, M. (2019). Research Article Determination of Nicotinic Acid and Nicotinamide Forms of Vitamin B3 (Niacin) in Fruits and Vegetables by HPLC Using Postcolumn Derivatization System. Pakistan Journal of Nutrition, 18(6), 563-570.

Chi, Y. X., Yang, L., Zhao, C. J., Muhammad, I., Zhou, X. B., & De Zhu, H. (2021). Effects of soaking seeds in exogenous vitamins on active oxygen metabolism and seedling growth under low-temperature stress. Saudi Journal of Biological Sciences, 28(6), 3254-3261.

Choudhary, S., Wani, K. I., Naeem, M., Khan, M. M. A., & Aftab, T. (2023). Cellular responses, osmotic adjustments, and role of osmolytes in providing salt stress resilience in higher plants: Polyamines and nitric oxide crosstalk. Journal of Plant Growth Regulation, 42(2), 539-553.

El Sabagh, A., Islam, M. S., Skalicky, M., Ali Raza, M., Singh, K., Anwar Hossain, M., Mahboob, W., Iqbal, M, A., Ratnasekera, D., Singhal, R, K., Ahmed, S., Kumari, A., Wasaya, A., Sytar, O., Brestic, M., ÇIG, F., Erman, M., Ur Rahman, M, H., Ullah, N., and Arshad, A. (2021). Salinity stress in wheat (*Triticum aestivum* L.) in the changing climate: Adaptation and management strategies. Frontiers in Agronomy, 3, 661932.

El-Bassiouny, H. M. S. (2005). Physiological responses of wheat to salinity alleviation by nicotinamide and tryptophan. International Journal of Agriculture & Biology, vol(7), 4, pp 653–659.

Elfanah, A. M. S., Darwish, M. A., Selim, A. I., Shabana, M. M. A., Elmoselhy, O. M. A., Khedr, R. A., Ali, A, M., and Abdelhamid, M. T. (2023). Spectral reflectance indices' performance to identify seawater salinity tolerance in bread wheat genotypes using genotype by yield* trait biplot approach. Agronomy, 13(2), 353.

Farooq, T. H., Bukhari, M. A., Irfan, M. S., Rafay, M., Shakoor, A., Rashid, M. H. U., Lin, Y., Saqib, M., Malik, Z., and Khurshid, N. (2022). Effect of Exogenous Application of Nicotinic Acid on Morpho-Physiological Characteristics of *Hordeum vulgare* L. under Water Stress. Plants, 11(18), 2443.

Gakière, B., Hao, J., de Bont, L., Pétriacq, P., Nunes-Nesi, A., & Fernie, A. R. (2018). NAD+ biosynthesis and signaling in plants. Critical Reviews in Plant Sciences, 37(4), 259-307.

Gasperi, V., Sibilano, M., Savini, I., & Catani, M. V. (2019). Niacin in the central nervous system: an update of biological aspects and clinical applications. International journal of molecular sciences, 20(4), 974.

Hmissi, M., Chaieb, M., & Krouma, A. (2023). Differences in the physiological indicators of seed germination and seedling establishment of durum wheat (*Triticum* durum Desf.) cultivars subjected to salinity stress. Agronomy, 13(7), 1718.

Hussein, M. M., Faham, S. Y., & Alva, A. K. (2014). Role of foliar application of nicotinic acid and tryptophan on onion plants response to salinity stress. Journal of Agricultural Science, 6(8), 41-51.

Khanishova, M. A., Tagiyeva, K. R., & Azizov, I. V. (2024). Effect of NaCl on Physiological Performance and Yield of Wheat Hybrids. Advanced Studies in Biology, 16(1), 1-12.

Khudair, T. Y., Albbas, F. A. A., & Kreem, K. A. A. (2019). Effect of Niacin (Nicotinamide) and Humic Acid on Growth and Chemical Traits of *Pelargonium hortorum* L. Indian J. Ecol., 46, 173-178.

Kononenko, N. V., Lazareva, E. M., & Fedoreyeva, L. I. (2023). Mechanisms of Antioxidant Resistance in Different Wheat Genotypes under Salt Stress and Hypoxia. International Journal of Molecular Sciences, 24(23), 16878.

Kwon, O. K., Mekapogu, M., & Kim, K. S. (2019). Effect of salinity stress on photosynthesis and related physiological responses in carnation (Dianthus caryophyllus). Horticulture, Environment, and Biotechnology, 60, 831-839.

Mahboob, W., Rizwan, M., Irfan, M., Hafeez, O. B. A., Sarwar, N., Akhtar, M., Munir, M., Rani, R., El Sabagh, A., and Shimelis, H. (2023). Salinity Tolerance In Wheat: Responses, Mechanisms And Adaptation Approaches. Applied Ecology & Environmental Research, 21(6).

Metzner, H., Rau, H., & Senger, H. (1965). Untersuchungen zur synchronisierbarkeit einzelner

pigmentmangelmutanten von Chlorella. Planta, 65(2), 186-194.

Mokhtarpour, H., Teh, C.B., Saleh, G., Selamat, A. B., Asadi, M. E. and Kamkar, B. (2010). Nondestructive estimation of maize leaf area, fresh weight, and dry weight using leaf length and leaf width. Communications in Biometry and Crop Science. 5(1):19-26.

Nassar, R. M., Kamel, H. A., Ghoniem, A. E., Alarcón, J. J., Sekara, A., Ulrichs, C., & Abdelhamid, M. T. (2020). Physiological and anatomical mechanisms in wheat to cope with salt stress induced by seawater. Plants, 9(2), 237.

Noctor, G., Hager, J., & Li, S. (2011). Biosynthesis of NAD and Its Manipulation in Plants. In Advances in botanical research Vol. 58, pp. 153-201, Academic Press.

Ramadan, E., Freeg, H. A., Shalaby, N., Rizk, M. S., Ma, J., Du, W., Ibrahim, O. M., Alwutayd, K. M., AbdElgawad, H., Jo, I., and El-Tahan, A. M. (2023). Response of nine triticale genotypes to different salt concentrations at the germination and early seedling stages. PeerJ, 11, e16256.

Salih, S. M., Abdulrraziq, A. A. (2023). The effects of indole butyric acid and seaweed (Posidonia oceanic) and their mixture in improving photosynthetic pigments of salt-stressed wheat cultivar (Marjawi). Scientific Journal for Faculty of Science-Sirte University, 3(1), 139-144.

Salih, S. M., Abdulrraziq, A. A., & Abdulwhab, O. A. (2023). The Evaluation of Tolerance of Six Triticum aestivum Genotypes to Salt Stress. Scientific Journal for Faculty of Science-Sirte University, 3(2), 105-109.

Sarkar, A. K., & Sadhukhan, S. (2023). Impact of Salinity on Growth and Development of Plants with the central focus on Glycophytes: an overview. Bull. Env. Pharmacol. Life Sci, 12, 235-266.

Sghayar, S., Debez, A., Lucchini, G., Abruzzese, A., Zorrig, W., Negrini, N., Morgutti, S., Abdelly, C., Sacchi, G. A., Pecchioni, N., and Vaccino, P. (2023). Seed priming mitigates high salinity impact on germination of bread wheat (*Triticum aestivum* L.) by improving carbohydrate and protein mobilization. Plant Direct, 7(6), e497.

Sharma, S., Joshi, J., Kataria, S., Verma, S. K., Chatterjee, S., Jain, M., Pathak, K., Rastogi, A., and Brestic, M. (2020). Regulation of the Calvin cycle under abiotic stresses: An overview. Plant life under changing environment, 681-717.

Singh, D. (2022). Juggling with reactive oxygen species and antioxidant defense system–A coping mechanism under salt stress. Plant Stress, 5, 100093.

Slama, I., Abdelly, C., Bouchereau, A., Flowers, T., & Savouré, A. (2015). Diversity, distribution and roles of osmoprotective compounds accumulated in halophytes under abiotic stress. Annals of botany, 115(3), 433-447.

Stojšin, M. M., Petrović, S., Jocković, B., Banjac, B., Zečević, V., Stefanović, V. M., & Perišić, V. (2023). Utilizing the Stability of Yield Parameters as a Technique to Select Salinity-Tolerant Wheat Genotypes. Contemporary Agriculture, 72(1-2), 64-74.

Tomar, R. S., Khamba, S., Kaushik, S., & Mishra, R. K. (2018). Role of Vitamins in Plant Growth and their Impact on Regeneration of Plants under Invitro Condition. International Journal for Research in Applied Science and Engineering Technology, 6(3), 423-426.

Yanagi, M. (2024). Climate change impacts on wheat production: Reviewing challenges and adaptation strategies. Advances in Resources Research, 4(1), 89-107.

Yaseen, F. K., Toma, R. S., & Carbonera, D. (2017). The effects of vitamins on micropropagation of Desiree and Mozart potatoes (*Solanum tuberosum* L.). Science Journal of University of Zakho, 5(1), 53-56.

Scientific Journal for the Faculty of Science-Sirte University Vol. 4, No. 1 (2024) 117-123

Scientific Journal for the Faculty of Science-Sirte University

Journal home page: http://journal.su.edu.ly/index.php/JSFSU/index

DOI: 10.37375/issn.2789-858X

Comparative Study of Hematological and Biochemical Parameters in Patients with Renal Failure depending on gender

Fawziya B. Marie[1], Fathia A. Mosa[2], Mabrouka B. Abdullah[1], and Samah A. Abdul[1], and Sondos S. Naji[1]

[1]*Department of Zoology, Faculty of Science, University of Sirte, Libya.*

[2]*Department of Chemistry, Faculty of Science, University of Sirte, Libya.*

DOI: https://doi.org/10.37375/sjfssu.v4i1.2642

ARTICLE INFO:

Received: 26 February 2024

Accepted: 04 April 2024

Published: 17 April 2024

Keywords: *Renal failure, urea, creatinine, haemoglobin, haematological parameters, CBC.*

A B S T R A C T

The research aimed to evaluate the hematological and biochemical parameters in patients with kidney failure who are being treated at the nephrology department. This study was performed on 100 samples (50 males and 50 females) of patients who attended the nephrology department at Ibn Sina University Hospital. The survey of these samples was carried out among patients attending from January to May 2023. This study depended on the analysis of individual samples obtained from patient records, expressed as complete blood count (CBC) as well as biochemical changes in kidney function. It was found that most patients suffered from a decrease in hemoglobin, WBCs, and RBCs levels. According to the obtained results in this study, we found a significant decrease in the concentrations of hemoglobin, platelets, and leukocytes in both genders, while we found a significant increase in the concentrations of urea and creatinine. The results revealed no decline in potassium ions in patients, but sodium ions slightly decreased somewhat in males alone and not in females.

1 Introduction

Kidney failure is defined as a disorder in which the kidneys lose their ability to remove the waste product from the bloodstream (Prasad, 2014). Kidney ailment is a serious and widespread health problem. The manifestations of this disease are changes that affect the ability of the kidneys to remove toxins, dysregulation of salt, and water balance (Perco et al., 2006). Impairment of normal kidney function affects the metabolic secretion of many endocrine hormones, including thyroid hormones, insulin, and sex hormones (Kaka et al., 2022). The physiological spectrum of kidney disease is divided into two general aspects, which are “acute kidney injury (AKI) and chronic kidney disease (CKD)” (Khan et al., 2005).

AKI is a quick deterioration in kidney function that worsens over days or weeks and is usually accompanied by smaller volumes of urine and increase creatinine concentrations in the bloodstream (Figure 1). Acute kidney disease coincides with a significant increase in mortality by 40-80% and thus also contributes to fatal acute anemia (Lafrance & Miller, 2010).

CKD is a worldwide public health problem that confuses many health institutions around the world (McClellan & Powe 2009). It can be explained as a significant decrease in kidney excretory function or evidence that the kidneys have suffered significant damage (Genovese et al., 2010). More than 200 papers were analyzed to better recognize the disease that exterminates more than 30,000 people each year (Priyadarshani et al., 2023). CKD is a clinically silent disease in up to 90% of individuals until it reaches a high-risk condition (Chadban et al., 2003; John et al., 2004).

***Corresponding author*: E-mail: fawziya.marie@su.edu.ly**

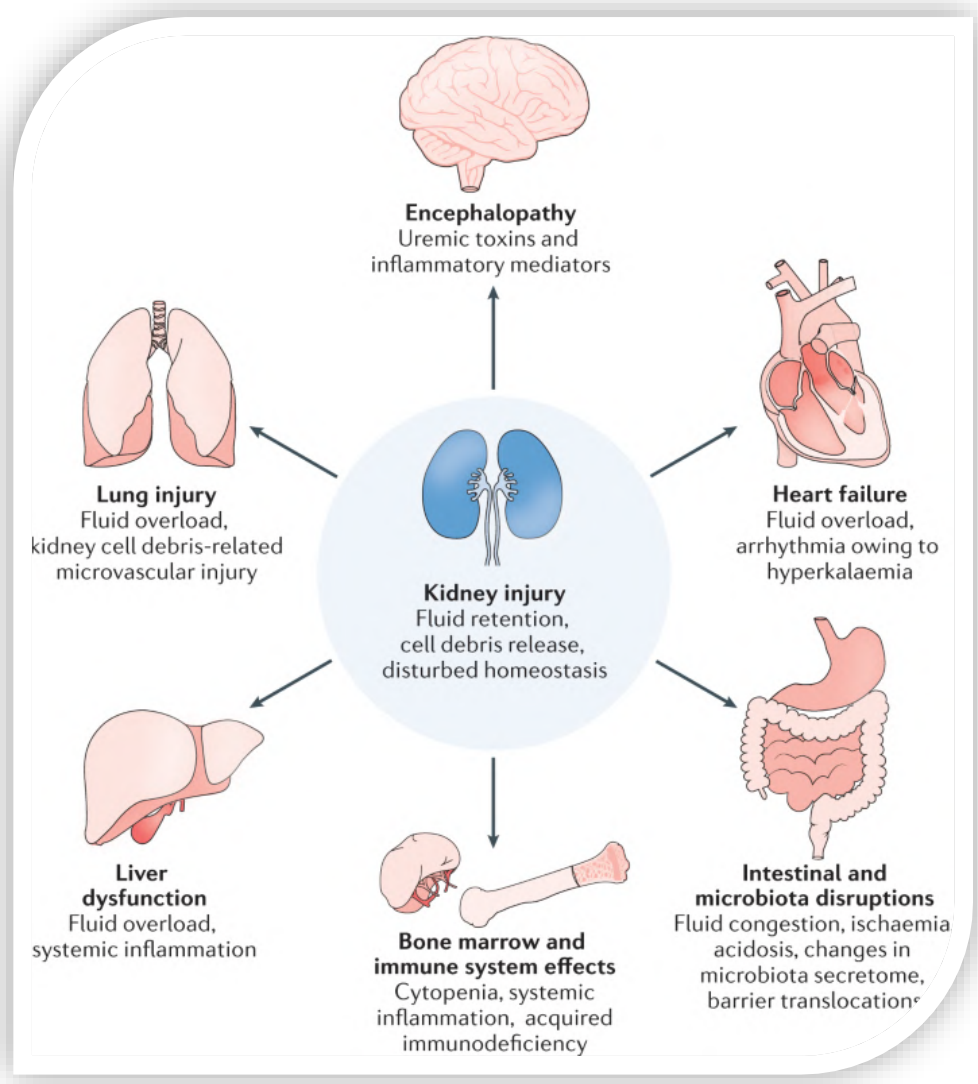

Figure (1) Systemic consequences of AKI (Kellum et al., 2021).

As for Libya, in 2003 the occurrence of the ailment was 200 patients per million people, and in 2007 the occurrence of the disease increased to 350 patients per million people. "Between 2007 and 2009, the number of patients undergoing dialysis in Libya increased from 2116 patients to 2417 patients, and the number of dialysis patients is expected to increase from 2417 patients in 2009 to 7667 patients in 2024" (Akkari 2013). Data published by the World Health Organization in 2012 revealed that the global occurrence of kidney failure was 282 individuals per million people, and the occurrence of the ailment increased to 624 individuals per million people (Goleg et al., 2014).

Chronic kidney failure is an irreversible destruction of the kidneys' nephrons that occurs slowly; the disease process is advanced and continuous until most of the kidney's nephrons are destroyed and replaced by fibrous tissue (Vaidya & Aeddula 2022). This failure may occur slowly in patients with normal diseases or kidney vesicular ailments, or it may result from injury to the kidneys (Figure 2). In chronic kidney failure, the kidneys lose their functions in filtering and maintaining blood balance due to inflammation of the kidney cells or nephrons (Kelly, et al, 1996).

Anemia is indicated by a low erythrocyte count or an inadequate quantity of hemoglobin (Hb) within erythrocytes (Begum & Latunde-Dada, 2019). It is estimated that more than half of those with CKD suffer from anemia (Bolignano et al., 2015). The lack of iron results when there is a need for more iron than can be released from iron reserves to promote Hb production (Nairz et al., 2016). Anemia can cause the heart muscles

to enlarge, increase the heart rate, and lead to cardiac failure in individuals with acute or chronic renal failure; this does not mean the heart stops functioning completely (Somvanshi et al., 2012).

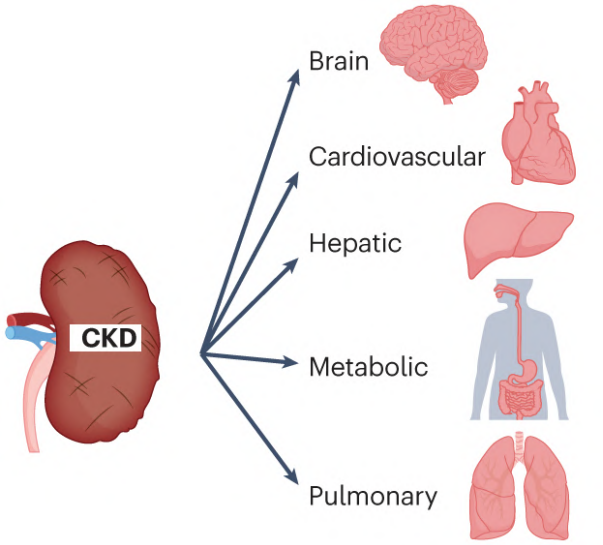

Figure (2) Systemic consequences of CKD (Benzing & Schumacher, 2023).

When the body lacks iron, it can result in a reduction in the formation of hemoglobin in red blood cells (RBCs), which can cause hypochromic anemia Srinivasan et al., 2016). Chronic anemia can be caused by a significant decrease in erythropoietin (EPO) hormone levels, as EPO hormone is responsible for the formation and increase of RBCs. Certain factors, such as signals sent from the bone marrow, can affect its production and release (Besarab et al., 2000).

2 Materials and Methods

This study aimed to investigate the hematological and biochemical variables in adult patients suffering from kidney failure. The variables evaluated included total white blood cell count (WBCs), estimated Hb concentration, total platelet count (PLT), and RBCs count, as well as creatinine, urea, sodium, and potassium. A total of 100 samples were analyzed, with an equal representation of both genders (50 males, 50 females) from the adult group.

A Chemistry AccentT 200 analyzer was utilized to measure various biochemical parameters. In addition, CBC Sysmex analyzer was employed to measure hematological parameters.

2.1 Data source and patients

100 patients have admitted to the Ibn Sina Teaching Hospital at Sirte (Libya) had been selected with age 40 years or above, who agreed to participate in the study. All of the selected patients (50 males and 50 females) had chronic kidney disease. A retrospective chart review was performed of those patients who attended *the nephrology department* between *January* 2023 and *May 2023*.

2.2 Statistical analysis

The analysis of the data was conducted through the utilization of IBM's Statistical Package for the Social Sciences (SPSS) software version 23.0 for windows (Armonk, New York: IBM Crops). Variables are compared using (cross tab) and Fisher's exact test, and differences between two means are used with (independent t-test). P value ≤ 0.05 was taken as level for statistical significance.

3 Results

The measurements of hematological and biochemical variables are summarized in Tables 1 and 2. There was a significant decrease (P-value ≤ 0.05) in haemoglobin concentration in both genders. This indicated the existence of anaemia in patients with kidney failure. There is a slight increase in the number of WBCs in the blood of patients with kidney failure compared to the normal range for this variable. The current results showed a significant decrease (P-value ≤0.05) in the number of platelets in the patients with kidney failure compared to the normal range of platelets.

The results of this study showed that the number of RBCs decreased significantly in patients with kidney failure, whether male or female, compared to normal levels, and that anaemia was noticeable in patients with chronic kidney failure. The results showed significant increases in both urea and creatinine compared to the normal levels of these variables.

The results in this study also indicated that there was a slight decrease in the concentration levels of sodium ions among patients with kidney failure compared to the normal levels of these variables. The results revealed no decline in potassium in patients with CKD.

Table (1) shows the hematological parameters (Hb level, WBC, red blood cell distribution width (RBC), and platelet counts) of the patients.

Hematological parameters	unit	Males		Females	
		Normal range*	**Mean ± S.D**	Normal range	**Mean ± S.D**
Hb	**g/dl**	14–18	9.6 ± 1.4	12–16	9.6 ± 1.4
WBCs	**$\times 10^9$/L**	4.8–10.8	6.3 ± 1.7	4.8–10.8	6.5 ± 2.1
RBCs	**$\times 10^{12}$/L**	4.5–6.0	3.1 ± 0.5	4.1–5.1	3.2 ± 0.5
PLT	**$\times 10^9$/L**	175–450	203.1 ± 77.3	175–450	218.4 ± 74.1
*from the references: (Billett, 1990; Marshall, 2022).					

Table (2) shows the biochemical parameters (urea, creatinine, sodium, and potassium) of the patients.

Biochemical parameters	SI Unit	Gender	Normal range*	Mean ± S.D
Creatinine	µmol/L	Male	61.9 - 114.9	131.75 ± 26.42
		Female	53 - 97.2	117.25 ± 37.14
Urea	mmol/L	Male	2.9 - 7.1	9.05 ± 1.86
		Female	2.9 - 7.1	8.099 ± 2.76
Sodium	mmol/L	Male	136 - 145	135.99 ± 3.04
		Female	136 - 145	136.595 ± 2.57
Potassium	mmol/L	Male	3.5 - 5.0	4.899 ± 0.74
		Female	3.5 - 5.0	4.366 ± 0.98
*from the references: (Lee, 2009 & Tyagi, 2023).				

4 Discussion

Hb levels in patients with kidney failure: "Many studies have indicated that anaemia represents one of the most important complications that accompany kidney failure" (Costa et al., 2008 & Hsu et al., 2001).This may be attributed to a deficiency in the secretion of the hormone EPO which is responsible for stimulating the process of forming RBCs (Erythropoiesis in the bone marrow) according to (Brunelli et al., 2009 & Erslev 1997). Additionally, the deficiency in the iron element in the patients with kidney failure suffer from (Kausz 2000). "Another reason that leads to the occurrence of anaemia in patients with kidney failure is the accumulation of nitrogenous wastes in the blood that inhibit the production of cells that generate RBCs in the bone marrow" (Besarab 2000).

WBCs count in patients with kidney failure: it found that there is a slight increase in the number of WBCs. This result did not reach agreement with what was mentioned by Kralova (2009). A notable increasing in WBCs is considered an inflammatory condition that is accompanied by uraemia, while it agreed with what was mentioned in the same study, as the slight increase is attributed to haemodialysis treatment, as neutrophils and monocytes are at the forefront of phagocytic cells whose number increases in response to any opportunistic stimulation.

PLTs count in patients with kidney failure: it found that there is a slight decline in the number of PLTs. This result agreed with Remuzzi (1989). It is believed that the decrease observed can be caused by the accumulation of nitrogenous compounds in the bloodstream. Nitrogenous wastes inhibited the formation of PLTs in the bone marrow. Moreover, the blood acidity was related to the decrease in PLT counts (Kopple et al., 2005). One of the important factors is the decrease in the level of the hormone thrombopoietin, which is responsible for regulating the formation process of PLTs and kidney excretion in the patients may be attributed to the accumulation of nitrogenous compounds in blood (Altun et al., 1999). Nitrogenous wastes inhibited the process of platelet formation in the bone marrow. Moreover, the blood acidity in patients with kidney failure was related to the decrease in platelet counts (Kopple et al., 2005). One of the important factors is the decrease in the level of the hormone thrombopoietin, which is responsible for regulating the formation process of platelets and kidney excretion (Altun et al. 1999).

RBCs count in patients with kidney failure: the number of RBCs decreased may be due to a lack of

secretion of the hormone (EPO), which is responsible for stimulating the process of Formation of RBCs in the bone marrow (Brunelli & Berns 2009; Erslev & Besarab 1997). Additionally, deficiencies in vitamin B12 and folate, and changes in red cell volume brought on by dialysis, might cause patients to exhibit macrocytic anemia (Shastry & Belurkar 2019). These patients have a lower hematocrit because of hemodilution.

There were noticeable similarities between both genders (Fig. 4) which suffering from kidney failure according to their levels of HB, WBCs, RBCs, sodium, potassium, and creatinine. Males exhibited higher mean PLT and urea levels than females. The outcomes point out that there are high connections between some parameters and gender differences that should be taken into account in future analyses.

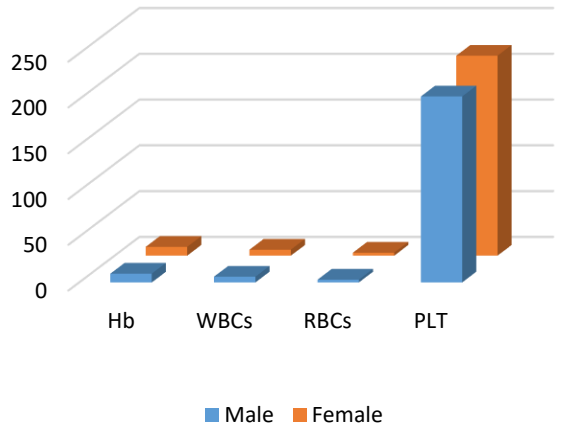

Figure (4) shows the hematological parameters of the patients

Creatinine and urea concentration in patients with kidney failure: It is known that urea and creatinine in blood serum are used as diagnostic tests for kidney function. The significant increases in urea and creatinine values are consistent with some previous studies (Zilve et al., 1989; Meri et al., 2022). The high concentration of urea and creatinine in the blood serum of patients with kidney failure may be attributed to the fact that they are metabolic wastes that are naturally excreted through urine, and in the case of kidney failure, a defect and decrease in kidney function occurs, leading to decreased excretion. These wastes accumulate and accumulate, increasing their concentration in the blood serum (Zilva et al., 1989). For the reason that urea is a substance that is reabsorbed again, it is not an indicator of kidney dysfunction. However, some studies have suggested that both serum creatinine and blood urea are the primary signs of kidney failure in both acute and chronic cases (Chhetri et al., 2008).

Sodium and potassium concentration in patients with kidney failure: The results revealed no decline in potassium in patients (Fig. 5), which differed with (Kumar 2004), as his study demonstrated that increased potassium can be attributed to causes many of them include the role of the kidney in excreting approximately (90-95%) of the potassium entering the body. When chronic kidney failure occurs, the efficiency of this process diminishes. However, the study of (Al-Abachi et al., 2012), in which the results of their study indicated that there is a decrease in the level of sodium and potassium concentration in the blood serum, and the deficiency of sodium and potassium ions in the blood serum among patients with kidney failure may be due to a deficiency of the hormone aldosterone, which it increases the loss of sodium and potassium ions in the urine (Al-Abachi et al., 2012).

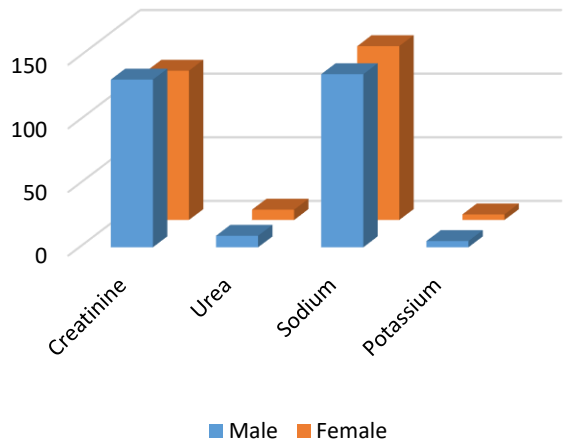

Figure (5) shows the biochemical parameters (urea, creatinine, sodium, and potassium) of the patients

5 Conclusions

Based on the results of this study, a significant decrease was observed in the concentration levels of haemoglobin, platelets, and RBCs in patients with kidney failure compared to the normal levels of these variables. Even though there was a slight decrease in the number of WBCs in the patients with kidney failure compared to normal levels for this variable. Furthermore, urea and creatinine were found to have significantly increased. While the results indicated a little decrease in sodium ions in the male group only and no decrease in the female group. There was no decrease in potassium ions in patients. Therefore, the results

revealed significant changes in both haematological parameters and some biochemical parameters, suggesting that kidney failure effects on the blood cell formation, and electrolyte balance.

Conflict of interest: The authors affirm that there are no conflicts of interest.

References

Akkari, K. (2022). Projecting requirements for end stage renal disease services in Libya 2014-2024. *Ibnosina Journal of Medicine and Biomedical Sciences*, *5*(06), 354-362.

Al-Abachi, S. Z., Mustafa, L. A., Hassan, D. S. K., & Al-Hadidi, A. A. (2012). Study of some biochemical changes in serum of patients with chronic renal failure. *Iraqi National Journal of Chemistry*, *12*(46), 270-280.

Begum, S., & Latunde-Dada, G. O. (2019). Anemia of Inflammation with An Emphasis on Chronic Kidney Disease. *Nutrients*, *11*(10), 2424. https://doi.org/10.3390/nu11102424

Benzing, T., & Schumacher, B. (2023). Chronic kidney disease promotes ageing in a multiorgan disease network. *Nature Reviews Nephrology*, *19*(9), 542–543. https://doi.org/10.1038/s41581-023-00729-6

Besarab, A., Amin, N., Ahsan, M., Vogel, S.E., Zazuwa, G., Frinak, S., Zazra, J.J., Anandan, J.V. & Gupta, A. (2000). Optimization of epoetin therapy with intravenous iron therapy in hemodialysis patients. *Journal of the American Society of Nephrology*, *11*(3), 530-538.

Billett, H. H. (1990). *Hemoglobin and hematocrit*. Clinical Methods - NCBI Bookshelf. https://www.ncbi.nlm.nih.gov/books/NBK259/

Bolignano, D., Lennartz, S., Leonardis, D., D'arrigo, G., Tripepi, R., Emrich, I.E., Mallamaci, F., Fliser, D., Heine, G. & Zoccali, C. (2015). High estimated pulmonary artery systolic pressure predicts adverse cardiovascular outcomes in stage 2–4 chronic kidney disease. *Kidney international*, *88*(1), 130-136.

Brunelli, S. M., & Berns, J. S. (2009). Anemia in chronic kidney disease and end-stage renal disease. *Nephrology Rounds*, *7*(8), 1-6.

Chadban, S. J., Briganti, E. M., Kerr, P. G., Dunstan, D. W., Welborn, T. A., Zimmet, P. Z., & Atkins, R. C. (2003). Prevalence of kidney damage in Australian adults: The AusDiab kidney study. *Journal of the American Society of Nephrology*, *14*(suppl_2), S131-S138.

Chhetri, P. K., Manandhar, D. N., Bhattarai, S. P., Pahari, L. R., & Shrestha, R. (2008). Chronic kidney disease 5 on hemodialysis in Nepal medical college teaching hospital. *Nepal Med Coll J*, *10*(1), 8-10.

Costa, E., Rocha, C., Rocha-Pereira, P., Castro, E., Miranda, V., Faria, M. D. S., Quntannilha, A.; Belo, L. & Santos-Silva, A. (2008). Band 3 profile as a marker of erythrocyte changes in chronic kidney disease patients. *The Open Clinical Chemistry Journal*, *1*(1): 57-63.

Erslev, A. J., & Besarab, A. (1997). Erythropoietin in the pathogenesis and treatment of the anemia of chronic renal failure. *Kidney International*, *51*(3), 622-630.

Genovese, G., Friedman, D.J., Ross, M.D., Lecordier, L., Uzureau, P., Freedman, B.I., Bowden, D.W., Langefeld, C.D., Oleksyk, T.K., Uscinski Knob, A.L. and Bernhardy, A.J. (2010). Association of trypanolytic ApoL1 variants with kidney disease in African Americans. *Science*, *329*(5993), 841-845.

Goleg, F. A., Kong, N. C. T., & Sahathevan, R. (2014). Dialysis-treated end-stage kidney disease in Libya: Epidemiology and risk factors. *International urology and nephrology*, *46*, 1581-1587.

Hsu, C. Y., Bates, D. W., Kuperman, G. J., & Curhan, G. C. (2001). Relationship between hematocrit and renal function in men and women. *Kidney international*, *59*(2), 725-731.

John, R., Webb, M., Young, A., & Stevens, P. E. (2004). Unreferred chronic kidney disease: a longitudinal study. *American Journal of Kidney Diseases*, *43*(5), 825-835.

Kaka, N., Sethi, Y., Patel, N., Kaiwan, O., Al-Inaya, Y., Manchanda, K., & Uniyal, N. (2022). Endocrine manifestations of chronic kidney disease and their evolving management: A systematic review. *Disease-A-Month*, *68*(12), 101466. https://doi.org/10.1016/j.disamonth.2022.101466

Kausz, A. T., Obrador, G. T., & Pereira, B. J. (2000). Anemia management in patients with chronic renal insufficiency. *American journal of kidney diseases*, *36*(6), S39-S51.

Kellum, J. A., Romagnani, P., Ashuntantang, G., Ronco, C., Zarbock, A., & Anders, H. (2021). Acute kidney injury. *Nature Reviews Disease Primers*, *7*(1). https://doi.org/10.1038/s41572-021-00284-z

Kelly, F.J., Anderson, S., Thompson, M.M., Oyama, T.T., Kennefick, T.M., Corless, C.L., Roman, R.J., Kurtzberg, L., Pratt, B.M. & Ledbetter, S. R. (1999). Acute and chronic renal effects of recombinant human TGF-β2 in the rat. *Journal of the American Society of Nephrology*, *10*(6), 1264-1273.

Khan, R. N., Vohra, E. A., & Suleman, W. (2005). Factors determining outcome of acute renal failure patients. *Journal-Pakistan Medical Association*, *55*(12), 526.

Kopple, J. D., Kalantar-Zadeh, K., & Mehrotra, R. (2005). Risks of chronic metabolic acidosis in patients with

chronic kidney disease. *Kidney International*, *67*(95), S21-S27.

Kralova, S., Leva, L., & Toman, M. (2009). Polymorphonuclear function in naturally occurring renal failure in dogs. *Veterinární medicína*, *54*(5), 236-243.

Kumar, A. (2003). Animal physiology. Discovery Publishing House.

Lafrance, J. P., & Miller, D. R. (2010). Acute kidney injury associates with increased long-term mortality. *Journal of the American Society of Nephrology: JASN*, *21*(2), 345.

Lee, M. (Ed.). (2009). *Basic skills in interpreting laboratory data*. ASHP.

Macdougall, I., Bock, A. H., Carrera, F., Eckardt, K. U., Gaillard, C. A., Van Wyck, D. B., ... & Roger, S. D. (2016). CHRONIC KIDNEY DISEASE ANAEMIA. *Nephrology Dialysis Transplantation*, *31*(1), i193-i199.

Marshall, A. L. (2022). Williams Manual of Hematology. Mcgraw-Hill Education.

McClellan, W. M., & Powe, N. R. (2009). Introduction to the Proceedings of a Centers for Disease Control and Prevention Expert Panel Workshop: Developing a comprehensive public health strategy for preventing the development, progression, and complications of CKD. *American Journal of Kidney Diseases*, *53*(3), S1-S3.

Meri, M. A., Al-Hakeem, A. H., Al-Abeadi, R. S., & Mahdi, D. M. (2022). Study of the changes of some biochemical parameters of patients with renal failure. *Bulletin of National Institute of Health Sciences*, *140*(3), 2925-2933.

Nairz, M., Theurl, I., Wolf, D., & Weiss, G. (2016). Iron deficiency or anemia of inflammation? Differential diagnosis and mechanisms of anemia of inflammation. *Wiener Medizinische Wochenschrift*, *166*(13-14), 411-423.

Perco, P., Pleban, C., Kainz, A., Lukas, A., Mayer, G., Mayer, B., & Oberbauer, R. (2006). Protein biomarkers associated with acute renal failure and chronic kidney disease. *European journal of clinical investigation*, *36*(11), 753-763.

Prasad, G. R. (2014). Metabolic syndrome and chronic kidney disease: Current status and future directions. *World journal of nephrology*, *3*(4), 210.

Priyadarshani, W. V. D., de Namor, A. F. D., & Silva, S. R. P. (2023). Rising of a global silent killer: critical analysis of chronic kidney disease of uncertain aetiology (CKDu) worldwide and mitigation steps. *Environmental geochemistry and health*, *45*(6), 2647-2662.

Remuzzi, G. (1989). Bleeding disorders in uremia: pathophysiology and treatment. *Advances in nephrology from the Necker Hospital*, *18*, 171-186.

Saxena, R., Sharma, G., & Gulati, N. (2018). Iron-deficiency Anemia and Chronic Kidney Disease: An Overview. *World Journal of Anemia*, *2*(3and4), 85–89. https://doi.org/10.5005/jp-journals-10065-0037

Shastry, I., & Belurkar, S. (2019). The spectrum of red blood cell parameters in chronic kidney disease: A study of 300 cases. *Journal of Applied Hematology*, *10*(2), 61-66.

Somvanshi, S., Khan, N. Z., & Ahmad, M. (2012). Anemia in chronic kidney disease patients. *Clinical Queries: Nephrology*, *1*(3), 198-204.

Srinivasan, R., Fredy, I. C., Chandrashekar, S., Saravanan, J., Mohanta, G. P., & Manna, P. K. (2016). Assessment of erythropoietin for treatment of anemia in chronic kidney failure-ESRD patients. *Biomedicine & Pharmacotherapy*, *82*, 44-48.

Tyagi, N. (2023) Serum Creatinine Test: Means, Normal Range, Price, Procedure, retrieved from: https://www.hexahealth.com/blog/serum-creatinine-test

Vaidya, S. R., & Aeddula, N. R. (2022, October 24). *Chronic kidney disease*. StatPearls - NCBI Bookshelf. https://www.ncbi.nlm.nih.gov/books/NBK535404/

Zilva, J. F., & Pannall, P. R. (1988). Clinical chemistry in diagnosis and treatment. 5th ed., Edward Arnold, London, UK.

Scientific Journal for the Faculty of Science-Sirte University Vol. 4, No. 1 (2024) 124-128

Scientific Journal for the Faculty of Science-Sirte University

Journal home page: http://journal.su.edu.ly/index.php/JSFSU/index

DOI: 10.37375/issn.2789-858X

Isolation and Study of the Phenotypic Characteristics of Some Soil-borne Fungi in two Different Locations in Omar AL-Mukhtar University, Albyda, Libya

Zainap Ab. Easa

Botany Department, Science Faculty, Omar Al-Mukhtar University, Al-Bayda –Libya.

DOI: https://doi.org/10.37375/sjfssu.v4i1.2635

ARTICLE INFO:

Received: 15 February 2024

Accepted: 04 April 2024

Published: 17 April 2024

***Keywords*:** *Isolation, Soil fungi, Libya, phenotypic*

A B S T R A C T

Fungi assume a significant role within the terrestrial ecological system, as they are accountable for numerous crucial processes that contribute to the preservation of ecological equilibrium. Notably, they facilitate the recycling of soil organic matter and mineral elements. They are widely recognized for their role as a stimulator of plant development, a biocontrol agent for plant diseases, and participants in bioremediation processes. This study involved the isolation of fungi from agricultural soil previously employed at the Glasshouse facility at Omar AL-Mukhtar University, situated in Albayda City, eastern Libya. The investigation of soil fungus diversity in this region remains unexplored. This investigation involved the collection of soil samples from two distinct places within the institution. The soil dilution soil method and PDA agar medium were employed to isolate soil fungi. A notable disparity in fungal diversity was noted between the two sites, with the findings indicating that the predominant genera identified were associated with the Ascomycota family, while the proportions of Zygomycota were comparatively lower. The frequent species were in decrescent order: *Aspergillus*, *Penicillium* spp, and *Trichoderma* spp.

1 Introduction

The fungal communities present in soil are of significant importance in influencing plant communities and sustaining the functioning of the environment. These communities exhibit a strong correlation with both plant communities and soil attributes (Hicks *et al.*, 2021). Soil functions as a reservoir for several microbial communities found in plants and herbs, facilitating the production of carbon dioxide (CO2) and nitrogen (N) cycles. Microbial composition changes the quality of soil through organic matter decomposition, nutrient recycling and biocontrol (Stefanis *et al.*, 2013). Typically, fungi remain inactive and exhibit modest growth, relying on a variety of organic compounds. In general, the concentration of microbes is greater near the roots of plants (rhizosphere), where its exudates are considered an important source of organic energy that enters from soils. Fungal organisms, particularly pathogenic fungi responsible for plant illnesses, are influenced by several living and non-living elements (Liu *et al.*, 2020). Fungi have a substantial impact on various aspects of human existence, including but not limited to their application in industry, agriculture, medicine, food industry, textiles, bioremediation, natural cycling, and as biofertilizers. This study aimed to investigate the distribution and genus-level identification of fungal isolates, whenever feasible, by analyzing macromorphological characteristics such as slow or rapid growth, topography,

Corresponding author: **E-mail:** zainap.abdulkarem@omu.edu.ly

and micromorphological features, including hyphae, macroconidia, microconidia, chlamydospores, and other distinctive fungal structures Materials and Methods.

Provide sufficient details to allow the work to be reproduced by an independent researcher. Methods that are already published should be summarized and indicated by a reference. If quoting directly from apreviously published method, use quotation marks and cite the source. Any modifications to existing methods should also be described.

2 Materials and Methods

2.1 Collection of soil samples

Two soil samples were obtained from different places within Omar AL-Mukhtar University in order to investigate the distribution of fungi. In this study the uppermost layer of soil was removed from each sample, measuring approximately 3 cm. Subsequently, three sub-samples were randomly extracted to a depth of 15 cm at each location, employing a sterile auger (Mailafia, et.al 2017). Soil samples were collected in each site, namely near the roots where the majority of microbial activity is concentrated (Burh, 2011 ; Han et al. 2023).

The fungal communities present in soil are of significant importance in laboratory settings, where they are stored in sterile polyethylene bags under aseptic conditions. Furthermore, the sub-samples from each site were combined to form a single compound sample that accurately represents the entire area. The soils were subjected to ambient temperature to facilitate the drying process. Once the samples had acquired a sufficient moisture content, they were subjected to sieving using a 2 mm screen to evaluate the soil characteristics.

2.2 Organic matter content of soil

It was determined according to Poudel (2020). A 1 gm of sieved soil was digested by chromic acid in the presence of 10 ml of K2Cr2O7 and 20 ml H2SO4 (for oxidation of organic matter to carbon dioxide), while the excess of chromic acid was titrated against standard ferrous sulfate solution using diphenylamine as an indicator.

2.3 pH value of soil

The soil pH was determined using a Beckman pH meter. The pH of the soil was calculated by quantifying the addition of 5 ml of distilled water to 1 g of soil, as described by (Zhang et al. 2021; Li et al. 2023).

2.4 Isolation and purification

To isolate fungi, the soil dilution plating technique was employed, which involved combining 10 g of soil sample with 100 ml of sterile distilled water, followed by agitation on a shaker at a speed of 100 rpm for a duration of 10 minutes. The soil was diluted to a concentration of 10-3. Subsequently, 1 ml of the resulting diluted soil solution, ranging from 10-1 to 10-3, was pipetted into a petri dish. This process was repeated three times. Approximately 9 milliliters of Potato Dextrose Agar were introduced into the petri dish containing diluted soil, gently swirled, and allowed to undergo solidification. Daily examinations were conducted on the soil plates, while fungal colonies were subsequently subcultured onto PDA. This study conducted a single spore isolation procedure on a fresh PDA medium to acquire pure fungal culture isolates (Noman et al. 2018; Soltani et al., 2022).

2.5 Identification of Fungi

Similar to the study conducted by Raja *et al.* (2022), fungal isolates were classified at both the genus and species levels, whenever feasible, based on morphological analysis, which involved examining colonies for characteristics such as rapid or slow growth, topography, texture, surface pigmentation, as well as micromorphological features including hyphae, macroconidia, microconidia, chlamydospores, and other distinctive fungal structures.

3 Results

According to the findings shown in Table 1, the soil organic matter content was determined to be 3.3% for cultivated sandy soil in the Faculty of Science region and 4.3% for cultivated sandy loam soil in the Faculty of Agriculture region. The soil samples from both locations had alkaline pH values, as indicated in Table 1. Where soil pH and organic matter content had no significant differences between the two locations.

Table (1) Characteristics of the soil samples and plant used for isolatio

Soil No	Locations of soil samples	Particle size distribution				pH	Organic matter %	Plant under cultivation
		Sand %	Silt %	Clay %	Texture			
1	Faculty of science	64.60	25.6	9.8	Sandy Loam	7.6	3.3	*Phagnallon rupestre*
2	Faculty of agriculture	65.66	21.64	12.69	Sandy Loam	7.9	4.3	*Portulaca oleracea*

The primary objective of this study was to isolate soil fungus from two distinct locations within Omar AL-Mukhtar University. Thirteen fungal isolates were obtained from the soil samples. The majority of species within the genus were classified as *Aspergillus*. The identified soil fungus, as presented in Table 2, include *Aspergillus niger*, *Aspergillus* spp., *Fusarium* sp., *Trichoderma* ssp., *Penicillium* spp., and *Rhizopus* sp. The species *Aspergillus* had the highest abundance in both sites, followed by *Penicillium* ssp. and *Trichoderma* ssp.

Table (2) The colony morphology of different species isolated from two different locations in Omar AL-Mukhtar University

Soil No	Size	Color	Nature of hyphae	Conidia shape	Species	Divisions
1	Large	Black	Septate	Globose	*Aspergillus niger*	Ascomycota
	Small	Green	Septate	Oval	*Aspergillus* sp.	Ascomycota
	Medium	White	Septate	Microconidia: Oval (one or two cells Macroconidia: (more than two cells) Chlamydospores: Oval	*Fusarium* sp.	Ascomycota
	Medium	White	Septate	Globose	*Trichoderma* sp.	Ascomycota
	Large	Green	Septate	Globose	*Trichoderma* sp.	Ascomycota
		Green	Septate	Oval	*Penicillium* sp.	Ascomycota
2	Large	Black	Septate	Oval	*Aspergillus niger*	Ascomycota
	Medium	Green	Septate	Oval	*Aspergillus* sp.	Ascomycota
	Small	Brown	Septate	Globose	*Aspergillus* sp.	Ascomycota
	Medium	Green	Septate	Oval	*Penicillium* sp.	Ascomycota
	Medium	Yellow-green	Septate	Oval	*Penicillium* sp.	Ascomycota
	Large	Green	Septate	Globose	*Trichoderma* sp.	Ascomycota
	Medium	Brown	Aseptate	Globose	*Rhizopus* sp.	Zygomycota

4 Discussion

Soil is a complex surface composed of mineral and organic elements that exist in solid, liquid, and gaseous phases, forming several layers. The composition and pH levels of soil are influenced by the processes of weathering and erosion on rock (Raja et al., 2022). The community structure of soil fungus is significantly influenced by soil pH. A previous study has indicated that alterations in fungal communities within the rhizosphere can occur in response to several environmental conditions, such as pH levels, temperature fluctuations, and nutrient availability (Timling et al., 2012). Deslippe et al. (2012) observed that the fungal community structure varied between mineral and organic soils, maybe due to differences in nutrient content and carbon ratio in the organic soil. In a study conducted by Wahegaonkar et al. (2011), a total of 45 genera were identified and spread over 85 species within agricultural soils.

In a study conducted by Gaddeyya in 2012, a total of 15 species belonging to six genera were isolated from agricultural areas. The most common isolates were *Trichoderma harzianum*, *Trichoderma viride*, *Aspergillus flavus*, *Fusarium solani*, and *Fusarium oxysporum*, which aligns with the present findings.

5 Conclusions

In brief, this study has provided a comprehension of the range of soil fungi present in various locations inside Omar AL-Mukhtar University. The pH level of soil is widely recognized as a significant determinant in the establishment of fungal communities. Furthermore, there exist other unmeasured environmental elements that could potentially influence the development of fungal communities in the soil, including climate and vegetation type. These factors will impact the composition of soil fungus populations. Hence, it is imperative to conduct further studies to validate the impact of vegetation cover on the dispersal of fungi.

Acknowledgements

The author would like to thank Dr. Soad Mohamed Omar and Head of the Department of Botany, Dr. Najat Al-hadad for them valuable assistance.

Conflict of interest: There are no financial, personal, or professional conflicts of interest to declare.

References

Burh, P. M. (2011). Microbial analysis of soil and water samples from Koel river in Rourkela, Odisha.

Deslippe, J. R., Hartmann, M., Simard, S. W., & Mohn, W. W. (2012). Long-term warming alters the composition of Arctic soil microbial communities. FEMS microbiology ecology, 82(2), 303-315. https://doi.org/10.1111/j.1574-6941.2012.01350.x

Gaddeyya, G., Niharika, P. S., Bharathi, P., & Kumar, P. R. (2012). Isolation and identification of soil mycoflora in different crop fields at Salur Mandal. Advances in Applied Science Research, 3(4), 2020-2026.

Han, M., Chen, Y., Sun, L., Yu, M., Li, R., Li, S., ... & Zhu, B. (2023). Linking rhizosphere soil microbial activity and plant resource acquisition strategy. Journal of Ecology, 111(4), 875-888. https://doi.org/10.1111/1365-2745.14067

Hicks, L. C., Lajtha, K., & Rousk, J. (2021). Nutrient limitation may induce microbial mining for resources from persistent soil organic matter. Ecology, 102(6), https://doi.org/10.1002/ecy.3328 e03328 .

Li, J., Wu, B., Zhang, D., & Cheng, X. (2023). Elevational variation in soil phosphorus pools and controlling factors in alpine areas of Southwest China. *Geoderma*, *431*, 116361. https://doi.org/10.1016/j.geoderma.2023.116361

Liu, X., Chen, L., Liu, M., García-Guzmán, G., Gilbert, G. S., & Zhou, S. (2020). Dilution effect of plant diversity on infectious diseases: latitudinal trend and biological context dependence. Oikos, 129(4), 457-465. https://doi.org/10.1111/oik.07027

Mailafia, S., Olabode, H. O. K., & Osanupin, R. (2017). Isolation and identification of fungi associated with spoilt fruits vended in Gwagwalada market, Abuja, Nigeria. Veterinary world, 10(4), 393. https://doi.org/10.14202%2Fvetworld.2017.393-397

Nilima Wahegaonkar, N. W., Salunkhe, S. M., Palsingankar, P. L., & Shinde, S. Y. (2011). Diversity of fungi from soils of Aurangabad, MS, India. https://doi.org/10.5555/20113163794

Noman, E., Al-Gheethi, A. A., Rahman, N. K., Talip, B., Mohamed, R., & Kadir, O. A. (2018, April). Single spore isolation as a simple and efficient technique to obtain fungal pure culture. In *IOP conference series: earth and environmental science* (Vol. 140, p. 012055). IOP Publishing. **https://doi.org**/10.1088/1755-1315/140/1/012055

Poudel, S. (2020). Organic Matter determination (Walkley-Black method).

Raja, M., Praveena, G., & William, S. J. (2017). Isolation and identification of fungi from soil in Loyola college campus, Chennai, India. Int J Curr Microbiol App Sci, 6(2), 1789-95. http://dx.doi.org/10.20546/ijcmas.2017.602.200

Soltani Nejad, M., Samandari Najafabadi, N., Aghighi, S., Shahidi Bonjar, A. H., Murtazova, K. M. S., Nakhaev, M. R., & Zargar, M. (2022). Investigating the Potential of Streptomyces spp. in Suppression of Rhizoctonia solani (AG1-IA) Causing Rice Sheath Blight Disease in Northern Iran. Agronomy, 12(10), 2292. https://doi.org/10.3390/agronomy12102292

Stefanis, C., Alexopoulos, A., Voidarou, C., Vavias, S., & Bezirtzoglou, E. (2013). Principal methods for isolation and identification of soil microbial communities. Folia microbiologica, 58, 61-68. https://doi.org/10.1007/s12223-012-0179-5

Timling, I., Dahlberg, A., Walker, D. A., Gardes, M., Charcosset, J. Y., Welker, J. M., & Taylor, D. L. (2012). Distribution and drivers of ectomycorrhizal fungal communities across the North American Arctic. Ecosphere, 3(11), 1-25. https://doi.org/10.1890/ES12-00217.1

Zhang, P., Luan, M., Li, X., Lian, Z., & Zhao, X. (2021). The distribution of soil fungal communities along an altitudinal gradient in an alpine meadow. Global Ecology and Conservation, 31, e01838. https://doi.org/10.1016/j.gecco.2021.e01838